

NOTE TO USERS

This reproduction is the best copy available.

UMI[®]

Energy modulated electron therapy: design, implementation, and evaluation of a novel method of treatment planning and delivery

Khalid Al-Yahya

Doctor of Philosophy

Department of Physics

McGill University

Montreal, Quebec

2006-12-12

A thesis submitted to the faculty of graduate studies and research in partial fulfillment of the requirements of the degree of Doctor of Philosophy

© Khalid Al-Yahya 2006



Library and
Archives Canada

Bibliothèque et
Archives Canada

Published Heritage
Branch

Direction du
Patrimoine de l'édition

395 Wellington Street
Ottawa ON K1A 0N4
Canada

395, rue Wellington
Ottawa ON K1A 0N4
Canada

Your file Votre référence

ISBN: 978-0-494-32135-5

Our file Notre référence

ISBN: 978-0-494-32135-5

NOTICE:

The author has granted a non-exclusive license allowing Library and Archives Canada to reproduce, publish, archive, preserve, conserve, communicate to the public by telecommunication or on the Internet, loan, distribute and sell theses worldwide, for commercial or non-commercial purposes, in microform, paper, electronic and/or any other formats.

The author retains copyright ownership and moral rights in this thesis. Neither the thesis nor substantial extracts from it may be printed or otherwise reproduced without the author's permission.

AVIS:

L'auteur a accordé une licence non exclusive permettant à la Bibliothèque et Archives Canada de reproduire, publier, archiver, sauvegarder, conserver, transmettre au public par télécommunication ou par l'Internet, prêter, distribuer et vendre des thèses partout dans le monde, à des fins commerciales ou autres, sur support microforme, papier, électronique et/ou autres formats.

L'auteur conserve la propriété du droit d'auteur et des droits moraux qui protègent cette thèse. Ni la thèse ni des extraits substantiels de celle-ci ne doivent être imprimés ou autrement reproduits sans son autorisation.

In compliance with the Canadian Privacy Act some supporting forms may have been removed from this thesis.

Conformément à la loi canadienne sur la protection de la vie privée, quelques formulaires secondaires ont été enlevés de cette thèse.

While these forms may be included in the document page count, their removal does not represent any loss of content from the thesis.

Bien que ces formulaires aient inclus dans la pagination, il n'y aura aucun contenu manquant.


Canada

ABSTRACT

Energy modulated electron therapy (EMET) is a promising treatment modality that has the fundamental capabilities to enhance the treatment planning and delivery of superficially located targets. Although it offers advantages over x-ray intensity modulated radiation therapy (IMRT), EMET has not been widely implemented to the same level of accuracy, automation, and clinical routine as its x-ray counterpart. This lack of implementation is attributed to the absence of a remotely automated beam shaping system as well as the deficiency in dosimetric accuracy of clinical electron pencil beam algorithms in the presence of beam modifiers and tissue heterogeneities. In this study, we present a novel technique for treatment planning and delivery of EMET. The delivery is achieved using a prototype of an automated “few leaf electron collimator” (FLEC). It consists of four copper leaves driven by stepper motors which are synchronized with the x-ray jaws in order to form a series of collimated rectangular openings or “fieldlets”. Based on Monte Carlo studies, the FLEC has been designed to serve as an accessory tool to the current accelerator equipment. The FLEC was constructed and its operation was fully automated and integrated with the accelerator through an in-house assembled control unit. The control unit is a portable computer system accompanied with customized software that delivers EMET plans after acquiring them from the optimization station. EMET plans are produced based on dose volume constraints that employ Monte Carlo pre-generated and patient-specific kernels which are utilized by an in-house developed optimization algorithm. The structure of the optimization software is demonstrated. Using Monte Carlo techniques to calculate dose allows for accurate modeling of the collimation system as well as the patient heterogeneous geometry and take into account their impact on optimization. The Monte Carlo calculations were validated by comparing them against output measurements with an ionization chamber. Comparisons with measurements using nearly energy-independent radiochromic films were performed to confirm the Monte Carlo calculation accuracy for 1-D and 2-D dose

distributions. We investigated the clinical significance of EMET on cancer sites that are inherently difficult to plan with IMRT. Several parameters were used to analyze treatment plans where they show that EMET provides significant overall improvements over IMRT.

ABRÉGÉ

La radiothérapie par modulation d'énergie d'électron (RTMEE) est un mode de traitement prometteur qui a la capacité fondamentale d'améliorer la planification du traitement et son application vers des cibles superficielles. Bien que ce mode de traitement présente des avantages par rapport à la radiothérapie par modulation d'intensité (RTMI) avec photon, l'expansion de l'implantation de la RTMEE n'a pas atteint le même niveau de précision, d'automatisation et de routine clinique que la RTMI. Ce retard d'implémentation est attribué à l'absence d'un système automatisé qui contrôle à distance la conformité du faisceau ainsi qu'à l'imprécision des algorithmes de calcul de dose en milieux hétérogènes pour les faisceaux d'électrons en conformité. Cette étude présente une technique innovatrice permettant de faire la planification et le traitement par RTMEE. Le traitement est donné en utilisant un prototype de « collimateur d'électron à peu de lames » (CEPL) automatisé. Celui-ci possède quatre lames de cuivre, guidées par des moteurs pas à pas, qui sont synchronisées avec les mâchoires du mode photon de l'accélérateur linéaire afin de former une série d'ouvertures rectangulaires « sous champs ». Une modélisation Monte-Carlo du CEPL a été réalisée pour optimiser sa conception et sa construction afin de servir d'outil complémentaire aux accélérateurs linéaires médicaux actuels. La mise en opération du CEPL est totalement automatisée et intégrée à l'accélérateur via une unité de contrôle locale. L'unité de contrôle consiste en un ordinateur portable accompagné d'un logiciel fait sur mesure qui contrôle les lames en fonction des plans de la RTMEE reçus via la station d'optimisation. La production des plans de la RTMEE est basée sur des contraintes de volume de dose et utilise des noyaux de calcul pré-calculés et spécifiques au patient traité utilisant un algorithme d'optimisation développé localement. La structure des logiciels d'optimisation est démontrée. L'utilisation des techniques de calcul de la dose par Monte-Carlo permet une modélisation précise à la fois du système de collimateur ainsi que de la géométrie

hétérogène du patient afin de prendre en considération leurs impacts sur l'optimisation. Les calculs de dose par Monte-Carlo sont validés en les comparant aux mesures obtenues avec une chambre d'ionisation. Des comparaisons avec des mesures indépendantes à l'énergie ont été obtenues en utilisant des films radiochromiques pour confirmer l'exactitude des calculs de Monte-Carlo pour les distributions de dose en 1-D et en 2-D. Nous avons aussi étudié la signification clinique de la RTMEE sur des sites de cancer qui sont par nature difficiles à planifier avec la RTMI avec rayons X. Plusieurs paramètres ont été utilisés pour analyser les planifications de traitement et ont démontré que la RTMEE offre des améliorations généralement plus significatives que la RTMI avec rayons X.

STATEMENT OF ORIGINALITY

The complexity of inverse techniques for treatment planning of energy modulated electron therapy (EMET) has limited its applications clinically. The successful implementation of EMET requires the utility of an automated beam shaping system that allows the manipulation of beam intensities in addition to an accurate dose calculation engine. Although EMET has been the subject of several other studies, planning accuracy and complications during delivery remain central problems. We have attempted to overcome these problems by presenting a novel automated few leaf electron collimator (FLEC) in conjunction with Monte Carlo-based inverse treatment planning optimization. The FLEC was constructed and incorporated within the clinical accelerator so as to be easily controlled from the treatment console. The FLEC is integrated with a Monte Carlo-based inverse planning process. We are the first to construct an electron collimator that acquires a sequence of aperture settings from an optimization algorithm and deliver the EMET plans automatically. None of the previously reported investigations addressed the ability to provide an accessory tool for the purpose of EMET that is practical and completely automated. Nor there have been Monte Carlo-based, optimized planning tools that were connected to any form of delivery units.

In the process of verifying our Monte Carlo dose calculation performance, we present an extensive set of measurements. We are the first to use the radiochromic films to show the 2-D dose distributions of complex intensity maps delivered by different electron beam energies where both measurements and calculations agree well. We also investigated the effects of the partial blocking of electron beams using x-ray collimators for the purpose of EMET. We report excellent agreement between Monte Carlo and measurements which includes: the effect of the beam output, the isodose lines representing the high dose region, and the leakage dose.

So far, very little research examined the dosimetric advantages of EMET compared to IMRT. All the previous research was purely theoretical because means of delivery were not established. We present a comprehensive dosimetric evaluation of EMET delivered with the FLEC. We show that it provides a valuable addition to the current treatment planning techniques when applied to superficially located tumors.

CONTRIBUTIONS OF AUTHORS

This thesis consists of two published papers and one submitted paper. I was responsible for writing the manuscripts and performing the experimental work. However, several authors have contributed to these manuscripts.

First paper: *Monte Carlo-based modulated electron beam treatment planning using a few leaf electron collimator – feasibility study*

- Dr. Jan Seuntjens: Provided the initial idea and guidelines of the proposed work. He offered his expertise for some aspects of programming. He evaluated the progress and supervised the work. He contributed to the quality of the text through his useful suggestions and revisions.
- Dr. Frank Verhaegen: Shared his expertise with Monte Carlo modeling and revised the manuscript.
- Dr. Dimitre Hristov: Provided me with the early version of the optimization algorithm. He discussed the details of adapting advanced visual system (AVS) modules for our purpose.

Second paper: *Energy modulated electron therapy using a few leaf electron collimator in combination with IMRT and 3D-CRT: Monte Carlo-based planning and dosimetric evaluation*

- Dr. Jan Seuntjens: Supervised the work. He arranged multiple meetings with the clinical staff to present our work. He revised the manuscript.
- Dr. Matthew Schwartz: Outlined the volumes for all the patients. He provided the dose prescriptions and approved the treatment plans for 3-D conformal radiation therapy and intensity modulated radiation therapy (IMRT).

- Dr. Carolyn Freeman: Selected the patient for the breast case and approved our clinical outcome conclusions. She revised the manuscript and provided helpful comments.
- Dr. George Shenouda: Selected the head & neck cases and discussed the advantages of our work in reducing the total body dose.
- Dr. Frank Verhaegen: Revised the manuscript and gave useful advices on the Monte Carlo modeling.

Third paper: Construction and dosimetry of a new automated collimator for delivery of Monte Carlo-based energy-intensity modulated electron therapy

- Dr. Jan Seuntjens: Supervised the work and provided the finances for the construction of the new device. He discussed the mechanical and electronic designs. He provided an adapted code that simplifies the communication with the linear accelerator. He gave many suggestions for the experimental work that greatly improved the quality of the paper. He also revised the manuscript.
- Dr. Frank Verhaegen: He discussed the results and provided helpful suggestions. He revised the manuscript.

ACKNOWLEDGMENTS

I owe a huge debt of gratitude to Dr. Jan Seuntjens for all the time, effort, and patience that he has put into this project. Without his tireless and unique contributions, this work would have never come about. I thank him for his constant support, guidance, encouragement, and for his unflagging positive energy.

I also thank Dr. Frank Verhaegen for his suggestions on many key issues in this research.

Special thanks to Dr. Ervin Podgorsak for his timely words of encouragement and his advices.

I would like to express my special appreciation to my colleagues Emily Heath, Kristen Stewart, Arman Sarfehnia, Keyvan Jabbari, and Andrew Alexander who generously helped me at various stages of my work.

Special thanks to Pierre Leger and Robin Van Gils for sharing their expertise and time. Pierre is also acknowledged for providing me with a space in his office.

Far too many people to mention individually have assisted in so many ways at McGill Medical Physics Unit. They all have my sincere gratitude. In particular, I would like to thank Dr. Wamied Abdel-Rahman, Dr. Francois Deblois, Michael Evans, Dr. Slobodan Devic, William Parker, Russel Ruo, Christopher Kauffman, and Horacio Patrocinio for their help at different stages of my project.

Finally, my and most heartfelt acknowledgment must go to my wife. Her support, encouragement, and companionship have turned my journey through graduate school into a pleasure. For all that, and for being everything I am not, she has my everlasting love.

DEDICATION

To Razan and Jude,
If they only knew

TABLE OF CONTENTS

DEDICATION	xi
TABLE OF CONTENTS	xii
LIST OF TABLES	xiv
LIST OF FIGURES.....	xv
Introduction	1
1.1 Radiation Therapy	1
1.2 Intensity Modulated Radiation Therapy (IMRT)	2
1.3 The Need for Dosimetric Accuracy.....	2
1.4 Modulated Electron Therapy, Why Not?	3
1.5 Hypothesis and Objectives	5
1.6 Thesis Outline	6
References	7
Introduction to Electron Beam Therapy	11
2.1 Electron Interactions	11
2.1.1 Stopping power.....	12
2.1.2 Absorbed dose	13
2.2 Treatment Units.....	14
2.2.1 Medical linear accelerator (linac)	15
2.2.2 Microtron	17
2.3 Characteristics of Clinical Electron Beams	17
2.3.1 Central axis depth dose	17
2.3.2 Output factors	20
2.3.3 Virtual electron source.....	21
2.3.4 Effects of oblique incidence and tissue heterogeneities.....	21
2.4 Dose Measurements	21
2.4.1 Phantom materials	21
2.4.2 Absolute and relative dosimetry	22
2.4.3 Dose measurement methods	22
2.4.4 Comparison of different dose measuring tools	27
2.5 Treatment Planning	27
2.6 Electron Transport Calculation.....	28
2.6.1 Analytical radiation transport-pencil beam algorithm	28
2.6.2 Monte Carlo transport.....	34
2.6.3 Pencil beam algorithm vs. Monte Carlo techniques	40
2.7. Clinical Use of Electron Therapy	40
References	41
Energy Modulated Electron Therapy	51
3.1 Bolus Conformal Therapy	52
3.2 Collimator-based Modulated Electron Therapy	55
3.2.1 Inverse treatment planning	55
3.2.2 Treatment delivery.....	58
3.3 Modulated Electron Arc Therapy (MEAT)	63
3.5 Conclusion.....	64
References	65
Monte Carlo-based Inverse Treatment Planning for Energy Modulated Electron Therapy	70
4.1 Introduction	72
4.2 Materials and Method.....	73
4.2.1 Design of few leaf electron collimator	73
4.2.2 Monte Carlo calculations.....	75
4.2.3 Treatment plan optimization.....	76

4.2.4	Treatment planning details	79
4.3	Results and Discussion.....	80
4.3.1	Homogeneous phantom	80
4.3.2	Head and neck case.....	82
4.4	Conclusions	84
	References	86
Clinical Significance of Energy Modulated Electron Therapy Using Few Leaf Electron Collimator		88
5.1	Introduction	90
5.2	Methods and Materials	92
5.2.1	Patient selection, volume definition, dose prescription	92
5.2.2	Treatment planning.....	93
5.2.3	Plan evaluation parameters	98
5.2.4	Assessment of whole body dose-equivalent (WBDE).....	100
5.3	Results	101
5.3.1	Parotid cancer cases.....	101
5.3.2	Left breast cancer post-mastectomy case.....	105
5.4	Discussion	107
5.4.1	3D-CRT vs. EMET-CRT.....	107
5.4.2	IMRT vs. IMRT-EMET.....	108
5.4.3	IMRT vs. EMET-CRT.....	108
5.5	Conclusion.....	109
	References	111
Construction and Validation of an Automated Few Leaf Electron Collimator		114
6.1	Introduction	115
6.2	Materials and Methods	118
6.2.1	Construction and automation of the few leaf electron collimator (FLEC)	118
6.2.2	Monte Carlo simulations.....	122
6.2.3	Ionization chamber measurements of output factors	122
6.2.4	Film measurements.....	124
6.3	Results	125
6.3.1.	FLEC prototype	125
6.3.2	Leaf and backup jaw optimization.....	127
6.3.3	Comparison of calculated and measured dose from FLEC-defined fields.....	130
6.4	Conclusions and Future Work	137
	References	140
Summary and Future Work		143
7.1	Summary	143
7.1.1	Construction and automation of the few leaf electron collimator (FLEC)	143
7.1.2	Monte Carlo dose calculation engine.....	144
7.1.3	Incorporating a Monte Carlo-based optimization algorithm.....	144
7.1.4	Integrated software for planning and delivery of EMET	145
7.1.5	Investigation of the clinical significance of EMET	145
7.1.6	Validation of Monte Carlo calculations	147
7.2	Future Work	147
Appendix A		149
McGill Monte Carlo Treatment Planning (MMCTP)		149
Appendix B		156
Waivers.....		156
Appendix C		167
Reprints of the Published Papers		167
Bibliography		195

LIST OF TABLES

Table 4-1: Target dose and organ dose-volume levels in EMET optimization for the phantom case.	79
Table 4-2: The total number of the prescribed monitor units obtained by the optimizer over the whole treatment. The beam-on time required to deliver one fraction remains within 5 minutes interval.	82
Table 5-1: Objective function parameters used in treatment planning and optimization.	92
Table 5-2: The total MUs to deliver the plans of the conventional 3D-CRT*, EMET-CRT [†] , IMRT ^{††} , and EMET-IMRT [†] . The addition of EMET reduces the photon beam contributions of the 3D-CRT and IMRT plans by transferring some weight to the electron beams. The electron MUs and the photon MUs are not additive since they contribute differently to the whole body dose. (* The number of MUs is prescribed by the CadPlan treatment planning system. [†] The number of MUs is prescribed by the EMET optimizer. ^{††} The number of MUs is prescribed by the CORVUS treatment planning system.)	95
Table 5-3: Comparison of dose for PTV and OARs using four planning techniques. min= minimum dose; max= maximum dose; mean= mean dose.	102
Table 5-4: Comparison of treatment planning evaluation parameters of the four planning techniques. *COIN95= Conformity Index. [†] SPIN50/10= Sparing Index. ^{††} HI90/110 = Homogeneity Index. [§] WBDE = Whole body dose equivalent.	105
Table 6-1: (a) Numerated factors obtained from the off-axis profiles of 9 and 18 MeV of different jaw openings corresponding to a certain FLEC opening (C6). (b) Dose penumbra 90/10, Y-Leakage Peak, and X-Leakage Peak for different fieldlets following the optimum jaw opening.	131
Table 6-2: Measured and calculated output factors for the 9, 12, 15, and 18 MeV electron beams for different fieldlets. Measurements were performed with a PPC40 parallel plate chamber in water and the localization of z_{max} was determined from ionization measurements about z_{max} . The output for each energy is normalized to the measured dose at the largest fieldlet (J9 C8).	132

LIST OF FIGURES

Figure 2-1: Representation of an electron traversing the field of an atom; “a” is the classical atomic radius, “b” is the classical impact parameter.....	Error! Bookmark not defined.
Figure 2-2: PDD curves for electron and photon beams of $10 \times 10 \text{ cm}^2$ field size at SSD=100 cm for all energies of the CL2300 measured with ionization chamber.	Error! Bookmark not defined.
Figure 2-3: Specifications of parameters that are used to characterize electron beam central axis depth dose curve.	Error! Bookmark not defined.
Figure 2-4: Schematic diagram of the original Hogstrom’s pencil beam algorithm representation. Reprinted with permission from IOP Publishing (from Hogstrom et al., <i>Physics in Medicine and Biology</i> ; 1982).	Error! Bookmark not defined.
Figure 2-5: A 3D image of a Monte Carlo model of Varian CL-2300 (18 MeV) using EGSnrc/BEAM.....	Error! Bookmark not defined.
Figure 3-1: (a) Custom made bolus electron bolus for postmastectomy chest wall case. (b) Isodose distribution using bolus for 16 MeV electron beam. Reprinted with permission from Elsevier (from Perkins et al., <i>International Journal of Radiation Oncology Physics</i> ; 2001).	53
Figure 3-2: (a) Retractable eMLC designed at M.D. Andersson Cancer Center. Reprinted with permission from Medical Physics Publishing (from Hogstrom et al., <i>Medical Physics</i> ; 2004). (b) eMLC prototype built at Stanford University. It is mounted on $25 \times 25 \text{ cm}^2$ applicator of Varian CL2100. Reprinted with permission from IOP publishing (from Ma et al., <i>Physics in Medicine and Biology</i> ; 2000).	60
Figure 3-3: Monte Carlo calculated dose profiles in a water phantom for 20 MeV electron beams collimated by an eMLC of 1.5 cm thick tungsten leaves for a single $4 \text{ cm} \times 4 \text{ cm}$ electron field (dotted) and a $4 \text{ cm} \times 4 \text{ cm}$ field formed by four $1 \text{ cm} \times 4 \text{ cm}$ electron fields (solid line) (a) at surface; and (b) at 3 cm depth. Reprinted with permission of IOP publishing (from Ma et al., <i>Physics in Medicine and Biology</i> ; 2000).....	61
Figure 3-4: Prototype of electron arc therapy-specific eMLC. The leaf resolution projects to 4 cm at isocenter. Reprinted with permission from Elsevier (from Leavitt et al., <i>International Journal of Radiation Oncology Physics</i> ; 1989).	63
Figure 4-1: (a) Position of few-leaf collimator (FLEC) relative to other components in the accelerator (not to scale). (b) Schematic drawing of beam’s eye view of FLEC.	74
Figure 4-2: A schematic diagram of the current EMET procedure.....	77

Figure 4-3: Dose distribution of an optimized EMET plan and DVHs for a hypothetical target and two organs at risk surrounding the PTV in a homogenous solid water phantom scanned by CT (PTV is outlined in yellow).	80
Figure 4-4: Comparison of (a) isodose distributions and (b) DVH for an outlined target using conventional two AP-PA wedged, MLC-shaped 6 MV beams mixed with one lateral 12 MeV electron beam and EMET technique using four fields of 9, 12, 15, and 18 MeV.	81
Figure 4-5: Dose distribution obtained by EMET shows that the algorithm takes the effect of the heterogeneity into account at the cost of the conformity.	81
Figure 4-6: XY scatter-plot for the weighted fluence obtained by the optimizer for each energy.	83
Figure 5-1: The intensity map of two energy fields based on the relative weights assigned by the EMET optimizer. The intensity map is normalized to the fieldlet with the highest MUs.	98
Figure 5-2: Schematic diagram of two plans that have the same coverage of the 95% isodose line to the PTV volume but with different conformity of the low isodose lines. The conformity index (COIN95) will be equivalent for both plans despite their differences. The sparing index (SPIN50/10) could be used to differentiate between them.	99
Figure 5-3: Off axis dose at depth of 2 cm in solid water phantom based on the number of MUs given by four techniques.	101
Figure 5-4: A comparison of the Monte Carlo calculated dose distributions and DVHs for all outlined organs produced by four plans: (I) 3D-CRT, (II) EMET-CRT, (III) IMRT, and (IV) EMET-IMRT. (a) and (b) are for the two parotid cases and (c) is for the breast case. The target is outlined in yellow.	104
Figure 6-1: (a) Flow chart of the software structure of the EMET controller. (b) Schematic diagram of the integrated EMET hardware that communicates with the Monte Carlo-based optimization station, the FLEC, and the linear accelerator.	120
Figure 6-2: Design drawing showing a side view of the FLEC prototype.	126
Figure 6-3: The FLEC prototype, including the necessary wiring, shows its compact design to fit in a clinical applicator.	127
Figure 6-4: (a) Calculated (symbols) and measured (full lines) off-axis profiles for three 18 MeV fieldlets with a fixed FLEC opening (at C6) and varying jaw openings (J8(◇), J7(▲), and J6(■)) based on a delivery of 1500 MUs. (b) The calculated normalized profiles of the three fieldlets	128
Figure 6-5: (a) Calculated (symbols) and measured (full lines) off-axis profiles for three 9 MeV fieldlets with a fixed FLEC opening (at C6) and varying jaw openings (J8(◇), J7(▲), and J6(■)) based on a delivery of 1500 MUs. (b) The calculated normalized profiles of the three fieldlets	129

Figure 6-6: Calculated (symbols) and measured (full lines) output factors for the 9, 12, 15, and 18 MeV electron beams for different fieldlet sizes. The output for each energy is normalized to the measured dose at the largest fieldlet (J9 C8).	133
Figure 6-7: (a) Calculated (symbols) and measured (full lines) depth dose distribution for three fieldlets with energy of 18 MeV and openings J9 C8(◇), J5 C4(▲), and J3 C3(■). (b) the differences (calculated- measured), expressed as the absolute difference.	134
Figure 6-8: Calculated (symbols) and measured (full lines) central depth dose distribution based on 1500 MUs given for three fieldlets with energies of 9 MeV and 18 MeV and openings J9 C8(◇), J7 C6(▲), and J5 C4(■).	135
Figure 6-9: Calculated (symbols) and measured (full lines) normalized depth dose distribution for two fieldlets (J9 C8 and J5 C4) for 9, 12, 15, and 18 MeV electron beams. The solid symbols represent the fieldlet J9 C8 and the open symbols represent the fieldlet J5 C4.	135
Figure 6-10: Absorbed dose distribution comparisons between HS film measurements (full lines) and Monte Carlo calculation (dotted lines) based on 2000 MUs irradiations at depth of 2.8 cm for (a) 9 MeV fieldlet with J7 C6, (b) 12 MeV fieldlet with J9 C8, (c) 15 MeV fieldlet, and (d) 18 MeV fieldlet. (e) and (f) Absorbed dose distribution comparison at depths of 3 cm (e) and 5 cm (f) for an intensity map formed by sum of the above four fieldlets with 750 MUs given to each of them. The Monte Carlo calculation accurately predicts the dose distribution of the mixed energy beam delivery at different depths.	138
Figure 7-1: The design of the FLEC prototype, including the necessary wiring, shows its compact design to fit in a clinical applicator.	144
Figure 7-2: The EMET controller is portable and can easily be linked to the FLEC and the linear accelerator through connectors.	145
Figure 7-3: Flow chart of the software structure that was developed to perform Monte Carlo-based optimization and delivery for EMET.	146
Figure A-1: The display of the main MMCTP window showing, in addition to the beam parameters list box, three canvas for axial, sagittal, and coronal views.	152
Figure A-2: Block diagram of the MMCTP structure. The shaded areas represent computer programs developed in-house.	154

Chapter 1**Introduction****1.1 Radiation Therapy**

Radiation therapy is the treatment of cancer with ionizing radiation where energy is transferred to the cells, thereby destroying them by damaging their DNA. The damage is caused directly or indirectly by ionizing the atoms that constitute the DNA chain. Most of the effects of radiation are caused by free radicals that are formed through ionization. Breaking the DNA on both strands of the DNA double helix is the most significant cellular perturbations caused by ionizing radiation that leads to diminishing cancer cells. Whether used as the main mode of treatment or in conjunction with surgery and/or chemotherapy, radiation therapy is considered a very important tool in the fight against cancer and is used in the treatment of as many as 50% of all cancer patients [1]. Clinically, radiation delivery is done either in the form of sealed radiation sources that are inserted inside the patient (brachytherapy) or using external beams. In the latter, particles are accelerated to high energies before being directed at the patient.

The treatment success rate increases with the increased number of killed tumor cells. Hence, the goal of any treatment is to maximize the damage to the cancerous cells by radiation [2]. Defined as the amount of energy deposited per unit mass of tissue, absorbed dose is directly related to the number of radiation-induced cell deaths [3]. But since the principles of radiation killing apply to both the tumor and normal cells, it is important for the dose distribution to conform to the shape of the tumor volume while minimizing the dose to the normal cells [4]. In order to spare surrounding tissue and

maximize the tumor dose, the beam of radiation may be partially blocked, modulated, or rotated around the patient's body. This process is referred to as "treatment planning". With the advent of 3D imaging, the location of the tumor and the extent of the disease can accurately be determined. Hence, treatment plans that match the optimum tumor control goals can be achieved. The recent developments in the design of external beams have provided us with ideal tools that enable tightened dose shaping through the delivery of complex fields.

1.2 Intensity Modulated Radiation Therapy (IMRT)

The ability to employ spatially modulated beam intensities in intensity modulated radiation therapy (IMRT) is regarded as the outcome of the latest developments in radiation therapy [5-11]. In IMRT, each beam is divided into a large number of radiation beamlets. Each beamlet is assumed to contribute to the overall dose to the organ by dose deposition coefficients (DDCs) that measure the dose deposited to a point per unit weight of the beamlet. By assuming that the intensity modulation is linearly mapped onto the dose vector by the DDC matrix, inverse treatment optimization algorithms are used to manipulate the beamlets in order to escalate the dose to the tumor while providing sufficient healthy tissue sparing. The beam portals are adjusted by the computer-controlled multi leaf collimators (MLCs) which offer a delicate control of delivered intensities.

1.3 The Need for Dosimetric Accuracy

There are several steps that are involved in the complex process of radiation therapy. Each step contributes to an overall uncertainty on the dose distribution which has a potential impact on tumor control or healthy tissue complications. These uncertainties are introduced through (1) patient setup, (2) accelerator beam output calibration, (3) patient data acquisition, and (4) dose calculation algorithms. In order to be consistent with the analysis and the outcome of clinical trials, the International Commission on Radiation Units and Measurements (ICRU) recommends achieving an accuracy that falls within the limits of 5% in dose delivery to the patient [12]. However, since the uncertainties in each procedure have independent nature, the required accuracy for each

of the four procedures should be limited to 2.5% in order to achieve an overall accuracy that matches the ICRU recommendations. The demand for accuracy in calculating the dose distribution within the treatment volume and normal tissue requires the application of a 3-dimensional treatment planning system. Such a system utilizes the information pertaining to the treatment machine in addition to the radiation transport properties influenced by the geometric patient data. The challenge of performing accurate dose calculations is due to: (1) the complicated shape and intensity distribution of the beam, and (2) the heterogeneous anatomy of the patient. Both problems have become more pronounced over the last years as the beam shaping is attaining more complexity. Currently, Monte Carlo simulation is undoubtedly the most accurate method that simulates radiation transport and predicts doses in complex heterogeneous media representing the human body [13-21]. Arguably, its main disadvantage, however, are the extremely long computing times that are required in order to obtain a dose distribution with a good statistical accuracy. Although this is still true to some extent, the use of modern computing power that is available nowadays along with the aid of valid approximations have considerably reduced the required computation times for Monte Carlo simulations. In recent years, manufacturers have developed commercial Monte Carlo-based clinical treatment planning systems [21-25].

1.4 Modulated Electron Therapy, Why Not?

High energy electron beams are used frequently in radiation therapy. They have unique characteristics that are not provided by x-rays or other forms of accelerated particles. Namely, a high surface dose followed by a rapid fall-off until the dose is reduced to a few percent of the maximum dose. Such advantages over x-ray therapy make electron therapy well-suited for superficial targets. Moreover, most clinical linear accelerators can produce electrons with a wide range of energies. With these characteristics, electron beams have the potential of being modulated with the same level of automation, accuracy and clinical routine as their x-ray counterpart [26-29]. Theoretically, all the advances in IMRT could be implemented so as to achieve electron beam modulation. Another advantage of electrons is that in addition to their intensity, their nominal energy is also a function of modulation. However, despite its potential

capabilities, energy modulated electron therapy (EMET) lagged behind IMRT. Two major reasons contributed to this lag: (1) the dosimetric complexity of electron beam planning and (2) the absence of a practical and automated collimation device.

The accuracy of the dose calculation algorithm is critical to the success of the inverse treatment optimization. It is the dose calculation algorithm that is responsible for producing the dose kernel data, i.e., DDCs, which are used by the optimizer algorithm to produce an optimal distribution. If the DDCs are poorly modeled, the optimization procedure will produce a “theoretical” plan that significantly differs from the “deliverable” one. Therefore, realistic dose kernel data are essential for a meaningful optimization outcome. In x-ray IMRT, analytical dose calculation algorithms are the most widely used. Despite recent indications that more accurate dose algorithms reduce the discrepancies between planned and delivered dose distributions [30-33], analytical algorithms generally show decent dosimetric accuracy for the task of optimization. However, for electron beams, they suffer from severe limitations that restrict their use in optimization algorithms. For example, the pencil beam algorithm, which is considered the best available analytical dose calculation algorithm, could yield an error of up to 20% in the case of oblique incidence on heterogeneous medium [13,19,20,34,35]. In addition, it fails to predict the beam output under beam collimation devices to within reasonable accuracy. If the dose per unit weight of the beamlet is not known precisely, the basic requirement of the optimization procedure is violated. Hence, analytical dose calculation algorithms, despite their current relative success in photon beams, are not suitable for EMET. Monte Carlo algorithms, on the other hand, have the ability to account for the fundamentals of electron transport through collimation devices and inside the heterogeneous patient. It is therefore proposed that Monte Carlo techniques can be the essence of a successful application of EMET [28].

The other major reason behind the limited applications of EMET is the absence of a remotely automated collimation system that is fully integrated into the optimization and the dose calculation algorithms. Although attempts were made to incorporate different collimation tools as upgrades to the existing technology [28,36-39], a full delivery system has not yet found its clinical implementation. These attempts tried to solve pieces of the puzzle without a comprehensive approach to deal with the problems of EMET. For

example, several authors discussed the possibility of employing an electron MLC (eMLC) for the purpose of EMET. But these approaches dealt only with the collimation problem isolated from the possibility of automated delivery and, more importantly, isolated from the impact of the presence of such collimator on the optimization procedure. There is no doubt that these studies shed some light on the problems encountered when dealing with EMET and proposed a number of solutions. However, EMET treatment planning and delivery remained only a research topic.

1.5 Hypothesis and Objectives

In this work, we present a novel technique of delivering EMET using an automated “few leaf electron collimator” (FLEC) prototype. The FLEC serves as an accessory tool to current-day accelerator equipments. It allows for an optimization technique that uses a limited number of Monte Carlo-generated and patient-specific kernels in order to perform inverse planning.

We hypothesize that the integration of Monte Carlo calculated dose distributions with an optimization algorithm that communicates with the FLEC leads to the clinical implementation of EMET. We consider the clinical implementation to be demonstrated when the FLEC collimation system is comprehensively automated to acquire the plans from the optimization algorithm and deliver them in a clinical setting. We also hypothesize that the Monte Carlo-calculated plans are accurate compared to the plan delivery verified experimentally. In addition, we hypothesize that the EMET technique will be superior to current treatment modalities for superficially located lesions.

In order to resolve the stated hypotheses, the work has the following objectives:

- Design, construction, and automation of the FLEC that fits on a frame that fits in the electron applicator.
- Incorporation of Monte Carlo-based inverse treatment planning software.
- Dosimetric evaluation of the significance of EMET compared to IMRT and three dimensional conformal therapy (3D-CRT).
- Dosimetric validation of the Monte Carlo calculations used to deliver the optimal plans.

1.6 Thesis Outline

This thesis consists of three manuscripts, two of which were published and the third one is still under review. Chapter 2 presents a brief introduction to electron beam therapy. It describes the fundamentals of electron beam characteristics, dosimetry, and treatment planning. It includes a comparison between the algorithms used for electron transport in treatment planning systems. In the third chapter, a comprehensive review of the literature discussing alternative approaches for EMET delivery is presented. Chapter 4 consists of a paper published in *Physics in Medicine and Biology*. It introduces the idea of the FLEC in conjunction with a Monte Carlo dose calculation engine. An in-house optimization algorithm that has been modified to perform EMET planning is presented. EMET treatment plans for a simple phantom and a realistic patient have been produced and compared to 3D-CRT. In chapter 5 we present a paper published in *Medical Physics* where we show the expected clinical advantages that would be obtained by using EMET delivered with the FLEC. A detailed dosimetric evaluation is presented for EMET, and is compared further to both 3D-CRT and IMRT. The construction and validation of the FLEC is discussed in chapter 6 which presents the results of a recently submitted paper to *Medical Physics*. It demonstrates the structure of a control unit that was built and integrated to deliver EMET plans. This study validates the Monte Carlo-calculated 1-D and 2-D dose distributions of energy modulated electron beams. Chapter 7 summarizes the main contributions of this work and proposes some future work. Finally, an appendix is included to briefly introduce the McGill Monte Carlo Treatment Planning (MMCTP). This appendix was not included in the manuscripts due to the required concise nature of the published papers. Finally, it is worth mentioning that slight modifications were made to the notations and abbreviations used in the original published manuscripts. These minor modifications, such as the use of italics and addition of spaces, were required to maintain consistency of formatting throughout the thesis. Reprints of the publications are included in a dedicated appendix.

References

- [1] National Cancer Institute 2006 <http://www.cancer.gov>.
- [2] M. Tubiana, Introduction to Radiobiology (Taylor & Francis, New York, 1990).
- [3] International Commission of Radiation Units and Measurements Report No. 33: Radiation quantities and units (ICRU, Washington, D.C., 1980).
- [4] International Commission of Radiation Units and Measurements Report No. 50: Prescription, recording, and reporting photon beam therapy (ICRU, Washington, D.C., 1993).
- [5] A. Brahme, "Optimal setting of multileaf collimators in stationary beam radiation therapy," *Strahlenther. Onkol.* **164**, 343-350 (1988).
- [6] T. Bortfeld, J. Burkelbach, R. Boesecke, and W. Schlegel, "Methods of image reconstruction from projections applied to conformation radiotherapy," *Phys. Med. Biol.* **35**, 1423-1434 (1990).
- [7] S. Webb, "Optimization by simulated annealing of three-dimensional, conformal treatment planning for radiation fields defined by a multileaf collimator: II. Inclusion of two-dimensional modulation of the x-ray intensity," *Phys. Med. Biol.* **37**, 1689-1704 (1992).
- [8] T.R. Mackie, T.W. Holmes, P.J. Reckwerdt, and J. Yang, "Tomotherapy: optimized planning and delivery of radiation therapy," *Int. J. Imaging Syst. Technol.* **6**, 43-55 (1995).
- [9] C.X. Yu, M.J. Symons, M.N. Du, A.A. Martinez, and J.W. Wong, "A method for implementing dynamic photon beam intensity modulation using independent jaws and a multileaf collimator," *Phys. Med. Biol.* **40**, 769-787 (1995).
- [10] S. Webb, Intensity modulated radiation therapy (Institute of Physics Publishing, Bristol, UK, 2000).
- [11] J.R. Palta and T.R. Mackie, Intensity modulated radiation therapy - the state of the art (Medical Physics Publishing, Madison, WI, 2004).
- [12] International Commission of Radiation Units and Measurements Report No. 24: Determination of absorbed dose in a patient irradiated by x or gamma rays in radiotherapy procedures (ICRU, Washington, D.C., 1976).
- [13] J. Cygler, J.J. Battista, J.W. Scrimger, E. Mah, and J. Antolak, "Electron dose distributions in experimental phantoms: a comparison with 2D pencil beam calculations," *Phys. Med. Biol.* **32**, 1073-1086 (1987).

- [14] A.F. Bielajew, D.W. Rogers, J. Cygler, and J.J. Battista, "A comparison of electron pencil beam and Monte Carlo calculation methods," in: *The Use of Computers in Radiation Therapy*, edited by A.D. Bruinvis (Elsevier, Amsterdam, 1987).
- [15] A. Nahum, "Overview of photon and electron Monte Carlo," in: *Monte Carlo Transport of Photons and Electrons*, edited by T.M. Jenkins, W.R. Nelson, A. Rindi (Plenum, New York, 1988).
- [16] P. Andreo, "Monte Carlo techniques in medical radiation physics," *Phys. Med. Biol.* **36**, 861-920 (1991).
- [17] J. Seuntjens, A. Van der Plaetsen, H. Thierens, and M. Piessens, "Comparison of measured and calculated dose distributions in lung after electron beam treatment of the chest wall," *Med. Phys.* **21**, 1959-1968 (1994).
- [18] M. Miften, M. Wiesmeyer, A. Kapur, and C.M. Ma, "Comparison of RTP dose distributions in heterogeneous phantoms with the BEAM Monte Carlo simulation system," *J. Appl. Clin. Med. Phys.* **2**, 21-31 (2001).
- [19] G.X. Ding, J.E. Cygler, G.G. Zhang, and M.K. Yu, "Evaluation of a commercial three-dimensional electron beam treatment planning system," *Med. Phys.* **26**, 2571-2580 (1999).
- [20] G.X. Ding, J.E. Cygler, C.W. Yu, N.I. Kalach, and G. Daskalov, "A comparison of electron beam dose calculation accuracy between treatment planning systems using either a pencil beam or a Monte Carlo algorithm," *Int. J. Radiat. Oncol. Biol. Phys.* **63**, 622-633 (2005).
- [21] J.E. Cygler, G.M. Daskalov, G.H. Chan, and G.X. Ding, "Evaluation of the first commercial Monte Carlo dose calculation engine for electron beam treatment planning," *Med. Phys.* **31**, 142-153 (2004).
- [22] E. Heath, J. Seuntjens, and D. Sheikh-Bagheri, "Dosimetric evaluation of the clinical implementation of the first commercial IMRT Monte Carlo treatment planning system at 6 MV," *Med. Phys.* **31**, 2771-2779 (2004).
- [23] J.E. Cygler, C. Lochrin, G.M. Daskalov, M. Howard, R. Zohr, B. Esche, L. Eapen, L. Grimard, and J.M. Caudrelier, "Clinical use of a commercial Monte Carlo treatment planning system for electron beams," *Phys. Med. Biol.* **50**, 1029-1034 (2005).
- [24] G.X. Ding, D.M. Duggan, C.W. Coffey, P. Shokrani, and J.E. Cygler, "First macro Monte Carlo based commercial dose calculation module for electron beam treatment planning--new issues for clinical consideration," *Phys. Med. Biol.* **51**, 2781-2799 (2006).

- [25] R.A. Popple, R. Weinber, J.A. Antolak, S.J. Ye, P.N. Pareek, J. Duan, S. Shen, and I.A. Brezovich, "Comprehensive evaluation of a commercial macro Monte Carlo electron dose calculation implementation using a standard verification data set," *Med. Phys.* **33**, 1540-1551 (2006).
- [26] S. Hyodynmaa, A. Gustafsson, and A. Brahme, "Optimization of conformal electron beam therapy using energy- and fluence-modulated beams," *Med. Phys.* **23**, 659-666 (1996).
- [27] M.G. Karlsson, M. Karlsson, and B. Zackrisson, "Intensity modulation with electrons: calculations, measurements and clinical applications," *Phys. Med. Biol.* **43**, 1159-1169 (1998).
- [28] C.M. Ma, T. Pawlicki, M.C. Lee, S.B. Jiang, J.S. Li, J. Deng, B. Yi, E. Mok, and A.L. Boyer, "Energy- and intensity-modulated electron beams for radiotherapy," *Phys. Med. Biol.* **45**, 2293-2311 (2000).
- [29] C.M. Ma, M. Ding, J.S. Li, M.C. Lee, T. Pawlicki, and J. Deng, "A comparative dosimetric study on tangential photon beams, intensity-modulated radiation therapy (IMRT) and modulated electron radiotherapy (MERT) for breast cancer treatment," *Phys. Med. Biol.* **48**, 909-924 (2003).
- [30] C. Boudreau, E. Heath, J. Seuntjens, O. Ballivy, and W. Parker, "IMRT head and neck treatment planning with a commercially available Monte Carlo based planning system," *Phys. Med. Biol.* **50**, 879-890 (2005).
- [31] J. Yang, J. Li, L. Chen, R. Price, S. McNeeley, L. Qin, L. Wang, W. Xiong, and C.M. Ma, "Dosimetric verification of IMRT treatment planning using Monte Carlo simulations for prostate cancer," *Phys. Med. Biol.* **50**, 869-878 (2005).
- [32] N. Sakthi, P. Keall, I. Mihaylov, Q. Wu, Y. Wu, J.F. Williamson, R. Schmidt-Ullrich, and J.V. Siebers, "Monte Carlo-based dosimetry of head-and-neck patients treated with SIB-IMRT," *Int. J. Radiat. Oncol. Biol. Phys.* **64**, 968-977 (2006).
- [33] L. Paelinck, B.D. Smedt, N. Reynaert, M. Coghe, W.D. Gersem, C.D. Wagter, B. Vanderstraeten, H. Thierens, and W.D. Neve, "Comparison of dose-volume histograms of IMRT treatment plans for ethmoid sinus cancer computed by advanced treatment planning systems including Monte Carlo," *Radiother. Oncol.* (2006).
- [34] M. Blomquist and M. Karlsson, "Test procedures for verification of an electron pencil beam algorithm implemented for treatment planning," *Radiother. Oncol.* **39**, 271-286 (1996).

- [35] A. Samuelsson, S. Hyodynmaa, and K.A. Johansson, "Dose accuracy check of the 3D electron beam algorithm in a treatment planning system," *Phys. Med. Biol.* **43**, 1529-1544 (1998).
- [36] M.G. Karlsson, M. Karlsson, and C.M. Ma, "Treatment head design for multileaf collimated high-energy electrons," *Med. Phys.* **26**, 2161-2167 (1999).
- [37] M.C. Lee, S.B. Jiang, and C.M. Ma, "Monte Carlo and experimental investigations of multileaf collimated electron beams for modulated electron radiation therapy," *Med. Phys.* **27**, 2708-2718 (2000).
- [38] K.R. Hogstrom, R.A. Boyd, J.A. Antolak, M.M. Svatos, B.A. Faddegon, and J.G. Rosenman, "Dosimetry of a prototype retractable eMLC for fixed-beam electron therapy," *Med. Phys.* **31**, 443-462 (2004).
- [39] A.T. Gauer, A.D. Albers, A.F. Cremers, A.R. Harmansa, A.R. Pellegrini, and A.R. Schmidt, "Design of a computer-controlled multileaf collimator for advanced electron radiotherapy," *Phys. Med. Biol.* **51**, 5987-6003 (2006).

Chapter 2**Introduction to Electron Beam Therapy**

Since the early 1950s, electron beam therapy has been considered a cornerstone modality for radiation therapy applications. The use of electron beams is continuously being enhanced with the remarkable developments in electron treatment machines, dose measurements, electron transport algorithms, and new advancements in energy modulated electron beam delivery. This chapter presents a general overview of the fundamentals and applications of high energy electron beams in radiation therapy. A basic introduction is provided to describe electron beam characteristics, dosimetry, and treatment planning.

2.1 Electron Interactions

Electrons may interact with matter in three basic ways: (1) soft collisions, (2) hard collisions, and (3) nuclear scattering. In the classical approach, these modes of interactions can be characterized depending on the relation between the classical impact parameter b and the classical atomic radius a , as shown in Fig. 2-1. The impact parameter is defined as the perpendicular distance between the incoming electron and the nucleus. It is dependant on the energy of the incoming electron and the atomic number.

Soft collisions occur when the impact parameter is much larger than the atomic radius causing a Coulomb interaction between the electron and the atom as a whole. Hard collisions occur when the impact parameter is of the same order of magnitude as the radius of the atom. Here, the incident electron interacts with an orbital electron resulting

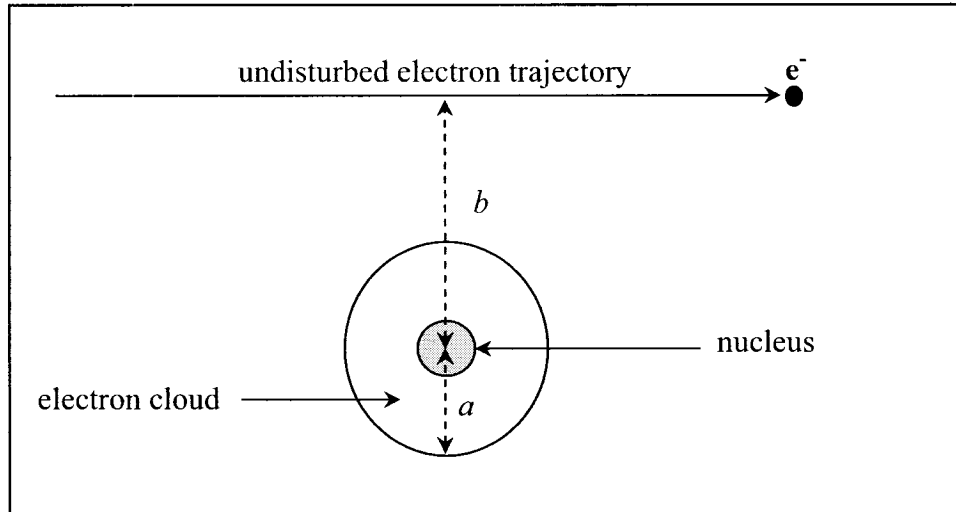


Figure 2-1: Representation of an electron traversing the field of an atom; “a” is the classical atomic radius, “b” is the classical impact parameter.

in the ejection of the orbital electron with considerable kinetic energy. The ejected electron, called a delta ray, is able to produce its own track that can potentially cause further series of ionizations and excitations in the absorber. If the impact parameter is much smaller than the atomic radius, the electron interacts with the electric field of the nucleus. In most of these interactions, the charged particle is scattered elastically without losing any energy. In the case of inelastic electron-nucleus interactions, the electron loses energy through the emission of radiation in a process referred to as bremsstrahlung production. The production of bremsstrahlung photons becomes more important for higher atomic number Z materials. As electrons travel through the absorbing medium, their energy is continuously degraded until they completely stop.

2.1.1 Stopping power

The average rate of energy loss dT of an electron per unit of path length dx is called the linear stopping power. From this definition, the stopping power S can be written as $S = \frac{dT}{dx}$.

Since thicknesses of the materials are often expressed in mass units, the stopping properties of the absorbing media are often defined in terms of the mass stopping power $\left(\frac{S}{\rho}\right)$. The mass stopping power can be subdivided into two components: the “mass

collision stopping power” $\left(\frac{S}{\rho}\right)_{\text{col}}$ which accounts for the energy loss through hard and soft collisions, and the “mass radiative stopping power” $\left(\frac{S}{\rho}\right)_{\text{rad}}$, which takes into account the energy loss due to radiative interactions.

According to Bethe and Heitler [1], with the aid of Møller’s [2] and Bhabha’s [3] work, the mass collision stopping power for electrons and positrons is defined as:

$$\left(\frac{S}{\rho}\right)_{\text{col}} = \frac{2\pi r_e^2 m_e c^2 N_A}{\beta^2} \frac{Z}{A} \left[\ln(T/I) + \ln\left(1 + \frac{\tau}{2}\right) + F^\pm(\tau) - \delta \right], \quad (2-1)$$

where r_e is the classical electron radius, I is the mean ionization/excitation potential, N_A is the Avogadro’s number, m_e is the electron mass, β is the incident particle velocity normalized to the speed of light, τ is the kinetic energy of the incident particle in units of $m_0 c^2$, T is the kinetic energy of the incident particle, δ is the density correction, and F^\pm is a function that depends on whether the incident particle is electron or positron. Equation 2-1 shows the dependence of the collision stopping power on the charge and energy of the incident particle.

The radiative stopping power can be expressed as

$$\left(\frac{S}{\rho}\right)_{\text{rad}} = \frac{1}{137} r_e^2 \frac{N_A Z^2}{A} (T + m_e c^2) \bar{B}_r, \quad (2-2)$$

where \bar{B}_r is a slowly varying function that is dependent on Z and T [4]. The radiative stopping power has a quadratic dependence on Z . In addition, the radiative energy loss increases linearly with the particle energy. Therefore, bremsstrahlung production becomes the predominant mechanism of energy loss for high energy electrons impinging on high Z materials.

2.1.2 Absorbed dose

The absorbed dose D is defined at a point inside a volume as the expectation value of the energy imparted to matter per unit mass and is represented by

$$D = \frac{d\bar{\epsilon}}{dm}. \quad (2-3)$$

The energy imparted (or absorbed) $\bar{\epsilon}$ is found by taking the sum of all energies entering the volume and subtracting all the energies leaving the volume while accounting for any

mass energy conversion within the volume. The SI unit for the absorbed dose is Gray (Gy) which is equivalent to 1 joule per kilogram.

When absorbed dose is calculated, two parameters are required: (1) electron fluence and (2) the “restricted” stopping power $\left(\frac{L}{\rho}\right)_{\text{col},\Delta}$ that refers to the rate of energy loss in collisions per unit path length in which the energy is absorbed “locally”. Hence, any electron with an energy that is higher than Δ is assumed to deposit its energy outside the unit mass where the dose is calculated. Hence, the absorbed dose can be calculated from the differential electron fluence spectrum $\frac{d\Phi}{dT}$ as

$$D = \int_{\Delta}^{E_0} \frac{d\Phi(T)}{dT} \cdot \left(\frac{L}{\rho}\right)_{\text{col},\Delta} dT + TE_{\Delta} \quad (2-4)$$

where TE_{Δ} is the track-end term which can be approximated by

$$TE_{\Delta} = \Delta \cdot \Phi(\Delta) \cdot \left(\frac{S(\Delta)}{\rho}\right)_{\text{coll}}. \quad (2-5)$$

2.2 Treatment Units

The use of high energy electrons in radiation therapy started with the development of the Van de Graaff and betatron accelerators. Despite being cumbersome, the Van de Graaff generator provided one of the earliest sources for producing electron beams in radiation therapy, as reported by Trump [5]. It is an electrostatic accelerator in which the particles cannot be accelerated to energies higher than the potential energy of the maximum voltage available in the machine. Because of its limited maximum energy, the Van de Graaff generator was only used for treating surface lesions.

Betatrons, based on the technology of cyclic accelerators, were able to accelerate electrons to much higher energies. In cyclic accelerators, particles are accelerated gradually by repeatedly following a closed path of variable electric and magnetic fields until a maximum kinetic energy is obtained. Cyclic acceleration was implemented in betatrons where electrons are accelerated using the electromagnetic induction by allowing them to circulate in a vacuum chamber that is placed between two magnet poles. Changing the flux of the magnetic field by using an alternating current applied to the magnets induces an electric field inside the vacuum chamber. The induced electric field

accelerates the electrons which are kept in circular orbits by the magnetic field. Because of their ability to produce high energy electron beams, betatrons provided an environment for early clinical research. The studies that discussed the design of scattering foils and collimators were initially investigated using betatrons. Also, with betatrons, the early calibration procedures and dose measurements were performed [6]. However, betatrons were bulky and noisy machines. They gradually lost their appeal with the development of medical linear accelerators (linacs) that were able to provide much higher dose rates and larger field sizes using quieter machines with more compact design allowing isocentric mounting.

2.2.1 Medical linear accelerator (linac)

Linacs are cyclic accelerators that use the microwave radiofrequency to accelerate electrons. After being initially produced thermionically from a filament and accelerated in an electrostatic accelerator, called an electron gun, electrons enter a loaded metallic accelerating waveguide. In the waveguide, high power radiofrequency waves produced by a microwave generator are propagated according to Maxwell's equations. The electron acceleration is gained by the transfer of energy from the radiofrequency fields to the electrons with the help of the specially designed loaded waveguide that allows the electrons to continuously "see" a positive potential ahead and a negative potential behind. Once the desired energy has been achieved, the electron beam is directed through a beam transport system to the linac head.

The design of the linac exhibits differences because of the variety of manufacturers. These differences include standing vs. traveling wave accelerating structures, magnetron vs. klystron microwave generators, and various bending magnet systems. However, all designs share common features of the treatment head in which they incorporate systems for (1) broadening and flattening, (2) dose monitoring, and (3) collimation of the beam.

The broadening and the flattening of the electron beam is achieved in modern linacs using a dual-foil scattering systems [7]. In this system, a primary thin foil made of a high Z material is separated by a few centimetres from a secondary foil made of a low Z material. Such a system minimizes the increase in energy spread [8,9] and the bremsstrahlung production while maximizing the flattened field size.

The use of monitor chambers is of critical importance because of the need to evaluate the beam output stability and measure the integrated dose of the flattened electron beam. The monitor chambers quantify the delivery of electron beams using a quantity called monitor unit (MU) which is adjusted to deliver a certain dose in Gy inside a water phantom. To avoid overdose delivery to the patient, linacs are equipped with safety interlocks that terminate the beam irradiation in case of any failure.

Collimators are considered a major component of the treatment head. They are designed to collimate the beam to different sizes in order to conform the irradiation to a localized volume. Because electrons suffer from significant in-air scattering, two sets of collimators are required. Hence, the collimation system in clinical linacs usually consists of a primary collimator that is close to the source and a secondary collimator that is close to the patient. The former is defined by the x-ray jaws and the latter can be in the form of inserts or trimmer bars. The movable x-ray collimators, consisting of two perpendicular pairs (jaws) of tungsten, define the primary collimation and are located approximately 60 cm from the isocenter of the beam. The lower collimators are auxiliary collimators that are provided in fixed attachable cones.

In addition to the basic components of the linac, an auxiliary system is also required to provide vacuum pumping, water cooling, microwave transmission, and shielding from radiation leakage. The advancements in modern electronics and computer control resulted in linacs that are easily operated and remotely controlled.

The type of the accelerator is usually defined by its frequency range (L-band for $\sim 10^3$ MHz, X-band for $\sim 10^4$ MHz, and S-band for 2856 MHz). S-band accelerators are the most commonly used waveguide structures in conventional linacs because of design practicality. X-band linacs are used in applications that require compactness (e.g., in robotic and CT-type gantry mounting) because of their short waveguide length. The design of medical linacs has been extensively reviewed [10-12] and a good basic introduction was provided by Podgorsak *et al.* [13].

In addition to linacs used in routine radiotherapy, special machines have been built to serve for intraoperative radiation therapy (IORT) purposes. Mobile X-band machines that can be moved into the operating room were designed to deliver single radiation fractions to the patient on a surgical bed [14-16].

2.2.2 Microtron

The microtron is another form of electron accelerator that accelerates the electrons by the oscillating electromagnetic field of a single microwave cavity. There are two available types of microtrons: circular and racetrack. For the former, a single magnet is used to accelerate electrons by allowing them to circulate multiple times through a microwave resonant cavity. The particle is kept in phase with the microwave power and the electron energy is gained in increments until a desired energy is obtained. As for the latter, it uses a multicavity structure similar to the one used in the linac through which the beam passes repeatedly and is bent by two D-shaped pole pieces. Although microtrons offer some advantages over linacs, such as smaller beam divergence and less energy spread in the spectrum, they are not widely implemented in radiation therapy clinics.

2.3 Characteristics of Clinical Electron Beams

2.3.1 Central axis depth dose

Electron beam depth dose curves exhibit features that are clinically advantageous in treatment of lesions at shallow depths. As shown in Fig. 2-2, when incident on water, a single electron beam with an energy ranging from 6 MeV to 22 MeV could deliver a high surface dose followed by a broad region of nearly maximum dose (plateau) and then a steep fall-off laterally and distally. These properties make electron beams well suited for treating superficial targets with minimized dose to the underlying organs at risk providing them with remarkable clinical advantages over the conventional photon beams. Electron beams with energies that are higher than approximately 22 MeV lose their rapid dose fall-off at depths beyond the depth of the maximum dose and behave similarly to photon beams due to bremsstrahlung energy loss.

Figure 2-3 shows a typical percentage depth-dose (*PDD*) curve. *PDD* is a dosimetric function that relates the dose delivered to a point along the central axis of the beam to the dose at the point of the maximum dose. According to the recommendations of ICRU 35 [17], the *PDD* is characterized by several parameters:

PDD_s : The relative surface dose at 0.5 mm depth.

PDD_x : The relative dose due to the x-ray component.

z_{max} : The depth of the maximum dose in water.

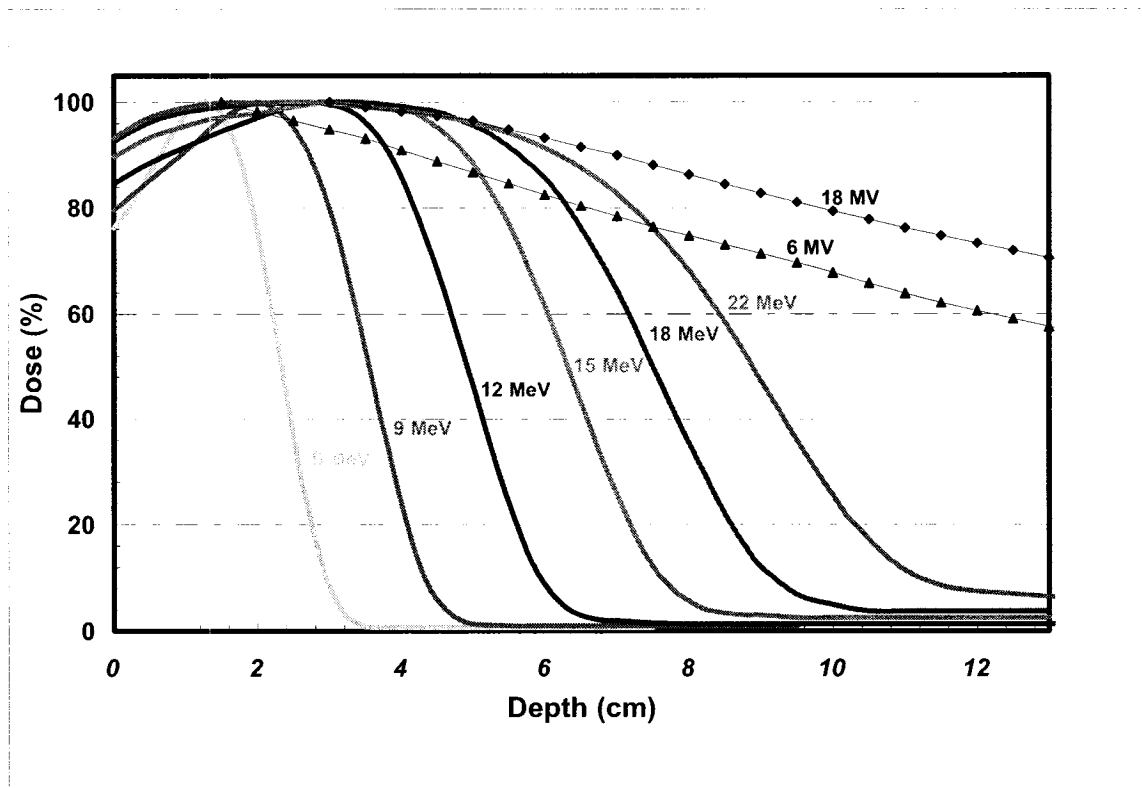


Figure 2-2: PDD curves for electron and photon beams of $10 \times 10 \text{ cm}^2$ field size at $\text{SSD}=100 \text{ cm}$ for all energies of the CL2300 measured with ionization chamber.

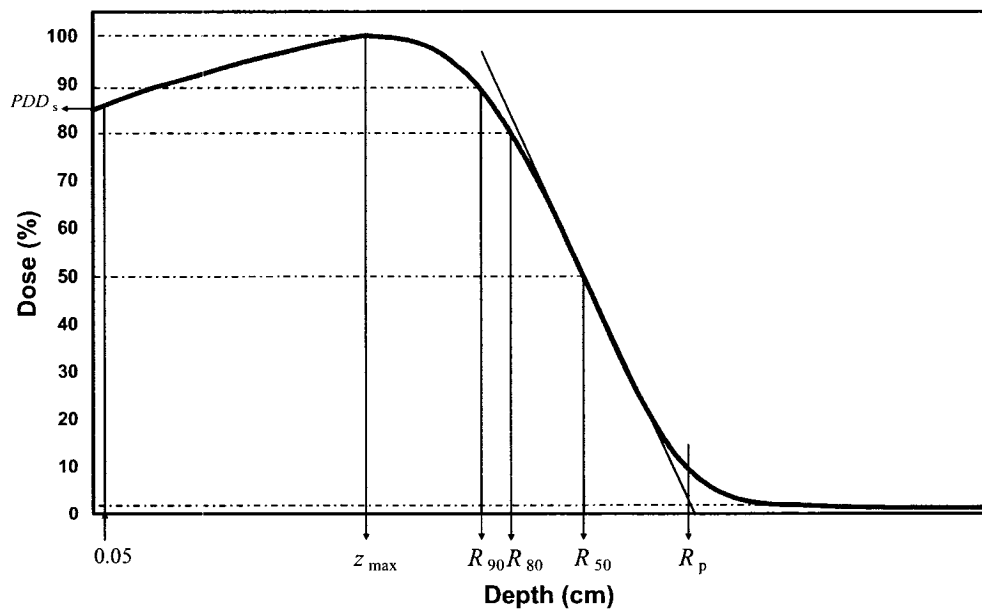


Figure 2-3: Specifications of parameters that are used to characterize electron beam central axis depth dose curve.

- R_t : The therapeutic range which varies between 90% and 80% of the maximum dose.
- R_{50} : The depth of the 50% dose level.
- R_p : The practical range. It corresponds to the point of intersection between the tangent at the inflection point of the fall-off portion of the *PDD* and the bremsstrahlung background extrapolated toward z_{\max} .
- G_0 : The normalized dose gradient that measures the steepness of the descending part of the *PDD*.

Of these parameters, R_{50} and R_p are the most important because of their role in determining the energy specifications of the electron beams. The energy of the pencil electron beam exiting the linac window is degraded because the electron beam passes through multiple components before hitting the surface. This results in the clinical beam consisting of a spectrum of energies. According to TG-25 [18], the energy parameters of the electron beam are characterized by (1) the most probable energy at the surface ($E_{p,0}$), (2) the mean energy on the surface (\bar{E}_0), and (3) the energy at depth z (\bar{E}_z).

($E_{p,0}$) is defined as:

$$E_{p,0} = C_1 + C_2 R_p + C_3 R_p^2, \quad (2-6)$$

where $C_1 = 0.22$ MeV, $C_2 = 1.98$ MeV cm⁻¹, and $C_3 = 0.0025$ MeV cm⁻². (\bar{E}_0) is obtained from:

$$\bar{E}_0 = C_4 R_{50}, \quad (2-7)$$

where $C_4 = 2.33$ MeV cm⁻¹. Finally (\bar{E}_z) is expressed, according to Harder's relationship [19], as:

$$\bar{E}_z = \bar{E}_0 \left(1 - \frac{z}{R_p} \right), \quad (2-8)$$

where z is the depth in phantom. These energy parameters are easily obtained from *PDD* measurements.

It should be noted that the *PDD* parameters are sensitive to small differences in energy, scattering foils, collimations and source surface distance (*SSD*). The surface dose

increases with increase in energy of the electron beams. Expressed in cm, the range parameters, R_p , R_{80} , and R_{90} , can be approximated as $\left(\frac{1}{2}\right)E_{p,0}$, $\left(\frac{1}{3}\right)E_{p,0}$, and $\left(\frac{1}{4}\right)E_{p,0}$, respectively, when $E_{p,0}$ is expressed in MeV. Although z_{\max} does not have an apparent dependence on the energy of the beam, it is dependent, however, on the size and shape of the field. Finally, the bremsstrahlung contamination is exhibited as a tail beyond R_p which increases with higher energies.

Because of its importance in clinical applications of electron beams, *PDD* data must be measured for all electron energies and possible applicators. The report AAPM TG-25 recommends a comprehensive procedure to determine the *PDD* data for a given linac [18].

2.3.2 Output factors

Output factors are defined as the ratio of dose per MU at z_{\max} for a given field size to the dose per MU at z_{\max} for a reference field size. Since the increase in field size as defined by the photon collimator leads to increased scatter from the collimator, the collimator setting has a significant influence on the electron dose. The output dependence on the x-ray jaw opening variations is large, especially at low electron energies [20]. Therefore, most linacs provide a fixed primary collimation and vary the secondary collimation. This keeps the variation in output measurements relatively small. Moreover, output factors are affected by a change in *SSD*. Hence, they should be measured properly for *SSDs* that differ from the reference *SSD*, i.e. $SSD \neq 100$ cm.

Various approaches were introduced for modeling the output of an arbitrary field size [6] after acquiring a significant amount of measurement data. In the model reviewed by Khan [21], output factors at a standard *SSD* are obtained using an equivalent square field size [20]. For extended *SSD*, the output is assumed to follow an inverse square relationship [22]. Hogstrom [23] reviewed an analytical model for predicting output based on the physics of electron transport.

Recently, Monte Carlo methods were used to perform output calculations [24-26]. Monte Carlo-based software that calculates output factors for Varian CL2300 accelerator was commissioned at the Medical Physics Unit, McGill University [27].

2.3.3 Virtual electron source

A virtual electron source is the point at which the pencil electron beam spreads into a broad beam. Unlike an x-ray beam that has a well defined point source at the target position, the electron beam point source needs to be obtained from measurements. Various methods were introduced to obtain the virtual electron source [22,28]. Reporting the virtual source values for all clinical situations is important for treatment planning and for analytical dose calculation algorithms.

2.3.4 Effects of oblique incidence and tissue heterogeneities

The dose distributions of electron beams are significantly affected by oblique incidence, surface curvatures, and tissue heterogeneities. Ekstrand and Dixon [29] discussed the impact of using oblique beams. Hogstrom [30] showed that the dependence of electron beam interactions on tissue heterogeneities may lead to unpredicted dose distribution results if the transport of electrons is not carefully studied.

2.4 Dose Measurements

2.4.1 Phantom materials

When used in radiation therapy, the term “phantom” refers to the material and geometry that can serve as a model for radiation transport in the patient. Since water is the main constituent of many body tissues, most dosimetric procedures are performed in water phantoms. The “water tank” is one of the most important tools that are available in every radiation therapy department. It is a computerized phantom used mainly for acceptance testing and commissioning of treatment units. Being automated, the water tank allows for dose measurement at any point in the phantom and performs scans along the three-dimensional axes. Smaller tanks that are manually controlled are also available. Despite its usefulness, the use of water in performing dose measurements is not always practical. Solid phantoms with radiological properties that are similar to those of water were developed to offer an alternative medium for routine measurements. Commercial Solid Water® is available and it is replacing the use of the conventional solid phantoms such as polystyrene and Lucite. Solid Water has a physical density of 1, an electron density of 1.02, an effective atomic number of 7.54, and a CT number of 15 (compared to the water properties of 1, 1, 7.4, and 0, respectively).

2.4.2 Absolute and relative dosimetry

Dose measurement for electron beams is divided into absolute and relative dosimetry. The aim of absolute dosimetry is to determine absorbed dose (in Gy) under standard irradiation conditions. It relates the relative amount of charge collected by the monitor chamber in the linac, referred to as a monitor unit (MU), to the absolute dose at a reference point. Such a relation is referred to as “calibration”. Relative dosimetry, however, describes the dosimetric functions that relate the dose at a point irradiated under certain conditions to the *reference point* at which the dose has been measured accurately. Examples of relative dosimetry are *PDD*, off-axis profiles, isodose distributions, and output factors.

Absolute dosimetry for electron beams can be performed using calorimetry [31-33] or chemical dosimetry [34,35]; however, because of technical difficulties, these dosimeters are not widely used. The routine absorbed dose calibration for electron beams in standard clinical departments is usually performed using ionization chambers. Relative dosimetry is carried out using thermoluminescent dosimeters (TLD), silicon diodes, and film.

2.4.3 Dose measurement methods

2.4.3.a Ionization chambers

Ionization chambers refer to dosimeters that measure the dose deposited by ionizing radiation through collecting the created charges inside an active volume of air sandwiched between two electrodes with an applied voltage operated between them. For electron beams, measurements that are performed with ionization chambers are assumed to follow Bragg-Gray cavity theory. Assuming that the chamber is small enough to prevent significant perturbations to the electron fluence, a direct proportionality is established between the number of collected charges inside the chamber volume and the dose at the same point without the chamber. However, applying the Bragg-Gray cavity theory in determining the absorbed dose for electrons requires accounting for mass collision stopping power ratios, mass of the gas inside the chamber, the perturbations caused by introducing the chamber into the phantom, and the effective point of measurement. The dependence of the mass stopping power ratios and perturbation factors

on the depth in the phantom is considered a disadvantage of using ionization chambers for electron beam dosimetry [18].

Determination of absorbed dose

Except for those at the National Physical Laboratory in the United Kingdom [36], there are no available international standards for absorbed dose in water for electron beams. The calibration of ionization chambers carried out by most standards laboratories is only provided for high energy photon beams but not for high energy electron beams. The use of photon beam-calibrated ionization chambers is therefore extended to electron beams by following national/international protocols. Depending on the quantity used for calibration (exposure, air kerma, absorbed dose) of an ionization chamber in a given photon beam, codes of practice were developed to use these photon-calibrated ionization chambers to determine absorbed dose in water for electrons of megavoltage energies. Protocols were developed, revised, and rewritten to accommodate the change in calibrating options [36-38] and they provide detailed discussions of the problems encountered with the use of ionization chambers for calibrating electron beams. Corrections are implemented for various effects, such as polarity effects, perturbation effects, and ion collection efficiency.

Types of clinical ionization chamber

Cylindrical chamber

Counted as the most frequently used dosimeter in medical physics, the cylindrical ionization chamber provides a reliable secondary standard for absolute absorbed dose calibrations. It was initially designed by Farmer with a relatively thin wall to reduce the electron fluence perturbation. The Farmer chamber contains an inner electrode made of aluminium which has an atomic number of 13 in order to compensate for the carbon wall that is made of graphite with an atomic number of 6. The materials were purposely chosen to provide a flat energy response. Originally, the farmer chamber had a nominal collecting volume of 0.6 cm^3 . Smaller ionization chambers were developed later with miniature dimensions. The Exradin A12 chamber, for example, has a collecting volume of 0.01 cm^3 . The use of a small chamber is advantageous in locations where steep dose gradients are suspected. The advantage of being symmetric simplifies the use of cylindrical chambers in profile measurements.

Parallel plate ionization chamber

Parallel plate ionization chambers were developed primarily for measurements of electron beams that inherently have steep depth dose gradients. These types of chamber have a thin wall and a small fixed electrode spacing (within 2 mm) that minimizes the cavity perturbations. Compared to the cylindrical chambers, parallel plate chambers can avoid the significant perturbations in the electron fields that result from the relatively large cavity size especially at low energies. Protocols usually describe a method to locally cross-calibrate parallel plate chambers with cylindrical chambers that are calibrated at standard laboratories.

2.4.3.b Thermoluminescent dosimeter (TLD)

TLDs are considered to be relative solid state dosimeters. They consist of crystals with imperfections in the form of impurities which, upon irradiation, may trap electrons and holes traveling through the conducting band and valence band, respectively, following irradiation of the crystal. The trapped charged carriers remain at a metastable energy state that is in the order of a few eV from the valence band. Heating the crystal increases the probability of the trapped charge carriers gaining enough energy to escape the trap. The electron rises to the conducting band and then falls to recombine with a positive hole trapped in a storage trap. Or conversely, a free hole moving through the valence band may recombine with an electron trapped in a storage trap. The recombination energy is released in the form of visible or ultraviolet light. Therefore, TLDs require a readout procedure that employs photomultiplier tubes to detect the emitted light.

The most noteworthy TLD material is lithium fluoride (LiF) doped with magnesium (Mg) which has an effective atomic number of 8.2 (comparable to the effective atomic number of soft tissue of 7.4). It has a useful dose range from 10^{-5} to 10 Gy and its response is essentially independent of the dose-rate.

Being highly sensitive, TLDs can be constructed in small dosimeters that are suitable for measurements in regions of steep dose gradient. Boone *et al.* [39] used TLDs to show the effects of tissue heterogeneity that simulates complex patient geometry on the dose distribution. TLDs, on the other hand, have difficulty providing measurements of the entire dose distributions in phantoms. When requiring 2D dose distributions, TLDs

are cumbersome and time consuming to use. Also, the readout of TLDs erases the dosimetric data making it impossible to be stored for archival purposes.

2.4.3.c Silicon diodes

Silicon diodes are another form of solid state detectors. By irradiating a doped layer of a semiconductor, the charged particles are set free allowing a signal current to flow. The diode has a sensitivity that is nearly 3 orders of magnitude higher than that of an ionization chamber for the same sensitive volume.

Because of their high sensitivity combined with their spontaneous dose read-out, diodes are well-suited for scanning devices. Silicon diodes offer the advantage of providing a constant ratio of stopping power (silicon-to-water) for a wide range of clinical electron energies. When scanned along the central axis, the measured ionization curve can be directly converted into dose. However, diodes suffer from directional dependence, temperature dependence, and radiation-induced damage in the sensitive layer. These shortcomings lead Khan *et al.* [18] to advise strongly that before accepting diode measurements, they should be compared with fully corrected ionization chamber measurements for central axis depth dose curves.

2.4.3.d Films

In electron therapy, films are used extensively because of their convenience and effective means of measuring 2D dose distributions. Since their review of film dosimetry of high energy electrons in 1969, the recommendations of Dutreix and Dutreix [40] are still implemented as the basis for film dosimetry [6,18]. After being irradiated and processed, films are analyzed using a densitometer to obtain a map of optical densities. The net optical density of an exposed film (after deducting the background fog) is related to the dose based on the sensitometric curve (also known as an H-D curve) which is a plot of optical density as a function of dose to the medium. An equation that fits the sensitometric curve establishes the relationship for determining the dose to the film based on various irradiations. It is recommended to obtain the equation for each batch of film without relying on previously reported equations because of the known variation of manufacturing characteristics of films [18,41].

Films have a high spatial resolution and can provide a lasting record of dose distributions that allows for multiple readouts. In addition, they are favoured for the

dosimetry of scanning electron beams since ionization chambers and diodes require significantly longer exposure time for data accumulation. Films can be positioned either perpendicularly to the beam's axis or parallel to it (in order to obtain spatial dose distributions). The perpendicular placement of films requires adequate compression of the phantom to avoid the presence of air gaps that may compromise the results [18,40]. Shiu *et al.* [42] showed a good agreement between results obtained using ionization chambers and radiographic films.

Types of films

Two types of film are used for dosimetry in radiation therapy:

Radiographic film

Radiographic film consists of a transparent film base that is coated from one or both sides with a radiosensitive emulsion containing crystals of silver bromide. After exposing the film to radiation, chemical reactions occur within the exposed crystals. After developing the film, these crystals darken with the extent of darkening being dependent on the radiation energy absorbed. The need for a light-tight packing and film development are considered the main disadvantages of radiographic films. The use of radiographic films in electron beams was discussed in AAPM Task Group report No. 25 [18].

Radiochromic film

Radiochromic film is considered a recent dosimetric tool developed to produce immediate permanent colored images of a radiation exposure pattern. Upon irradiation, a solid state polymerization of colorless molecules is initiated which changes the color of the film from transparent to varying shades of blue. The dose is determined based on the absorption spectrum. AAPM Task Group report No. 55 provides guidelines for dosimetry using radiochromic films [41].

Being self-developing, nearly tissue equivalent, and nearly energy independent are considered the main advantages offered by radiochromic film over radiographic film. The relative small change in response to change in energy makes the radiochromic films useful for modulated electron beams. Radiochromic films are used extensively for brachytherapy dose measurements where the high spatial dose resolution and tissue equivalence are required.

It was mentioned by many authors that the use of film should be restricted to relative dosimetry because of different sources that affect the optical density readout such as changes in processing conditions and emulsions [18]. However, in avoiding the special developmental procedures needed for radiographic films, as stated by TG-55 [41], the use of radiochromic film to obtain absorbed dose with an acceptable precision is feasible.

2.4.4 Comparison of different dose measuring tools

Results of relative dose distributions that are obtained with different dosimeters should be comparable with reasonable accuracy. Ten Haken *et al.* [43] compared depth dose curves in water/polystyrene for multiple electron energies using films, diodes, two different cylindrical chambers, two parallel plate chambers, TLDs and radiographic films. With careful implementation of the recommendations of TG-25, excellent agreement with an average difference of less than 1% or 1 mm could be achieved [43].

2.5 Treatment Planning

The electron treatment is planned such that a uniform prescribed dose is delivered to the planning target volume (PTV) with minimal dose given to normal tissues and critical structures. The planning starts with delineation of the PTV on images obtained by a computed tomography (CT) scanner. This is followed by the selection of appropriate beam energies and field sizes. In certain situations, extra photon beams may be required to enhance the uniformity of dose distributions inside the PTV. In addition, accessory tools are commonly used to achieve the treatment objectives. One of the standard tools often used is a field shaping cutout that is inserted at the end of the treatment cone to provide irregular field shapes that match the PTV. Skin collimation and internal collimation are two forms of field shaping that are implemented for certain types of treatments. Placement of bolus (near-water-equivalent material) on the skin surface to provide extra scattering and/or energy degradation of the electron beam is also a common practice. Bolus is used also to serve as a missing tissue compensator that flattens out irregular surfaces. The thickness of bolus is determined as part of the treatment planning procedure.

In addition to its contribution to localizing and specifying tumors, CT provides significant patient information about the patient geometry that is critical for dose

calculation. A 3D model of the patient is reconstructed based on its variable tissue types and densities. The correlation between CT numbers and electron densities plays an important role in computerized calculation algorithms.

Computerized treatment planning systems have been developed and are commercially available to facilitate patient data acquisition and calculate dose distributions. Each treatment planning system is characterized by the way it models the electron transport in its dose calculation algorithm. It is the dose calculation algorithm that is considered the most important and unique feature of any treatment planning system.

2.6 Electron Transport Calculation

2.6.1 Analytical radiation transport-pencil beam algorithm

Analytical radiation transport is a formalism that characterizes and calculates the clinical beam parameters based on scattering models. This formalism requires performing a set of measurements using the treatment machines to obtain beam data that are fed into an algorithm. Derived from the input data, the algorithm processes the transport parameters based on the scattering model to evaluate dose distributions for any selected geometry.

The scattering model derived from the Fermi-Eyges theory was the first model to be used for electron beam transport. Eyges [44] included the energy loss as an extension to the cosmic ray theory of multiple Coulomb scatter for thick targets developed by Fermi. Brahme [45] applied the Fermi-Eyges theory to characterize electron beams [45] and their transport through air leading to a momentous contribution in designing beams and patient dose calculations.

2.6.1.a Early developments of pencil beam algorithm

By mid seventies, Lillicrap *et al.* [46] had shown that a measured broad incident beam could be divided into a grid of smaller narrow constituents called “pencil beams”. The dose at any point of interest is computed from the sum of all contributing individual pencils. But the presence of tissue heterogeneities limited the proposed approach due to the impracticality of measuring all the pencils in different media. However, the introduction of the Fermi-Eyges theory in electron beams stimulated several researchers

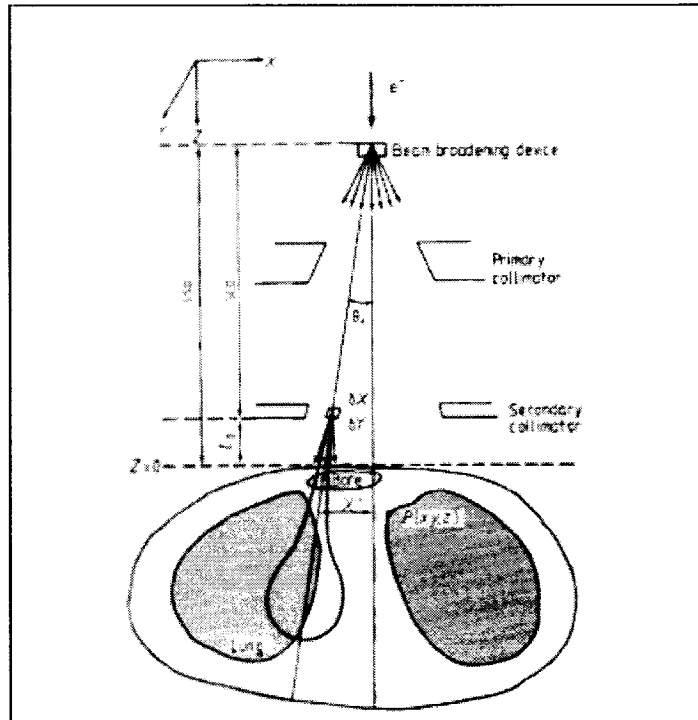


Figure 2-4: Schematic diagram of the original Hogstrom's pencil beam algorithm representation. Reprinted with permission from IOP Publishing (from Hogstrom et al., *Physics in Medicine and Biology*; 1982).

to investigate independently its application in dose calculations [47-49]. The most significant model was Hogstrom's pencil beam algorithm (HPBA) that received a wide acceptance in the commercial and research treatment planning systems (Fig. 2-4). With the limited computer power that was available at the time of its development, the HPBA offered a sufficiently fast dose calculation algorithm that provided a decent accuracy in dose calculation and could be easily implemented to allow for beam and patient modeling. The power of the HPBA lies in its ability to account for irregularly-shaped electron fields, variable air gaps, and surface curvatures while using CT data to correct for internal heterogeneities. The detailed history of evolution of the electron pencil beam algorithm was discussed in depth by Jette [50].

2.6.1.b Pencil beam definition

A pencil beam is a pixel that identifies the most elementary type of a broad electron beam. It is defined as all electrons that pass through a pixel of a divided broad

beam and is characterized by its energy, the root mean square spread of the electron distribution function about its mean direction, and the planar fluence of electrons. The electrons passing through a point within the pixel are not differentiated from electrons passing through the center since they are all assumed to be uniformly distributed with equivalent angular distributions. The algorithm assumes “perfect” collimators and ignores the scattering from them. A pencil beam impinging perpendicularly on a semi-infinite slab creates an energy deposition kernel. The basic task of a pencil beam algorithm is to generate the kernel distribution based on the geometry of the beam/patient configuration. In the HPBA, the complex angular distribution of a pencil beam at any point in the patient geometry is approximated by a Gaussian distribution. Another model was developed to use the sum of three Gaussian distributions to represent the dose profile of a pencil beam at each depth [51-53]. It is referred to as the generalized Gaussian pencil beam algorithm (GGPBA).

2.6.1.c General formalism

For a broad beam, the dose to a point (x, y, z) is calculated at a given depth by convolving the relative primary fluence distribution with the profile of the pencil beam distribution as follows:

$$D_e(x, y, z) = \int \int \Phi(x'', y'') d(x'' - x, y'' - y, z) dx'' dy'', \quad (2-9)$$

where $D_e(x, y, z)$ is the dose delivered by the electron component which includes the effects of beam modifiers, heterogeneities, and surface curvature and $\Phi(x'', y'')$ represents the relative weight along the fan line at the point (x'', y'') . The convolution kernel, $d(x'' - x, y'' - y, z)$, is the dose contribution at (x, y, z) from the pencil beam at (x'', y'') . The dose distribution of a pencil beam is separated into a central-axis term, derived from the measured depth dose distribution in water and corrected for heterogeneities based on CT numbers, and an off-axis term, equivalent to the lateral distribution derived from the Fermi-Eyges theory.

The formalism implemented by Hogstrom *et al.* [48,54] expressed the dose to a point as an integral of the doses delivered by Gaussian pencil beams according to

$$\begin{aligned}
D_e(x, y, z) = & \int_{-\infty}^{\infty} \int_{-\infty}^{\infty} dx'' dy'' \Phi(x'', y'') \\
& \times \left\{ \frac{I}{2\pi\sigma_{\text{air}}^2} \iint_{\text{coll}(z)} dx' dy' \exp \left[-\frac{(x' - x'')^2 + (y' - y'')^2}{2\sigma_{\text{air}}^2} \right] \right\} \\
& \times D_e^{\text{meas}} \left[0, 0, d_{\text{eff}}(x'', y'', z) \right] \left[\frac{SSD + d_{\text{eff}}(x'', y'', z)}{SSD + z} \right]^2, \\
& \times \frac{1}{2\pi\sigma_{\text{MCS}}^2(x'', y'', z)} \exp \left[-\frac{(x - x'')^2 + (y - y'')^2}{2\sigma_{\text{MCS}}^2(x'', y'', z)} \right]
\end{aligned} \tag{2-10}$$

where $d_{\text{eff}}(x, y, z)$ is the effective depth at the point (x, y, z) corrected from the actual depth in water based on CT numbers. It is calculated by integrating the ratio of linear collision stopping power (tissue to water) along the ray from the source to the point (x, y, z) . The central-axis depth dose curve at the effective depth, represented by $D_e^{\text{meas}}[0, 0, d_{\text{eff}}(x'', y'', z)]$, is a quantity derived from measured central-axis depth dose curve in water. The inner integrals in the second term are taken over the area defined by the projection of the irregular shape of the collimator at depth z . σ_{MCS}^2 and σ_{air}^2 are two moments of the linear angular scattering power (σ) that characterizes the beam spread as explained by Hogstrom [48], where:

$$\sigma^2 = \sigma_{\text{air}}^2 + \sigma_{\text{MCS}}^2. \tag{2-11}$$

The first beam spread term, σ_{air}^2 , is the transformation of the root mean square of the projected angular distribution at the plane of final calculation to the plane at the depth of calculation. The second term, σ_{MCS}^2 , is the integrated linear angular scattering power over a fan line from the patient surface to the plane of calculation.

The common feature in the pencil beam formalism is that all integrals over Gaussians are evaluated in terms of the difference between two error functions as indicated in the equation:

$$\int f(x) \exp \left[-\frac{x^2}{g(x)} \right] dx = \sum_i f \left(x_i \frac{[\pi g(x_i)]^{1/2}}{2} \left\{ \text{erf} \left[\frac{x_i + \Delta x/2}{\sqrt{g(x_i)}} \right] - \text{erf} \left[\frac{x_i - \Delta x/2}{\sqrt{g(x_i)}} \right] \right\} \right). \tag{2-12}$$

Precalculated and tabulated, the error function tables provide accessible fast solutions to solve for dose distributions.

In addition to the CT data tables that are needed to perform the dose calculations in correlated heterogeneous media [48], Hogstrom described the specifications of the input beam data required for HBRA [54]. These specifications include:

- (1) *Most probable electron energy* ($E_{p,0}$) calculated from the practical range that is obtained from the measured depth dose curve.
- (2) *Depth dose data and off-axis ratios* for each nominal electron energy for a set of square fields.
- (3) *Initial angular divergence* determined by measuring the penumbral width as a function of distance from the collimator.
- (4) *Source-to-surface distance (SSD)* and *Source-to-Collimator distance (SCD)* which represents the distance from the virtual source position (as defined by Khan *et al.*[18]) to the standard treatment plane and to the location of the final collimation, respectively.

The clinical implementation of HPBA in 3D treatment planning system was described by Starkschall *et al.* [55]. Incorporating reconstructed equations with precalculated error functions along with different optimization procedures has lead to significant improvement in computational efficiency. Consequently, it established the basis for electron dose calculations for commercial 3D systems such as Pinnacle and FOCUS.

2.6.1.d Limitations of pencil beam algorithm

Despite their usefulness for broad beam electron dose calculations in radiation therapy, pencil beam models encounter significant limitations as discussed in depth by Hogstrom [56]. The most significant properties that primarily lead to considerable inaccuracies in dose calculations are:

(1) The assumption of slab geometry:

The original pencil beam model was formulated with the assumption of semi-infinite slab approximation. Therefore, when evaluating dose contributions, it is the anatomy along the axis of the central ray of each pencil that defines the slab heterogeneity characteristics and, therefore, is used to calculate the dose. Since the anatomy along the central axis could be different from that along the mean path of the electrons, a considerable error could occur. The errors are more pronounced when differences in scattering properties between adjacent tissues are significant. Lax [57] showed that the presence of bone heterogeneities at deep depths (beyond half of the

electron range) leads to an overestimation of the dose calculation within the tissue. He showed that the slab geometry assumption is behind that overestimation. Also, due to that assumption, the dose in the air cavities is also underestimated.

(2) The Gaussian scatter distribution function

The pencil beam model was developed based on Fermi-Eyges small angle scattering theory. The model predicts that the root mean square spread of the Gaussian increases with depth. However, the “pure” Gaussian model does not represent a true distribution as electrons scatter through large angles in the tail region. Electrons that scatter with larger angles have shorter ranges. The GGPBA model that calculates the radial dose distribution as the sum of three Gaussians, takes better account of large angle scattering events. This leads to an overall improvement in the accuracy of the calculation especially at the penumbra region where the electrons exhibit a larger angular scattering.

(3) The inability to account for secondary electrons

The effect of electron-electron scattering is neglected in the original HPBA. This implies inaccurate prediction of the dose for small fields, causing the maximum dose build-up to occur at depths deeper than those calculated, with a steeper fall-off beyond the therapeutic depth [58].

2.6.1.e Pencil beam algorithm in commercial electron treatment planning systems

Following the reported results of evaluating pencil beam algorithm [48,54,59-62], the algorithm was implemented in 3D commercial treatment planning systems. Different studies were performed to evaluate the accuracy of the clinically-used dose calculation algorithms in treatment planning systems.

FOCUS

Muller-Runkel and Cho [58] tested the accuracy of HPBA in the FOCUS treatment planning system (Computerized Medical Systems Inc., St. Louis, MO) for different data sets that represent clinical applications for electron beam therapy. They showed that FOCUS is well implemented within the limitations of HPBA. Good agreement between measurements and algorithm was found for straight-on beams in homogeneous water phantoms except for the lower isodoses. They also showed that the small field sizes are poorly modeled and that the oblique beam models show severe discrepancies due to the violation of the inherent assumption of slab geometry.

CADPLAN

The dose calculation algorithm in CADPLAN (Varian Medical Systems, Palo Alto, CA) was investigated by Samuelsson *et al.*[63]. CADPLAN uses a model of GGPBA. The standard setup of perpendicular incidence in water phantom showed a more accurate calculation than was reported by Muller-Runkel where the error in the penumbra was eliminated. For complicated situations that involve tissue heterogeneities, the deviations were up to 10%. The profiles for geometries with a gantry angle of 30 degrees also showed large deviations. Ding *et al.*[64] performed another study to evaluate the accuracy of CADPLAN for various energies and field sizes in different phantoms. CADPLAN fails to calculate the magnitude of dose changes in complex heterogeneous geometries.

Helax-TMS

Both HPBA and GGPBA are implemented in the dose calculation algorithm in Helax-TMS commercial treatment planning system. Blomquist *et al.*[65] used a comprehensive data set to evaluate the system. HELAX-TMS retrieves precalculated pencil beam kernels that were computed based on the GGPBA model that accounts for small and large angle scattering. Prior to entering the patient, the pencil beams are modeled according to HPBA to handle the initial angular spread and air transport. The results showed that small heterogeneities and obliquity are problematic and cause errors outside the acceptable limits.

2.6.1.f Summary

During the past two decades, significant modifications have been introduced to improve the accuracy of the originally proposed pencil beam algorithm. This includes the phase-space evolution algorithm [66,67] and pencil beam redefinition algorithm (PRBA) [68]. Although these modifications have now reached a satisfactory degree of development, they still exhibit what Hogstrom and Almond [6] described as a “failure” of practice for radiation therapy because of their inability to model actual treatments [6].

2.6.2 Monte Carlo transport

Monte Carlo transport calculations have been continuously gaining a more important role in the field of medical physics. In his review paper, Rogers [69] stated that the number of published papers on Monte Carlo has doubled every five years during the

period from 1967 to 2000 in the journal of Physics in Medicine and Biology. Because of its wide acceptance as a powerful tool for modeling radiation transport, Monte Carlo techniques were used in a wide range of implementations in order to derive physical quantities that are relevant to radiation therapy. Monte Carlo was used in optimizing the design of linacs [70], deriving dose deposition kernels for treatment planning systems [71,72], obtaining source spectra [70,73-75], calculating stopping power ratios [76-78], analyzing detector response [79-81], studying and optimizing portal imaging [82-84], and it is still continuing to be a lively field of research [85]. In addition to its ability to provide a wide range of data, Monte Carlo techniques offer solutions that are able to go beyond measurement capabilities. For example, Monte Carlo techniques have the aptitude to extract the fractions of either primary or scattered dose and proceed with only one of them. It is also possible when performing calculations to know the contribution from each component in the treatment head to the total dose.

2.6.2.a Overview

In the context of radiation therapy, Monte Carlo transport calculations usually refer to algorithms that allow the determination of the dose deposited in a certain volume by following the path of representative particles as they travel inside a medium. After generating a particle (following a distribution that describes the source of radiation), the particle is tracked through the medium for a certain distance before it scatters into another direction and/or energy. The transport of the particle is governed by probability distributions and cross sectional data that are obtained from well-known fundamental laws of radiation physics. While a particle is traveling in a geometry, it gives birth to a shower of secondary particles until it is totally absorbed by the scoring volume or departs to another volume of interest. In a Cartesian coordinate system, the sub-volume in which the particle is scored is referred to as a voxel. The transport of a primary incident particle, including its progeny, until its complete absorption or escape from the voxel geometry is referred to as “history”.

Theoretically, a patient that is treated with a radiation dose of 40 Gy is bombarded with the order of 10^{12} particles. This translates to more than 10^{16} particles that are transported through the system including the treatment head and the patient. Even with the aid of the fast computers currently available, processors are still unable to follow the

track of each individual particle and perform the consequent calculations within a reasonable time. Therefore, to accelerate this process, the tracks of randomly selected particles are followed as a sample representing the average behaviour of all particles. These representative particles are sampled using a computer based pseudo-random number generator. This introduces a statistical uncertainty in the quantities calculated by Monte Carlo which is dependent on the number of simulated histories.

The inclusion of electron transport adds a new dimension to Monte Carlo simulation. In principle, direct simulation that includes all kinds of possible interactions could be used for electrons in a similar fashion as that used for photon transport. However, due to the fact that a high energy electron undergoes on the order of 10^5 interactions in its slowing down process, processors cannot handle the tracking of each individual particle on an event-by-event basis. Berger [86] proposed the use of condensed history techniques for calculating electron transport where interactions are grouped into steps and the angular deflection and the energy loss are evaluated on a step by step basis. The transition from one step to the next step accounts for many interactions where multiple collision models, such as multiple scattering or restricted stopping power, are considered. Since its introduction, the condensed history technique has become the basis for all current codes that handle electron transport for energies above 10 keV.

Variance reduction techniques were developed to improve the simulation efficiency by reducing the statistical uncertainties for a fixed computational time. In such techniques, the “natural” physics as well as the scoring procedures are “manipulated” in a number of different ways so as to increase the relative occurrence of certain events. Forced interactions, Russian roulette, particle splitting, range rejection, geometrical symmetry, and PRESTA are commonly used techniques in Monte Carlo codes. In his review chapter, Sheikh-Bagheri *et al.* [87] offered excellent explanations for variance reduction techniques and their impact on the improvement of Monte Carlo calculations.

Because of its intensive computing time, there had been a traditional belief that Monte Carlo is impractical for routine clinical treatment planning despite its ability to accurately predict dose distributions in highly complex geometries. However, this belief started to fade away with the ever continuing increase in computer power and parallel processing along with the variance reduction techniques that improve the computational

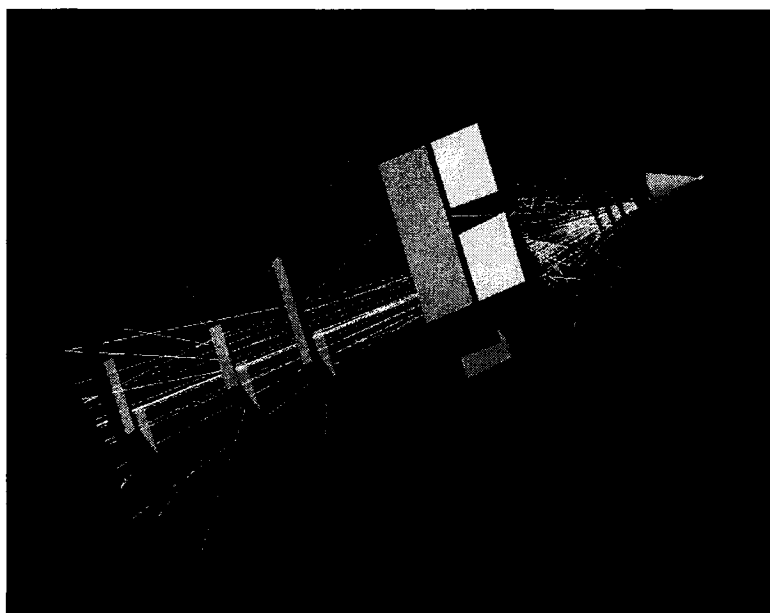


Figure 2-5: *A 3D image of a Monte Carlo model of Varian CL-2300 (18 MeV) using EGSnrc/BEAM.*

efficiency. Although not yet published at the time of the writing of this thesis, the AAPM is preparing to approve a Task Group report on application of Monte Carlo techniques to clinical treatment planning [69].

2.6.2.b Monte Carlo codes for radiation therapy

There are wide varieties of Monte Carlo codes that are used in radiation therapy. ETRAN/ITS [88,89], Electron Gamma Shower EGS4/EGSnrc [90,91], MCNP4/MCNP5 [92-94], PENELOPE [95], and GEANT3/GEANT4 [96,97] are all available Monte Carlo packages that significantly contributed to the impact of Monte Carlo applications. The BEAM/EGS4 user interface [98], which was later upgraded to EGSnrc/BEAM [99], facilitated easy modeling of radiation therapy accelerators leading to significant growth in the research of photon and electron beams (Fig. 2-5). Many studies have been performed to compare the results of different codes for clinical electron beams [100,101].

As the trend to use Monte Carlo calculation in treatment planning grew, the demand for simplified Monte Carlo algorithms increased. Monte Carlo packages were originally designed to provide solutions for a wide range of radiation transport problems

that were beyond the interest of radiation therapy. Customized codes were introduced to avoid time-consuming complications caused by built-in options that are integrated within Monte Carlo packages.

Macro Monte Carlo (MMC)

Macro Monte Carlo (MMC) was first proposed by Mackie and Battista [102] to apply precalculated kernels for treatment planning. The kernels are stored in large look-up tables that include the electron transport characteristics. Neuenschwander *et al.* [103] implemented the MMC algorithm in spherical volume elements called kugels. The code tabulates the probability of electrons exiting the kugel as a function of the exit location, energy, and direction. When it was introduced, MMC offered a faster calculation algorithm than EGS4. However, it suffered from a lack of accuracy in comparison with EGS due to the lack of modeling of the transport of secondary electrons and bremsstrahlung photons [103].

Super Monte Carlo (SMC)

Keall and Hoban [104] introduced Super Monte Carlo (SMC) that incorporates the precalculated kernels to construct probability distributions for electron transport. SMC differentiates itself from MMC by performing rigorous step-by-step calculation for each electron step. Compared to EGS, SMC provided dose accuracy within 1.5% but without substantial gain in the calculation time.

Voxel Monte Carlo (VMC/XVMC)

Voxel Monte Carlo (VMC) [105,106] is a fast Monte Carlo code designed to simulate electron transport under certain restrictions specifically designed for radiotherapy purposes. Unlike EGS, which is designed for a wide range of energies and materials, the VMC code is applicable only within an energy range of 1-30 MeV and for low Z materials that have physical densities between 0 to 3 g/cm³. With the aid of multiple uses of each simulated history, VMC was able to perform calculations faster than EGS by a factor of 30, although it still uses an advanced transport algorithm. After benchmarking the VMC code for electron transport, a new code (XVMC) [107] was introduced for coupled photon and electron transport. Doucet *et al.* [108] showed that XVMC calculations performed for electron beams in heterogeneous phantoms provide excellent agreement with both measurements and EGSnrc.

2.6.2.c Monte Carlo in commercial electron treatment planning systems

Until recently, Monte Carlo-based treatment planning systems remained predominantly research tools [101,109,110]. However, introducing Monte Carlo algorithms in commercial treatment planning systems designed for electron beams is becoming a trend for new treatment planning systems. Two commercial systems have been reviewed in scientific literature:

Eclipse

Eclipse (Varian Medical Systems) is a commercial electron dose calculation software that implements the MMC algorithm. Within one month, two independent studies evaluating Eclipse were published. Popple *et al.* [111] evaluated the accuracy of Eclipse by comparing the calculations with a set of measurements. Results similar to that previously reported in validation of MMC were shown. Expected deviations for small fields with low energy beams were also demonstrated. Ding *et al.* [112] investigated more geometries and different setups including extended SSDs and oblique beams. Concerns arising from using Monte Carlo in commercial treatment planning systems were discussed in depth by Ding *et al.* [112]. This includes a comparison between reporting the dose-to-medium versus dose-to-water. The effect of statistical uncertainties on point dose prescription was also discussed. Eclipse is configured for Varian electron beams only.

Theraplan Plus

Cygler *et al.* [113] tested the accuracy of VMC algorithm implemented in the dose calculation engine of a commercial treatment planning system software developed within Theraplan Plus (MDS Nordion, Ottawa, ON, Canada). The software consists of a linac head model and a VMC++ code (VMC code rewritten in C++) for electron and photon transport through the patient anatomy. It was shown that the software could be faster than EGS by two orders of magnitude with the same level of accuracy. Excellent agreements (within 2.5%) were obtained between calculations and measurements performed in heterogeneous phantoms. Results showed that discrepancies are sensitive to size of the voxels. Errors as high as 5% at material interfaces were found when voxel sizes were poorly selected. However, based on their results, it was concluded that Monte

Carlo-based treatment planning offers the best approach for modern clinical treatment planning [113].

2.6.3 Pencil beam algorithm vs. Monte Carlo techniques

Scientific literature is accumulating evidence that Monte Carlo techniques are superior to pencil beam algorithms [113,114]. In a study by Ding *et al.* [115], comparisons of dose calculations in equivalent phantoms were performed between pencil beam-based and Monte Carlo-based commercial treatment planning systems. When compared to the Monte Carlo-based algorithm, the pencil beam-based algorithm results in large errors in phantoms containing three-dimensional heterogeneities. Coleman *et al.* [116], however, claimed that pencil beam-based algorithms offer modest accuracy and can be used as an alternative in the case of unavailability of Monte Carlo-based treatment planning systems. Antolak *et al.* [117] demanded a higher standard of agreements between Monte Carlo calculations and measurements where the criteria of acceptance was raised to be within 2% of z_{\max} or 1 mm over the entire range of clinical parameters. Such requirements continue the challenge to improve the applications of Monte Carlo in radiation therapy.

2.7. Clinical Use of Electron Therapy

The unique characteristics of the electron beam made it a preferred therapeutic modality for treating malignant lesions located at superficial depths. Most of the applications of the electron beam revolve around its distinct advantage of delivering a total dose to tumors while maintaining minimum irradiation to the normal tissues. Electron beams are used in many applications including: total skin irradiation [118], total scalp irradiation [119,120], craniospinal irradiation [121], and electron arc therapy [122-125]. However, these techniques are often implemented as special procedures in regional centers. Still, the main role of electron beams in radiation therapy will continue to be in the management of superficially located disease. Newer modalities that benefit from the advantages offered by electron beams are being developed. Discussion of these modalities is the topic of the next chapter.

References

- [1] H. Bethe and W. Heitler, "On the stopping of fast particles and on the creation of positive electrons," Proc. Roy. Soc. **146**, 0083-0112 (1934).
- [2] C. Moller, "Zur Theories des Durchgangs schneller Elektronen durch Materie," Ann. Phys. **14**, (1932).
- [3] H.J. Bhabha, "The scattering of positrons by electrons with exchange on Dirac's theory of the positron," Proc. Roy. Soc. **154**, 0195-0206 (1936).
- [4] H. Attix, Introduction to radiological physics and radiation dosimetry (Whily & Son, New York, NY, 1986).
- [5] J.G. Trump, K.A. Wright, W.W. Evans, J.H. Anson, H.F. Hare, J.L. Fromer, G. Jacque, and K.W. Horne, "High energy electrons for the treatment of extensive superficial malignant lesions," Am. J. Roentgenol. Radium. Ther. Nucl. Med. **69**, 623-629 (1953).
- [6] K.R. Hogstrom and P.R. Almond, "Review of electron beam therapy physics," Phys. Med. Biol. **51**, R455-489 (2006).
- [7] E. Grusell, A. Montelius, A. Brahme, G. Rikner, and K. Russell, "A general solution to charged particle beam flattening using an optimized dual-scattering-foil technique, with application to proton therapy beams," Phys. Med. Biol. **39**, 2201-2216 (1994).
- [8] A.D. Green, Modeling of dual foil scattering systems for clinical electron beams. M.S. Thesis, University of Texas Health Science Center, 1991.
- [9] E.E. Klein, D.A. Low, and J.A. Purdy, "Changes in electron beam dosimetry with a new scattering foil-applicator system on a CL2100C," Int. J. Radiat. Oncol. Biol. Phys. **32**, 483-490 (1995).
- [10] C.J. Karzmark and N.C. Pering, "Electron linear accelerators for radiation therapy: history, principles and contemporary developments," Phys. Med. Biol. **18**, 321-354 (1973).
- [11] C.J. Karzmark, "Advances in linear accelerator design for radiotherapy," Med. Phys. **11**, 105-128 (1984).
- [12] C.J. Karzmark, C. Nunan, and E. Tanabe, Medical Electron Accelerator (McGraw Hill, New York, 1993).
- [13] E.B. Podgorsak, P. Metcalfe, and J. Van Dyk, "Medical Accelerators," in: *The Modern Technology of Radiation Oncology*, edited by J. Van Dyk (Medical Physics Publishing, Madison, 1999), pp. 351-435.
- [14] M.L. Meurk, D.A. Goer, G. Spalek, and T. Cook, "The Mobetron: a new concept for IORT," in: *Intraoperative Radiation Therapy in the Treatment of Cancer: 6th Int. IORT*

- Symposium and 31st San Francisco Cancer Symposium (September 1996) (Frontiers of Radiation Therapy and Oncology vol 31)*, edited by J.L. Meyer, W. Hinkelbein (Karger, Basle, 1997), pp. 65-70.
- [15] M.D. Mills, L.C. Fajardo, D.L. Wilson, J.L. Daves, and W.J. Spanos, "Commissioning of a mobile electron accelerator for intraoperative radiotherapy," *J. Appl. Clin. Med. Phys.* **2**, 121-130 (2001).
- [16] A.S. Beddar and S. Krishnan, "Intraoperative radiotherapy using a mobile electron LINAC: a retroperitoneal sarcoma case," *J. Appl. Clin. Med. Phys.* **6**, 95-107 (2005).
- [17] International Commission of Radiation Units and Measurements Report No. 35: Radiation dosimetry: electron beams with energies between 1 and 50 MeV (ICRU, Washington, D.C., 1984).
- [18] F.M. Khan, K.P. Doppke, K.R. Hogstrom, G.J. Kutcher, R. Nath, S.C. Prasad, J.A. Purdy, M. Rozenfeld, and B.L. Werner, "Clinical electron-beam dosimetry: report of AAPM Radiation Therapy Committee Task Group No. 25," *Med. Phys.* **18**, 73-109 (1991).
- [19] D. Harder, "Energiespektren schneller Elektronen in verschiedenen Tiefen," in: *Symp. on High-Energy Electrons*, edited by A. Zuppinger, G. Poretti (Springer, Berlin, 1965), pp. 260.
- [20] P.J. Biggs, A.L. Boyer, and K.P. Doppke, "Electron dosimetry of irregular fields on the Clinac 18," *Int. J. Radiat. Oncol. Biol. Phys.* **5**, 433-440 (1979).
- [21] F.M. Khan, *The Physics of Radiation Therapy* (Lippincott, Williams & Wilkins, Philadelphia, PA, 2003).
- [22] F.M. Khan, W. Sewchand, and S.H. Levitt, "Effect of air space and depth dose in electron beam therapy," *Radiology* **126**, 249-251 (1978).
- [23] K.R. Hogstrom, R.E. Steadham, P.F. Wong, and A.S. Shiu, "Monitor unit calculations for electron beams," in: *Monitor Unit Calculations for External Photon and Electron Beams*, edited by J.P. Gibbons (Advanced Medical Publishing, Madison, WI, 2000), pp. 113-125.
- [24] G.G. Zhang, D.W. Rogers, J.E. Cygler, and T.R. Mackie, "Monte Carlo investigation of electron beam output factors versus size of square cutout," *Med. Phys.* **26**, 743-750 (1999).
- [25] F. Verhaegen, C. Mubata, J. Pettingell, A.M. Bidmead, I. Rosenberg, D. Mockridge, and A.E. Nahum, "Monte Carlo calculation of output factors for circular, rectangular, and square fields of electron accelerators (6-20 MeV)," *Med. Phys.* **28**, 938-949 (2001).

- [26] P. Bjork, T. Knoos, and P. Nilsson, "Measurements of output factors with different detector types and Monte Carlo calculations of stopping-power ratios for degraded electron beams," *Phys. Med. Biol.* **49**, 4493-4506 (2004).
- [27] C. Albaret, Automatic system for Monte Carlo determination of cutout factors of arbitrarily shaped electron and experimental verification of Monte Carlo calculated dose distributions. M.S. Thesis, Medical Physics Unit, McGill University, 2004.
- [28] P.M. Ostwald and T. Kron, "Variation in calculated effective source-surface distances with depth," *Phys. Med. Biol.* **41**, 2067-2078 (1996).
- [29] K.E. Ekstrand and R.L. Dixon, "The problem of obliquely incident beams in electron-beam treatment planning," *Med. Phys.* **9**, 276-278 (1982).
- [30] K.R. Hogstrom and R.S. Fields, "Use of CT in electron beam treatment planning: current and future development," in: *Computed Tomography in Radiation Therapy*, edited by C.C. Ling (Raven, New York, 1983), pp. 241-252.
- [31] J.S. Laughlin, "Calorimetric determination of absorbed dose with electrons," in: *Symp. on High-Energy Electrons (Montreaux, Switzerland)*, edited by A. Zuppinger, G. Poretti (Springer, Berlin, 1965), pp. 65-71.
- [32] P.R. Almond, "The physical measurements of electron beams from 6 to 18 Mev: absorbed dose and energy calibration," *Phys. Med. Biol.* **12**, 13-24 (1967).
- [33] A.P. Pinkerton, "Comparison of calorimetric and other methods for the determination of absorbed dose," *Ann. N. Y. Acad. Sci.* **161**, 63-76 (1969).
- [34] G. Hettinger and C. Pettersson, "Determination of Frick G-value for 30 MeV electrons with the use of a calorimetric technique," in: *Symp. on High-Energy Electrons (Montreaux, Switzerland)*, edited by A. Zuppinger, G. Poretti (Springer, Berlin, 1965), pp. 57-61.
- [35] R.J. Shalek and C.E. Smith, "Chemical dosimetry for the measurement of high-energy photons and electrons," *Ann. N. Y. Acad. Sci.* **161**, 44-62 (1969).
- [36] D.I. Thwaites, A.R. DuSautoy, T. Jordan, M.R. McEwen, A. Nisbet, A. Nahum, and W.G. Pitchford, "The IPEMB code of practice for electron dosimetry for radiotherapy beams of initial energy from 2 to 50 MeV based on an air kerma calibration. Institution of Physics and Engineering in Medicine and Biology," *Phys. Med. Biol.* **41**, 2557-2603 (1996).
- [37] International Atomic Energy Agency Technical Report No. 277: Absorbed dose determination in photon and electron beams: an international code of practice (IAEA, Vienna, 1987).

- [38] "A protocol for the determination of absorbed dose from high-energy photon and electron beams," *Med. Phys.* **10**, 741-771 (1983).
- [39] M.L. Boone, P.R. Almond, and A.E. Wright, "High-energy electron dose perturbations in regions of tissue heterogeneity," *Ann. N. Y. Acad. Sci.* **161**, 214-232 (1969).
- [40] J. Dutreix and A. Dutreix, "Film dosimetry of high-energy electrons," *Ann. N. Y. Acad. Sci.* **161**, 33-43 (1969).
- [41] A. Niroomand-Rad, C.R. Blackwell, B.M. Coursey, K.P. Gall, J.M. Galvin, W.L. McLaughlin, A.S. Meigooni, R. Nath, J.E. Rodgers, and C.G. Soares, "Radiochromic film dosimetry: recommendations of AAPM Radiation Therapy Committee Task Group 55. American Association of Physicists in Medicine," *Med. Phys.* **25**, 2093-2115 (1998).
- [42] A.S. Shiu, V.A. Otte, and K.R. Hogstrom, "Measurement of dose distributions using film in therapeutic electron beams," *Med. Phys.* **16**, 911-915 (1989).
- [43] R.K. Ten Haken, B.A. Fraass, and R.J. Jost, "Practical methods of electron depth-dose measurement compared to use of the NACP design chamber in water," *Med. Phys.* **14**, 1060-1066 (1987).
- [44] L. Eyges, "Multiple Scattering with Energy Loss," *Phys. Rev.* **74**, 1534-1535 (1948).
- [45] A. Brahme, "Geometric parameters of clinical electron beams," *Acta Radiol. Suppl.* **364**, 11-19 (1983).
- [46] S.C. Lillicrap, P. Wilson, and J.W. Boag, "Dose distributions in high energy electron beams: production of broad beam distributions from narrow beam data," *Phys. Med. Biol.* **20**, 30-38 (1975).
- [47] D.J. Perry and J.G. Holt, "A model for calculating the effects of small inhomogeneities on electron beam dose distributions," *Med. Phys.* **7**, 207-215 (1980).
- [48] K.R. Hogstrom, M.D. Mills, and P.R. Almond, "Electron beam dose calculations," *Phys. Med. Biol.* **26**, 445-459 (1981).
- [49] B.L. Werner, F.M. Khan, and F.C. Deibel, "A model for calculating electron beam scattering in treatment planning," *Med. Phys.* **9**, 180-187 (1982).
- [50] D. Jette, "Electron beam dose calculations," in: *Radiation Therapy Physics*, edited by A.R. Smith (Springer, Berlin, 1995), pp. 95-121.
- [51] A. Brahme, I. Lax, and P. Andreo, "Electron beam dose planning using discrete Gaussian beams. Mathematical background," *Acta Radiol. Oncol.* **20**, 147-158 (1981).
- [52] I. Lax, A. Brahme, and P. Andreo, "Electron beam dose planning using Gaussian beams. Improved radial dose profiles," *Acta Radiol. Suppl.* **364**, 49-59 (1983).

- [53] I. Lax and A. Brahme, "Electron beam dose planning using Gaussian beams. Energy and spatial scaling with inhomogeneities," *Acta Radiol. Oncol.* **24**, 75-85 (1985).
- [54] K.R. Hogstrom, M.D. Mills, J.A. Meyer, J.R. Palta, D.E. Mellenberg, R.T. Meoz, and R.S. Fields, "Dosimetric evaluation of a pencil-beam algorithm for electrons employing a two-dimensional heterogeneity correction," *Int. J. Radiat. Oncol. Biol. Phys.* **10**, 561-569 (1984).
- [55] G. Starkschall, A.S. Shiu, S.W. Bujnowski, L.L. Wang, D.A. Low, and K.R. Hogstrom, "Effect of dimensionality of heterogeneity corrections on the implementation of a three-dimensional electron pencil-beam algorithm," *Phys. Med. Biol.* **36**, 207-227 (1991).
- [56] K.R. Hogstrom, "Clinical Electron Beam Dosimetry: Basic Dosimetry Data," in: *AAPM 1990 Summer School*, edited by A.J. Purdy (American Institute of Physics, New York, 1992), pp. 390-490.
- [57] I. Lax, "Inhomogeneity corrections in electron-beam dose planning. Limitations with the semi-infinite slab approximation," *Phys. Med. Biol.* **31**, 879-892 (1986).
- [58] R. Muller-Runkel and S.H. Cho, "Evaluation of a commercial three-dimensional electron pencil beam algorithm," *Med. Phys.* **24**, 91-101 (1997).
- [59] D.L. McShan, B.A. Fraass, and R.K. Ten Haken, "Dosimetric verification of a 3-D electron pencil beam dose calculation algorithm," *Med. Phys.* **21**, 13-23 (1994).
- [60] H.M. Kooy and H. Rashid, "A three-dimensional electron pencil-beam algorithm," *Phys. Med. Biol.* **34**, 229-243 (1989).
- [61] J. Seuntjens, A. Van der Plaetsen, H. Thierens, and M. Piessens, "Comparison of measured and calculated dose distributions in lung after electron beam treatment of the chest wall," *Med. Phys.* **21**, 1959-1968 (1994).
- [62] J. Cygler, J.J. Battista, J.W. Scrimger, E. Mah, and J. Antolak, "Electron dose distributions in experimental phantoms: a comparison with 2D pencil beam calculations," *Phys. Med. Biol.* **32**, 1073-1086 (1987).
- [63] A. Samuelsson, S. Hyodynmaa, and K.A. Johansson, "Dose accuracy check of the 3D electron beam algorithm in a treatment planning system," *Phys. Med. Biol.* **43**, 1529-1544 (1998).
- [64] G.X. Ding, J.E. Cygler, G.G. Zhang, and M.K. Yu, "Evaluation of a commercial three-dimensional electron beam treatment planning system," *Med Phys* **26**, 2571-2580 (1999).
- [65] M. Blomquist and M. Karlsson, "Test procedures for verification of an electron pencil beam algorithm implemented for treatment planning," *Radiother. Oncol.* **39**, 271-286 (1996).

- [66] H. Huizenga and P.R. Storchi, "Numerical calculation of energy deposition by broad high-energy electron beams," *Phys. Med. Biol.* **34**, 1371-1396 (1989).
- [67] J.J. Janssen, D.E. Riedeman, M. Morawska-Kaczynska, P.R. Storchi, and H. Huizenga, "Numerical calculation of energy deposition by high-energy electron beams: III. Three-dimensional heterogeneous media," *Phys. Med. Biol.* **39**, 1351-1366 (1994).
- [68] A.S. Shiu and K.R. Hogstrom, "Pencil-beam redefinition algorithm for electron dose distributions," *Med. Phys.* **18**, 7-18 (1991).
- [69] D.W. Rogers, "Fifty years of Monte Carlo simulations for medical physics," *Phys. Med. Biol.* **51**, R287-301 (2006).
- [70] R.C. McCall, R.D. McIntyre, and W.G. Turnbull, "Improvement of linear accelerator depth-dose curves," *Med. Phys.* **5**, 518-524 (1978).
- [71] T.R. Mackie, J.W. Scrimger, and J.J. Battista, "A convolution method of calculating dose for 15-MV x rays," *Med. Phys.* **12**, 188-196 (1985).
- [72] R. Mohan, C. Chui, and L. Lidofsky, "Differential pencil beam dose computation model for photons," *Med. Phys.* **13**, 64-73 (1986).
- [73] J.P. Patau, C.E. Vernes, M. Terrissol, and M. Malbert, "Calcul des caracteristiques qualitatives (TEL, F.Q., equivalent de dose) d'un faisceau de photons de freinage a usage medical, par simulation de sa creation et de son transport," in: *Proc. the 6th Symposium on Microdosimetry*, edited by J. Booz, H.G. Ebert (Harwood Academic, London, 1978), pp. 579-588.
- [74] B.A. Faddegon, C.K. Ross, and D.W. Rogers, "Forward-directed bremsstrahlung of 10- to 30-MeV electrons incident on thick targets of Al and Pb," *Med. Phys.* **17**, 773-785 (1990).
- [75] B.A. Faddegon, C.K. Ross, and D.W. Rogers, "Angular distribution of bremsstrahlung from 15-MeV electrons incident on thick targets of Be, Al, and Pb," *Med. Phys.* **18**, 727-739 (1991).
- [76] A.E. Nahum, "Water/air mass stopping power ratios for megavoltage photon and electron beams," *Phys. Med. Biol.* **23**, 24-38 (1978).
- [77] P. Andreo and A.E. Nahum, "Stopping-power ratio for a photon spectrum as a weighted sum of the values for monoenergetic photon beams," *Phys. Med. Biol.* **30**, 1055-1065 (1985).
- [78] P. Andreo and A. Brahme, "Stopping power data for high-energy photon beams," *Phys. Med. Biol.* **31**, 839-858 (1986).

- [79] J.E. Bond, R. Nath, and R.J. Schulz, "Monte Carlo calculation of the wall correction factors for ionization chambers and A_{eq} for ^{60}Co gamma rays," *Med. Phys.* **5**, 422-425 (1978).
- [80] A.E. Nahum and M. Kristensen, "Calculated response and wall correction factors for ionization chambers exposed to ^{60}Co gamma rays," *Med. Phys.* **9**, 925-929 (1982).
- [81] P. Andreo, A. Nahum, and A. Brahme, "Chamber-dependent wall correction factors in dosimetry," *Phys. Med. Biol.* **31**, 1189-1199 (1986).
- [82] B.M. McCurdy and S. Pistorius, "Photon scatter in portal images: physical characteristics of pencil beam kernels generated using the EGS Monte Carlo code," *Med. Phys.* **27**, 312-320 (2000).
- [83] E. Spezi and D.G. Lewis, "Full forward Monte Carlo calculation of portal dose from MLC collimated treatment beams," *Phys. Med. Biol.* **47**, 377-390 (2002).
- [84] S. Flampouri, P.M. Evans, F. Verhaegen, A.E. Nahum, E. Spezi, and M. Partridge, "Optimization of accelerator target and detector for portal imaging using Monte Carlo simulation and experiment," *Phys. Med. Biol.* **47**, 3331-3349 (2002).
- [85] J.P. Seuntjens and P.N. Mobit, Recent developments in accurate radiation dosimetry (Medical Physics Publishing, Madison, 2002).
- [86] M.J. Berger, "Monte Carlo calculation of the penetration and diffusion of fast charged particles," *Methods Comput. Phys.* **1**, 135-215 (1963).
- [87] D. Sheikh-Bagheri, I. Kawrakow, B.R. Walters, and D.W. Rogers, "Monte Carlo simulations: efficiency improvements techniques and statistical considerations," in: *Integrating new technologies into the clinic: Monte Carlo and Image-Guided Radiation Therapy- Proceedings of 2006 AAPM Summer School*, edited by (Medical Physics Publishing, Madison, WI, 2006), pp. 71-91.
- [88] J.A. Halbeib, "Structure and operation of the ITS code system," in: *Transport of Electrons and Photons*, edited by T.M. Jenkins, W.R. Nelson, A. Rindi (Plenum, New York, 1988), pp. 249-262.
- [89] S.M. Seltzer, "Electron-photon Monte Carlo calculations: the ETRAN code," *Appl. Radiat. Isot.* **42**, 917 (1991).
- [90] W.R. Nelson, H. Hirayama, and D.W. Rogers, "The EGS4 code system, Stanford Linear Accelerator Center Report SLAC-265," (1985).
- [91] I. Kawrakow, "Accurate condensed history Monte Carlo simulation of electron transport. I. EGSnrc, the new EGS4 version," *Med. Phys.* **27**, 485-498 (2000).

- [92] J.F. Briesmeister, "MCNP-a general Monte Carlo n-particle transport code, Version 4C Technical Report No LA-13709-M Los Alamos National Laboratory," (2000).
- [93] J.S. Hendricks, K.J. Adam, T.E. Booth, J.F. Briesmeister, L.L. Carter, L.J. Cox, J.A. Favorite, R.A. Forster, G.W. McKinney, and R.E. Prael, "Present and future capabilities of MCNP," *Appl. Radiat. Isot.* **53**, 857-861 (2000).
- [94] RSICC 2003 <http://www-rsicc.ornl.gov/SOFTWARE.html>.
- [95] J. Sempau, "An algorithm for Monte Carlo simulation of coupled electron-photon transport," *Nucl. Inst. Methods B* **132**, 377 (1997).
- [96] GEANT, Application Software Group Computing and Networks Division-Detector Description and Simulation Tool, in: CERN Program Library Long Writeup W5013 (CERN, Geneva, 1995).
- [97] GEANT4 2003 <http://geant4.web.cern.ch/geant4/>.
- [98] D.W. Rogers, B.A. Faddegon, G.X. Ding, C.M. Ma, J. We, and T.R. Mackie, "BEAM: a Monte Carlo code to simulate radiotherapy treatment units," *Med. Phys.* **22**, 503-524 (1995).
- [99] D.W. Rogers, C.M. Ma, B.R. Walters, G.X. Ding, D. Sheikh-Bagheri, and G.G. Zhang, "BEAMnrc Users Manual, National Research Council of Canada, Ottawa, Report PIRS-0509(A)G," (2002).
- [100] R. Jeraj, P.J. Keall, and P.M. Ostwald, "Comparisons between MCNP, EGS4 and experiment for clinical electron beams," *Phys. Med. Biol.* **44**, 705-717 (1999).
- [101] W. van der Zee, A. Hogenbirk, and S.C. van der Marck, "ORANGE: a Monte Carlo dose engine for radiotherapy," *Phys. Med. Biol.* **50**, 625-641 (2005).
- [102] T.R. Mackie and J.J. Battista, A macroscopic Monte Carlo method for electron beam dose calculations: a proposal, in: *Proc. 8th Conf. of Use of Computers in Radiation Therapy* (IEEE, Toronto, 1984) 123-127.
- [103] H. Neuenschwander, T.R. Mackie, and P.J. Reckwerdt, "MMC--a high-performance Monte Carlo code for electron beam treatment planning," *Phys. Med. Biol.* **40**, 543-574 (1995).
- [104] P.J. Keall and P.W. Hoban, "Super-Monte Carlo: a 3-D electron beam dose calculation algorithm," *Med. Phys.* **23**, 2023-2034 (1996).
- [105] I. Kawrakow, M. Fippel, and K. Friedrich, "3D electron dose calculation using a Voxel based Monte Carlo algorithm (VMC)," *Med. Phys.* **23**, 445-457 (1996).

- [106] M. Fippel, I. Kawrakow, and K. Friedrich, "Electron beam dose calculations with the VMC algorithm and the verification data of the NCI working group," *Phys. Med. Biol.* **42**, 501-520 (1997).
- [107] I. Kawrakow and M. Fippel, "Investigation of variance reduction techniques for Monte Carlo photon dose calculation using XVMC," *Phys. Med. Biol.* **45**, 2163-2183 (2000).
- [108] R. Doucet, M. Olivares, F. DeBlois, E.B. Podgorsak, I. Kawrakow, and J. Seuntjens, "Comparison of measured and Monte Carlo calculated dose distributions in inhomogeneous phantoms in clinical electron beams," *Phys. Med. Biol.* **48**, 2339-2354 (2003).
- [109] C.M. Ma, E. Mok, A. Kapur, T. Pawlicki, D. Findley, S. Brain, K. Forster, and A.L. Boyer, "Clinical implementation of a Monte Carlo treatment planning system," *Med. Phys.* **26**, 2133-2143 (1999).
- [110] C.M. Ma, J.S. Li, T. Pawlicki, S.B. Jiang, J. Deng, M.C. Lee, T. Koumrian, M. Luxton, and S. Brain, "A Monte Carlo dose calculation tool for radiotherapy treatment planning," *Phys. Med. Biol.* **47**, 1671-1689 (2002).
- [111] R.A. Popple, R. Weinber, J.A. Antolak, S.J. Ye, P.N. Pareek, J. Duan, S. Shen, and I.A. Brezovich, "Comprehensive evaluation of a commercial macro Monte Carlo electron dose calculation implementation using a standard verification data set," *Med. Phys.* **33**, 1540-1551 (2006).
- [112] G.X. Ding, D.M. Duggan, C.W. Coffey, P. Shokrani, and J.E. Cygler, "First macro Monte Carlo based commercial dose calculation module for electron beam treatment planning--new issues for clinical consideration," *Phys. Med. Biol.* **51**, 2781-2799 (2006).
- [113] J.E. Cygler, G.M. Daskalov, G.H. Chan, and G.X. Ding, "Evaluation of the first commercial Monte Carlo dose calculation engine for electron beam treatment planning," *Med. Phys.* **31**, 142-153 (2004).
- [114] J.S. Li, T. Pawlicki, J. Deng, S.B. Jiang, E. Mok, and C.M. Ma, "Validation of a Monte Carlo dose calculation tool for radiotherapy treatment planning," *Phys. Med. Biol.* **45**, 2969-2985 (2000).
- [115] G.X. Ding, J.E. Cygler, C.W. Yu, N.I. Kalach, and G. Daskalov, "A comparison of electron beam dose calculation accuracy between treatment planning systems using either a pencil beam or a Monte Carlo algorithm," *Int. J. Radiat. Oncol. Biol. Phys.* **63**, 622-633 (2005).

- [116] J. Coleman, C. Park, J.E. Villarreal-Barajas, P. Petti, and B. Faddegon, "A comparison of Monte Carlo and Fermi-Eyges-Hogstrom estimates of heart and lung dose from breast electron boost treatment," *Int J Radiat Oncol Biol Phys* **61**, 621-628 (2005).
- [117] J.A. Antolak, M.R. Bieda, and K.R. Hogstrom, "Using Monte Carlo methods to commission electron beams: a feasibility study," *Med Phys* **29**, 771-786 (2002).
- [118] AAPM, "Total skin electron therapy: technique and dosimetry," Report no 23, American Association of Medical Physicists (December 1987).
- [119] C. Akazawa, "Treatment of the scalp using photon and electron beams," *Med. Dosim.* **14**, 129-131 (1989).
- [120] S.S. Tung, A.S. Shiu, G. Starkschall, W.H. Morrison, and K.R. Hogstrom, "Dosimetric evaluation of total scalp irradiation using a lateral electron-photon technique," *Int. J. Radiat. Oncol. Biol. Phys.* **27**, 153-160 (1993).
- [121] M.H. Maor, R.S. Fields, K.R. Hogstrom, and J. van Eys, "Improving the therapeutic ratio of craniospinal irradiation in medulloblastoma," *Int. J. Radiat. Oncol. Biol. Phys.* **11**, 687-697 (1985).
- [122] K.R. Hogstrom and D.D. Leavitt, "Dosimetry of electron arc therapy," in: *Radiation Oncology Physics 1986: Proc. 1986 Summer School of the AAPM*, edited by H. Elson, C. Born (AIP, New York, 1987), pp. 265-295.
- [123] L.K. McNeely, G.M. Jacobson, D.D. Leavitt, and J.R. Stewart, "Electron arc therapy: chest wall irradiation of breast cancer patients," *Int. J. Radiat. Oncol. Biol. Phys.* **14**, 1287-1294 (1988).
- [124] J.R. Stewart, D.D. Leavitt, and J. Prows, "Electron arc therapy of the chest wall for breast cancer: rationale, dosimetry, and clinical aspects," *Front. Radiat. Ther. Oncol.* **25**, 134-150 (1991).
- [125] M. Olivares-Pla, E.B. Podgorsak, and C. Pla, "Electron arc dose distributions as a function of beam energy," *Med. Phys.* **24**, 127-132 (1997).

Chapter 3**Energy Modulated Electron Therapy**

The innovations in computer-controlled medical linear accelerators heightened the interest in x-ray intensity modulated radiation therapy (IMRT) [1-6]. Most importantly was the advent of multileaf collimators (MLCs) which provided a tool to employ non-uniform fluence distributions that is able to design optimum intensity modulated beams. By manipulating the intensities of individual subdivisions of beams (beamlets), a desired optimum pattern of dose can be achieved. Being an inverse treatment planning problem, an optimization algorithm is required to satisfy certain constraints which can be defined based on clinical relevant parameters. Examples of these constraints are: uniformity of the dose, conformity to the planning target volume (PTV), and sparing of the organs at risk (OARs). IMRT has become a well established treatment modality and a major research specialty that is served by several commercial systems.

Although IMRT has been widely used for treating deep-seated tumors [7-11], it has been less effective for superficially located tumors. This is mainly because of the low surface dose exhibited by the x-ray beams. Furthermore, the slow attenuation of x-ray beams results in a high exit dose and a large integral dose in the patient. It has been reported that a large volume that receives low radiation doses may introduce a long term risk of developing radiation-induced cancers [12].

To overcome these shortcomings and because of the nature of the electron beams, some studies have investigated the possibility of adding single electron beams, which offer high surface doses, to photon IMRT in order to improve treatment planning for shallow targets [13-15]. However, energy modulated electron therapy (EMET) has garnered increasing interest for delivering high conformal dose to targets near the surface

[16-20]. For a successful EMET delivery, three main ingredients are required; namely: (1) an accurate dose calculation algorithm to model the electron transport and dose deposition, (2) an optimization algorithm that solves the inverse problem, and (3) a delivery unit. This chapter explores the state-of-the-art methods of delivering EMET.

3.1 Bolus Conformal Therapy

The electron bolus is a tissue equivalent material that is customarily placed on the skin surface in order to provide extra scattering and energy degradation of the electron beam. Because of the irregular surface of the patient, the use of a spatially uniform electron beam is not always optimal. The irregular surfaces often lead to non uniform dose distributions within the target. Such non-uniformity is represented as hot spots (over-dosing) and cold spots (under-dosing). In addition, the variable depth of the distal surface of the planning target volume (PTV) causes overdosing of normal tissues that are adjacent to the PTV. These potential deficiencies can be eliminated with the use of bolus which offers useful advantages to the treatment planning due to its ability to compensate for the missing tissues. Bolus is often used to flatten out the irregular surfaces and to reduce the penetration of the electrons.

Since the variation in the bolus thickness corresponds to a variation in the practical electron range, a spatially dependent energy modulation can be achieved by the modulation of the bolus thickness. For example: energy modulation with a step as low as 0.2 MeV can be achieved because of its equivalence to a 1 mm bolus thickness. Hence, the custom-shaped bolus represents a means of EMET despite its frequent use in conventional three dimensional conformal therapy (3D-CRT) for forward treatment planning.

The methodology for computer aided design of electron bolus was initiated at M. D. Anderson Cancer Center (Houston, TX) by Low *et al.* [21]. Low *et al.* [21,22] designed bolus based on ray tracing from the electron source to the patient surface that tracks the distal surface of the PTV. The goal of the design is to have a total radiological thickness of (bolus+PTV) that is equivalent to the therapeutic range in water (R_{90}). The radiological thickness refers to the effective thickness accounting for the differences in

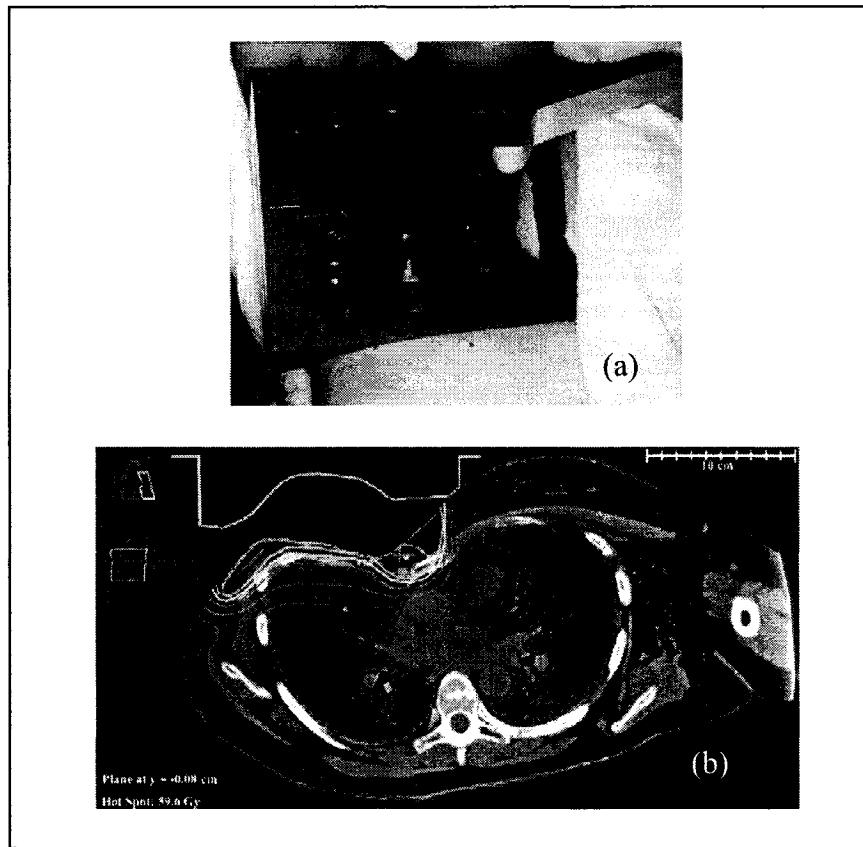


Figure 3-1: (a) Custom made bolus electron bolus for postmastectomy chest wall case. (b) Isodose distribution using bolus for 16 MeV electron beam. Reprinted with permission from Elsevier (from Perkins et al., *International Journal of Radiation Oncology Physics*; 2001).

tissue densities. Once the initial grid of bolus thicknesses is determined, it undergoes some design modifications in order to homogenize the dose distribution based on calculations that are performed using the pencil beam algorithm. The grid is then adjusted so that it smoothes the bolus thickness. Different operators were introduced to assist the optimal design of bolus. They have been implemented in a local treatment planning system at the M. D. Anderson Center [22,23].

The fabrication of the bolus to a high level accuracy is labour intensive and requires large milling machines that are not likely to be available in radiation therapy clinics. Therefore, in the case of M. D. Anderson Center, the final design is provided

electronically to a third party company that performs the milling and ship the custom-made bolus back to the institution.

After receiving the fabricated bolus, the patient undergoes another CT procedure with the bolus placed on him/her. It is important to verify the accuracy of the milling by verifying the positioning of the bolus and ensuring that minimum air gaps are present in order to avoid any perturbation to the planned dose distribution [23]. The dose distribution is then computed using the treatment planning system. Although the effects of the presence of bolus are measurable and consequently quantifiable, the quality assurance procedure does not require measurements that validate the 2-D dose distribution nor point dose measurements [23]. Rather, it assumes that the dose distribution calculated by the treatment planning system is accurate without further verification.

Results have been demonstrated for the applications of custom-made bolus at M. D. Anderson Cancer Center. Comparisons between conventional treatment planning and bolus technique were presented for different clinical sites including paraspinal muscles [22], post-mastectomy irradiation [24], and head and neck [23]. In these studies, the use of bolus technique showed modest improvements on the coverage of the PTV and reduced dose to the organs at risk (Fig. 3-1).

Although this technique was implemented for treatment of many patients [25], there are still some concerns regarding some of its disadvantages. Most notably, its dependence on the accuracy of the pencil beam algorithm which cannot calculate dose within 4% accuracy in conditions of tissue heterogeneities and surface irregularities. Because of this, Kudchadker *et al.* [26] reported that the dose spread in the PTV was found to be as much as 20% which violates the goal of maintaining the uniformity to within 10% limits [26]. It was suggested that further electron beam modulation is required to restore the dose uniformity [26]. However, although not available presently, beam modulation requires a considerable amount of resources that are similar to those required by IMRT.

Another disadvantage of the bolus technique is that it is labour-intensive and time consuming. It requires the procedure of outlining volumes from CT scans to be performed twice. Planning is also performed in two stages: preplanning and post-

planning. In addition, the quality assurance procedure requires extensive verification of treatment positioning to ensure the best possible fit which might cause the need for another round of refabrication of bolus.

It has been reported, also, that the use of the bolus technique raises a risk of developing complications due to the increase in the skin dose. Therefore, long-term follow up were suggested to assess the potential risk for skin fibrosis complications [24].

Finally, the use of bolus design technology is still limited and has not been widely implemented. Despite being available for more than a decade, none of the commercial treatment planning systems has adopted the automated bolus designing procedure. The technology remained localized in one region without feasible efforts to transfer it to widespread use.

3.2 Collimator-based Modulated Electron Therapy

3.2.1 Inverse treatment planning

In inverse planning, the beam parameters are optimized to match the prescribed dose distributions defined by an objective function that ranks the treatment plan merits. The objective function is formulated such that it reflects the treatment quality through clinically relevant criteria. These objectives could be either physical (which depend on measurable physical quantities) or biological (which depend on radiation response models). It is assumed that the objective function is dependent on the vector representing the beam modulation weights. This section presents a brief introduction to the optimization algorithms used for radiation therapy applications.

3.2.1.a Optimization algorithms

In radiation therapy, an optimization algorithm refers to a mathematical method that searches through successive iterations for the lowest objective function. The optimization usually starts with an initial guess of beam weights. It is then followed by modifying these weights to produce new dose data that is used to evaluate the objective function and its convergence. This procedure is repeated until the goals are met.

Searching for the optimum solution can be deterministic or stochastic. In the deterministic method, the algorithm modifies and approves different solutions based on predefined mathematical formulae. The stochastic method, on the other hand, approves

different iterates in a probabilistic manner. The deterministic method is by far faster than the stochastic one. However, the final solution obtained by the deterministic method is critically dependent on the initial values of the parameters which might lead to entrapment of the objective function in local minima. Such dependence is avoided by extensive searches throughout the solution space exhibited by the stochastic method which comes at the expense of the speed.

(1) Deterministic method: steepest gradient optimization

The steepest gradient method minimizes the objective function, $F(\mathbf{w})$, with respect to the weight vector \mathbf{w} , following these general steps:

- (1) Starting with an initial weight \mathbf{w}_n , a decent direction \mathbf{d}_n is computed by taking the gradient of the objective function at the current weight.
- (2) A feasible step λ is then calculated such that it satisfies the condition $F(\mathbf{w}_n + \lambda \times \mathbf{d}_n) < F(\mathbf{w}_n)$.
- (3) The weight is updated as $\mathbf{w}_{n+1} = \mathbf{w}_n + \lambda \times \mathbf{d}_n$.
- (4) The process is continued until the maximum number of iterations is achieved or until the relative change in the objective function is smaller than a cut-off value.

(2) Stochastic method: simulated annealing optimization

Simulated annealing is a process that is analogous to the physical annealing where a heated system is slowly cooled so that it reaches its lowest energy state. If the annealing concept is applied to the optimization, the global minimum is reached in the same way as a heated system reaches its final state. The optimization follows the analogy by corresponding the objective function to the free energy system while linking the optimization parameters to the physical system components. The correct functioning of the optimization requires concise representations of the objective function and the state space. In addition, the properly designed simulated annealing process should consist of three major components:

- (1) Generating function that keeps generating new solutions within a feasible range.
- (2) Acceptance function that determines whether the newly generated iterate is acceptable. This function applies the so-called Metropolis criterion

where it does not reject the inferior state immediately. Rather, even if the new objective function does not satisfy the convergence conditions, it might be accepted based on the Boltzmann probability (p_B):

$$p_B = e^{\frac{-\Delta F}{kT}} = e^{\frac{-[F(w_{new}) - F(w_{old})]}{kT}},$$

where ΔF is the difference in the objective function between the new and the old solutions, k is the Boltzmann constant, and T is the system temperature.

- (3) An annealing function that updates the system temperature which is crucial since it affects the probability of the acceptance of new solutions. The annealing scheme requires properly selected initial temperature, optimal cooling rate, and sampling sizes of iterations at each temperature step.

3.2.1.b Aperture vs. beamlet-based optimization

In IMRT, the inverse problem is solved based on the assumption that a broad beam could be divided into a number of small radiation beamlets (defined by MLC) which are modulated in an iterative process until the objectives are met. By varying the weights of the beamlets, the ideal dose distribution could be constructed after adding the contribution of each individual beamlet. The weights of the beamlets are converted into a 2-D intensity map that is deliverable using MLC. It is crucial to assume that the beamlet-by-beamlet addition is equal to the dose that is delivered by the leaf sequence. Although such assumption has been successful in IMRT, the scattering behavior of electrons makes this approach nearly impossible in the beam delivery for EMET. The effects of scattering and leakage severely distort the fluence profiles especially when small beamlets are used. The problem is even magnified when a certain beamlet is assigned a low weight while surrounded by high weight beamlets. To circumvent this problem, Lee *et al.* [27] proposed the use of a second optimization to account for the bremsstrahlung leakage electron scattering. However, the second optimization was reported to be computation intensive and time inefficient [28].

“Aperture-based” optimization was introduced as an alternative approach instead of the beamlet-based optimization [29,30]. In this approach, the use of intensity maps is

avoided by using a sequence of deliverable apertures that could be divided virtually into beamlet grid. A typical initial aperture as large as $7 \times 7 \text{ cm}^2$, compared to $1 \times 1 \text{ cm}^2$ beamlets, were reported suitable for EMET purposes [29]. Since the beamlet-based optimization has much more free parameters, the dose distribution that results from the beamlet-based optimization is expected to be better. However, when such a plan is undeliverable, aperture-based optimization offers an adequate alternative.

The use of pencil beam algorithm in the planning for EMET, delivered with any form of electron collimators, encounter a number of difficulties. The algorithm suffers from inherent limitations that reduce its accuracy in oblique incidence, extended air gaps, mixing of energies, and heterogeneous phantoms. Because of the dependence of the optimization process on accurate modeling of the beamlet (or aperture) calculation inside the patient geometry, Ma *et al.* [31] showed that the use of Monte Carlo algorithm as a calculation engine is more suitable for EMET.

3.2.2 Treatment delivery

3.2.2.a Using xMLC

Introducing x-ray multileaf collimators (xMLC) revolutionized the practice of radiation therapy. The xMLC allows the delivery of complex field shapes in rapid succession. Since it is computer controlled with the ability to deliver automatic leaf sequence, it offered an attractive approach to be used for electron beam collimation.

Different studies have investigated the possibility of utilizing the xMLC for isocentric delivery of electron beams. But because of the large air gap between the xMLC and the patient in addition to the presence of the scattering foil systems, the penumbra of the collimated electron beams was found too high. Klein *et al.* [32] concluded that the use of xMLC for electron beams in conventional linear accelerators is only acceptable for short source-surface distances (*SSDs*) that are less than 70 cm. Du Plessis *et al.* [33] favoured the use of even shorter *SSD* (60 cm) to provide a collimation suitable for electron planning. Therefore, isocentric treatments with the available xMLC are impossible.

However, the MM50 racetrack microtron, designed by Brahme [34], was reported to be a treatment machine that can produce highly collimated electron beams using xMLC with relatively sharp penumbra [35]. It uses a scanning beam technique that

avoids the need for the scattering foils. Having a treatment head that is filled with helium gas and a doubly focused xMLC that is only 35 cm above the isocenter, electron penumbra could be kept sufficiently small. Karlsson and Zackrisson [18,36,37] showed improvements in dose distribution in the patient for several applications by matching multileaf collimated of mixed electron and x-ray beams. Hence, the use of scanned electron beam has the potential capability for intensity and/or energy modulation of electron beams [16,20]. Nevertheless, the width of the dose kernels was reported to be excessively large at lower energies which limit their applications for electron modulation [25]. Also, scanned beam technology is not commonly used in clinical accelerators and this type of machine is only available at a handful centers around the world.

In order to use the xMLC as a means of electron modulation, significant changes are required to modify the commercially available treatment heads. Karlsson *et al.* [38] suggested replacing air atmosphere in the treatment head with helium, changing the position of the scattering foils, and lowering the xMLC plane so that the electron beam characteristics are clinically acceptable. The implementation of such modifications requires an unfeasible redesign of the complete treatment head and cannot be a simple upgradeable solution.

3.2.2.b Using eMLC

Similar to the adaptation of the xMLC, electron multileaf collimator (eMLC) was introduced to replace the need for labor intensive fabrication of custom blocking and to allow EMET delivery. The implementation of eMLC was initiated after the reported difficulties encountered with the possibility of using the existing xMLC for modulated electron therapy. Therefore, an alternative approach was introduced that employs the use of an electron specific MLC that is located approximately 40 cm closer to the patient than xMLC. Different prototypes of eMLC were constructed.

Ravindran *et al.* [39] designed a manual eMLC that could be added as an accessory to the Siemens Mevatron 15×15 cm² applicator. It consists of 30 pairs of low melting point alloy (LMA) with a leaf thickness of 1.6 cm, a leaf width of 0.48 cm, and a length of 12 cm. Aimed for the simplest application of eliminating the use of electron cutouts, the basic dosimetric properties of the eMLC were compared to those of the cutouts. That included depth dose curves, beam profiles, and output factors. However, the

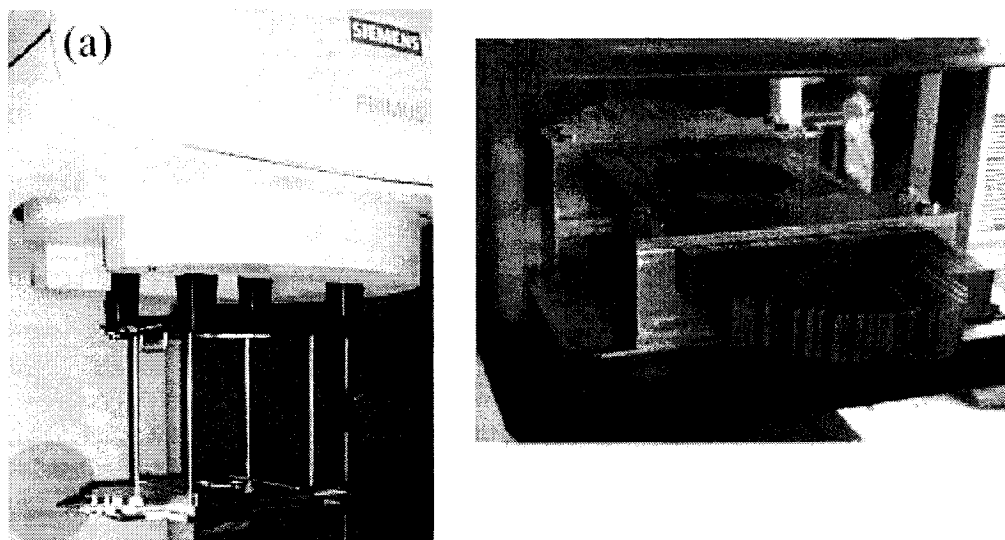


Figure 3-2: (a) Retractable eMLC designed at M.D. Andersson Cancer Center. Reprinted with permission from Medical Physics Publishing (from Hogstrom et al., *Medical Physics*; 2004). (b) eMLC prototype built at Stanford University. It is mounted on $25 \times 25 \text{ cm}^2$ applicator of Varian CL2100. Reprinted with permission from IOP publishing (from Ma et al., *Physics in Medicine and Biology*; 2000).

reported long time that is required to manually shape the irregular fields, along with an approximately 8 kg weight of the device, were considered major disadvantages of the eMLC. It did not show more appealing convenience over the use of cutouts.

Ma et al. [31] developed another prototype of manual eMLC (Fig. 3-2(b)) intended for the application of EMET (it was called in their study as modulated electron radiation therapy (MERT)). In their prototype, 30 steel leaf pairs were mounted on a steel frame attachable to the $25 \times 25 \text{ cm}^2$ applicator of Varian Clinac 2100C. Each leaf has straight ends with the dimensions of 0.48 cm width, 2.54 cm thickness, and 20 cm length. The eMLC, weighing more than 12 kg, gives an air-gap clearance of 10 cm above the surface of $SSD=100 \text{ cm}$ and is able to form a field size of $15.7 \times 15.7 \text{ cm}^2$. The characteristics of individual beamlets were investigated, especially for the purpose of forming large fields. When comparing a square field defined by the eMLC to the square field that is formed by the addition of multiple beamlets, results show fluctuations in the dose distributions under the field and an increased leakage dose outside the area projected

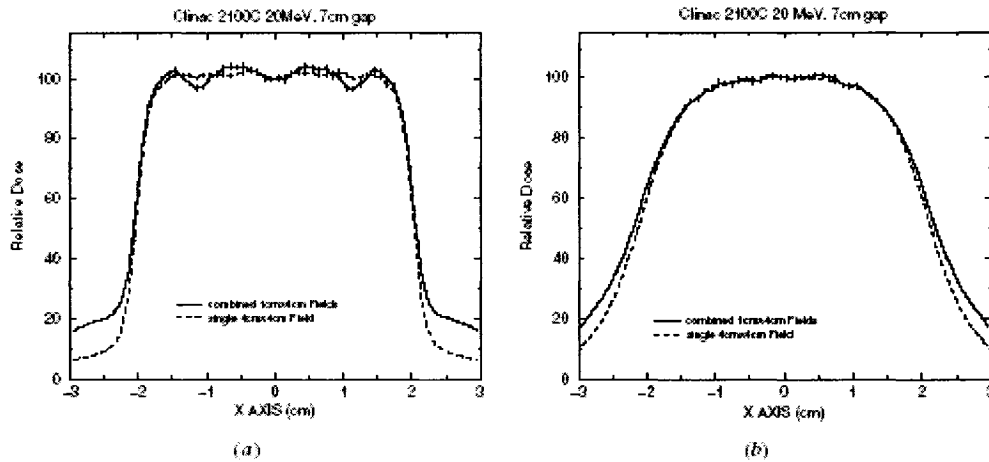


Figure 3-3: Monte Carlo calculated dose profiles in a water phantom for 20 MeV electron beams collimated by an eMLC of 1.5 cm thick tungsten leaves for a single 4 cm \times 4 cm electron field (dotted) and a 4 cm \times 4 cm field formed by four 1 cm \times 4 cm electron fields (solid line) (a) at surface; and (b) at 3 cm depth. Reprinted with permission of IOP publishing (from Ma *et al.*, *Physics in Medicine and Biology*; 2000)

by the field (Fig. 3-3). Part of their investigations included a comparison of the beamlet dose distributions in a heterogeneous medium between Monte Carlo calculations and pencil beam algorithm. They recommended the use of Monte Carlo calculations as dose calculation algorithm for EMET. Lee *et al.* [40] performed further investigations of the prototype where new specifications for eMLC were recommended. That included the use of 1.5 cm thick tungsten leaf, instead of the 2.54 cm thick steel, in order to reduce the leakage effects. The implementation of these recommendations have not yet been made nor clinically studied nor was there a discussion about automating the new collimator.

A different manual eMLC was constructed by Hogstrom *et al.* [41] with a retractable feature that, theoretically, allows for isocentric treatments and arc therapy in addition to the standard SSD treatments (Fig. 3-2(a)). Built to be compatible with a Siemens Primus linac, the eMLC consists of 21 pairs of rounded brass alloy leaves to project up to 20 \times 21 cm² if it is at the standard position. The leaf has a thickness of 3 cm, a length of 26 cm, and a width of 0.9 cm. This eMLC, unlike the ones previously mentioned, was not designed as an addition to the existing applicator. Rather it fits in a specially constructed treatment applicator. Comparisons between this model of eMLC

and the model designed by Ravindran *et al.* were shown for the basic dosimetric properties. Although such eMLC has the potential to work on an isocentric setup, the results were shown only for a normal beam incident with a gantry angle at 0° due to the weight of the eMLC that causes sagging of the gantry and/or the leaves. This represents a major concern for the potential use of this prototype. Also, the excessive length of the leaf in the direction of the leaf travel raises another concern when the eMLC is close to the patient for certain clinical situations such as parotid-neck treatments. In their conclusion, they planned to fabricate a final version with 2.0 cm thick and 0.5 wide tungsten leaves. In addition, there was a brief mention of the incorporation of motors that will be added to each individual leaf. As far as known, the final version is still under development.

Finally, plans for an automated eMLC were announced recently by Gauer *et al.* [42] who designed and studied a manual eMLC in Germany. The study focused on the characteristics of the leaf design and provided minimal discussions on the dosimetric properties of the beamlets defined by their model of eMLC. For example, variations of the x-ray jaws were mentioned as a mean of providing enhanced profile distribution but there was no mention of their impact on the beam output. Also, the proposed automated design will include trimmer bars between the x-ray jaws and the eMLC to reduce electron scattering above eMLC. However, the effects that result from these trimmer bars were neither measured nor simulated. The manual eMLC weighed approximately 20 kg with more weight that is expected due to the addition of motors and the extra electronics. The automated eMLC is being assembled by 3D Line Medical Systems (Schwarzenbruck, Germany).

3.2.3.c Summary

Using eMLC, EMET treatment plans were designed and showed superiority over 3D-CRT and IMRT treatments for some clinical cases [27,43]. However, these plans remained only as research topics without attempts of delivering them. Despite the numerous reports showing the potential use of eMLCs for EMET purposes, there is, yet, no available delivery unit that is able to perform sophisticated treatments obtained from an inverse treatment planning system. Moreover, the quality assurance of implementing this technique has not been discussed.

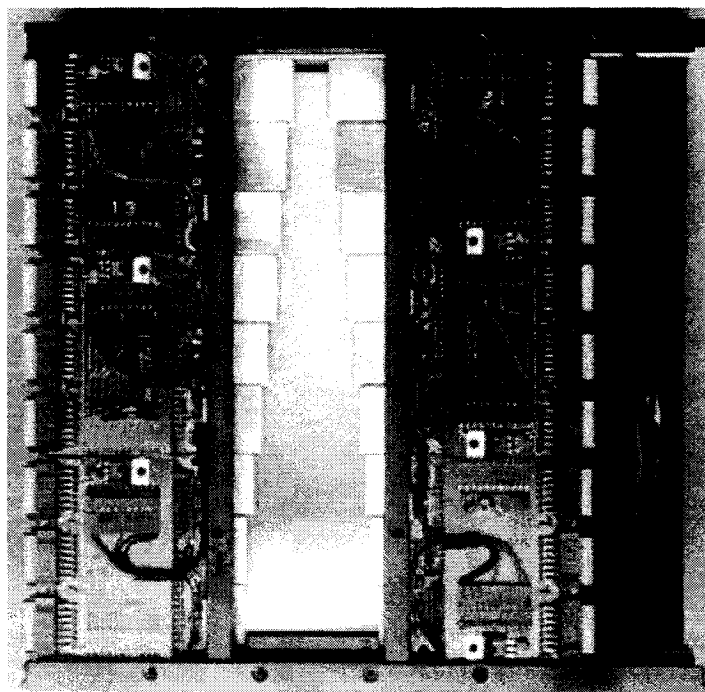


Figure 3-4: *Prototype of electron arc therapy-specific eMLC. The leaf resolution projects to 4 cm at isocenter. Reprinted with permission from Elsevier (from Leavitt et al., International Journal of Radiation Oncology Physics; 1989).*

3.3 Modulated Electron Arc Therapy (MEAT)

Modulated electron arc therapy (MEAT) refers to an irradiation technique that conforms the prescribed dose to a large superficial curved volume by utilizing multiple arced beams of differing energies and intensities. In this technique, the electron energy/intensity is partitioned in angular segments based on the depth of the PTV.

In the early proposed applications, MEAT was planned using cutout inserts with fixed shapes that are chosen to account for the variation in the patient radius of curvatures between transverse planes [44]. This approach assumes that the radius curvature within a single transverse plane is constant. Since this assumption neglects the considerable variations in the radius of curvatures, another approach was proposed. Leavitt *et al.* [45] demonstrated that in order to achieve a homogeneous dose distribution, the shape of the secondary collimator should be variable as a function of the angle of the arc. The shaping of variable fields was accomplished by a prototype computer-controlled eMLC (Fig. 3-4)

[45,46]. The advantages benefited by superposition of multiple electron energies showed an improved radial depth dose uniformity [47].

The treatment planning of MEAT requires each arc to have special specifications that include the angle of rotation, monitor unit prescriptions, collimator width, and nominal energy. Commercial treatment planning systems still lack adequate 3D dose calculation algorithms designed for that purpose. The eMLC designed for MEAT has a resolution of 4 cm which is considered coarse for electron planning. It was designed exclusively for MEAT and was not shown to be practical for other EMET applications. Also, rigorous quality assurance procedures have not been developed [25]. Despite these disadvantages, inversely optimized MEAT has the potential to be beneficial if accurate dose calculation algorithms are employed.

3.5 Conclusion

In this chapter, different methods of delivering EMET were presented. Although clinical utilities were demonstrated, these methods are unable to offer full solutions that can provide adequate tools for plan optimization, dose calculation, treatment delivery and quality assurance. In all the mentioned approaches, only partial solutions are proposed where they either propose a delivery tool without investigating the effects of the dose calculation algorithm or discuss the optimization without addressing the means of delivery. Until becoming commercially available, the proposed systems are not likely to achieve widespread applications.

The plan optimization in EMET is much more complex than in IMRT because of the significant effects of beam collimation on the dose distributions. Such dependence requires faithful calculation of the dose kernels that are fed in the optimization algorithms. In addition, having a simple accessible treatment delivery device that is fully automated is essential to demonstrate clinical significance. To achieve an optimal application of EMET, the effects of the delivery unit should be integrated in the optimization algorithm. Hence, the fundamentals of electron transport through the collimators and inside the heterogeneous patient should be used in post-hoc optimization step. This must be followed by verifying that the planned dose distribution is truly delivered through the development of careful quality assurance procedures.

References

- [1] A. Brahme, "Optimal setting of multileaf collimators in stationary beam radiation therapy," *Strahlenther. Onkol.* **164**, 343-350 (1988).
- [2] T. Bortfeld, J. Burkelbach, R. Boesecke, and W. Schlegel, "Methods of image reconstruction from projections applied to conformation radiotherapy," *Phys. Med. Biol.* **35**, 1423-1434 (1990).
- [3] D.J. Convery and S. Webb, "Generation of discrete beam-intensity modulation by dynamic multileaf collimation under minimum leaf separation constraints," *Phys. Med. Biol.* **43**, 2521-2538 (1998).
- [4] S. Webb, "Optimization by simulated annealing of three-dimensional, conformal treatment planning for radiation fields defined by a multileaf collimator: II. Inclusion of two-dimensional modulation of the x-ray intensity," *Phys. Med. Biol.* **37**, 1689-1704 (1992).
- [5] T.R. Mackie, T.W. Holmes, P.J. Reckwerdt, and J. Yang, "Tomotherapy: optimized planning and delivery of radiation therapy," *Int. J. Imaging Syst. Technol.* **6**, 43-55 (1995).
- [6] C.X. Yu, M.J. Symons, M.N. Du, A.A. Martinez, and J.W. Wong, "A method for implementing dynamic photon beam intensity modulation using independent jaws and a multileaf collimator," *Phys. Med. Biol.* **40**, 769-787 (1995).
- [7] C.C. Ling, C. Burman, C.S. Chui, G.J. Kutcher, S.A. Leibel, T. LoSasso, R. Mohan, T. Bortfeld, L. Reinstein, S. Spirou, X.H. Wang, Q. Wu, M. Zelefsky, and Z. Fuks, "Conformal radiation treatment of prostate cancer using inversely-planned intensity-modulated photon beams produced with dynamic multileaf collimation," *Int. J. Radiat. Oncol. Biol. Phys.* **35**, 721-730 (1996).
- [8] A.L. Boyer, P. Geis, W. Grant, and M. Carol, "Modulated beam conformal therapy for head and neck tumors," *Int. J. Radiat. Oncol. Biol. Phys.* **39**, 227-236 (1997).
- [9] D. Verellen, N. Linthout, D. van den Berge, A. Bel, and G. Storme, "Initial experience with intensity-modulated conformal radiation therapy for treatment of the head and neck region," *Int. J. Radiat. Oncol. Biol. Phys.* **39**, 99-114 (1997).
- [10] K. Sultanem, H.K. Shu, P. Xia, C. Akazawa, J.M. Quivey, L.J. Verhey, and K.K. Fu, "Three-dimensional intensity-modulated radiotherapy in the treatment of nasopharyngeal carcinoma: the University of California-San Francisco experience," *Int. J. Radiat. Oncol. Biol. Phys.* **48**, 711-722 (2000).

- [11] R.A. Price, G.E. Hanks, S.W. McNeeley, E.M. Horwitz, and W.H. Pinover, "Advantages of using noncoplanar vs. axial beam arrangements when treating prostate cancer with intensity-modulated radiation therapy and the step-and-shoot delivery method," *Int. J. Radiat. Oncol. Biol. Phys.* **53**, 236-243 (2002).
- [12] E. Glatstein, "Intensity-modulated radiation therapy: the inverse, the converse, and the perverse," *Semin. Radiat. Oncol.* **12**, 272-281 (2002).
- [13] X. Mu, L. Olofsson, M. Karlsson, R. Sjogren, and B. Zackrisson, "Can photon IMRT be improved by combination with mixed electron and photon techniques?," *Acta Oncol.* **43**, 727-735 (2004).
- [14] J.G. Li, S.S. Williams, D.R. Goffinet, A.L. Boyer, and L. Xing, "Breast-conserving radiation therapy using combined electron and intensity-modulated radiotherapy technique," *Radiother. Oncol.* **56**, 65-71 (2000).
- [15] S.K. Das, M. Bell, L.B. Marks, and J.G. Rosenman, "A preliminary study of the role of modulated electron beams in intensity modulated radiotherapy, using automated beam orientation and modality selection," *Int. J. Radiat. Oncol. Biol. Phys.* **59**, 602-617 (2004).
- [16] E.P. Lief, A. Larsson, and J.L. Humm, "Electron dose profile shaping by modulation of a scanning elementary beam," *Med. Phys.* **23**, 33-44 (1996).
- [17] S. Hyodynmaa, A. Gustafsson, and A. Brahme, "Optimization of conformal electron beam therapy using energy- and fluence-modulated beams," *Med. Phys.* **23**, 659-666 (1996).
- [18] B. Zackrisson and M. Karlsson, "Matching of electron beams for conformal therapy of target volumes at moderate depths," *Radiother. Oncol.* **39**, 261-270 (1996).
- [19] M.A. Ebert and P.W. Hoban, "Possibilities for tailoring dose distributions through the manipulation of electron beam characteristics," *Phys. Med. Biol.* **42**, 2065-2081 (1997).
- [20] M.G. Karlsson, M. Karlsson, and B. Zackrisson, "Intensity modulation with electrons: calculations, measurements and clinical applications," *Phys. Med. Biol.* **43**, 1159-1169 (1998).
- [21] D.A. Low, G. Starkschall, S.W. Bujnowski, L.L. Wang, and K.R. Hogstrom, "Electron bolus design for radiotherapy treatment planning: bolus design algorithms," *Med. Phys.* **19**, 115-124 (1992).
- [22] D.A. Low, G. Starkschall, N.E. Sherman, S.W. Bujnowski, J.R. Ewton, and K.R. Hogstrom, "Computer-aided design and fabrication of an electron bolus for treatment of the paraspinal muscles," *Int. J. Radiat. Oncol. Biol. Phys.* **33**, 1127-1138 (1995).

- [23] R.J. Kudchadker, J.A. Antolak, W.H. Morrison, P.F. Wong, and K.R. Hogstrom, "Utilization of custom electron bolus in head and neck radiotherapy," *J. Appl. Clin. Med. Phys.* **4**, 321-333 (2003).
- [24] G.H. Perkins, M.D. McNeese, J.A. Antolak, T.A. Buchholz, E.A. Strom, and K.R. Hogstrom, "A custom three-dimensional electron bolus technique for optimization of postmastectomy irradiation," *Int. J. Radiat. Oncol. Biol. Phys.* **51**, 1142-1151 (2001).
- [25] K.R. Hogstrom, J.A. Antolak, R.J. Kudchadker, C.M. Ma, and D.D. Leavitt, "Modulated Electron Therapy," in: *Intensity-Modulated Radiation Therapy, The State of the Art: Proceedings of the 2003 Summer School*, edited by J.R. Palta, T.R. Mackie (Medical Physics Publishing, Madison, 2003), pp. 749-786.
- [26] R.J. Kudchadker, K.R. Hogstrom, A.S. Garden, M.D. McNeese, R.A. Boyd, and J.A. Antolak, "Electron conformal radiotherapy using bolus and intensity modulation," *Int. J. Radiat. Oncol. Biol. Phys.* **53**, 1023-1037 (2002).
- [27] M.C. Lee, J. Deng, J. Li, S.B. Jiang, and C.M. Ma, "Monte Carlo based treatment planning for modulated electron beam radiation therapy," *Phys. Med. Biol.* **46**, 2177-2199 (2001).
- [28] J. Deng, M.C. Lee, and C.M. Ma, "A Monte Carlo investigation of fluence profiles collimated by an electron specific MLC during beam delivery for modulated electron radiation therapy," *Med. Phys.* **29**, 2472-2483 (2002).
- [29] S.B. Jiang, T. Pawlicki, and C.-M. Ma, An aperture-based inverse planning algorithm for modulated electron radiation therapy, in: *Engineering in Medicine and Biology Society, 2000. Proceedings of the 22nd Annual International Conference of the IEEE*, Vol. 1 (2000) 116-118 vol.111.
- [30] S.B. Jiang, T. Pawlicki, E. Gracia, T. Guerrero, M.C. Lee, J.S. Li, J. Deng, D.R. Goffinet, A.L. Boyer, and C.M. Ma, "Modulated electron radiation therapy: A new treatment modality," *Int. J. Radiat. Oncol. Biol. Phys.* **48**, 218 (2000).
- [31] C.M. Ma, T. Pawlicki, M.C. Lee, S.B. Jiang, J.S. Li, J. Deng, B. Yi, E. Mok, and A.L. Boyer, "Energy- and intensity-modulated electron beams for radiotherapy," *Phys. Med. Biol.* **45**, 2293-2311 (2000).
- [32] E.E. Klein, Z. Li, and D.A. Low, "Feasibility study of multileaf collimated electrons with a scattering foil based accelerator," *Radiother. Oncol.* **41**, 189-196 (1996).
- [33] F.C.P. du Plessis, A. Leal, S. Stathakis, W. Xiong, and C.M. Ma, "Characterization of megavoltage electron beams delivered through a photon multi-leaf collimator (pMLC)," *Phys. Med. Biol.* **51**, 2113-2129 (2006).

- [34] A. Brahme, "Design principles and clinical possibilities with a new generation of radiation therapy equipment. A review," *Acta Oncol.* **26**, 403-412 (1987).
- [35] M. Karlsson, H. Nystrom, and H. Svensson, "Electron beam characteristics of the 50-MeV racetrack microtron," *Med. Phys.* **19**, 307-315 (1992).
- [36] M. Karlsson and B. Zackrisson, "Matching of electron and photon beams with a multi-leaf collimator," *Radiother. Oncol.* **29**, 317-326 (1993).
- [37] M. Karlsson and B. Zackrisson, "Exploration of new treatment modalities offered by high energy (up to 50 MeV) electrons and photons," *Radiother. Oncol.* **43**, 303-309 (1997).
- [38] M.G. Karlsson, M. Karlsson, and C.M. Ma, "Treatment head design for multileaf collimated high-energy electrons," *Med. Phys.* **26**, 2161-2167 (1999).
- [39] B.P. Ravindran, I.R. Singh, S. Brindha, and S. Sathyan, "Manual multi-leaf collimator for electron beam shaping--a feasibility study," *Phys. Med. Biol.* **47**, 4389-4396 (2002).
- [40] M.C. Lee, S.B. Jiang, and C.M. Ma, "Monte Carlo and experimental investigations of multileaf collimated electron beams for modulated electron radiation therapy," *Med. Phys.* **27**, 2708-2718 (2000).
- [41] K.R. Hogstrom, R.A. Boyd, J.A. Antolak, M.M. Svatos, B.A. Faddegon, and J.G. Rosenman, "Dosimetry of a prototype retractable eMLC for fixed-beam electron therapy," *Med. Phys.* **31**, 443-462 (2004).
- [42] A.T. Gauer, A.D. Albers, A.F. Cremers, A.R. Harmansa, A.R. Pellegrini, and A.R. Schmidt, "Design of a computer-controlled multileaf collimator for advanced electron radiotherapy," *Phys. Med. Biol.* **51**, 5987-6003 (2006).
- [43] C.M. Ma, M. Ding, J.S. Li, M.C. Lee, T. Pawlicki, and J. Deng, "A comparative dosimetric study on tangential photon beams, intensity-modulated radiation therapy (IMRT) and modulated electron radiotherapy (MERT) for breast cancer treatment," *Phys. Med. Biol.* **48**, 909-924 (2003).
- [44] K.R. Hogstrom, R.G. Kurup, A.S. Shiu, and G. Starkschall, "A two-dimensional pencil-beam algorithm for calculation of arc electron dose distributions," *Phys. Med. Biol.* **34**, 315-341 (1989).
- [45] D.D. Leavitt, J.R. Stewart, J.H. Moeller, W.L. Lee, and G.A. Takach, Jr., "Electron arc therapy: design, implementation and evaluation of a dynamic multi-vane collimator system," *Int. J. Radiat. Oncol. Biol. Phys.* **17**, 1089-1094 (1989).
- [46] D.D. Leavitt, L. Earley, and J.R. Stewart, "Design and production of customized field shaping devices for electron arc therapy," *Med. Dosim.* **15**, 25-31 (1990).

- [47] D.D. Leavitt, J.R. Stewart, and L. Earley, "Improved dose homogeneity in electron arc therapy achieved by a multiple-energy technique," *Int. J. Radiat. Oncol. Biol. Phys.* **19**, 159-165 (1990).

Chapter 4

Monte Carlo-based Inverse Treatment Planning for Energy Modulated Electron Therapy

In order to implement energy modulated electron therapy (EMET) clinically, we propose a simplified collimation system that is easily automated and integrated with a Monte Carlo-based inverse treatment planning. To achieve this goal, a planning process was built which involves developing (1) a Monte Carlo treatment planning system [see Appendix A] and (2) an optimization algorithm. We chose to improve the existing in-house developed optimization algorithm that was initially programmed in our department to study x-ray intensity modulated radiation therapy (IMRT) planning [1]. This research tool has been modified in order to communicate with the Monte Carlo treatment planning system. Different routines have been introduced to obtain the dose deposition coefficients (DDCs) for each organ, required to perform the optimization, from the Monte Carlo calculated dose distributions.

In addition to the treatment planning requirement, a delivery method was also investigated. The few leaf electron collimator (FLEC), fitted on a standard electron applicator and backed up by the x-ray collimator, was introduced to facilitate the delivery of a flexible combination of different energies and intensities. Its light-weight design accompanied by the proposed automation, gives the FLEC the potential to overcome the limitations of other proposed electron collimation systems. Also, the rectangular fields (fieldlets) that are delivered by FLEC can be fully simulated through the beam configuration and the patient geometry. Using the detailed information of realistic deliverable beam ports, the optimization process determines the weights in the form of the prescribed number of monitor units given to each fieldlet. This “aperture-based”

optimization was recommended, as discussed in the previous chapter, as a realistic approach for optimizing EMET plans.

In this chapter, we present a paper published in *Physics in Medicine and Biology*. It discusses the feasibility of using the FLEC for EMET purposes. It describes the general vision of the FLEC and shows the structure of our approach for obtaining EMET plans. The ability to perform EMET treatment planning is demonstrated. Comparisons with conventional treatment planning are shown for a theoretical target in a homogeneous water phantom. Also, the advantages of using EMET for a head & neck treatment case are shown.

Title: Monte Carlo-based modulated electron beam treatment planning using a few leaf electron collimator – feasibility study

Authors: Khalid Al-Yahya, Dimitre Hristov, Frank Verhaegen, and Jan Seuntjens

Published in Physics in Medicine and Biology vol. 50 p. 847-857 (2005).

Submitted: 6 July 2004; revised: 14 October 2004; published: 17 February 2005.

Abstract

Energy modulated electron beam therapy with conventional clinical accelerators has lagged behind photon IMRT despite its potential to achieve highly conformal dose distributions in superficial targets. One of the reasons for this is the absence of an automated collimating device that allows for the flexible delivery of a series of variable field openings. Electron-specific multileaf collimators attached to the bottom of the applicator require the use of a large number of motors and suffer from being relatively bulky and impractical for head and neck sites. In this work we investigate the treatment planning aspects of a proposed “few-leaf” electron collimator (FLEC) that consists of four motor-driven trimmer bars at the end of the applicator. The device is designed to serve as an accessory to standard equipment and allows for the shaping of any irregular field by combination of rectangular fieldlets. Using a Monte Carlo model of the FLEC, dose distributions are optimized using a simulated annealing inverse planning algorithm based on a limited number of Monte Carlo pre-generated, realistic phantom-specific dose kernels and user-specified dose-volume constraints. Using a phantom setup with an artificial target enclosed by organs at risk (OAR) as well as using a realistic patient case we demonstrate that highly conformal distributions can be generated. Estimates of delivery times are made and show that a full treatment fraction can be kept to 15 minutes or less.

4.1 Introduction

Energy Modulated Electron Therapy (EMET) has the ability to provide conformal dose distributions to superficial tumors for which it could be competitive to the intensity modulated radiation therapy (IMRT). The high surface dose followed by a steep fall-off make the electron beams well suited for treating shallow targets. However, EMET has not yet been clinically used to its full potential in contrast to photon IMRT. The main reasons for this lag in clinical implementation are: (1) the lack of dosimetric accuracy of electron pencil beam algorithms in the presence of heterogeneities and beam modifiers and (2) the absence of a practical automated collimation device that allows the delivery of series of different field openings (fieldlets) during one treatment. Although a high degree of accuracy of the dose calculation could be achieved if Monte Carlo techniques are used

[2-4], the development of a beam shaping device that is able to preserve the electron beam characteristics and yet allow for flexible use of multiple fieldlets remains challenging.

In recent years, significant efforts have addressed the feasibility, implementation and clinical utility of EMET which employs a thin-leaf multileaf collimator attached onto a frame at the bottom of an existing electron applicator [5-10]. To automate such collimator in a clinical setting, this approach requires the presence of a large number of motors at the bottom of the electron applicator and suffers from being relatively bulky and impractical to handle.

The use of inverse techniques for treatment planning of EMET is more complex than in photon beam IMRT since collimation has a profound effect on electron scattering and the dose gradients in a specific sub-field. In addition, accurate dose calculations in and near patient heterogeneities are essential for a successful application of EMET. Having detailed information about the effect of both the collimation devices and the complex patient geometry on the dose provided to the optimization algorithm would lead to a truly optimal treatment plan. Hence, the output and the dose distribution realized through the combination of multiple sub-fields requires the electron transport to be faithfully modeled through the collimating system and inside the patient. Any optimization algorithm that does not make use of realistic dose deposition kernel data will inevitably produce segment weights that lead to suboptimal and/or undeliverable dose distributions.

In this work we introduce an approach to deliver EMET plans using a simplified model for an automated collimation device. This feasibility study is based on Monte Carlo calculations where the fundamentals of electron transport and scattering through collimating devices and in the heterogeneous patient are all taken into account.

4.2 Materials and Method

4.2.1 Design of few leaf electron collimator

To facilitate the formation of irregular electron fields and to allow the flexible combination of different energies and intensities, a few leaf electron collimator (FLEC) is proposed as an add-on accessory that could fit on a light-weight frame at the bottom of an

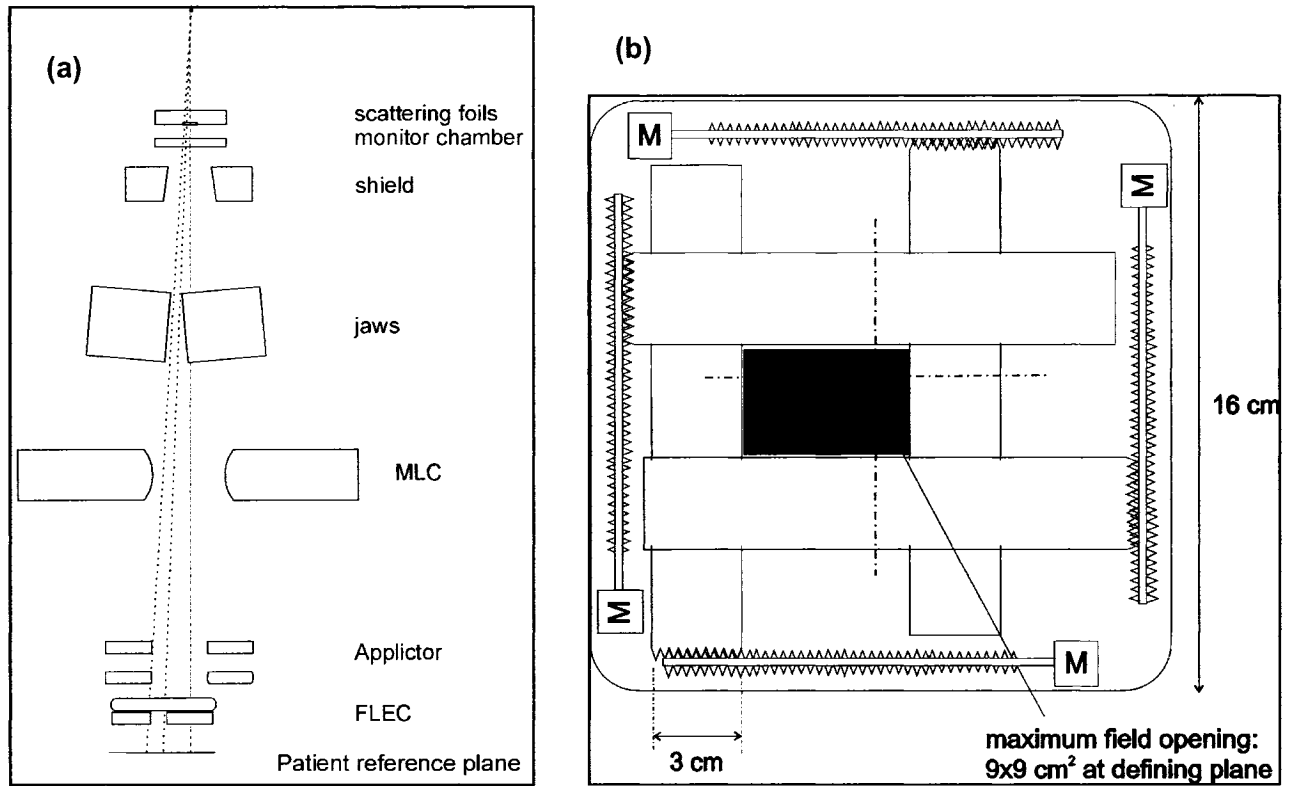


Figure 4-1: (a) Position of few-leaf collimator (FLEC) relative to other components in the accelerator (not to scale). (b) Schematic drawing of beam's eye view of FLEC.

electron applicator. In its most basic appearance (as shown in Fig. 4-1), this collimator consists of four blades (or trimmer bars) driven by motors so as to form arbitrary square or rectangular fields with an area between zero and nominally $9 \times 9 \text{ cm}^2$ (for the $15 \times 15 \text{ cm}^2$ electron applicator) and between zero and $14 \times 14 \text{ cm}^2$ (for the $20 \times 20 \text{ cm}^2$ electron applicator). Any irregular irradiation field can be made up by a combination of rectangular and square fields which possibly could involve the use of collimator rotation in a more evolved stage. The function of the FLEC is an automated final re-collimation of electron fields, previously collimated by jaws and/or the photon MLC that will be used as backup collimation devices. Hence, the blades, made of copper, can be relatively thin. In our study, their thickness was 1.5 cm and their width was 3 cm. To first order, the delivery of complex dynamic electron fields will be performed in a step-and-shoot approach, whereby every sub-field is formed by simultaneous collimation of the electron

beam by the jaws and the FLEC. We verified the ability of our clinical accelerators to dynamically control jaws when run in electron mode.

4.2.2 Monte Carlo calculations

In this study, the BEAM/EGSnrc [11] Monte Carlo code was used to simulate a CL2300 CD linear accelerator for the electron energies 6, 9, 12, 15, 18 and 22 MeV as well as for the photon energies of 6 and 18 MV. The transport parameters used in EGS accelerator simulations were E_{CUT}= A_E= 700 keV cutoff for electron transport, P_{CUT}= A_P= 10 keV for photon transport, and the electron step is 1% (i.e. ESTEPE= 0.01). After validation of the simulated beams against standard dosimetric data that includes the validation of the model in the presence of the beam modifiers, the Monte Carlo model was used to generate a master phase space file above the jaws for all energies. The procedure for the selection and calculation of fieldlet arrangement is conducted as follows:

- 1) A user-specified number of fieldlets is geometrically selected and positioned to conform the shape of the projected target. The fieldlets are chosen such that they are matched at the edges of the projected 3D volume of the PTV. An algorithm for optimizing the best fieldlet configuration based on the 3D PTV contour is being developed. For the purpose of this feasibility study, the fieldlets were selected manually.
- 2) Using the master phase space file, we proceeded with the simulation of the fieldlet-specific jaw openings as well as with the lower part of the accelerator including the FLEC. For each fieldlet setting of FLEC, the secondary jaws are set so as to project an opening equal to the one projected by the FLEC plus a margin of 0.5 cm on all sides. The phase space file of a fully simulated fieldlet, for all energies, is scored at a source-surface distance (*SSD*) of 95 cm.
- 3) The final phase space file of the fieldlet is then transported through the patient geometry using the XVMC code [12,13]. The patient is modeled by converting the CT-data into a density matrix with a size of 128×128× (number of slices) with the dimensions of the voxel size varying from 0.25 to 0.35 cm.
- 4) Once the dose distribution of each fieldlet is generated, a Monte Carlo dose distribution given in absorbed dose to tissue per particle is converted to absorbed dose to tissue per monitor unit. This is obtained using energy-dependent calibration factors

obtained from simulations that are performed under accelerator calibration conditions ($10 \times 10 \text{ cm}^2, z_{max}$). The Monte Carlo calculated dose distribution provided by each fieldlet -after it is “properly” normalized- represents the dose deposition kernel whose weight is modulated by the optimization algorithm. The number of simulated particle histories was chosen to achieve a statistical uncertainty on the dose calculation of 1% or less per fieldlet.

4.2.3 Treatment plan optimization

Figure 4-2 shows a schematic diagram of the inverse treatment planning system. The optimization is performed using the simulated annealing (SA) algorithm proposed by Sait and Youssef [14]. The optimizer selects the fieldlets, their energies, and their associated intensities that correspond to the optimal plan while the rejected fieldlets receive the weight of zero.

The dose-volume objective function, $F^{DV}(\mathbf{w})$, is represented by

$$F^{DV}(\mathbf{w}) = F_{TV}^D(\mathbf{w}) + F_{OAR}^V(\mathbf{w}) \quad (4-1)$$

where \mathbf{w} stands for the array of fieldlet weights, $F_{TV}^D(\mathbf{w})$ represents the (dose-based) target objective term and $F_{OAR}^V(\mathbf{w})$ represents the (volume-based) organs at risk (OAR) objective term. The objective functions are calculated as follows:

$$F_{TV}^D(\mathbf{w}) = \pi_{TV}^{max} \sum_{p \in TV} \Theta(D_{TV,p}(\mathbf{w}) - D_{TV}^{max}) \left[\frac{D_{TV,p}(\mathbf{w}) - D_{TV}^{max}}{D_{TV}^{max}} \right]^2 + \pi_{TV}^{min} \sum_{p \in TV} \Theta(D_{TV}^{min} - D_{TV,p}(\mathbf{w})) \left[\frac{D_{TV}^{min} - D_{TV,p}(\mathbf{w})}{D_{TV}^{min}} \right]^2, \text{ and} \quad (4-2)$$

$$F_{OAR}^V(\mathbf{w}) = \sum_i \pi_{OAR_i} \left[\frac{\sum_{p \in OAR_i} \Theta(D_{OAR_i,p}(\mathbf{w}) - D_{OAR_i}^{max}) dV - V_{OAR_i}^{max}}{V_{OAR_i}} \right]^2, \quad (4-3)$$

where π_{TV}^{max} and π_{TV}^{min} refer to the penalty parameters of the target maximum and minimum dose constraints respectively, Θ defines the Heaviside or step function, and $D_{TV,p}(\mathbf{w})$ is

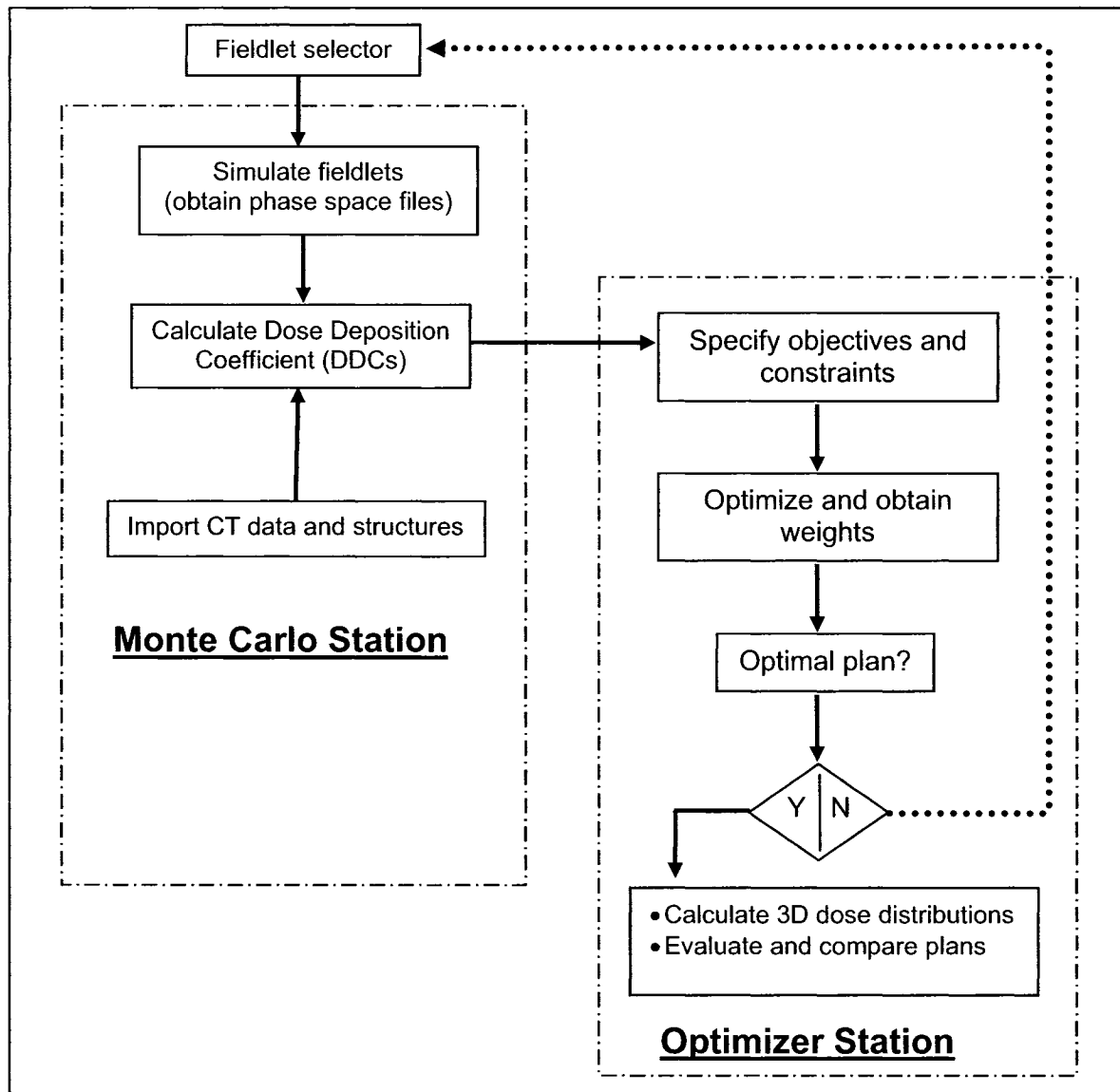


Figure 4-2: A schematic diagram of the current EMET procedure.

the dose deposited to point p of the target (denoted by TV) which contains a total of N_{TV} dose points. The dose to the target volume is constrained by the user-specified maximum and minimum dose D_{TV}^{max} and D_{TV}^{min} and relevant dose-volume relations for critical organs are specified by the dose-volume constraints of $(D_{OAR_l}^{max}, V_{OAR_l}^{max})$, where l labels all the organ constraints. Each constraint in the OAR is assigned a penalty value π_{OAR} that weighs the individual penalty contribution to the overall objective function.

The optimization algorithm was developed in an in-house built inverse treatment planning system that is developed within a visual software environment (AVS 5.4, Advanced Visual Systems, MA), running under SUSE LINUX. Software has been developed to interface the optimizer with the Monte Carlo calculated kernels so that the dosimetric data as well as the contour data required for the optimization algorithm could be extracted. The software also extracts the dose deposition coefficients (DDCs) which define the relative dose contribution from each fieldlet to each voxel contained in a specific contour. Moreover, the optimal fluence data obtained by the optimization algorithm are interfaced again with the kernels and then fed back to the clinical planning system (CadPlan 6.2.7) to display the final dose distribution. Another optimization algorithm, based on the deterministic steep dose volume histogram (DVH) minimization [15], has been developed within the same environment and objective function. It will be used for future studies for comparison with the simulated annealing algorithm to check the ability of both of the two algorithms to achieve the optimum optimization goals. That would include the study of the effect of the dependence of the generated fieldlet weights on the initial condition that might result in entrapment in a local minimum of the objective function if the deterministic approach is used.

Note that, since we work *a priori* with realistic and deliverable beam port dose distributions, there are no additional steps involved (analogous to an MLC leaf sequence calculator in IMRT) in determining the delivery of the distribution. The combined dose distribution is also truly optimized since the effects of both the presence of the heterogeneities as well as the bremsstrahlung produced by the collimation device are taken into account without the need to correct the final dose distribution for the leakage and transmission. As shown in Fig. 4-2, in the event that no convergence can be achieved

Structure	Dose (Gy)	Volume (%)	Penalty Value
Target	50	100	1
Target	60	0	1
Organ 1	40	2	0.3
Organ1	30	10	0.3
Organ 2	40	2	0.3
Organ 2	30	10	0.3

Table 4-1: Target dose and organ dose-volume levels in EMET optimization for the phantom case.

in the optimization process with the existing fieldlets new beams have to be added and the optimization process repeated. An example of such a case could be the need to reduce skin dose through the use of one or more conventionally shaped photon beams. As only a limited number of additional fieldlets would be required, the incremental time needed for this process is limited.

4.2.4 Treatment planning details

4.2.4.a Simple water phantom

We have planned for EMET on a three dimensional homogeneous solid water phantom geometry as well as for a realistic head and neck case. For the homogeneous phantom case, contours and CT data were acquired from the CART files, the file format used by CadPlan treatment planning system. We used a phantom scanned through CT to emulate the planning procedure where our calculations will be performed. The target was drawn to be surrounded by critical structures shown in Fig. 4-3. The lateral extent of the target was 8 cm and the inferior-superior extent was 6 cm while the depth varies laterally. The isocenter was placed at the surface so that the phantom is at an SSD 100 cm. With each electron energy, five fieldlets were simulated: two of them were adjacent to cover the PTV laterally (along x -axis) with a size of $4.5 \times 7 \text{ cm}^2$ each; two were chosen to cover the PTV widely (along z -axis) with a size of $9 \times 3.5 \text{ cm}^2$, and one fieldlet that was of the size of $9 \times 7 \text{ cm}^2$ to properly cover the PTV. Table 4-1 summarizes the dose and dose-volume constraints prescribed for this case.

4.2.4.b Head and neck case

For the head and neck case, we generated two plans: (1) the conventional tangential wedged photon beams with cutout-shaped electron boost and (2) EMET with four electron fields in addition to the wedged photon beams. In plan 1, the dose

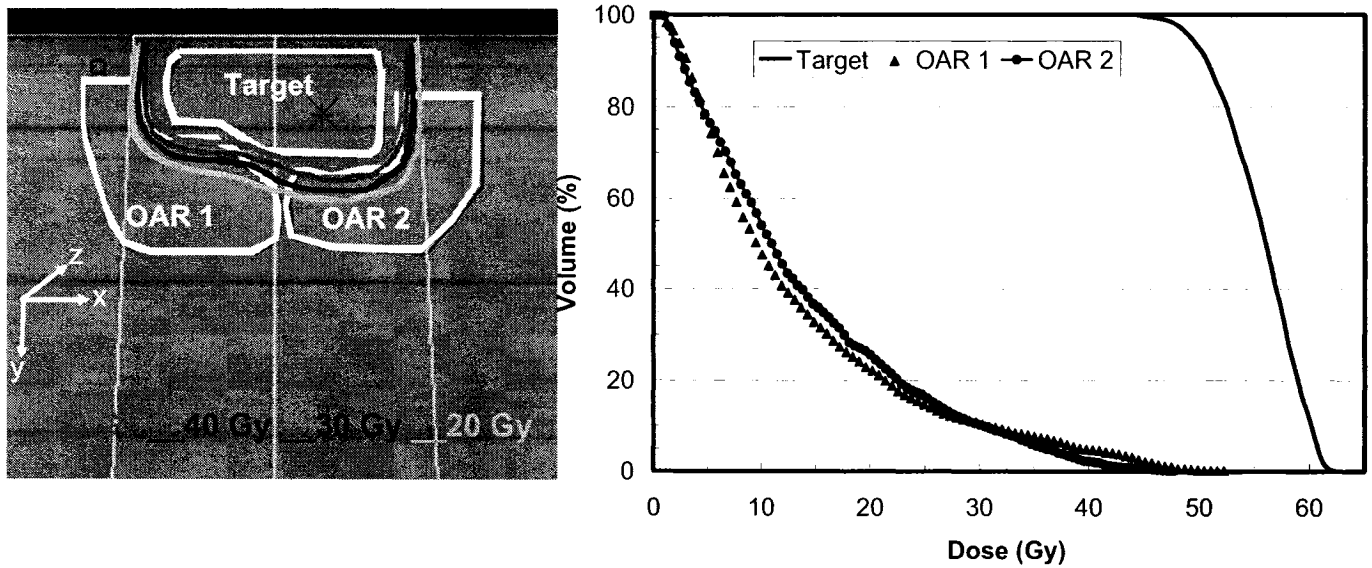


Figure 4-3: Dose distribution of an optimized EMET plan and DVHs for a hypothetical target and two organs at risk surrounding the PTV in a homogenous solid water phantom scanned by CT (PTV is outlined in yellow).

distribution was calculated after the simulation of the MLC-shaped wedged beams using our in-house Monte Carlo-based treatment planning system. We acquired the beam modifiers as well as the monitor unit settings to perform the simulation for each beam and add the individual normalized dose distributions to be displayed in the clinical treatment planning system. In plan 2, the four electron fields were 9, 12, 15, 18 MeV with 6 fieldlets each such that the PTV is fully covered. In addition, we considered each photon field as a fieldlet and allowed the optimization algorithm to decide whether or not to use its contribution in the final plan.

4.3 Results and Discussion

4.3.1 Homogeneous phantom

Using our automated EMET system, we calculated the dose distribution for an imaginary PTV outlined in a homogeneous solid water phantom that has been scanned by CT. Fig 4-3(a) shows the conformity of the isodose distribution obtained by EMET at the isocenter slice based on a 50 Gy prescription. The corresponding DVHs are shown in Fig. 4-3(b) for the PTV and the OARs. The DVH confirms the coverage of the PTV with the

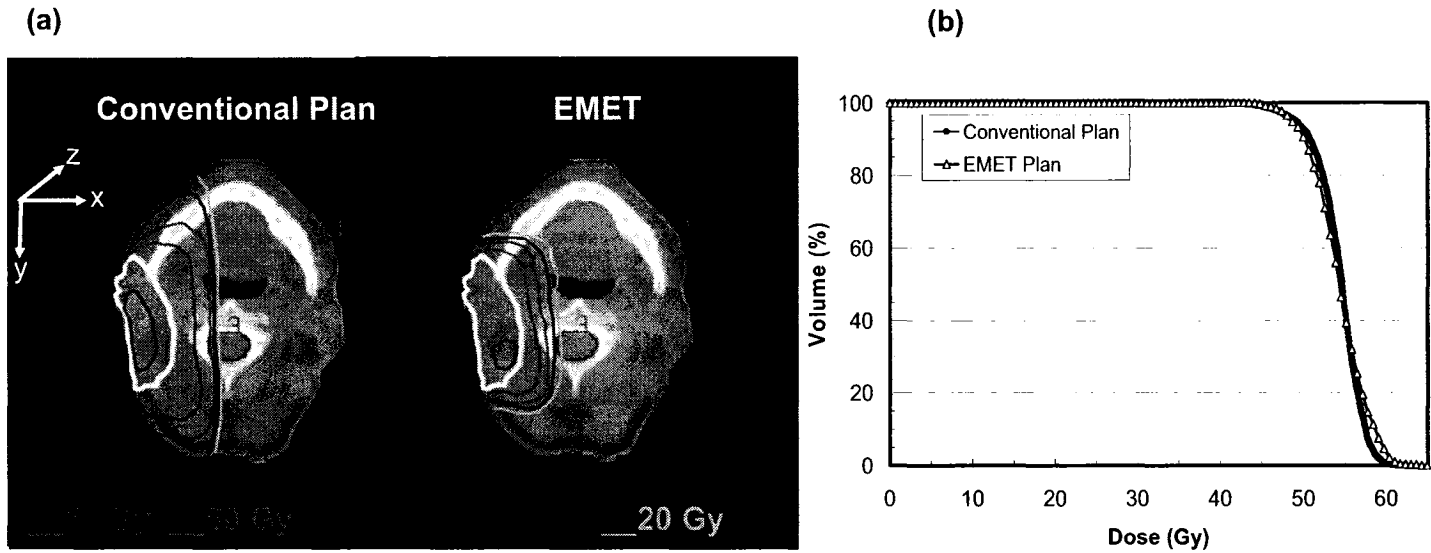


Figure 4-4: Comparison of (a) isodose distributions and (b) DVH for an outlined target using conventional two AP-PA wedged, MLC-shaped 6 MV beams mixed with one lateral 12 MeV electron beam and EMET technique using four fields of 9, 12, 15, and 18 MeV.

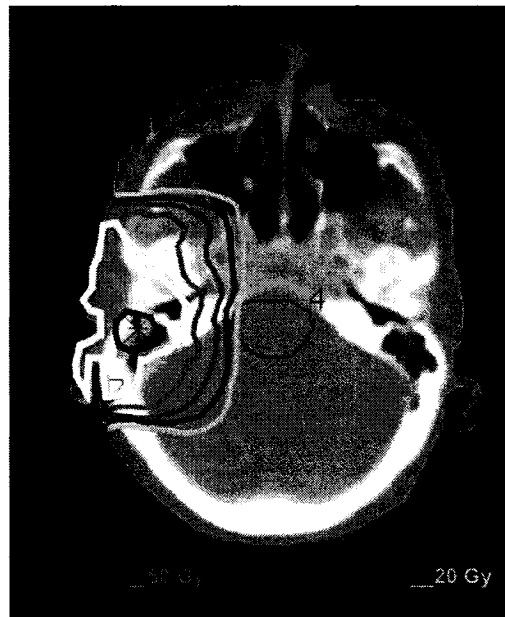


Figure 4-5: Dose distribution obtained by EMET shows that the algorithm takes the effect of the heterogeneity into account at the cost of the conformity.

<i>Fieldlet</i>	9 MeV	12 MeV	15 MeV	18 MeV	6 MV	
<i>1</i>	2310	450	3000	0	<i>ANT</i>	0
<i>2</i>	7425	0	400	76	<i>POS</i>	1240
<i>3</i>	315	1408	1590	1372		
<i>4</i>	360	736	60	1892		
<i>5</i>	4750	36	0	0		
<i>6</i>	855	1536	120	252		
<i>7</i>	1980	0	270	1036		
<i>8</i>	495	0	0	0		

Table 4-2: *The total number of the prescribed monitor units obtained by the optimizer over the whole treatment. The beam-on time required to deliver one fraction remains within 5 minutes interval.*

prescribed dose but it shows also the presence of hot spots due to the use of limited number of fieldlets where the bulging effect that occurs at the edge of the fieldlets causes the appearance of dose heterogeneity wherever the fieldlets are junctioned. For this particular case, the effect could be reduced by the use of a photon field that covers the PTV to create more uniformity within the target. The hot spots could be eliminated by feathering the field edges using dynamic delivery of the fieldlets. Although it has not been implemented yet, it is a potential topic of future study.

4.3.2 Head and neck case

To demonstrate the ability of EMET to deal with more realistic scenarios, a plan was generated for a head and neck case and compared with the conventional treatment technique. Figure 4-4(a) shows the comparison between the Monte Carlo calculated isodose distribution for a conventional plan using two wedged and MLC-shaped photon beams boosted by a lateral 12 MeV electron beam with an optimized plan provided by EMET. It is shown that the EMET plan provides better conformity of the prescribed 50 Gy to the PTV as opposed to the conventional plan where the 50 Gy isodose line extends to cover more volume of the healthy tissues. It is also shown that the low-dose isodose line (20 Gy), obtained by EMET, covers a small volume compared to the conventional plan. If we consider any tissue outside the PTV as an OAR, then EMET would show

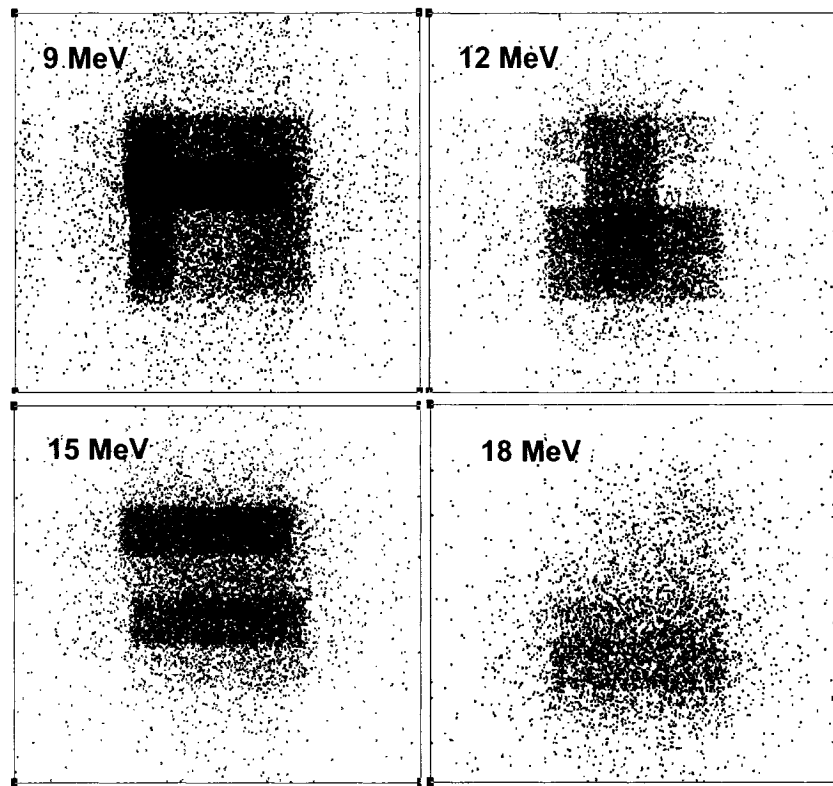


Figure 4-6: XY scatter-plot for the weighted fluence obtained by the optimizer for each energy.

superior behavior in saving such OAR. The DVHs, shown in Fig. 4-4(b), of both plans show that they both converge to the same maximum dose with more uniformity within the PTV if the conventional plan is used. Hot spots were observed to be spread along the PTV for the EMET plan due to the junctioning effect, while in the conventional plan the hotspots are localized in the soft tissue. Figure 4-5 shows the dose distribution obtained by EMET for a slice that contains part of the target located in bone tissues. It shows that the PTV is fully covered with the prescription dose of 50 Gy even though the slice shows a high level of heterogeneity. With the use of realistic Monte Carlo simulated fieldlets kernels *a priori*, where the patient heterogeneities have been accounted for in the optimization algorithm, the EMET plan is truly optimized with its initial requirements. However, due to the competing goals in the objective function between covering the PTV adequately and conforming the prescribed dose to it, the final outcome depends on which

goal has higher priority. In this case, the coverage of the heterogeneous tissue came at the cost of the conformity.

The intensity maps for each energy field, obtained by weighing the Monte Carlo simulated fieldlets to their contribution provided by the optimizer, are shown in Fig. 4-6. The map shows the dominance of the 9 MeV electron field. Such dominance is due to the shallow depth of the tumor. There is also a significant fraction of the high energy electron fieldlets at the positions which is attributed to the presence of bone tumor heterogeneity along the path of that specific fieldlets. Table 4-2 shows the final output provided by the optimizer converted to monitor unit settings. Note that these numbers represent the setting of the complete delivery and need to be fractionated based on the number of fractions prescribed by the physician. The minimum output to be given by the optimizer was set to be one monitor unit, yet several fieldlets were given a zero weight including the anterior photon beam. The posterior photon beam, however, was given a relatively high weight which improved the homogeneity of the distribution as specified by the constraints.

The calculation time required to obtain phase files of 24 fieldlets used in this EMET plan was a total of 24 hours with a 10 Pentium III CPUs cluster. Calculating all dose distributions based on the generated phase space files is estimated to be 30 minutes in the same cluster. The optimization process produces its results within 2 hours. Most of the time consumed in the process is due to the production of the phase space files that could be significantly reduced by the use of the beam models or by building up a library of selected phase space files.

4.4 Conclusions

In this work, we studied the feasibility of a simplified collimation device to deliver conformal electron beam dose distributions. Our results show that EMET offers advantages over the conventional treatments and leads to a significant reduction of the dose delivered to the healthy tissues. In the case studied, the beam-on time for one fraction would be within 5 minutes if the accelerator was set to run 500 MU per minute. The transition time for the 6 fieldlets for each of the four energies used is estimated to be around 8 minutes based on the basic characteristics of standard motors and the pitch of

typical driving screws. Given the fact that we used a limited number of fieldlets, the optimization algorithm could provide weights that conform to the target within reasonable delivery time. More work is needed in the selection of fieldlets and in investigating the use of beam models. A prototype of FLEC is under construction in our department. Comparisons between EMET and IMRT is being investigated and the feasibility of using a practical combined plan is underway

Acknowledgments

This work has been partially supported by the Canadian Institute of Health Research (CIHR) operating grant MOP 57828. J.S. is a research scientist of the National Cancer Institute of Canada (NCIC) appointed with funds provided by the Canadian Cancer Society. The Saudi Arabian Cultural Bureau is also acknowledged for its financial contributions.

References

- [1] E. Sham, Simulated annealing algorithm for inverse treatment planning. M.S. Thesis, Medical Physics Unit, McGill University, 2002.
- [2] A.F. Bielajew, D.W. Rogers, J. Cygler, and J.J. Battista, "A comparison of electron pencil beam and Monte Carlo calculation methods," in: *The Use of Computers in Radiation Therapy*, edited by A.D. Bruinvis (Elsevier, Amestrdam, 1987).
- [3] I. Kawrakow, M. Fippel, and K. Friedrich, "3D electron dose calculation using a Voxel based Monte Carlo algorithm (VMC)," *Med. Phys.* **23**, 445-457 (1996).
- [4] C.M. Ma, B. Faddegon, D.W. Rogers, and T.R. Mackie, "Accurate characterization of Monte Carlo calculated electron beams for radiotherapy," *Med. Phys.* **24**, 401-406 (1997).
- [5] M.C. Lee, S.B. Jiang, and C.M. Ma, "Monte Carlo and experimental investigations of multileaf collimated electron beams for modulated electron radiation therapy," *Med. Phys.* **27**, 2708-2718 (2000).
- [6] C.M. Ma, T. Pawlicki, M.C. Lee, S.B. Jiang, J.S. Li, J. Deng, B. Yi, E. Mok, and A.L. Boyer, "Energy- and intensity-modulated electron beams for radiotherapy," *Phys. Med. Biol.* **45**, 2293-2311 (2000).
- [7] M.C. Lee, J. Deng, J. Li, S.B. Jiang, and C.M. Ma, "Monte Carlo based treatment planning for modulated electron beam radiation therapy," *Phys. Med. Biol.* **46**, 2177-2199 (2001).
- [8] B.P. Ravindran, I.R. Singh, S. Brindha, and S. Sathyan, "Manual multi-leaf collimator for electron beam shaping--a feasibility study," *Phys. Med. Biol.* **47**, 4389-4396 (2002).
- [9] C.M. Ma, M. Ding, J.S. Li, M.C. Lee, T. Pawlicki, and J. Deng, "A comparative dosimetric study on tangential photon beams, intensity-modulated radiation therapy (IMRT) and modulated electron radiotherapy (MERT) for breast cancer treatment," *Phys. Med. Biol.* **48**, 909-924 (2003).
- [10] K.R. Hogstrom, R.A. Boyd, J.A. Antolak, M.M. Svatos, B.A. Faddegon, and J.G. Rosenman, "Dosimetry of a prototype retractable eMLC for fixed-beam electron therapy," *Med. Phys.* **31**, 443-462 (2004).
- [11] D.W. Rogers, B.A. Faddegon, G.X. Ding, C.M. Ma, J. We, and T.R. Mackie, "BEAM: a Monte Carlo code to simulate radiotherapy treatment units," *Med. Phys.* **22**, 503-524 (1995).
- [12] M. Fippel, "Fast Monte Carlo dose calculation for photon beams based on VMC electron algorithm," *Phys. Med. Biol.* **26**, 1466-1475 (1999).

- [13] I. Kawrakow and M. Fippel, "Investigation of variance reduction techniques for Monte Carlo photon dose calculation using XVMC," *Phys. Med. Biol.* **45**, 2163-2183 (2000).
- [14] S.M. Sait and H. Youssef, *Iterative Computer Algorithms with Applications in Engineering: Solving Combinatorial Optimization Problems* (Angela Burgess, Los Alamitos, CA, 1999).
- [15] D. Hristov, P. Stavrev, E. Sham, and B.G. Fallone, "On the implementation of dose-volume objectives in gradient algorithms for inverse treatment planning," *Med. Phys.* **29**, 848-856 (2002).

Chapter 5

Clinical Significance of Energy Modulated Electron Therapy Using Few Leaf Electron Collimator

Energy modulated electron therapy (EMET) is capable of delivering high conformal dose tailored to superficially located targets which are inherently difficult to plan with x-ray intensity modulated radiation therapy (IMRT). This chapter presents a paper published in *Medical Physics* showing the advantages gained from introducing EMET. Following the preliminary results of the previous chapter, we extend our comparison of dosimetric studies to include IMRT. We introduce multiple plan evaluation parameters to examine the significance of EMET compared to the available treatment modalities; namely, conventional three-dimensional conformal radiation therapy (3D-CRT) and IMRT.

Title: Energy modulated electron therapy using a few leaf electron collimator in combination with IMRT and 3D-CRT: Monte Carlo-based planning and dosimetric evaluation

Authors: Khalid Al-Yahya, Matthew Schwartz, George Shenouda, Frank Verhaegen, Carolyn Freeman, and Jan Seuntjens

Published in Medical Physics vol. 32 p. 847-857 (2005).

Submitted: 3 May 2005; revised: 17 June 2005; accepted: 7 July 2005; published: 30 August 2005

Abstract

Energy modulated electron therapy (EMET) based on Monte Carlo dose calculation is a promising technique that enhances the treatment planning and delivery of superficially located tumors. This study investigated the application of EMET using a novel few-leaf electron collimator (FLEC) in head & neck and breast sites in comparison with three dimensional conventional radiation therapy (3D-CRT) and intensity modulated radiation therapy (IMRT) techniques. Treatment planning was performed for two parotid cases and one breast case. Four plans were compared for each case: 3D-CRT, IMRT, 3D-CRT in conjunction with EMET (EMET-CRT), and IMRT in conjunction with EMET (EMET-IMRT), all of which were performed and calculated with Monte Carlo techniques. For all patients, dose volume histograms (DVHs) were obtained for all organs of interest and the DVHs were used as a means of comparing the plans. Homogeneity and conformity of dose distributions were calculated, as well as a sparing index that compares the effect of the low isodose lines. In addition, the whole-body dose equivalent (WBDE) was estimated for each plan. Adding EMET delivered with the FLEC to 3D-CRT improves sparing of normal tissues. For the two head & neck cases the mean dose to the contralateral parotid and brain stem was reduced relative to IMRT by 43% and 84%, and by 57% and 71%, respectively. Improved normal tissue sparing was quantified as an increase in sparing index of 47% and 30% for the head & neck and the breast cases, respectively. Adding EMET to either 3D-CRT or IMRT, results in preservation of target conformity and dose homogeneity. When adding EMET to the treatment plan, the WBDE was reduced by between 6% and 19% for 3D-CRT and by between 21% and 33% for IMRT, while WBDE for EMET-CRT was reduced by up to 72% when compared with IMRT. FLEC offers a practical means of delivering modulated electron therapy. Although adding EMET delivered using the FLEC results in perturbation of target conformity when compared to IMRT, it significantly improves normal tissue sparing while offering enhanced target conformity to the 3D-CRT planning. The addition of EMET systematically leads to a reduction in WBDE especially when compared with IMRT.

5.1 Introduction

Electron beams offer significant advantages over megavoltage photon beams in terms of delivery of high dose at shallow depths, rapid fall off of the dose distribution beyond the treatment volume, and low exit dose. Nevertheless, the use of modulated electron beams still lags behind that of photon intensity modulated radiation therapy (IMRT). Compared with IMRT, energy modulated electron therapy (EMET) has not been widely implemented due to problems inherent to electron beams such as dosimetric accuracy and verification as well as a lack of systems for automatic delivery. Studies have shown the fundamental capability of modulated electron beams for the delivery of tailored dose distribution and different delivery approaches have been proposed [1]. An automated system of bolus modulation was proposed to design and produce patient specific bolus [2-5]. But such system is expensive and planning and treatment with bolus-modulated electron beams remain time consuming and cumbersome.

Electron multileaf collimators (eMLC) [6-8] have been designed for use in their own support frame and have the potential to serve for modulated electron radiation therapy applications [8]. Aside from being relatively bulky, due to the presence of a large number of motors in close proximity to the patient, automation of such a complex system has not been satisfactorily addressed.

We have recently proposed and studied the feasibility of a simplified “few-leaf electron collimator” (FLEC) for delivering EMET [9]. The FLEC is designed as an added accessory tool able to automatically form a sequence of rectangular openings (fieldlets) to compose any irregular electron field. It consists of four copper bars driven by stepper motors that are electronically coupled to the motors controlling the photon jaws so that both of them simultaneously project the same opening at $SSD=100$ cm. Being backed up by the jaws, the e-collimator blades have a thickness of only 1.1 cm and a width of 3 cm. These limited lateral dimensions ensure that the collimator fits within a regular clinical electron applicator.

The use of inverse planning techniques for EMET is more complex than for photon beam IMRT since collimation has a profound effect on electron scattering and the dose gradients in a specific fieldlet. In addition, accurate dose calculations in and near patient heterogeneities are essential to ensure that the optimizer has the dose information

required for calculation of fieldlet weights that lead to an optimal treatment plan. Hence, the output and the dose distribution realized through the combination of multiple sub-fields requires faithful modeling of electron transport through the collimation system and inside the patient.

The total body dose resulting, mainly, from scatter and leakage in photon beams is considered to be a significant disadvantage to IMRT [10-12]. To deliver an equivalent target dose, IMRT techniques require a considerable increase in beam-on time compared to conventional techniques (between 2 - 5 times longer) [13,14]. The increased number of monitor units (MUs) leads to a greater whole-body dose to the patient due to the leakage and scattering of x-rays, thereby increasing the risk of radiation induced malignancies [15]. In contrast, electron beams are not associated with the hazard of the increased total body dose due to the absence of the target and the flattening filter that produce and flatten photon beams and cause leaking and scattering away from the beam direction.

In this work, we investigated the clinical significance of a “few-leaf” collimator with an associated inverse Monte Carlo-based planning algorithm for electron beams. As the use of a limited number of electron fieldlets may result in undesirable dose heterogeneity within the target when applied as a sole treatment modality, the combination of EMET with either traditional photon beams or IMRT beams is of greater interest because it achieves the conformity and target uniformity desired in an optimal plan with better sparing of normal tissues. EMET planning was thus performed either in conjunction with photon beams used in three dimensional conformal therapy (EMET-CRT) or in conjunction with IMRT (EMET-IMRT). We studied three clinical cases: two parotid gland cases and a breast case. We estimated the whole body dose-equivalent (WBDE) of the conventional 3D-CRT, IMRT, EMET-CRT, and EMET-IMRT plans using measured dose data at various distances from the isocenter. This work represents the results of a feasibility study and the full application of the technique awaits the implementation and validation of a QA program that verifies the accuracy of the delivery using similar techniques as those used in IMRT.

Parotid Cases				
	Goal (Gy)	Vol Below Goal (%)	Min (Gy)	Max (Gy)
Target	60	2	57.5	68
	Limit (Gy)	Vol Above Limit(%)		Max (Gy)
Tissue	50	20		68
Eye(L)	40	2		45
Eye(R)	40	2		45
Lens(L)	8	1		8
Lens(R)	8	1		8
Spinal Cord	40	4		45
Brain	50	33		53
Brain Stem	50	33		53
Larynx	50	50		50
Breast Case				
	Goal (Gy)	Vol Below Goal (%)	Min (Gy)	Max (Gy)
Target	50	3	48	55
	Limit (Gy)	Vol Above Limit(%)		Max (Gy)
Tissue	50	1		50
Heart	20	10		45
Lung	20	10		50

Table 5-1: Objective function parameters used in treatment planning and optimization.

5.2 Methods and Materials

5.2.1 Patient selection, volume definition, dose prescription

Two parotid cancer patients post-surgical resection previously treated with adjuvant radiation were selected. Each patient had been immobilized with a thermoplastic mask, and had had a planning computed tomography (CT) scan of the head and neck with 5 mm slices. The clinical target volume (CTV), planning target volume (PTV), and organs at risk (OARs) (brain, brain stem, spinal cord, eyes, lenses, larynx, and contralateral parotid) had been contoured for each patient. The CTV included the post-surgical bed and areas at risk for microscopic disease. The PTV included the CTV and a 3 mm margin. The dose prescribed to the PTV was 60 Gy, at 2 Gy per fraction. For inverse planning, dose constraints to the OARs are seen in Table 5-1.

One patient with left sided breast cancer post mastectomy previously treated with adjuvant radiation was selected. The patient had been immobilized with a breast board, and had had a planning CT scan of the thoracic cavity with 5 mm slices. The clinical

target volume (CTV) and organs at risk (lungs, heart, contralateral breast, skin, and ribs) had been contoured. The skin was outlined for a depth of 2-3 mm. The CTV included the left chest-wall as defined on the planning CT scan. The dose prescribed to the CTV was 50 Gy, at 2 Gy per fraction. For inverse planning, dose constraints to the OARs are seen in Table 5-1. The IMRT plan dose constraints did not include the skin or ribs as we did not want to compromise the target coverage. For all cases, the normal tissues excluding the OARs and target volumes were defined.

5.2.2 Treatment planning

5.2.2.a Treatment planning system

To ensure consistency of the comparison between different plans, all plans computed in this work were Monte Carlo recalculated using the dose engine embedded in the MMCTP (McGill Monte Carlo Treatment Planning) system. This planning interface was developed with the capability of importing treatment plans from different planning systems from which it reads the CT data, beam arrangements and the MU prescription. After acquiring the plan information, the patient-specific beam arrangements are simulated using the Monte Carlo EGS/BEAMnrc package [16] to obtain the phase space data (PSD) representing the beam energy and particle properties. For each energy, the MU calibration of the system is obtained based on a dose calculation in reference calibration conditions. The PSD of each beam is stored in a file from which each particle is transported through the patient density matrix ($256 \times 256 \times (\text{number of slices})$) derived from CT data (voxel size varying from 0.15 to 0.2 cm) using the fast Monte Carlo code XVMC [17]. The beams are added based on their MU weights to obtain a final dose distribution displayed in MMCTP.

Simulation of the photon beams of all plans included importing the MLC file from the clinical treatment planning system (CadPlan®) and converting them to an input file readable by the DYNVMLC module [18] in BEAM/EGSnrc. The DYNVMLC has the ability to fully model the details of the leaves used in the Millennium 120 leaf collimator including the difference on the thickness of the inner and the outer leaves, leaf holes, tips, air gaps. For dynamic delivery in IMRT plans, the leaf sequence files were extracted from the IMRT system station and converted to a format suitable for the BEAMnrc DYNVMLC component module in which the physical openings at the MLC

plane are calculated and the MLC segments are sampled based on the MU settings. MMCTP is equipped to process the IMRT plan and provide a Monte Carlo-recalculated dose distribution for each approved plan. The wedges were simulated using the WEDGE module developed by van der Zee and Welleweerd [19] and modified to work within the BEAMnrc environment. While the validation of the simulations of DYNVMLC has been reported in another study [18], the simulations of the WEDGE module have been extensively studied over a wide set of experimental setups and the differences between measurements and calculations were less than 3%.

5.2.2.b Energy modulated electron therapy planning

EMET was planned and the delivery was calculated as described in a previous study [9]. Briefly, it involves the use of the automated FLEC in conjunction with Monte Carlo-calculation of patient-specific dose deposition coefficients (DDC). Keeping the outer dimensions of the FLEC not larger than the currently existing standard electron applicators has the consequence that geometrical restrictions associated with the electron treatment of head & neck patients can be overcome. The weight of the FLEC is estimated to be around 3-4 kg in addition to the weight of a clinical electron treatment applicator. In the first order, the delivery of complex dynamic electron fields will be performed in a step-and-shoot approach, whereby every sub-field is formed by simultaneous collimation of the electron beam by the jaws and FLEC. A complete fraction from a typical treatment plan consisting of a combination of 25 subfields of 4 energies can be delivered within a 15 minute timeframe [9]. The DDCs are obtained by manual selection of suitable fieldlets that geometrically conform to the target followed by full Monte Carlo simulation of each fieldlet for all energies using the BEAMnrc code to obtain a phase space representation of the fieldlets. Particles from this phase space are then transported through the patient model using the XVMC code. The dose distribution of each simulated fieldlet is considered a kernel that is fed into an optimization algorithm. Each fieldlet's phase space file contains 2-6 million particles depending on its dimensions which results to a negligible latent uncertainty. In a previous study, the accuracy of the Monte Carlo engine for clinical electron beams has been commissioned and compared to measurements in heterogeneous phantoms and the overall accuracy was less than 3% near maximum dose [20]. The number of simulated histories was selected so as to achieve a statistical

<i>Case 1 (Parotid)</i>											
3D-CRT			EMET-CRT			IMRT			EMET-IMRT		
Energy	Angle	MU	Energy	Angle	MU	Energy	Angle	MU	Energy	Angle	MU
6 MV	345	142	6 MV	345	86	6 MV	240	259	6 MV	240	297
6 MV	200	141	6 MV	200	199	6 MV	280	199	6 MV	280	89
6 MV	270	97	6 MV	270	39	6 MV	310	226	6 MV	310	67
			6 MeV	270	48	6 MV	350	160	6 MV	350	131
			9 MeV	270	53	6 MV	30	216	6 MV	030	219
			12 MeV	270	251				6 MeV	270	50
									9 MeV	270	60
									12 MeV	270	279
<i>Case 2 (Parotid)</i>											
3D-CRT			EMET-CRT			IMRT			EMET-IMRT		
Energy	Angle	MU	Energy	Angle	MU	Energy	Angle	MU	Energy	Angle	MU
6 MV	10	165	6 MV	10	211	6 MV	330	209	6 MV	330	158
6 MV	190	155	6 MV	190	76	6 MV	100	209	6 MV	100	102
6 MV	90	134	6 MV	90	11	6 MV	130	207	6 MV	130	171
			9 MeV	90	159	6 MV	170	212	6 MV	170	111
			12 MeV	90	135	6 MV	30	198	6 MV	30	146
			15 MeV	90	320	6 MV	60	247	6 MV	60	206
									9 MeV	90	43
									12 MeV	90	74
									15 MeV	90	219
<i>Case 3 (Breast)</i>											
3D-CRT			EMET-CRT			IMRT			EMET-IMRT		
Energy	Angle	MU	Energy	Angle	MU	Energy	Angle	MU	Energy	Angle	MU
6 MV	302	205	6 MV	302	156	6 MV	302	207	6 MV	302	137
6 MV	127	205	6 MV	127	156	6 MV	312	184	6 MV	312	120
			6 MeV	46	370	6 MV	322	196	6 MV	322	101
			9 MeV	46	414	6 MV	127	185	6 MV	127	130
						6 MV	117	228	6 MV	117	144
						6 MV	107	243	6 MV	107	150
									6 MeV	46	570
									9 MeV	46	805

Table 5-2: The total MUs to deliver the plans of the conventional 3D-CRT*, EMET-CRT[†], IMRT^{††}, and EMET-IMRT^{††}. The addition of EMET reduces the photon beam contributions of the 3D-CRT and IMRT plans by transferring some weight to the electron beams. The electron MUs and the photon MUs are not additive since they contribute differently to the whole body dose. (* The number of MUs is prescribed by the CadPlan treatment planning system.[†] The number of MUs is prescribed by the EMET optimizer.^{††} The number of MUs is prescribed by the CORVUS treatment planning system.)

uncertainty within 2% or less per fieldlet in the voxels receiving 10% or more of maximum dose. Ma *et al.* illustrated that such small statistical uncertainties in modulated electron beams will not affect the final results represented in DVHs [21].

The in-house developed optimization software operates under a graphical programming system (Application Visualization System, AVS Inc.) and uses the deterministic steep dose volume histogram (DVH) minimization algorithm [22] as an optimization technique. The software manages the extraction of the dosimetric information from the Monte Carlo calculated kernels which includes the contour data and the DDCs that characterize the relative dose contribution from each kernel to each point confined in an individual contour. Obtaining both contour data and DDCs for the PTV and OARs is followed by assigning the prescription, the dose-volume constraints, and their related penalties. The EMET optimizer evaluates the role of each fieldlet in the overall dose distribution and assigns a relative weight to it. After an optimum plan is achieved, the EMET optimizer returns the energies of the contributing fieldlets along with their associated relative intensities in the form of number of MUs. Fieldlets that receive a weight of zero by the optimizer are considered rejected. In this work, the Monte Carlo simulated photon beams are considered as fieldlets in both EMET-CRT and EMET-IMRT plans. The EMET optimizer determines the weight of the entire field in the same fashion it deals with an electron fieldlet. Thus, the optimizer reweighs the overall delivered IMRT treatment but does not change the leaf sequence of each of the individual IMRT fields.

5.2.2.c Treatment techniques

For each patient, we have used four planning techniques that are summarized in Table 5-2

Technique 1: 3D conformal radiotherapy (3D-CRT) technique

For each of the two parotid cases, three wedged 6 MV photon beams from a Varian Clinac 2100EX accelerator (Varian Medical Systems, Palo Alto, CA) were used. The perpendicular beams (the 270° beam for the first case and the 90° beam for the second case) were given a reduced weight to obtain a more homogeneous dose distribution. The fields were shaped by means of the beam's eye view (BEV) feature in ACQSIM (Philips, Andover, MA) and a 120 multileaf collimator (MLC) was used with a 6-mm consistent

margin around the PTV to reduce the dose to the OARs. For the breast case, two tangential rectangular 6 MV photon fields were chosen based on the BEV feature to entirely cover the CTV. A wedge angle of 30 degrees was selected to provide a uniform dose distribution within the CTV.

Technique 2: IMRT

The commercial inverse planning system (CORVUS 5.0, NOMOS Inc., Cranberry Township, PA) was used to generate the IMRT plans. The IMRT technique used five step-and-shoot 6 MV beam orientations for the first parotid case and six gantry angles for the second parotid case and the breast case. The optimization procedure was performed without considering the effect of tissue inhomogeneities. Although the CORVUS treatment planning system allows one to use heterogeneity corrections in the optimization procedure, Yang *et al.* showed that this leads to only a negligible difference when compared to the CORVUS plan obtained without the heterogeneity correction for coplanar plans [23]. The effect of this approximation is manifested as discrepancies between the predicted DVH by the optimization algorithm and the “actual” DVH obtained after calculating the dose distribution with Monte Carlo simulations which rigorously accounts for the effect of tissue inhomogeneities.

Once the IMRT plans are approved, leaf sequence files were produced for each beam orientation derived from the intensity maps required to achieve the fluence proposed by the optimization algorithm and the dose distribution is then recalculated by Monte Carlo methods.

Techniques 3 and 4: EMET-CRT and EMET-IMRT

For case 1, 10 fieldlets of 6, 9, and 12 MeV in addition to the newly-weighted three beams of the conventional plan were selected for the EMET-CRT and the same electron fieldlets (with different intensities) were also selected in conjunction with the 5 IMRT fieldlets for the EMET-IMRT. Case 2 employed 12 fieldlets with energies of 9, 12, and 15 MeV. The intensity maps of the 9 and 12 MeV electron fields are shown in Fig. 5-1. The breast case used 8 fieldlets of 6 and 9 MeV. Table 5-2 shows the MU settings for the four techniques where the settings of the EMET plans were provided by the EMET optimizer.

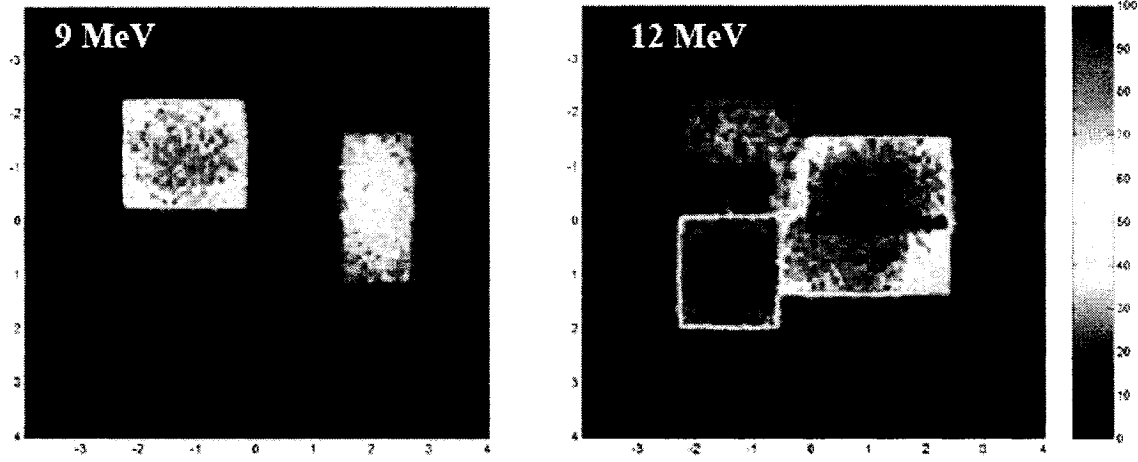


Figure 5-1: The intensity map of two energy fields based on the relative weights assigned by the EMET optimizer. The intensity map is normalized to the fieldlet with the highest MUs.

5.2.3 Plan evaluation parameters

For each case studied, the mean dose, minimum dose, and maximum dose to the target were calculated for each of the four plans. As per Nutting *et al.* [24], the minimum dose is defined as the dose received by $\geq 99\%$ of the target volume and the maximum dose is defined as the dose received by $\leq 1\%$ of the target. DVHs were obtained for each of the four treatment plans for the target and OARs delineated. Only the mean dose and the maximum dose were reported for the OARs.

Conformity was compared by calculating the conformity index (COIN95) defined by Baltas *et al.* [25] for each plan. COIN95 is defined as the product of the fraction of the target covered by higher than 95% ($\frac{PTV_{95}}{PTV}$) of the prescribed dose and the ratio of the volume of the target receiving at least 95% of the prescribed dose to the total volume of tissue receiving at least 95% of the prescribed dose ($\frac{PTV_{95}}{V_{95}}$):

$$COIN95 = \frac{PTV_{95}}{PTV} \frac{PTV_{95}}{V_{95}}. \quad (5-1)$$

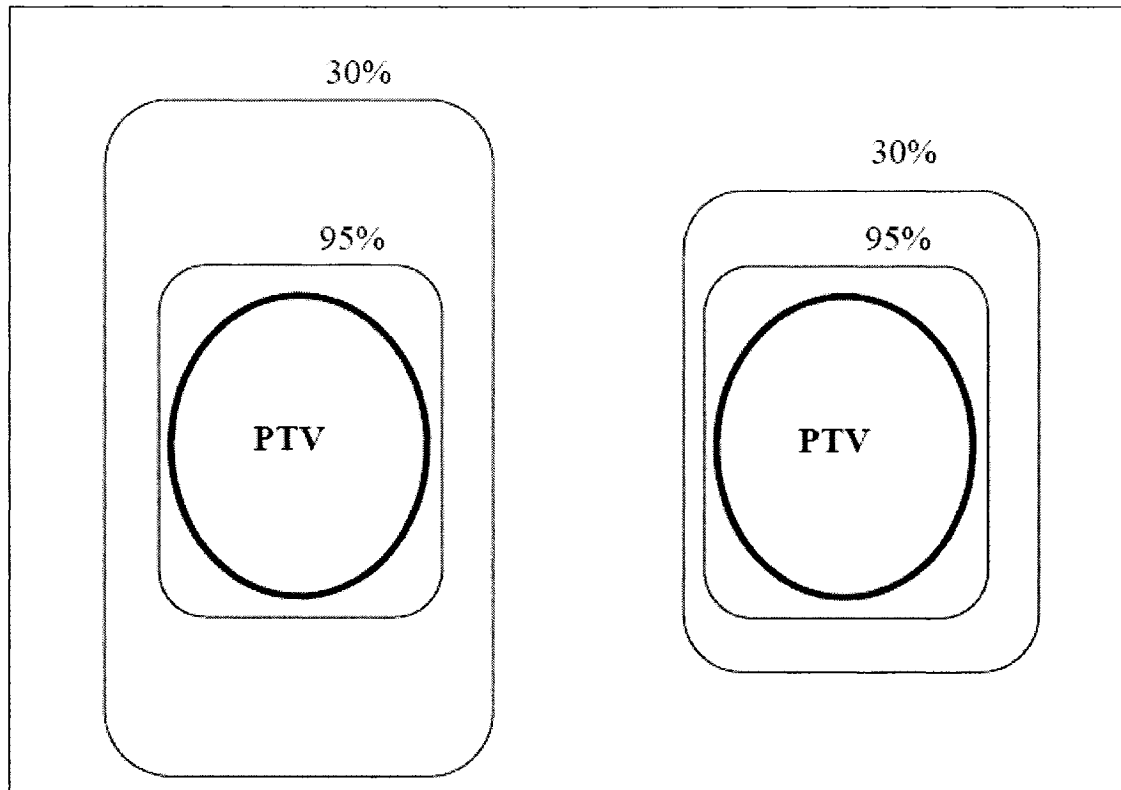


Figure 5-2: Schematic diagram of two plans that have the same coverage of the 95% isodose line to the PTV volume but with different conformity of the low isodose lines. The conformity index (COIN95) will be equivalent for both plans despite their differences. The sparing index (SPIN50/10) could be used to differentiate between them.

However, although COIN95 provides reasonable evaluation of the conformity surrounding the target for the high dose values, it does not consider the volume that lies in the low dose region. As shown in Fig. 5-2, having two plans delivering the same 95% coverage will not be differentiated by the COIN95 factor if one plan extends the 30% line to cover larger volume which is undesirable if it could be avoided. We therefore propose the use of a new term, the sparing index (SPIN50/10), to quantify the volume that receives between 50% and 10% of the prescribed dose. We have defined this as:

$$SPIN50/10 = 1 - V_{10}^{50}, \quad (5-2)$$

where V_{10}^{50} is the ratio of the volume of tissue that receives between 10% and 50% of the prescribed dose to the irradiated volume. The irradiated volume was defined as the

volume of tissue that receives 0.5% of the prescribed dose. SPIN50/10 can not stand alone without being evaluated in conjunction with COIN95 where both values, ideally, should approach 1.

We also used the homogeneity index HI90/110 to compare plans in terms of the ability to deliver homogeneous dose distribution to the target. HI90/110 is defined as the percentage of the target volume with a dose higher than 90% and lower than 110% of the prescribed dose. These parameters assist in comparing plans that have the same volume of the PTV and irradiated volume since there is a central dependence of these parameters on the planning volume in relation to normal tissue.

5.2.4 Assessment of whole body dose-equivalent (WBDE)

The dose was measured using a cylindrical Farmer ionization chamber placed at a depth of 2 cm in a solid water phantom and positioned at 35, 55, 75 and 95 cm away from the edge of the field. To resemble the patient geometry, a semi-spherical solid water phantom that mimics a head was placed at the isocenter while the other parts of the body were mimicked using bolus bags to account for the effect of the internal scatter. Dose per MU was obtained for a 7×7 cm² field (a typical field collimated with jaws and FLEC used in EMET) at all energies (6, 9, 12, 15 MeV), as well as the dose per MU for 10×10 cm² of the 6 MV photon field which agreed with the results obtained by other authors [26]. Using the total number of MUs acquired from the CadPlan treatment planning system for the conventional plan, from the CORVUS treatment planning system for the IMRT plan, and from the EMET system for both the EMET-CRT and EMET-IMRT plan, WBDE was estimated by multiplying the total MUs of each field by the dose value per MU measured at 40 cm from the isocenter. This value was used as a reasonable approximation to determine WBDE resulting from the 60 Gy prescribed dose for head & neck cases and the 50 Gy prescribed dose for the breast case. Figure 5-3 illustrates the comparison of the behavior of the peripheral dose caused by the four techniques based on the total MUs prescribed for the breast case. It is important to note that this estimate of the total body dose assessment serves only as a first order approximation due to the vital dependence of the WBDE on the treatment technique of each plan. In this work, we have used WBDE only to relatively compare different planning techniques.

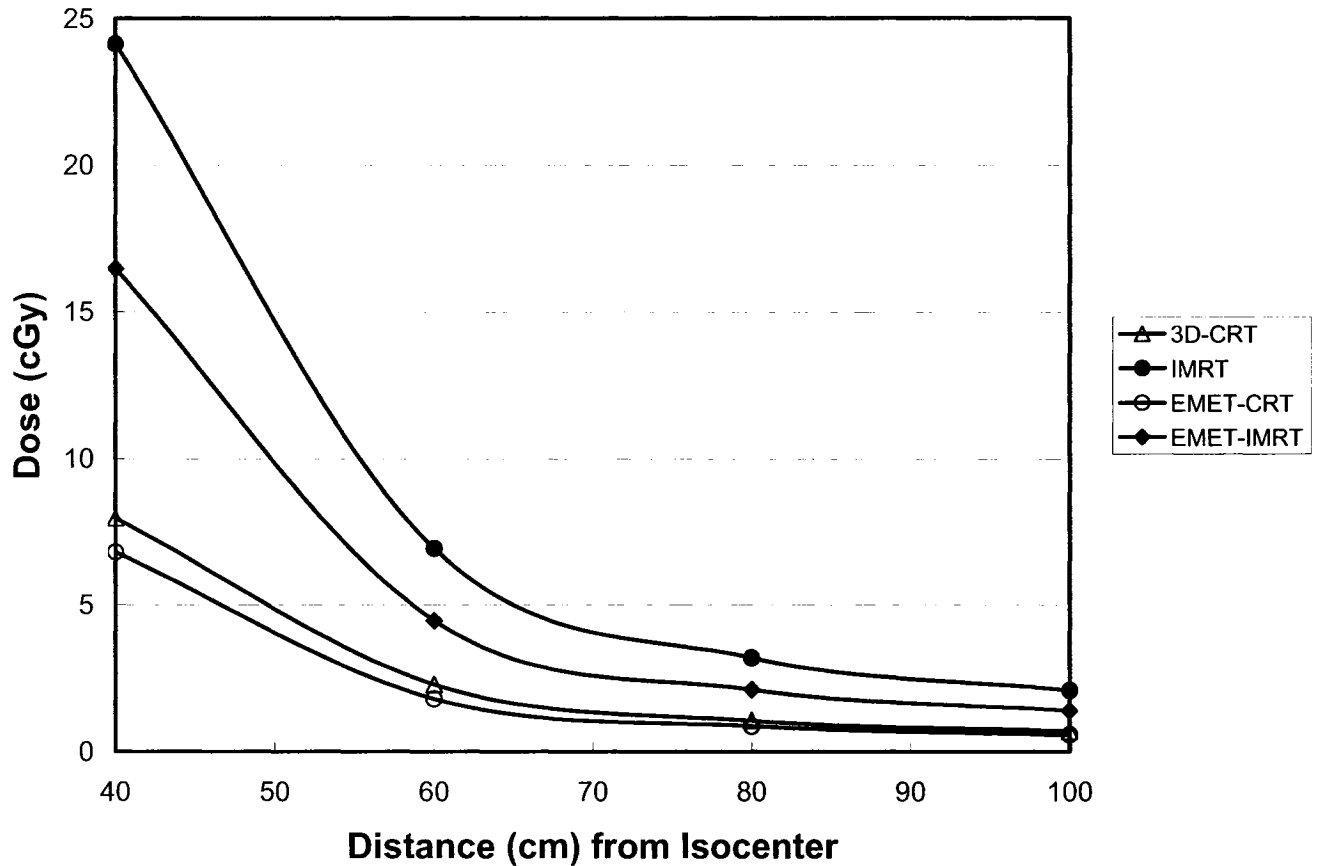


Figure 5-3: Off axis dose at depth of 2 cm in solid water phantom based on the number of MUs given by four techniques.

5.3 Results

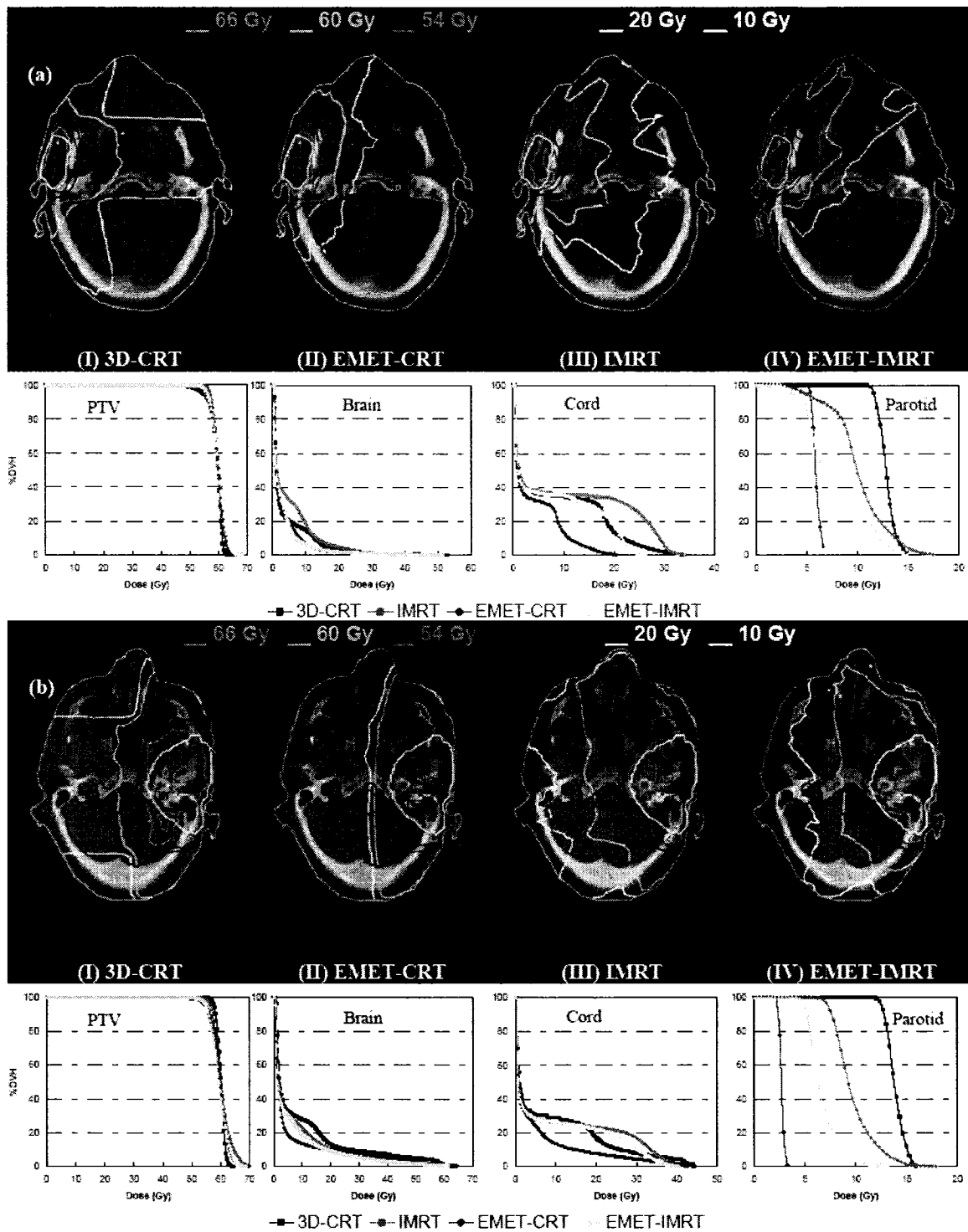
5.3.1 Parotid cancer cases

The isodose distributions of the four different plans with the DVHs of the outlined organs for the two cases are shown in Figures 5-4(a) and (b). Table 5-3 shows the summary of the DVH analysis of the four treatment plans for each case where the minimum, maximum, and mean doses to the target are reported. COIN95, SPIN50/10, HI90/110, and the estimate for the WBDE are shown in Table 5-4.

The target was well covered by all four plans. However, the IMRT plan gave the highest conformity to the target, followed by the EMET-IMRT plan. The use of IMRT and EMET-CRT produced hot spots, but these were within the target volume and were considered acceptable. For case 2, the hot spots with the EMET-CRT plan were within

	Plan	PTV			Brain		Brain Stem		Cord		Contralateral Parotid	
		mean	min	max	mean	max	mean	max	mean	max	mean	max
<i>Case 1</i>	<i>(Parotid)</i>											
	3D-CRT	59.1	49.6	62.2	3.60	24.5	16.0	19.9	7.5	31.6	12.7	14.7
	IMRT	59.7	55.9	64.7	4.82	29.2	17.2	25.1	9.9	32.2	9.9	16.3
	EMET-CRT	59.5	50.7	63.6	2.79	23.9	7.4	11.3	3.8	18.2	5.7	6.7
	EMET-IMRT	59.9	54.7	65.4	2.9	23.5	9.1	14.5	7.2	24.2	7.5	14.3
<i>Case 2</i>	<i>(Parotid)</i>											
	3D-CRT	59.9	56.9	63.1	9.01	59.3	18.4	29.3	8.1	43.2	13.7	15.7
	IMRT	60.3	55.1	68.9	6.64	52.2	17.8	38.4	8.6	39.9	9.5	15.1
	EMET-CRT	59.6	52.2	65.9	5.94	55.4	5.3	18.7	4.6	40.7	2.5	3.1
	EMET-IMRT	59.3	53.2	66.1	6.15	51.8	14.0	34.5	7.8	37.3	6.5	11.1
	Plan	Breast			Lung		Heart		Skin		Ribs	
		mean	min	max	mean	max	mean	max	mean	max	mean	max
<i>Case 1</i>	<i>(Breast)</i>											
	3D-CRT	52.4	47.3	55.5	14.3	48.7	2.1	6.2	41.7	51.9	12.2	52.2
	IMRT	51.7	48.1	56.3	11.2	42.8	4.3	17.2	40.7	55.6	9.5	49.4
	EMET-CRT	52.5	48.5	55.4	12.4	45.1	2.3	10.1	42.6	51.4	11.8	49.9
	EMET-IMRT	52.4	48.7	56.2	10.1	41.3	3.8	17.3	41.7	53.7	10.3	49.5

Table 5-3: Comparison of dose for PTV and OARs using four planning techniques. min= minimum dose; max= maximum dose; mean= mean dose.



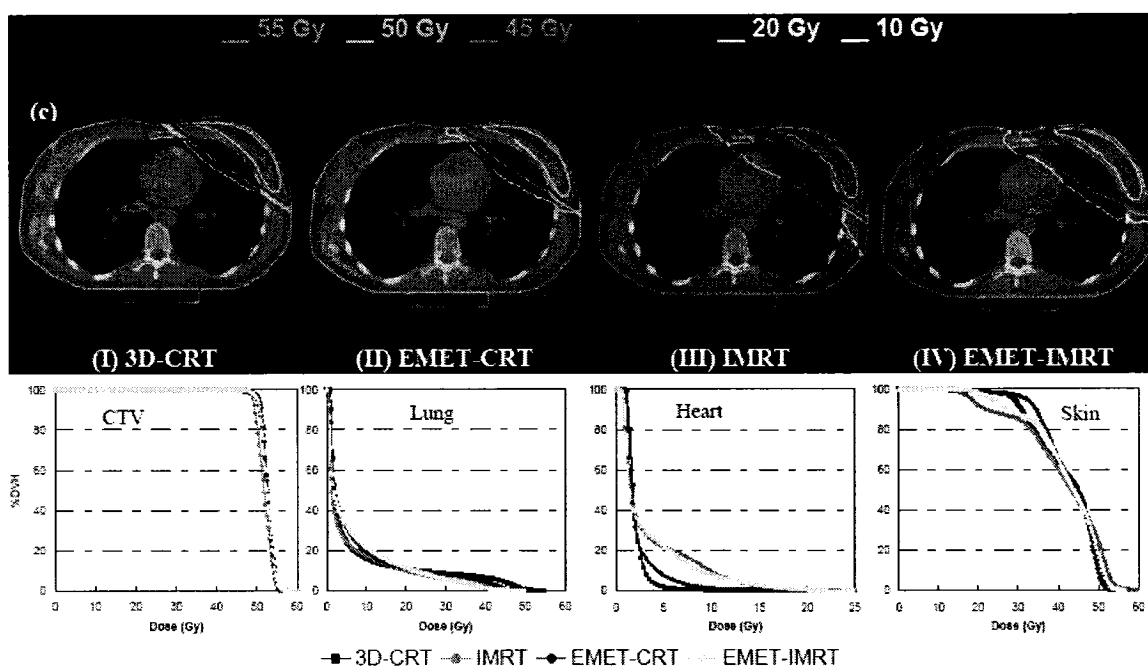


Figure 5-4: A comparison of the Monte Carlo calculated dose distributions and DVHs for all outlined organs produced by four plans: (I) 3D-CRT, (II) EMET-CRT, (III) IMRT, and (IV) EMET-IMRT. (a) and (b) are for the two parotid cases and (c) is for the breast case. The target is outlined in yellow.

the air-filled cavities of the temporal bone in the mastoid air cells. Since the dose distribution was calculated by Monte Carlo, the dose that is reported is the actual dose that is deposited in the air cavities. The hot spots with the IMRT plan were in the soft tissues due to the heterogeneities that were not taken into account in the optimization. As expected, the high isodose curves were very conformal with both the IMRT and EMET-CRT plans, but the low isodose curves for the IMRT plan contained a much larger volume of normal tissue compared with the EMET-CRT plan as seen in Fig. 5-4. This corresponds to the EMET-CRT plan having a much higher SPIN50/10 value than the IMRT plan (Table 5-4). If the SPIN 50/10 is accepted as a measure of the ability of a given plan to spare the normal tissues in the low dose regions, then the EMET-CRT plan had a 47% higher sparing on average compared to the IMRT plan.

	Plan	COIN95*	SPIN50/10 [†]	HI90/110 ^{††}	WBDE [§] (mSv)
<i>Case 1</i>					
<i>(Parotid)</i>	3D-CRT	0.56	0.49	0.957	9.4
	IMRT	0.68	0.52	0.997	26.3
	EMET-CRT	0.59	0.77	0.956	8.9
	EMET-IMRT	0.62	0.59	0.985	20.8
<i>Case 2</i>					
<i>(Parotid)</i>	3D-CRT	0.54	0.69	0.987	11.3
	IMRT	0.69	0.61	0.935	31.8
	EMET-CRT	0.62	0.88	0.957	9.4
	EMET-IMRT	0.64	0.60	0.973	23.4
<i>Case 3</i>					
<i>(Breast)</i>	3D-CRT	0.30	0.93	0.949	8.5
	IMRT	0.54	0.67	0.956	25.7
	EMET-CRT	0.43	0.88	0.980	7.2
	EMET-IMRT	0.57	0.71	0.960	17.4

Table 5-4: Comparison of treatment planning evaluation parameters of the four planning techniques. *COIN95= Conformity Index. [†]SPIN50/10= Sparing Index. ^{††}HI90/110 = Homogeneity Index. [§]WBDE = Whole body dose equivalent.

IMRT has been shown to reduce the dose to the contralateral parotid, brain, and spinal cord [24,27]. In our series, IMRT decreased the mean dose to the contralateral parotid by 27% on average when compared to the 3D-CRT plan (Table 5-3). The use of EMET-CRT further reduced the dose to the contralateral parotid dose by an additional 58%. The amount of normal brain tissue treated with a given technique is also an important issue when comparing different treatment techniques. The mean dose to the brain was 27% lower on average with the EMET-CRT plan as compared to the IMRT plan. The maximum dose to the spinal cord was 22% lower on average with the EMET-CRT plan when compared to the IMRT plan.

The estimate of WBDE (in mSv) is shown in Table 5-4. The WBDE was lowest for the EMET-CRT plans and the highest for the IMRT plans for all cases. The use of EMET-CRT resulted in a 69% decrease in the whole body dose on average compared to the IMRT plan.

5.3.2 Left breast cancer post-mastectomy case

Table 5-3 summarizes the quantitative comparison between different plans for the target volume and OARs. The minimum, maximum, and mean doses to the target,

ipsilateral lung, heart, skin overlying the treated breast, and ribs are given for each of the treatment plans. COIN95, SPIN50/10, HI90/110, and the WBDE are given for each plan in Table 5-4. Figure 5-4 (c) compares the isodose distributions for each of the treatment plans.

The mean doses to the target were similar with each of the plans. However when using the conformity index, the EMET-IMRT plan had the highest conformity followed by the IMRT plan, EMET-CRT plan, and the 3D-CRT plan the lowest. EMET-CRT gave the most homogeneous dose distribution to the target as shown by the HI90/110 seen in Table 5-4. The SPIN50/10 showed that the 3D-CRT plan had highest value due to the poor conformity, shown in COIN95, that increased the volume of normal tissues irradiated with high isodose lines while lessening the volume covered by low isodose lines. The sparing of the 3D-CRT plan is followed by the EMET-CRT plan, EMET-IMRT plan, and the IMRT plan.

An important concern with left-sided breast cancer patients treated with radiotherapy is the dose to the heart. Table 5-3 gives the doses to the heart according to the different techniques. The 3D-CRT technique gave the lowest mean heart dose followed by the EMET-CRT plan, EMET-IMRT plan, and the IMRT plan. The use of EMET-CRT in this case gave a similar conformity as IMRT, but with a decrease in the dose to the heart. The EMET-CRT plan gave a 47% lower mean heart dose and a 41% lower maximum heart dose as compared to the IMRT plan.

The ipsilateral lung often receives significant dose with conventional radiotherapy using tangential fields. Table 5-3 shows the doses to the ipsilateral lung by the different techniques. The EMET-IMRT technique gave the lowest mean dose to the lung, which resulted in a 10% decrease in the mean lung dose compared to the IMRT plan. The dose to the contralateral lung was negligible since it was not in the path of any irradiation field. In addition, the skin and rib doses were analyzed, and the IMRT plan gave the lowest mean doses to each. The higher mean dose to the skin seen with the EMET-CRT plan is likely due to the location of the CTV 3 - 4 mm below the surface so that the skin is in the build-up region. However, the maximum skin dose was the highest with IMRT and the lowest with EMET-CRT. The increased dose to the skin seen with IMRT is likely due to the fact that the skin is in the buildup region for photons, and IMRT uses

multiple tangential beams to deliver a homogenous dose to the target. This effect has been seen with patients treated with IMRT for head & neck cancers [28]. The EMET-CRT plan had an 8% lower maximum skin dose when compared to the IMRT plan.

WBDE is shown in Table 5-4. It was lowest for the EMET-CRT plan followed by the 3D-CRT plan, EMET-IMRT plan, and the IMRT plan. The EMET-CRT plan was 72% lower than the IMRT plan with respect to the estimated whole body radiation dose.

5.4 Discussion

In this study, we introduce a novel EMET technique using a FLEC as a modality for use in conjunction with 3D-CRT and/or IMRT in the context of mixed beam treatment planning and delivery. The automated FLEC circumvents the challenge of remotely shaping the electron fields required for the clinical application of EMET. This technique was applied to two parotid cases and a breast case for which comparisons with Monte Carlo-recalculated conventional 3D-CRT and IMRT plans were performed. Although the FLEC involves the use of limited beam ports and large fieldlets compared to the fine MLC beamlets used in IMRT, the results show a significant overall improvement in several parameters used to analyze treatment plans.

5.4.1 3D-CRT vs. EMET-CRT

Conformity is significantly enhanced when EMET was added to the 3D-CRT plan. The conformity effect was more pronounced with the breast case where the high isodose lines extend to the lung covering some portion of it with the prescribed dose while with EMET-CRT plan, as shown in Fig. 5-4, the 45 Gy isodose line conforms to the breast tissues, sparing the lung from irradiation by high doses. The volume of lung that receives the prescribed dose as seen from the DVH was reduced by 50% using EMET. Sparing was also significantly improved with the use of EMET-CRT in both head & neck cases, leading to considerable reduction of the mean dose to all OARs including the contralateral parotid. Sparing could also be achieved by replacing the lateral photon field with a lateral conventional cutout-shaped electron field. However, this would lead to extremely unfavorable heterogeneities in the dose distribution appearing as an extended tail in the DVH of the PTV. Target dose uniformity was affected by the addition of EMET to the 3D-CRT in the head & neck cases, but the reduction to the HI90/110 caused

by EMET remained modest. Homogeneity could possibly be enhanced by assigning more penalty to it in the optimization procedure but this will cause competing goals in the objective function that might sacrifice conformity and/or reduce sparing of the other organs. In the breast case, however, the homogeneity of the dose distribution was improved with the use of EMET. The addition of a relatively large number of electron MUs did not increase the WBDE; EMET-CRT showed systematic reduction of the WBDE by reducing the photon MUs which are the dominant source of radiation outside the beam and replacing them with electron MUs which make a minimal contribution to the whole body dose.

5.4.2 IMRT vs. IMRT-EMET

Optimizing the EMET fieldlets with the IMRT whole fields that are added to form the IMRT-EMET plan does not represent the best possible optimization as only the weight of the entire IMRT field is varied and not the weight of the individual beamlets since the current technology has not yet been clinically implemented for Monte-Carlo based optimization of photon beams. Using EMET-IMRT for the head & neck cases showed reduced conformity relative to IMRT alone. This is not the case for the breast case where conformity was enhanced with the EMET-IMRT plan. This is attributed to the relative large size of the fieldlets compared to the projection of the small PTV. In the parotid cases, due to the small size of the PTV, the effect of the edges of the fieldlets appeared to be significant while this effect diminished in the breast case where a large target is irradiated. Overall, homogeneity is preserved with the addition of EMET. Sparing, however, systematically improves with EMET due to the lower exit dose of electrons compared to photons. Improvement of sparing was seen as the SPIN50/10 as well as the mean dose and the maximum dose to the OARs, all of which were consistently reduced when EMET fields were optimized with IMRT. EMET-IMRT has the advantage of lowering the WBDE because of the reduction of the photon beam-on time.

5.4.3 IMRT vs. EMET-CRT

Although the conformity achieved by IMRT cannot be challenged with the EMET-CRT due to the use of rather large fieldlets, the sparing attained by EMET-CRT is superior even with such limited fieldlets. The significant reduction of dose to the

contralateral parotid suggests that EMET-CRT has the potential to improve the quality of life, while the reduction of dose to the spinal cord is important since it allows the patient to receive further radiation treatment if needed. Target dose homogeneity was modestly improved with the breast case where the hot spots caused by the tangential effect of the IMRT fields could be avoided. The maximum dose to the skin in the breast case was reduced by 8% with EMET-CRT compared to IMRT. In the second parotid case, the hot spots in the IMRT plan were in the soft tissues while they were in the air cavities in the EMET-CRT plan. This effect cannot be differentiated when comparisons are made through DVHs only but it might have clinical implications. This study also underlies the concern of the inclusion of the air cavities in the PTV especially when true Monte Carlo optimization is implemented [29]. For the WBDE, EMET-CRT shows major reduction of the estimate of WBDE (in the order of 70%).

5.5 Conclusion

In summary, we investigated the use of energy modulated electron beam treatment planning and delivery using a few-leaf electron collimator in a context of mixed beam treatment planning with conventional radiation therapy and IMRT. We used Monte Carlo techniques to calculate treatment plans for conventional 3D-CRT planning and IMRT alone or combined with EMET. We have shown that EMET delivered with the FLEC could be a valuable addition to current treatment techniques especially when applied to superficially located tumors that are inherently difficult to plan using IMRT. Since the FLEC can be readily automated and remotely controlled, the complexity of EMET delivery will not exceed what is deemed acceptable in IMRT. The characteristics of quality assurance procedures are expected to be similar to those for IMRT treatments. For two head & neck cases and for one breast case we showed that target conformity and homogeneity are preserved while drastically improving normal tissue sparing. As a result of reducing the number of photon MUs for delivery, the addition of EMET systematically leads to a reduction in whole body dose, especially when compared to IMRT. The application of EMET to other treatment sites is currently being investigated.

Acknowledgments:

This work has been supported in part by the Canadian Institutes of Health Research through grant MOP 57828 and by National Cancer Institute of Canada, Terry Fox Foundation, grant No. 016298. K.A. acknowledges support from the Saudi Cultural Bureau. J. S. is a Research Scientist of the National Cancer Institute of Canada appointed with funds provided by the Canadian Cancer Society.

References

- [1] K.R. Hogstrom, J.A. Antolak, R.J. Kudchadker, C.M. Ma, and D.D. Leavitt, "Modulated Electron Therapy," in: *Intensity-Modulated Radiation Therapy, The State of the Art: Proceedings of the 2003 Summer School*, edited by J.R. Palta, T.R. Mackie (Medical Physics Publishing, Madison, 2003), pp. 749-786.
- [2] D.A. Low, G. Starkschall, S.W. Bujnowski, L.L. Wang, and K.R. Hogstrom, "Electron bolus design for radiotherapy treatment planning: bolus design algorithms," *Med. Phys.* **19**, 115-124 (1992).
- [3] D.A. Low, G. Starkschall, N.E. Sherman, S.W. Bujnowski, J.R. Ewton, and K.R. Hogstrom, "Computer-aided design and fabrication of an electron bolus for treatment of the paraspinal muscles," *Int. J. Radiat. Oncol. Biol. Phys.* **33**, 1127-1138 (1995).
- [4] G.H. Perkins, M.D. McNeese, J.A. Antolak, T.A. Buchholz, E.A. Strom, and K.R. Hogstrom, "A custom three-dimensional electron bolus technique for optimization of postmastectomy irradiation," *Int. J. Radiat. Oncol. Biol. Phys.* **51**, 1142-1151 (2001).
- [5] R.J. Kudchadker, K.R. Hogstrom, A.S. Garden, M.D. McNeese, R.A. Boyd, and J.A. Antolak, "Electron conformal radiotherapy using bolus and intensity modulation," *Int. J. Radiat. Oncol. Biol. Phys.* **53**, 1023-1037 (2002).
- [6] M.C. Lee, S.B. Jiang, and C.M. Ma, "Monte Carlo and experimental investigations of multileaf collimated electron beams for modulated electron radiation therapy," *Med. Phys.* **27**, 2708-2718 (2000).
- [7] C.M. Ma, T. Pawlicki, M.C. Lee, S.B. Jiang, J.S. Li, J. Deng, B. Yi, E. Mok, and A.L. Boyer, "Energy- and intensity-modulated electron beams for radiotherapy," *Phys. Med. Biol.* **45**, 2293-2311 (2000).
- [8] K.R. Hogstrom, R.A. Boyd, J.A. Antolak, M.M. Svatos, B.A. Faddegon, and J.G. Rosenman, "Dosimetry of a prototype retractable eMLC for fixed-beam electron therapy," *Med. Phys.* **31**, 443-462 (2004).
- [9] K. Al-Yahya, D. Hristov, F. Verhaegen, and J. Seuntjens, "Monte Carlo-based modulated electron beam treatment planning using a few leaf electron collimator - feasibility study," *Phys. Med. Biol.* **50**, 847-857 (2005).
- [10] E. Glatstein, "Intensity-modulated radiation therapy: the inverse, the converse, and the perverse," *Semin. Radiat. Oncol.* **12**, 272-281 (2002).
- [11] A.C. Paulino and M. Skwarchuk, "Intensity-modulated radiation therapy in the treatment of children," *Med. Dosim.* **27**, 115-120 (2002).

- [12] D. Verellen and F. Vanhavere, "Risk assessment of radiation-induced malignancies based on whole-body equivalent dose estimates for IMRT treatment in the head and neck region," *Radiother. Oncol.* **53**, 199-203 (1999).
- [13] "Intensity-modulated radiotherapy: current status and issues of interest," *Int. J. Radiat. Oncol. Biol. Phys.* **51**, 880-914 (2001).
- [14] D. Followill, P. Geis, and A. Boyer, "Estimates of whole-body dose equivalent produced by beam intensity modulated conformal therapy," *Int. J. Radiat. Oncol. Biol. Phys.* **38**, 667-672 (1997).
- [15] E.J. Hall and C.S. Wu, "Radiation-induced second cancers: the impact of 3D-CRT and IMRT," *Int. J. Radiat. Oncol. Biol. Phys.* **56**, 83-88 (2003).
- [16] D.W. Rogers, B.A. Faddegon, G.X. Ding, C.M. Ma, J. We, and T.R. Mackie, "BEAM: a Monte Carlo code to simulate radiotherapy treatment units," *Med. Phys.* **22**, 503-524 (1995).
- [17] I. Kawrakow and M. Fippel, "Investigation of variance reduction techniques for Monte Carlo photon dose calculation using XVMC," *Phys. Med. Biol.* **45**, 2163-2183 (2000).
- [18] E. Heath, J. Seuntjens, and D. Sheikh-Bagheri, "Dosimetric evaluation of the clinical implementation of the first commercial IMRT Monte Carlo treatment planning system at 6 MV," *Med. Phys.* **31**, 2771-2779 (2004).
- [19] W. van der Zee and J. Welleweerd, "A Monte Carlo study on internal wedges using BEAM," *Med. Phys.* **29**, 876-885 (2002).
- [20] R. Doucet, M. Olivares, F. DeBlois, E.B. Podgorsak, I. Kawrakow, and J. Seuntjens, "Comparison of measured and Monte Carlo calculated dose distributions in inhomogeneous phantoms in clinical electron beams," *Phys. Med. Biol.* **48**, 2339-2354 (2003).
- [21] C.M. Ma, J.S. Li, S.B. Jiang, T. Pawlicki, W. Xiong, L.H. Qin, and J. Yang, "Effect of statistical uncertainties on Monte Carlo treatment planning," *Phys. Med. Biol.* **50**, 891-907 (2005).
- [22] D. Hristov, P. Stavrev, E. Sham, and B.G. Fallone, "On the implementation of dose-volume objectives in gradient algorithms for inverse treatment planning," *Med. Phys.* **29**, 848-856 (2002).
- [23] J. Yang, J. Li, L. Chen, R. Price, S. McNeeley, L. Qin, L. Wang, W. Xiong, and C.M. Ma, "Dosimetric verification of IMRT treatment planning using Monte Carlo simulations for prostate cancer," *Phys. Med. Biol.* **50**, 869-878 (2005).

- [24] C.M. Nutting, C.G. Rowbottom, V.P. Cosgrove, J.M. Henk, D.P. Dearnaley, M.H. Robinson, J. Conway, and S. Webb, "Optimisation of radiotherapy for carcinoma of the parotid gland: a comparison of conventional, three-dimensional conformal, and intensity-modulated techniques," *Radiother. Oncol.* **60**, 163-172 (2001).
- [25] D. Baltas, C. Kolotas, K. Geramani, R.F. Mould, G. Ioannidis, M. Kekchidi, and N. Zamboglou, "A conformal index (COIN) to evaluate implant quality and dose specification in brachytherapy," *Int. J. Radiat. Oncol. Biol. Phys.* **40**, 515-524 (1998).
- [26] M. Stovall, C.R. Blackwell, J. Cundiff, D.H. Novack, J.R. Palta, L.K. Wagner, E.W. Webster, and R.J. Shalek, "Fetal dose from radiotherapy with photon beams: report of AAPM Radiation Therapy Committee Task Group No. 36," *Med. Phys.* **22**, 63-82 (1995).
- [27] C.M. Bragg, J. Conway, and M.H. Robinson, "The role of intensity-modulated radiotherapy in the treatment of parotid tumors," *Int. J. Radiat. Oncol. Biol. Phys.* **52**, 729-738 (2002).
- [28] N. Lee, C. Chuang, J.M. Quivey, T.L. Phillips, P. Akazawa, L.J. Verhey, and P. Xia, "Skin toxicity due to intensity-modulated radiotherapy for head-and-neck carcinoma," *Int. J. Radiat. Oncol. Biol. Phys.* **53**, 630-637 (2002).
- [29] C. Boudreau, E. Heath, J. Seuntjens, O. Ballivy, and W. Parker, "IMRT head and neck treatment planning with a commercially available Monte Carlo based planning system," *Phys. Med. Biol.* **50**, 879-890 (2005).

Chapter 6

Construction and Validation of an Automated Few Leaf Electron Collimator

Subsequent to the verified clinical significance of the Monte Carlo-based inverse planning for energy modulated electron therapy (EMET), we proceeded with constructing the collimation device in order to provide a full solution that integrates treatment planning with delivery. In this chapter we present a paper submitted to *Medical Physics* which explains the details of the hardware and software structure of the proposed automated few leaf electron collimator (FLEC). It also shows the comprehensive sets of measurements that were used to validate the Monte Carlo calculations. Compared to previous methods of electron beam collimation, this represents the first automated delivery unit that is incorporated with a flexible optimization algorithm.

Title: Construction and dosimetry of a new automated collimator for delivery of Monte Carlo-based energy-intensity modulated electron therapy.

Authors: Khalid Al-Yahya, Frank Verhaegen, and Jan Seuntjens

Submitted: 11 November 2005

Abstract

Energy modulated electron therapy (EMET) with conventional clinical accelerators is lagging behind photon intensity modulated therapy (IMRT). Despite the capability of EMET to achieve highly conformal dose distributions in superficial targets, it has not been widely implemented due to problems inherent to electron beam radiotherapy such as planning dosimetry accuracy and verification as well as a lack of systems for automated delivery. In previous work, we proposed a novel technique to deliver EMET using an automated “few leaf electron collimator” (FLEC) that consists of four motor-driven leaves fit in a standard clinical electron beam applicator. Integrated with a Monte Carlo-based optimization algorithm fed with patient-specific dose kernels, a treatment delivery was incorporated within the linear accelerator operation. Based on Monte Carlo simulations, the FLEC was envisioned to work as an accessory tool added to the clinical accelerator. In this paper, we present the design and construction of the FLEC prototype that match our compact design goals. It is controlled using an in-house developed EMET controller. The structure of the software and the hardware characteristics of the EMET controller are demonstrated. Using a parallel plate ionization chamber, output measurements were obtained to validate the Monte Carlo calculations for a range of fields with different energies and sizes. Further verifications were also performed for comparing 1-D and 2-D dose distributions using energy independent radiochromic films. Comparisons between Monte Carlo calculations and measurements of complex intensity map deliveries show an overall agreement to within $\pm 3\%$.

6.1 Introduction

Energy modulated electron therapy (EMET) is a promising treatment modality that offers the fundamental capability to achieve highly conformal electron dose distributions tailored to superficial targets [1]. However, due to the absence of an automated collimation system that allows electron beam modulation and due to the lack of dosimetric accuracy of clinical electron pencil beam algorithms in the presence of beam modifiers, the EMET has lagged behind photon IMRT.

Considerable efforts were made to investigate the potential of delivering the EMET using bolus electron conformal therapy [2-5]. However, using custom-made bolus

remains time consuming and expensive especially there is a need to restore dose homogeneity in the target using further beam modulations [5]. An attractive alternative approach was to use a separate add-on electron collimator that could offer a simple upgradeable solution to complement the existing radiation technology. Different designs of electron multileaf collimators (eMLC) that are attachable to radiotherapy accelerators were introduced to demonstrate potential capabilities of delivering EMET [6-9]. Nevertheless, the weight of a bulky eMLC raised concerns not only in terms of lack of practicality of installing and removing such a heavy device, but also in terms of its use with gantry angles that might cause sagging of the eMLC and even of the gantry [9]. Moreover, the automation of eMLC has so far not adequately been addressed.

We have recently studied the feasibility of an automated “few-leaf electron collimator” (FLEC) for delivering the EMET using a sequence of rectangular fieldlets [10]. The FLEC is essentially composed of two pairs of trimmer bars that allow electron shaping using a combination of arbitrary rectangles. In our study, the FLEC was envisioned to serve as an add-on accessory tool. The collimation of the FLEC is backed up by the photon jaws and a sequence of apertures can form a series of fieldlets to compose a desired irregular electron field.

The delivery of complex electron fields is performed in a step-and-shoot approach. In addition to its compactness, the foremost characteristic of the prototype FLEC lies in its capability to deliver a full EMET plan in an automated fashion. The feasibility of this approach was supported by a Monte Carlo dose calculation engine and an inverse planning system was developed for this purpose. Patient-specific dose deposition kernels extracted from Monte Carlo calculations were fed into an in-house optimization algorithm that was used to select fieldlet energies and their associated intensities corresponding to the optimal plan [10].

In another study, we have shown that EMET delivered with FLEC in the context of mixed beam treatment planning could be a valuable addition to the currently available treatment techniques especially when applied to superficial tumors that are inherently difficult to plan using the IMRT [11]. Compared to the IMRT, the EMET preserves target conformity and homogeneity while significantly improving normal tissue sparing. Also, as a result of reducing the number of photon beam monitor units (MUs) for complete

dose delivery, the addition of the EMET systematically leads to a reduction in the whole body dose equivalent [11].

The photon jaw position affects the output of electron beams much more than it affects the photon beam output [12-14]. The dose delivered by electron beams, unlike with photon beams, cannot be divided into primary and secondary components. Rather, it is mainly due to the multiple scattered electrons that show their highest contribution at the depth of maximum dose (z_{\max}). This creates a critical dependence on the photon jaw collimation and, thus, emphasizes the need for accurate characterization of the energy/shape-dependent fieldlets. Although Monte Carlo techniques were previously proven to predict successfully the beam output in conventional electron beams [15-18], there has been no quantitative study to investigate the accuracy of Monte Carlo simulations in the setups that involve back-up photon jaw collimation. Therefore, further validation studies were required to evaluate the accuracy of the Monte Carlo model of the FLEC system for measurements of output, central axis dose distributions, and off-axis dose profiles as well as for measurements in regions where the presence of leakage dose is suspected. For modulated electron beams, the spatial validation can be achieved with the use of radiochromic films with their favorable energy independence characteristics [19].

In this study we present design, construction and validation of the novel automated FLEC. We also demonstrate the structure of a control unit that was built and integrated to deliver EMET plans. The accuracy of the calculated electron beam output factors has been tested against measurements performed with parallel plate ionization chamber for a range of fieldlets. Also, we have validated the Monte Carlo-calculated 1-D and 2-D dose distributions of energy modulated electron beams by comparing the distributions with results of film measurements using energy-independent HS GafChromic film.

6.2 Materials and Methods

6.2.1 Construction and automation of the few leaf electron collimator (FLEC)

6.2.1.a Design considerations

The design and materials of the FLEC prototype were guided by a series of Monte Carlo studies to optimize material/thickness/width of the FLEC and to achieve the optimal photon jaw opening associated with each desired FLEC opening (fieldlet). An optimal photon jaw opening is needed to preserve typical clinical electron beam characteristics with a narrow penumbra region and a minimized peripheral leakage dose from in-air scattering through peripheral field areas that are not covered by the FLEC leaves. To simplify the characterization of the square fieldlets, each fieldlet is designated by three parameters: the electron beam nominal energy (in MeV), photon jaw opening (represented by a number following J), and the FLEC opening collimator (represented by a number following C). For example, “18J8C7” represents a fieldlet with an energy of 18 MeV, jaw opening of $8 \times 8 \text{ cm}^2$, and collimator opening of $7 \times 7 \text{ cm}^2$. This notation applies for square fieldlets only. For the rectangular fieldlets, the exact opening for the four jaws and four FLEC collimators are required.

The collimator thickness ideally should be sufficient to stop the direct passage of all electrons as well as the produced bremsstrahlung photons of the highest energy used in the EMET optimization procedure, e.g., 18 MeV. Different material types were investigated, including tungsten, lead, and copper. A copper leaf, with a thickness of 1.2 cm, offers a good compromise among the three materials, since it is suitable to attenuate high energy electrons and also has a relatively lower yield of bremsstrahlung photons. Since we are striving to develop a light-weight collimation device and for reasons of cost and machinability, copper was selected as the leaf material for our prototype FLEC.

In the initial prototype, a leaf width of 3 cm was chosen to limit the effect of the lateral electron leakage. Despite the use of the photon jaws as backup collimation, the increased multiple Coulomb scattering exhibited by lower-energy electrons could lead to an unacceptable lateral electron leakage for the lowest energy (9 MeV) through areas that are not covered by the FLEC. Further studies were performed to minimize the lateral leakage by optimizing the margin of jaws openings (the shielding margin). Monte Carlo-calculated profiles for 18 MeV and 9 MeV electron beams were obtained for a fixed

FLEC opening projecting to a $6 \times 6 \text{ cm}^2$ field while varying the shielding margin by modifying the jaw settings to have openings of $6 \times 6 \text{ cm}^2$, $7 \times 7 \text{ cm}^2$, and $8 \times 8 \text{ cm}^2$. This is represented in our notation convention as (18J6C6, 18J7C6, and 18J8C6) for the 18 MeV fieldlets and as (9J6C6, 9J7C6, and 9J8C6) for the 9 MeV fieldlets.

The dosimetric characteristics of a fieldlet can be optimized by maximizing the output, minimizing the width of the dose penumbra and reducing the percentage dose beyond the outer edge of the leaf. Maximizing the output is favored in order to increase the efficiency of the fieldlet delivery.

The *dose penumbra 90/10* was quantified by the lateral distance between 90% and 10% points along the in-plane profile and the peripheral leakage was represented by the point of maximum leakage along the major axes (*maximum X-Leakage* for cross-plane axis and *maximum Y-leakage* for in-plane axis). These parameters were obtained from profiles calculated in Solid Water® at a depth of 2.8 cm for the 18 MeV fieldlets and at a depth of 1.5 cm for the 9 MeV fieldlets. The calculated profiles were subsequently verified by comparing them with measured profiles obtained by irradiating radiochromic HS films under the same conditions and following the protocol described below.

6.2.1.b FLEC electronics

The primary difference between the FLEC and previously reported means of electron collimation for delivering EMET is that we have opted to have a design that is completely automated without compromising compactness and practicality. To serve this purpose, each leaf is connected to a miniature stepper motor, micro-limit switch and micro-encoder taking into account the proximity of delicate electrical connections. A two-phase stepper motor with a 4-wire configuration (ARSAPE, Switzerland) was chosen to drive each leaf. Its miniature physical dimensions (a weight of 3.3 g and a front shaft length of 1.4 cm) combined with its powerful torque of 1 mN·m that is adequate to lift the copper leaf against gravity were the two main characteristics that dictated our choice. Optimal control of the FLEC requires the leaf positions to be independently verifiable. Hence, micro-encoders were incorporated to provide a feedback about the leaf movements in a “closed-loop” application. Switches were also added to simplify the automation procedure and to report further information of any electronic/mechanical failures. All the wires emerging from the FLEC were incorporated into two connectors

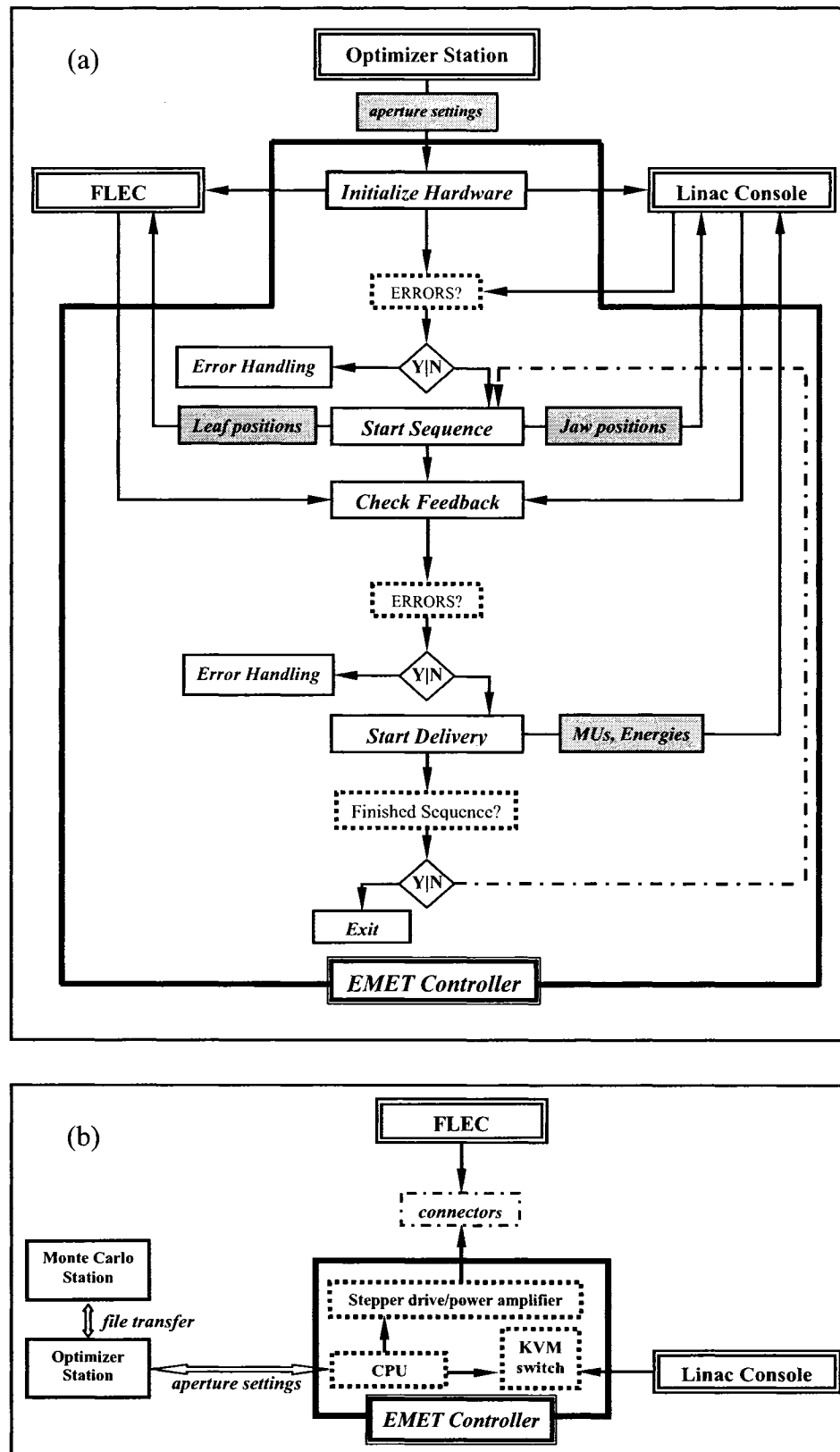


Figure 6-1: (a) Flow chart of the software structure of the EMET controller. (b) Schematic diagram of the integrated EMET hardware that communicates with the Monte Carlo-based optimization station, the FLEC, and the linear accelerator.

that communicate with an external controller using twisted pair cables. These cables were shielded for reduced noise susceptibility and enhanced signal integrity to avoid lost counts or reduced accuracy due to erroneous operations.

6.2.1.c EMET controller

The EMET controller is a delivery unit that was programmed to communicate with the optimization station and was locally assembled to accomplish the task of comprehensive delivery automation. It is a portable computer system accompanied with customized software to acquire the plan details from the optimization station and deliver the beam configuration of the optimal plan to the FLEC and the linac console.

EMET controller software

Figure 6-1(a) shows a flow chart of the structure of the EMET controller software that is programmed in C++ and operates in Windows® environment. At the end of the planning optimization process, a file is produced containing the prescribed fieldlets along with their associated energies and intensities (in terms of MUs). Four parameters are required for each prescribed fieldlet: (1) the positions of the FLEC leaves, (2) the photon jaw settings, (3) the beam nominal energy, and (4) the MU settings. The EMET controller software manages the translations of the text file containing the fieldlet prescriptions into binary commands that are sent to the FLEC as well as to the accelerator. A full treatment system has been integrated and a delivery can be performed entirely in a remotely controlled fashion. This includes initialization of the devices, sending binary signals to both the accelerator and the FLEC, reading the feedback of the positions of leaves/jaws, setting up the energies and MUs, and, finally, detecting the errors and limitations. The software was written to communicate with VARIAN accelerators operated in Service Mode.

EMET controller hardware

In terms of hardware, the EMET controller consists of three components (1) a PIII CPU equipped with a PCI -7334 board (National Instruments, Austin, TX), RS-232 port, and a Microsoft Visual Basic package; (2) MID-7604 Integrated axis stepper drive with power amplifier (National Instruments, Austin, TX); and (3) KVM switch (short for Keyboard, Video monitor, and Mouse). Built and assembled in-house, the EMET controller serves as a complete power supply and system interface that simultaneously

controls the stepper motors, analyzes the feedback from the encoders, detects the signals from switches, and, also offers a full control over the linac options.

The communication between the EMET Controller and the FLEC is carried through the shielded cables that are attached to the connectors, as previously described. On the other hand, the communication with the linac console is mediated through a KVM switch that is connected to the EMET controller through an RS-232 port from one end and to the console's keyboard from the other end. The use of the KVM switch allows a simplified "external" access for controlling the linac by emulating keyboard strokes, thus avoiding any modifications in the accelerator controller. Combining the portability of the EMET controller with the compactness of the FLEC adds to the efficiency of the system and enables the use of the FLEC with any available clinical accelerator.

6.2.2 Monte Carlo simulations

In all our Monte Carlo studies presented in this paper, the electron beams were modeled using the BEAMnrc [20,21] accelerator model to calculate phase space files for each fieldlet. The phase space files were used as source inputs that were transported through a simulated solid water phantom, with a voxel size dimension of 0.2 cm, using the XVMC [22] fast Monte Carlo code. The geometry of the FLEC was fully simulated and incorporated in our previously validated Monte Carlo model of McGill Varian CL2300 [10]. The BEAMnrc simulation parameters were set to ECUT=0.700 MeV, AE=0.521 MeV, PCUT=0.010 MeV and PRESTA II electron step algorithm. The number of initial histories ranged from 120×10^6 for 9 MeV electron beams to 80×10^6 for 18 MeV electron beams. The number of histories was chosen to ensure a statistical uncertainty (1σ) of 0.5% or less in the absorbed dose calculations surrounding regions with more than 80% of the maximum dose.

6.2.3 Ionization chamber measurements of output factors

Output factors for the electron fieldlets formed by the FLEC are defined in this work as follows:

$$OF = \frac{D_{\max}(E, \text{fieldlet})}{D_{\max}(EJ9C8)}, \quad (6-1)$$

which represents the ratio of the absorbed dose to water at the depth of maximum dose for a square fieldlet with a certain energy E to the absorbed dose to water at the depth of

maximum dose of the maximum opened fieldlet (J9C8) of the same energy at source-surface distance (SSD)=100 cm. The measured and calculated output factors were normalized to the output of the J9C8 fieldlet in order to be consistent within the same applicator/FLEC settings. Normalization in this fashion, in contrast to normalization to the standard 10×10 cm² field configuration without the FLEC, avoids manual replacement of the applicator which causes unnecessary delays and limits the automation of the QA procedure. However, this procedure does require establishment of reference dosimetry at the depth of maximum dose in the J9C8 fieldlet and therefore requires an adaptation of the TG-51 protocol [23] factors to this irradiation geometry.

Using the PPC-40 plane-parallel ionization chamber, measurements of output factors were performed at 9, 12, 15, and 18 MeV for various fieldlets. The PPC-40 chamber was cross-calibrated to the Exradin A12 Farmer chamber (Standard Imaging, Middleton) following the procedures described in the TG-51 protocol. After obtaining the parameter $k_{\text{ecal}} N_{D,w}^{60Co}$ valid for the TG-51 reference depth, the PPC-40 was positioned with its effective point of measurement at z_{max} in a water phantom of $50 \times 50 \times 40$ cm³ for each fieldlet. This depth was determined by measuring percentage depth doses ($PDDs$) using the same chamber after correcting for Monte Carlo calculated stopping power ratios water-to-air. At the reference depth corrected charge for influence quantities was determined. Thus, $D_{\text{max}}(EJ9C8)$ is obtained as:

$$D_{\text{max}}(EJ9C8) = M \cdot k'_{R_{50}} \cdot k_{\text{ecal}} N_{D,w}^{60Co} \cdot \frac{\left(\left(\frac{L}{\rho} \right)_{\text{air}}^{\text{water}} \right)_{EJ9C8}}{\left(\left(\frac{L}{\rho} \right)_{\text{air}}^{\text{water}} \right)_{10 \times 10}} \cdot \frac{(P_{\text{wall}} P_{\text{fl}})_{EJ9C8}}{(P_{\text{wall}} P_{\text{fl}})_{10 \times 10}}, \quad (6-2)$$

where M is the collected charge at z_{max} corrected for influence quantities, polarity, and ion recombination. The parameter $k_{\text{ecal}} N_{D,w}^{60Co}$ is determined from the cross calibration and $k'_{R_{50}}$ is obtained from the TG-51 formula for the Roos ionization chamber. It is reasonable to assume that the ratios of P correction factors can be neglected. The depth-dependent stopping power ratios, water to air, were obtained from Monte Carlo calculation using the EGSnrc/SPRZnrc code. The stopping power ratio was calculated for each fieldlet at the z_{max} and the correction was applied to determine the output as shown above.

6.2.4 Film measurements

6.2.4.a Film analysis

Calibration and dose measurement of HS films were performed following the protocol proposed by Devic *et al.* [24]. Multiple film pieces were exposed to a range of electron beam dose irradiations. A calibration curve, fitted with a 6th order polynomial, was determined in order to convert optical density change to dose. This calibration curve was examined for multiple electron energies so as to confirm its energy independence. The film sheets were consistently placed at the same position in the center of an Agfa Arcus II desktop flat-bed document scanner and were scanned using the AGFA FotoLook 3.5 software with a scanning resolution of 0.2 mm/pixel in the 48-bit RGB transparent mode. The scanned images were transferred into an in-house developed MATLAB routine (Version 6.5.0 The Math Works, Natick, MA), where they were processed to obtain net optical densities of the exposed films and from there the corresponding dose values. The response of the scanner was analyzed to eliminate faulty pixels and to correct the readings of the pixels that are dependent on both the position and the optical intensity. It has been reported that applying this protocol for HS GafChromic® films results in an improved dose uncertainty ranging from 3% for doses above 5 Gy to 2% for doses above 10 Gy [24].

6.2.4.b 1-D measurements

HS GafChromic film was used for comparison between calculation and measurements of central axis depth doses and profiles. Radiochromic films have been shown to be nearly energy independent [19], hence, they can be used for *PDD* measurements with the electron beam axis parallel to the film. Reporting the dose in absolute terms, using radiochromic films for central axis depth dose and profile measurements served also as a verification of output measurement to confirm our previously described reference dose measurements. In addition, the HS films show relative output differences for different beam energies with the same FLEC settings. The drawback of using films to measure *PDDs*, however, is the film's inaccurate dose measurement in regions at depths less than 1 cm, as discussed by Shiu *et al.* [25] and partly attributed to edge effects of radiochromic films [24,26].

PDD curves were measured at 100 cm *SSD* for four fieldlets: J9C8, J7C6, J5C4, and J3C2 for energies of 9, 12, 15, and 18 MeV. A sheet of HS film with dimensions of $2.5 \times 12 \text{ cm}^2$ was inserted between two slabs of Solid Water® with dimensions of $(30 \times 30 \times 10 \text{ cm}^3)$. A special device was constructed to press the slabs together to minimize airgaps. The linac output was measured before and after the irradiation using a cylindrical ionization chamber to determine the dose delivered to the film. To obtain the absorbed dose, the Monte Carlo calculated dose, which is reported in terms of dose per particle, is converted to dose in Gy/MU by assigning the dose/MU measured by the ionization chamber for the J9C8 fieldlet to the calculation dose under the same settings. This normalization procedure is applied only once per energy and all the subsequent calculations for the other fieldlets are reported with respect to this calibration.

6.2.4.c 2-D measurements

2-D isodose curve distributions were measured by HS films for various fieldlets as well as for an intensity map based on the sum of these fieldlets at different depths. Standard HS film sheets ($12.7 \times 12.7 \text{ cm}^2$) were irradiated with 2000 MUs after being sandwiched between layers of Solid Water® at a depth of 2.8 cm for fieldlets 12J9C8 and 9J5C4. To examine the behavior of the off-axis fieldlets, two additional sheets were irradiated at the same depth under fieldlets having energies of 15 MeV and 18 MeV with asymmetric jaws/FLEC configurations that partially blocked the electron beams.

Following the irradiation of these individual fieldlets, two sheets, placed at depths of 3 cm and 5 cm, were exposed to a combination of the four fieldlets with a prescription of 750 MUs given to each of them. The 2-D isodose lines were obtained and compared to the calculation.

6.3 Results

6.3.1. FLEC prototype

Based on the results of the Monte Carlo simulations, a prototype of the FLEC was designed and machined using CAD technology. The FLEC is comprised of two perpendicular sets of 2 leaves where each copper leaf has a thickness of 1.2 cm and a width of 3.0 cm. Figure 6-2 shows the computer design of the FLEC. It consists, in verification of the position of the leaves independently from the motor driving software.

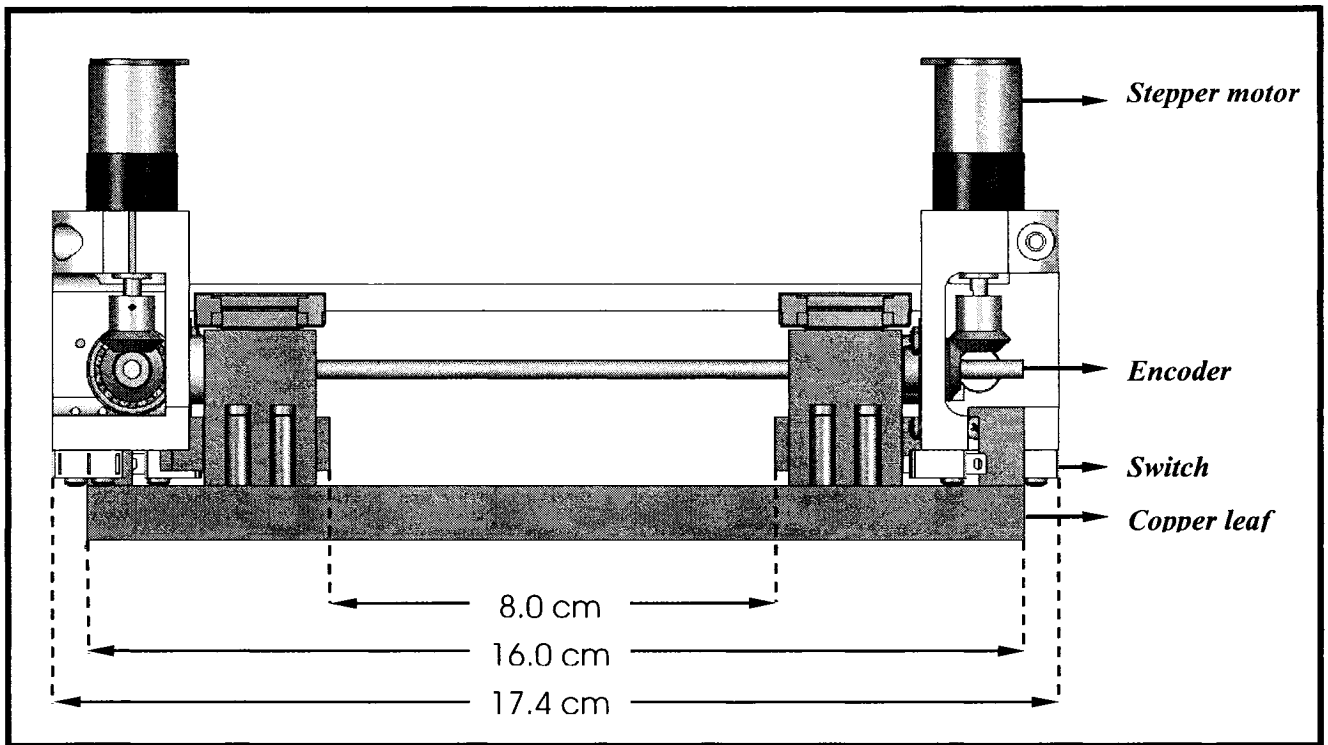


Figure 6-2: Design drawing showing a side view of the FLEC prototype.

Each leaf moves on a linear ball-bearing in order to minimize friction. With all these considerations, the FLEC maximum fieldlet opening is $8 \times 8 \text{ cm}^2$. Using the same electronic parts, a field size of $13 \times 13 \text{ cm}^2$ is achievable with a FLEC designed to fit in a $20 \times 20 \text{ cm}^2$ applicator and a field size of $18 \times 18 \text{ cm}^2$ is also feasible with the FLEC mounted in the $25 \times 25 \text{ cm}^2$ applicator.

Figure 6-3 shows the compact prototype of the FLEC compatible with Varian's clinical $15 \times 15 \text{ cm}^2$ electron applicator. The downstream edge of the lower part of the FLEC is 5 cm above the isocenter. Although in the current prototype the leaf ends have straight edges, the FLEC design allows replacement of these leaves by leaves with rounded ends but this is a topic requiring further investigations. The manufacturing followed a design where all the parts could be replaced easily in case of mechanical and/or electrical failure. The total FLEC weight is less than 2.5 kg.

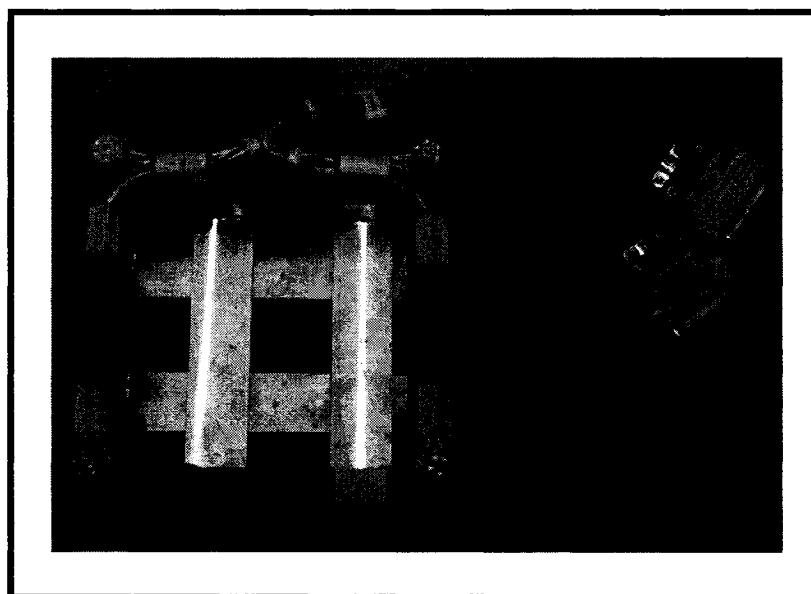


Figure 6-3: *The FLEC prototype, including the necessary wiring, shows its compact design to fit in a clinical applicator.*

Powered and controlled through two external connectors, the FLEC was automated and the controlling software was integrated in the EMET controller running under Windows®.

6.3.2 Leaf and backup jaw optimization

Figure 6-4(a) shows measured and calculated off-axis dose distributions of 18 MeV electron beams for multiple settings of jaw collimation, while maintaining the opening of the FLEC to project a field of $6 \times 6 \text{ cm}^2$ at $SSD=100 \text{ cm}$. Both the profile shape and output change by varying the shielding margin. When normalized to the maximum dose (Fig. 6-4(b)) at the centre of the profile, the dependence of the relative fall-off in the penumbra region on the jaw settings becomes clear. Figure 6-4(b) also shows the shielding margin effects on the relative peripheral leakage dose in the areas not covered by the leaves. At lower energies, the output dependence on the jaw settings is more pronounced and the leakage dose effects are magnified due to the in-air increased multiple Coulomb scattering. As shown in Figures 6-5(a) and (b), measurements and calculations for 9 MeV verify the manifestation of the leakage dose with the use of lower energies.

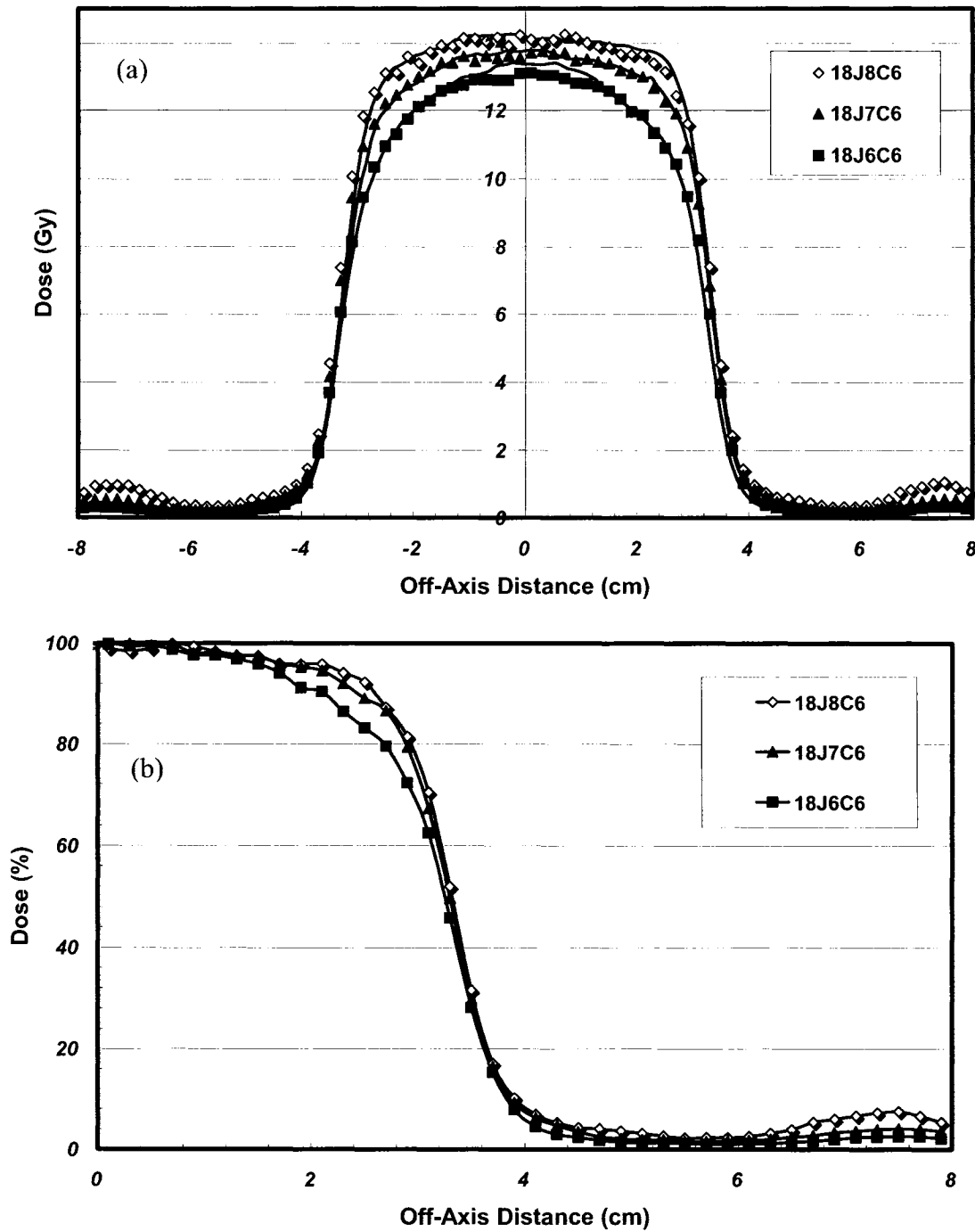


Figure 6-4: (a) Calculated (symbols) and measured (full lines) off-axis profiles for three 18 MeV fieldlets with a fixed FLEC opening (at C6) and varying jaw openings (J8(◇), J7(▲), and J6(■)) based on a delivery of 1500 MUs. (b) The calculated normalized profiles of the three fieldlets .

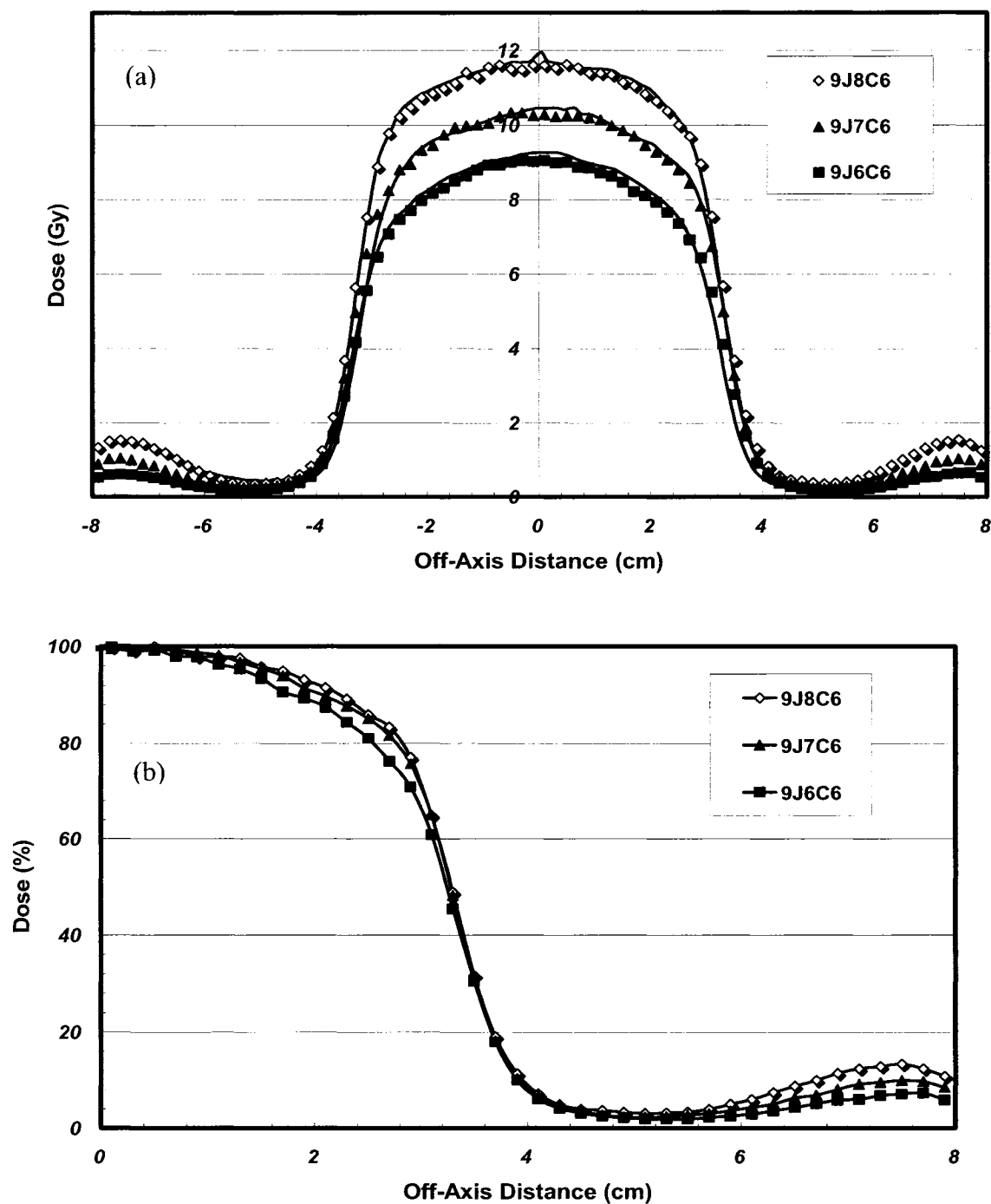


Figure 6-5: (a) Calculated (symbols) and measured (full lines) off-axis profiles for three 9 MeV fieldlets with a fixed FLEC opening (at C6) and varying jaw openings (J8(◇), J7(▲), and J6(■)) based on a delivery of 1500 MUs. (b) The calculated normalized profiles of the three fieldlets.

Three parameters (namely: the *Dose penumbra 90/10*, *maximum Y-Leakage*, and output factor) that quantify the relative differences between different jaw settings were used to evaluate the dosimetric characteristics of the fieldlets. Table 6-1(a) shows the effect of the shielding margin on these characteristics. The fieldlets that have jaw settings that project a shielding margin of 2 cm (18J8C6 and 9J8C6) provide the highest output and lowest penumbra but they also provide the highest undesirable *maximum Y-Leakage*. In contrast, jaw openings that have no margin (18J6C6 and 9J6C6) show the lowest leakage but the output and the penumbra width are deteriorated for both 18 MeV and 9 MeV.

Jaw openings that project to the same opening of the FLEC with an added projected margin of 1 cm (18J7C6 and 9J7C6) showed to be the configuration that optimizes the dosimetric quality of the fieldlet. The profiles that are measured along the in-plane axis (denoted as *Y-axis*) would follow the projection of the upper jaws and, therefore, would cause more significant leakage dose than the profiles measured along the cross-plane axis (denoted as *X-axis*) under the lower jaws that are closer to *SSD*=100 cm. Thus, the profiles shown in Figures 6-4 and 6-5 and their consecutive parameters represent the extreme case while the profiles that are calculated along the cross-plane would exhibit a reduced leakage dose.

Table 6-1(b) shows the *Dose penumbra 90/10*, *maximum Y-leakage*, and *maximum X-leakage* for different fieldlets following the optimum configuration of jaw settings. Although the leakage dose should be minimized to improve the efficacy of the inverse planning optimization procedure, our Monte Carlo-based optimization algorithm takes the “actual” leakage dose into account during optimization and in the final dose distribution. The optimizer has the complete dose information that allows it to evaluate the role of the leakage doses in the objective function. Based on their contribution (or their violation) to the optimal plan, the fieldlets that exhibit high leakage dose are accepted for modulation (or rejected).

6.3.3 Comparison of calculated and measured dose from FLEC-defined fields

6.3.3.a Output measurements at the reference point

A comparison between measured and calculated output factors for a selection of square fieldlets is shown in Table 6-2 for 9-18 MeV electron beams. The output was

(a)

Fieldlet	Dose penumbra 90/10 (mm)	Y-Leakage Peak (%)	Output
18 J8 C6	13.5	6.6	0.987
18 J7 C6	15	3.6	0.964
18 J6 C6	17.5	2.4	0.925
9 J8 C6	18	11.4	0.94
9 J7 C6	20	8.0	0.837
9 J6 C6	22	5.8	0.741

(b)

Fieldlet	Dose penumbra 90/10 (mm)	Y-Leakage Peak (%)	X-Leakage Peak (%)
18 J9 C8	16	2.1	1.4
18 J7 C6	15	3.6	1.9
18 J5 C4	14.5	2.9	1.8
18 J3 C2	10	2.5	1.3
9 J9 C8	21.5	3.1	2.2
9 J7 C6	20	8.0	3.4
9 J5 C4	15.5	8.5	3.6
9 J3 C2	11	8.6	3.7

Table 6-1: (a) Numerated factors obtained from the off-axis profiles of 9 and 18 MeV of different jaw openings corresponding to a certain FLEC opening (C6). (b) Dose penumbra 90/10, Y-Leakage Peak, and X-Leakage Peak for different fieldlets following the optimum jaw opening.

Nominal Energy	Fieldlet	z_{max}	Measured Output	Calculated Output	% diff
9 MeV	9 J9 C8	2.2	1.000	1.000	
	9 J7 C6	2.2	0.835	0.837	0.3
	9 J5 C4	2.2	0.541	0.535	0.9
	9 J3 C2	1.3	0.221	0.224	-1.1
12 MeV	12 J9 C8	2.8	1.000	1.000	
	12 J7 C6	2.7	0.906	0.900	0.6
	12 J5 C4	1.9	0.717	0.696	2.9
	12 J3 C2	1.3	0.356	0.363	-1.9
15 MeV	15 J9 C8	3.2	1.000	1.000	
	15 J7 C6	2.2	0.972	0.950	2.2
	15 J5 C4	1.7	0.829	0.799	3.6
	15 J3 C2	1.3	0.469	0.476	-1.4
18 MeV	18 J9 C8	2.8	1.000	1.000	
	18 J7 C6	2.8	0.973	0.964	0.9
	18 J5 C4	2.1	0.878	0.855	2.5
	18 J3 C2	1.5	0.558	0.572	-2.4

Table 6-2: Measured and calculated output factors for the 9, 12, 15, and 18 MeV electron beams for different fieldlets. Measurements were performed with a PPC40 parallel plate chamber in water and the localization of z_{max} was determined from ionization measurements about z_{max} . The output for each energy is normalized to the measured dose at the largest fieldlet (J9 C8).

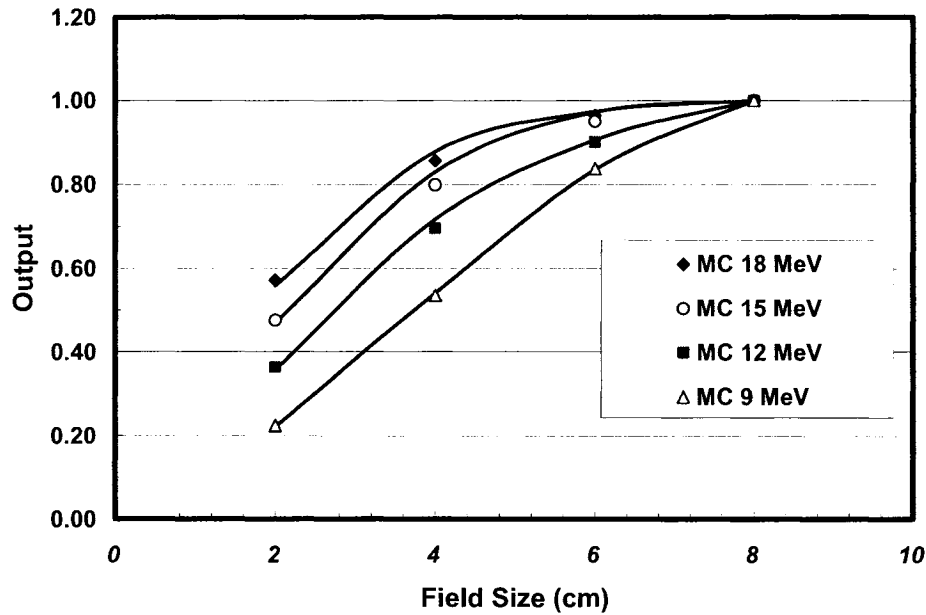


Figure 6-6: Calculated (symbols) and measured (full lines) output factors for the 9, 12, 15, and 18 MeV electron beams for different fieldlet sizes. The output for each energy is normalized to the measured dose at the largest fieldlet (J9 C8).

measured at z_{\max} and normalized to the open fieldlet formed by the FLEC (J9C8). Similarly, the calculated value at the corresponding depth, which is reported in dose per particle, was also normalized to the dose per particle value calculated for J9C8. For consistency, the measured z_{\max} was chosen as the reference in case of differences occurring in defining z_{\max} between measurements and calculations (the position of z_{\max} agreed within ± 2 mm). As shown in Table 6-2, the predicted Monte Carlo output is generally in good agreement with measurements with only one case showing a difference that exceeds 3%. We have no explanation for the latter disagreement.

For all energies, the measured output is higher than the calculation except at the lowest opening with a (J3C2) configuration where the measured output becomes lower. This could be attributed to the contribution of backscattered electrons from the jaws into the monitor ionization chamber, hence reducing the measured dose as demonstrated in a study by Verhaegen *et al.* [27].

Figure 6-6 shows the measured and the calculated output and their dependence on both energy and field size. Although, the output demonstrates a similar sharp fall-off with

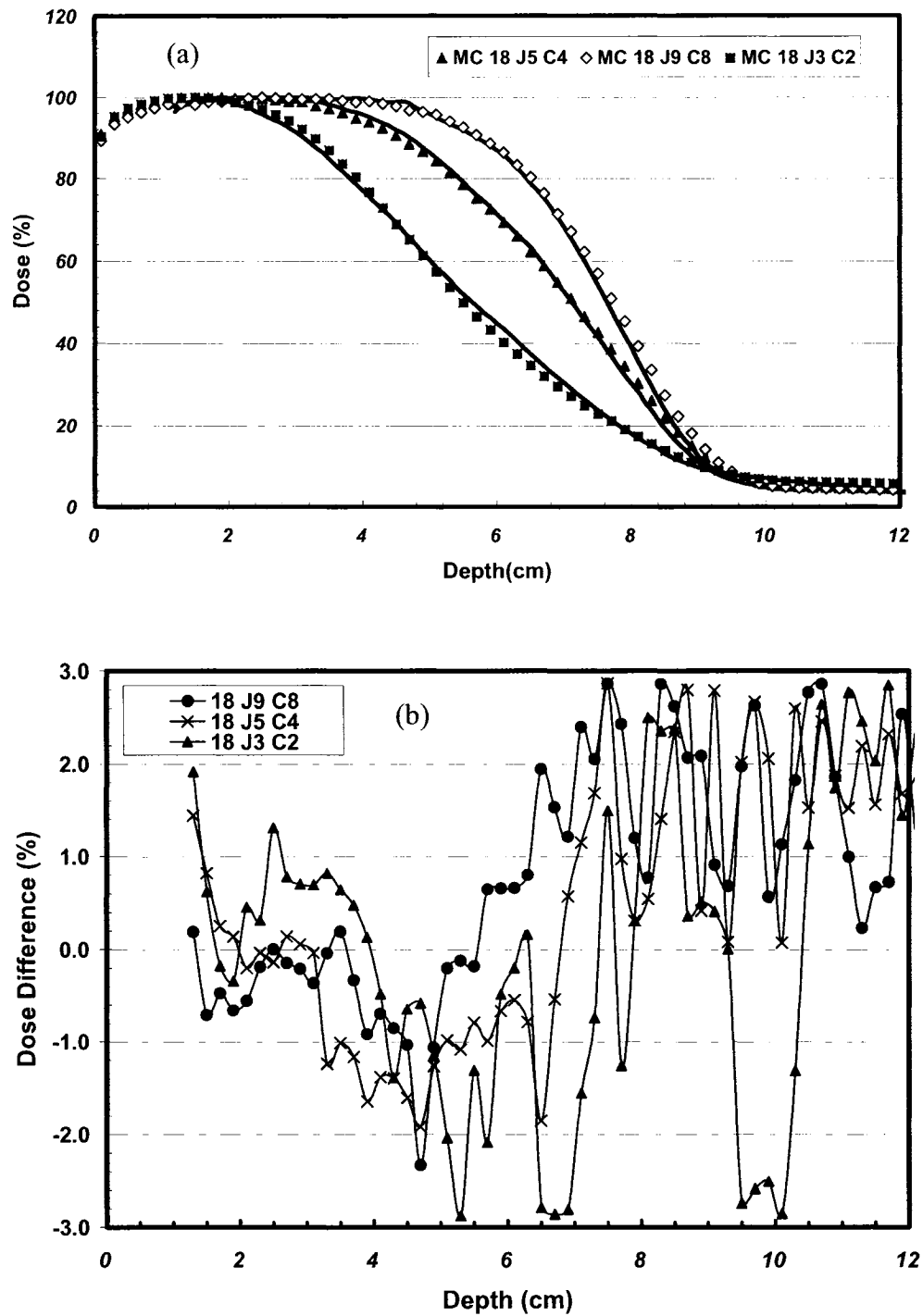


Figure 6-7: (a) Calculated (symbols) and measured (full lines) depth dose distribution for three fieldlets with energy of 18 MeV and openings J9 C8(◇), J5 C4(▲), and J3 C3(■). (b) the differences (calculated- measured), expressed as the absolute difference.

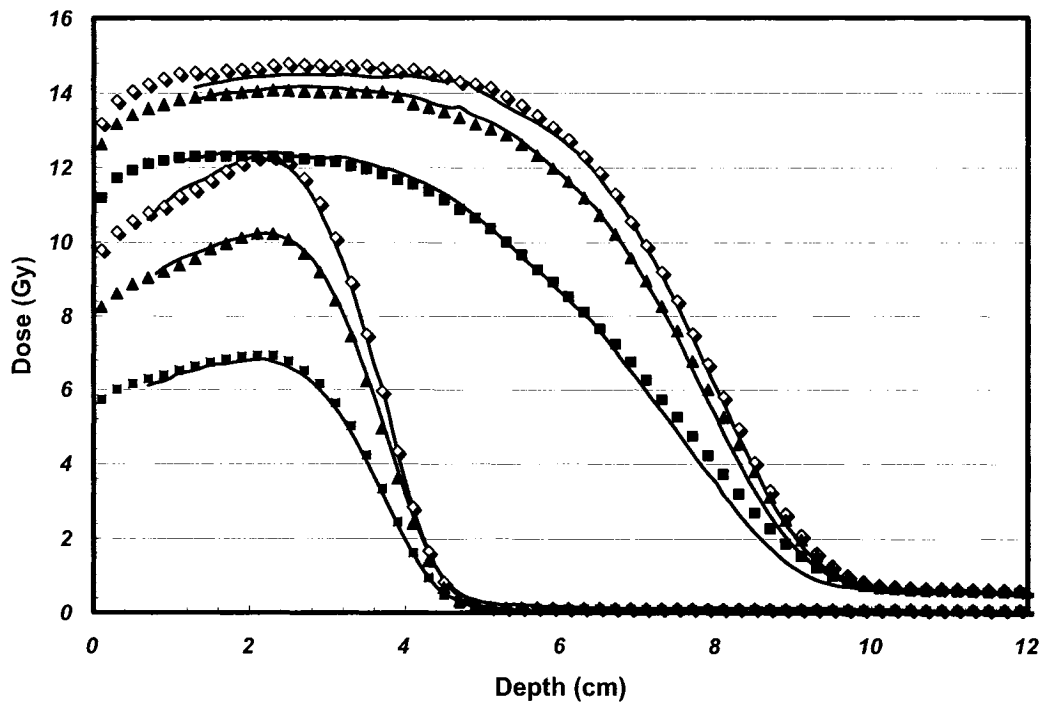


Figure 6-8: Calculated (symbols) and measured (full lines) central depth dose distribution based on 1500 MUs given for three fieldlets with energies of 9 MeV and 18 MeV and openings J9 C8(\diamond), J7 C6(\blacktriangle), and J5 C4(\blacksquare).

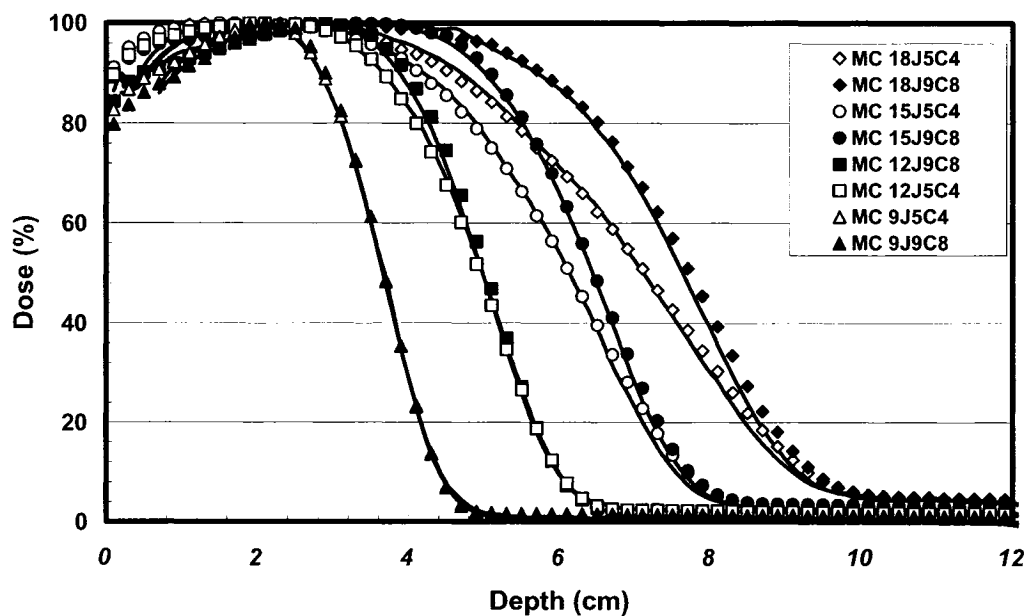


Figure 6-9: Calculated (symbols) and measured (full lines) normalized depth dose distribution for two fieldlets (J9 C8 and J5 C4) for 9, 12, 15, and 18 MeV electron beams. The solid symbols represent the fieldlet J9 C8 and the open symbols represent the fieldlet J5 C4.

decreasing field size for all energies, the field size dependence for lower energies is more significant.

6.3.3.b Central axis depth dose

Figure 6-7(a) shows measured and calculated depth dose distributions in Solid Water® for 18 MeV electron beams for fieldlets 18J9C8, 18J5C4, and 18J3C2. The calculated depth dose was normalized to the integrated dose under the curves in the region between 0.5 cm and the depth corresponding to 80% of the maximum dose. This procedure was necessary to avoid the propagation of statistical uncertainties that could result from normalizing to a Monte Carlo point dose calculation. Figure 6-7(b) shows the difference between calculation and measurement in terms of percentage dose for the three fieldlets. Generally, a good agreement is found with a maximum deviation of less than 3%. Most of the significant deviations appear at depths associated with the bremsstrahlung tail where the Monte Carlo statistical uncertainty is usually higher (up to 1.5%, one sigma). The difference between the measured and calculated depth doses in the high dose gradient region was within 1.5 mm.

Expressed in absolute dose, the comparison of measurement vs. calculation in central axis dose distribution is shown in Fig. 6-8 for 18 MeV and 9 MeV for the fieldlets J9C8, J7C6, and J5C4. Calculation and measurements agree well for both the output factors and the depth dose behavior. For the six fieldlets shown, the discrepancy in output is well within 1% around z_{\max} and the differences for other depths are never worse than 1 mm except for the lower part of the 18J5C4 fieldlet where the difference was within 2 mm. The calculation was corroborated by the consistency of the output factor measurements obtained by both film and ionization chamber.

Figure 6-9 shows the validation of the normalized Monte Carlo calculated *PDDs* when compared to film measurements for two fieldlets (J9C8 and J5C4) for the energies 9, 12, 15, and 18 MeV. R_{90} , R_{80} , R_{50} , and z_{\max} were predicted well by the calculation. Figure 6-9 also shows the ability of the calculation to account for the effect of the field size on the *PDD* behavior that appears most clearly with the highest energy. The differences vanish for the lowest energy.

The good agreement between Monte Carlo calculations and measurements that was shown for multiple profiles in the previous section is considered as another form of

the 1-D validation where it proved the ability of the model to predict precisely the shape of the measured profile distribution including the leakage effect.

6.3.3.c 2-D dose distributions

Figures 6-10(a) and 6-10(b) compare the resulting calculated and film-measured dose distributions for the fieldlets 9J7C6 and 12J9C8 based on an irradiation with 2000 MUs. With a same amount of delivered MUs, the comparison of dose distributions of partially blocked fields for 15 MeV and 18 MeV are shown in Figures 6-10(c) and 6-10(d). The summation of four fieldlets of different energies and with different jaws/FLEC configurations produces dose distributions that are shown in Figures 6-10(e) and 6-10(f) at depths of 3 cm and 5 cm, respectively. The isodose lines obtained from Monte Carlo calculations and measurements, reported in absorbed dose in Gy, are in excellent agreement. The similarity in the intensity maps includes the effect of the beam output, the isodose lines representing the high dose region, and the low-isodose lines. The leakage dose is well predicted except at the edges of the film where artifacts are present.

6.4 Conclusions and Future Work

The results of this work confirm our design objectives and support the potential of using the prototype FLEC for automated EMET. The FLEC was designed and constructed based on Monte Carlo simulations and was incorporated within the clinical accelerator operation so as to be easily controlled using the in-house developed EMET controller.

Monte Carlo simulations, which represent the dose calculation engine for our proposed EMET, generally showed good agreement with measurements for different experimental setups including output factors, *PDDs*, off-axis profiles, and 2-D dose distributions. For all energies studied, the dosimetric properties observed with measurements for the electron beams collimated using the FLEC were well predicted by Monte Carlo simulations.

With its current design, the FLEC is able to deliver treatment plans in step-and-shoot for *SSD* settings. Based on a previous study, a full EMET delivery is feasible within a 15 minutes time slot [10]. Since the FLEC is automated, we plan to investigate its use in dynamic deliveries, such as arc therapy and also in an operation mode

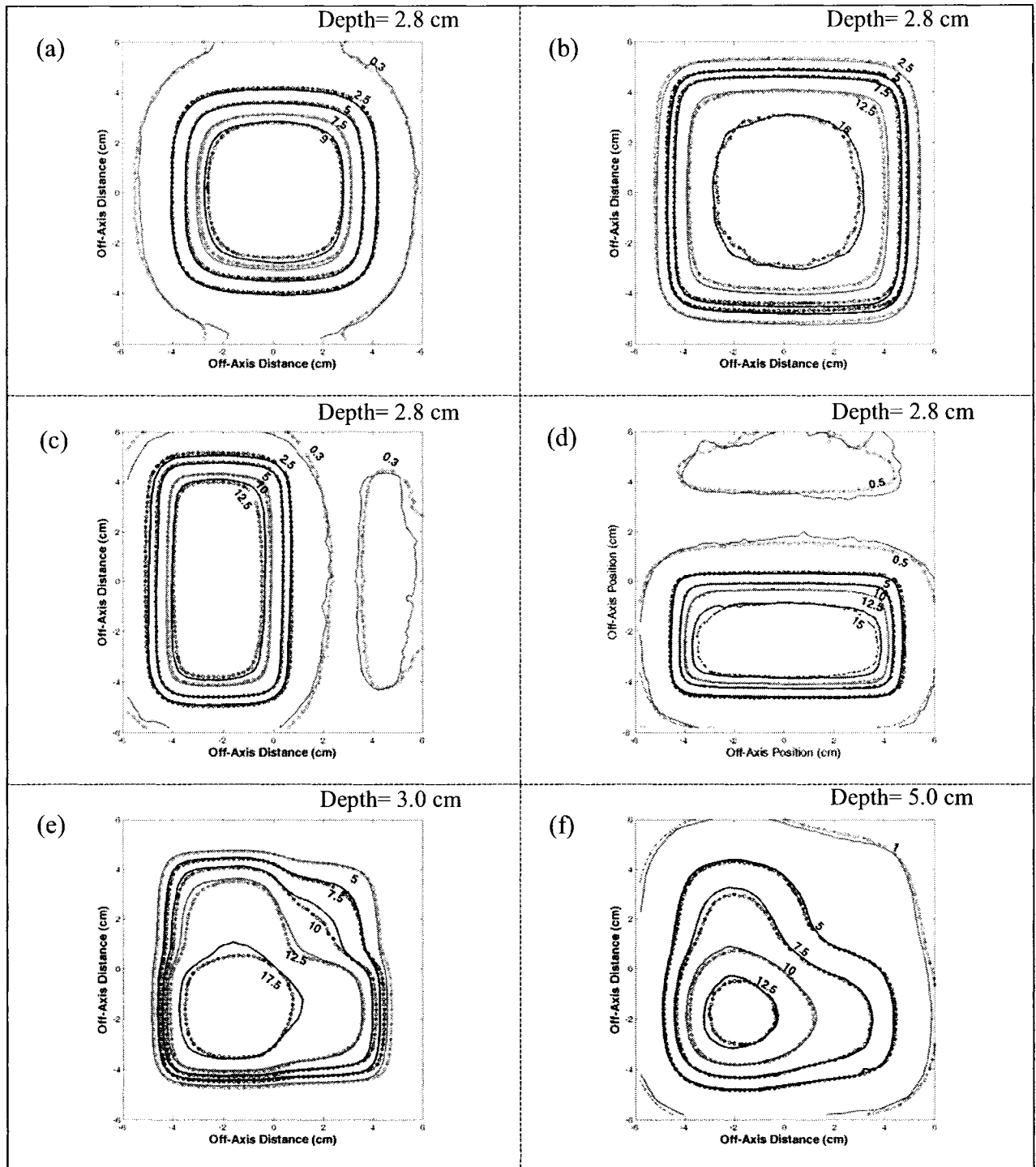


Figure 6-10: Absorbed dose distribution comparisons between HS film measurements (full lines) and Monte Carlo calculation (dotted lines) based on 2000 MUs irradiations at depth of 2.8 cm for (a) 9 MeV fieldlet with J7 C6, (b) 12 MeV fieldlet with J9 C8, (c) 15 MeV fieldlet, and (d) 18 MeV fieldlet. (e) and (f) Absorbed dose distribution comparison at depths of 3 cm (e) and 5 cm (f) for an intensity map formed by sum of the above four fieldlets with 750 MUs given to each of them. The Monte Carlo calculation accurately predicts the dose distribution of the mixed energy beam delivery at different depths.

synonymous to a dynamic wedge in photon beam therapy. This would require developing a new component module for BEAMnrc that efficiently simulates the movement with high accuracy in similar fashion to the dynamic wedge module [28] and the DYNMLC module [29] that was previously developed in our department. Also, we plan to design a new retractable applicator that allows isocentric deliveries, including arc therapy.

Acknowledgments:

The authors would like to thank Dr. Ervin Podgorsak for correcting the manuscript and Dr. Slobodan Devic for helpful discussions of this work. This work has been supported in part by the Canadian Institutes of Health Research through grant MOP 79448 and by Terry Fox Foundation grant No. 016298. K.A. acknowledges support from the Saudi Cultural Bureau. J. S. is a Research Scientist of the National Cancer Institute of Canada appointed with funds provided by the Canadian Cancer Society. F.V. is a Research Scientist supported by Fonds de recherche en santé du Québec.

References

- [1] K.R. Hogstrom, J.A. Antolak, R.J. Kudchadker, C.M. Ma, and D.D. Leavitt, "Modulated Electron Therapy," in: *Intensity-Modulated Radiation Therapy, The State of the Art: Proceedings of the 2003 Summer School*, edited by J.R. Palta, T.R. Mackie (Medical Physics Publishing, Madison, 2003), pp. 749-786.
- [2] D.A. Low, G. Starkschall, S.W. Bujnowski, L.L. Wang, and K.R. Hogstrom, "Electron bolus design for radiotherapy treatment planning: bolus design algorithms," *Med. Phys.* **19**, 115-124 (1992).
- [3] D.A. Low, G. Starkschall, N.E. Sherman, S.W. Bujnowski, J.R. Ewton, and K.R. Hogstrom, "Computer-aided design and fabrication of an electron bolus for treatment of the paraspinal muscles," *Int. J. Radiat. Oncol. Biol. Phys.* **33**, 1127-1138 (1995).
- [4] G.H. Perkins, M.D. McNeese, J.A. Antolak, T.A. Buchholz, E.A. Strom, and K.R. Hogstrom, "A custom three-dimensional electron bolus technique for optimization of postmastectomy irradiation," *Int. J. Radiat. Oncol. Biol. Phys.* **51**, 1142-1151 (2001).
- [5] R.J. Kudchadker, K.R. Hogstrom, A.S. Garden, M.D. McNeese, R.A. Boyd, and J.A. Antolak, "Electron conformal radiotherapy using bolus and intensity modulation," *Int. J. Radiat. Oncol. Biol. Phys.* **53**, 1023-1037 (2002).
- [6] B.P. Ravindran, I.R. Singh, S. Brindha, and S. Sathyan, "Manual multi-leaf collimator for electron beam shaping--a feasibility study," *Phys. Med. Biol.* **47**, 4389-4396 (2002).
- [7] C.M. Ma, T. Pawlicki, M.C. Lee, S.B. Jiang, J.S. Li, J. Deng, B. Yi, E. Mok, and A.L. Boyer, "Energy- and intensity-modulated electron beams for radiotherapy," *Phys. Med. Biol.* **45**, 2293-2311 (2000).
- [8] M.C. Lee, S.B. Jiang, and C.M. Ma, "Monte Carlo and experimental investigations of multileaf collimated electron beams for modulated electron radiation therapy," *Med. Phys.* **27**, 2708-2718 (2000).
- [9] K.R. Hogstrom, R.A. Boyd, J.A. Antolak, M.M. Svatos, B.A. Faddegon, and J.G. Rosenman, "Dosimetry of a prototype retractable eMLC for fixed-beam electron therapy," *Med. Phys.* **31**, 443-462 (2004).
- [10] K. Al-Yahya, D. Hristov, F. Verhaegen, and J. Seuntjens, "Monte Carlo-based modulated electron beam treatment planning using a few leaf electron collimator - feasibility study," *Phys. Med. Biol.* **50**, 847-857 (2005).
- [11] K. Al-Yahya, M. Schwartz, G. Shenouda, F. Verhaegen, C. Freeman, and J. Seuntjens, "Energy modulated electron therapy using a few leaf electron collimator in combination

- with IMRT and 3D-CRT: Monte Carlo-based planning and dosimetric evaluation," *Med. Phys.* **32**, 2976-2986 (2005).
- [12] L. Olofsson, M.G. Karlsson, and M. Karlsson, "Photon and electron collimator effects on electron output and abutting segments in energy modulated electron therapy," *Med. Phys.* **32**, 3178-3184 (2005).
- [13] M.D. Mills, K.R. Hogstrom, and R.S. Fields, "Determination of electron beam output factors for a 20-MeV linear accelerator," *Med. Phys.* **12**, 473-476 (1985).
- [14] M.D. Mills, K.R. Hogstrom, and P.R. Almond, "Prediction of electron beam output factors," *Med. Phys.* **9**, 60-68 (1982).
- [15] P. Bjork, T. Knoos, and P. Nilsson, "Measurements of output factors with different detector types and Monte Carlo calculations of stopping-power ratios for degraded electron beams," *Phys. Med. Biol.* **49**, 4493-4506 (2004).
- [16] F. Verhaegen, C. Mubata, J. Pettingell, A.M. Bidmead, I. Rosenberg, D. Mockridge, and A.E. Nahum, "Monte Carlo calculation of output factors for circular, rectangular, and square fields of electron accelerators (6-20 MeV)," *Med. Phys.* **28**, 938-949 (2001).
- [17] G.X. Ding, J.E. Cygler, G.G. Zhang, and M.K. Yu, "Evaluation of a commercial three-dimensional electron beam treatment planning system," *Med. Phys.* **26**, 2571-2580 (1999).
- [18] A. Kapur, C.M. Ma, E.C. Mok, D.O. Findley, and A.L. Boyer, "Monte Carlo calculations of electron beam output factors for a medical linear accelerator," *Phys. Med. Biol.* **43**, 3479-3494 (1998).
- [19] A. Niroomand-Rad, C.R. Blackwell, B.M. Coursey, K.P. Gall, J.M. Galvin, W.L. McLaughlin, A.S. Meigooni, R. Nath, J.E. Rodgers, and C.G. Soares, "Radiochromic film dosimetry: recommendations of AAPM Radiation Therapy Committee Task Group 55. American Association of Physicists in Medicine," *Med. Phys.* **25**, 2093-2115 (1998).
- [20] D.W. Rogers, B.A. Faddegon, G.X. Ding, C.M. Ma, J. We, and T.R. Mackie, "BEAM: a Monte Carlo code to simulate radiotherapy treatment units," *Med. Phys.* **22**, 503-524 (1995).
- [21] D.W. Rogers, C.M. Ma, B.R. Walters, G.X. Ding, D. Sheikh-Bagheri, and G.G. Zhang, "BEAMnrc Users Manual, National Research Council of Canada, Ottawa, Report PIRS-0509(A)G," (2002).
- [22] I. Kawrakow and M. Fippel, "Investigation of variance reduction techniques for Monte Carlo photon dose calculation using XVMC," *Phys. Med. Biol.* **45**, 2163-2183 (2000).

- [23] P.R. Almond, P.J. Biggs, B.M. Coursey, W.F. Hanson, M.S. Huq, R. Nath, and D.W. Rogers, "AAPM's TG-51 protocol for clinical reference dosimetry of high-energy photon and electron beams," *Med. Phys.* **26**, 1847-1870 (1999).
- [24] S. Devic, J. Seuntjens, E. Sham, E.B. Podgorsak, C.R. Schmidlein, A.S. Kirov, and C.G. Soares, "Precise radiochromic film dosimetry using a flat-bed document scanner," *Med. Phys.* **32**, 2245-2253 (2005).
- [25] A.S. Shiu, V.A. Otte, and K.R. Hogstrom, "Measurement of dose distributions using film in therapeutic electron beams," *Med. Phys.* **16**, 911-915 (1989).
- [26] S. Devic, J. Seuntjens, G. Hegyi, E.B. Podgorsak, C.G. Soares, A.S. Kirov, I. Ali, J.F. Williamson, and A. Elizondo, "Dosimetric properties of improved GafChromic films for seven different digitizers," *Med. Phys.* **31**, 2392-2401 (2004).
- [27] F. Verhaegen, R. Symonds-Tayler, H.H. Liu, and A.E. Nahum, "Backscatter towards the monitor ion chamber in high-energy photon and electron beams: charge integration versus Monte Carlo simulation," *Phys. Med. Biol.* **45**, 3159-3170 (2000).
- [28] F. Verhaegen and H.H. Liu, "Incorporating dynamic collimator motion in Monte Carlo simulations: an application in modelling a dynamic wedge," *Phys. Med. Biol.* **46**, 287-296 (2001).
- [29] E. Heath, J. Seuntjens, and D. Sheikh-Bagheri, "Dosimetric evaluation of the clinical implementation of the first commercial IMRT Monte Carlo treatment planning system at 6 MV," *Med. Phys.* **31**, 2771-2779 (2004).

Chapter 7**Summary and Future Work****7.1 Summary**

Energy modulated electron therapy (EMET) has been proposed to deliver highly conformal treatments to superficial targets that are less suitable for conventional x-ray intensity modulated radiation therapy (IMRT). However, EMET has not yet been used to its full potential due to the absence of a practical automated collimating device that is able to provide a series of different field openings (beamlets) during the treatment and the difficulties arising from limited dosimetric accuracy when using pencil beam algorithms in conjunction with beam modifiers. The main objective of this work was to develop, implement, and validate a practical technique of delivering EMET. This technique (1) allows for flexible, Monte Carlo-based inverse planning of modulated electron treatment and (2) employs the use of a custom-made automated electron collimator as a delivery method. Designed and constructed in-house, the few leaf electron collimator (FLEC) serves as an accessory to the current-day accelerator equipment. More importantly, the operation of the FLEC is comprehensively integrated into the planning process. The work in this thesis is summarized as follows.

7.1.1 Construction and automation of the few leaf electron collimator (FLEC)

Guided by a series of Monte Carlo studies, a prototype of the FLEC was designed and machined so that it is suitable to be attached to a clinical electron applicator. Figure 7-1 shows the final computer design and the realization of the compact and light-weighted FLEC. It fits in the electron applicator and is readily automated with controlling

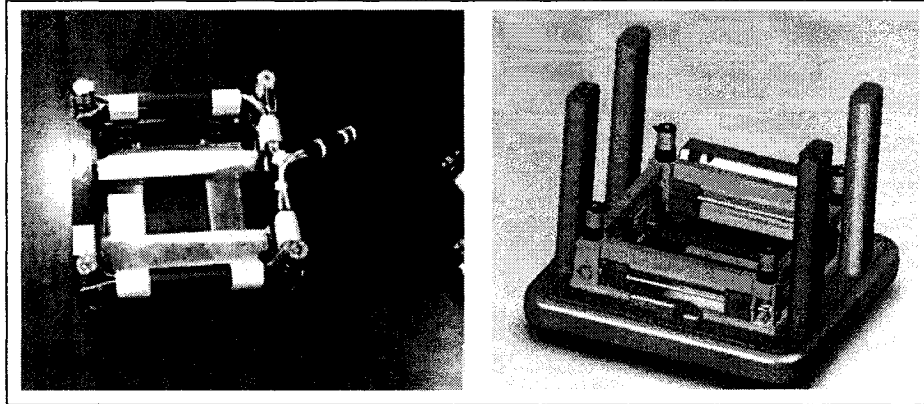


Figure 7-1: *The design of the FLEC prototype, including the necessary wiring, shows its compact design to fit in a clinical applicator.*

software that has been developed to run in the Windows® environment. The controlling software has been customized to acquire plan details and deliver the beam configuration while monitoring the performance of the delivery. A portable control unit (shown in Fig. 7-2) was assembled and integrated with the operation of VARIAN accelerators.

7.1.2 Monte Carlo dose calculation engine

We implemented the EGSnrc/BEAM and XVMC Monte Carlo codes for radiation therapy dose calculations. The accelerator specifications were modeled for all energies, including the FLEC, according to the information supplied by the manufacturer/designer. The beam model is used to obtain phase space representations which are then transported through the patient model derived from the computed tomography (CT) images.

7.1.3 Incorporating a Monte Carlo-based optimization algorithm

The optimizer was developed to acquire Monte Carlo-calculated and patient-specific dose kernels in order to provide an optimal plan that satisfies user-specified dose-volume constraints. In the optimization procedure, because of the nature of Monte Carlo, the effects of the tissue heterogeneities are included while also taking into account the leakage and the bremsstrahlung produced by the FLEC. The use of deliverable beam ports eliminates the need for leaf sequencing and any additional steps that require further optimizations.

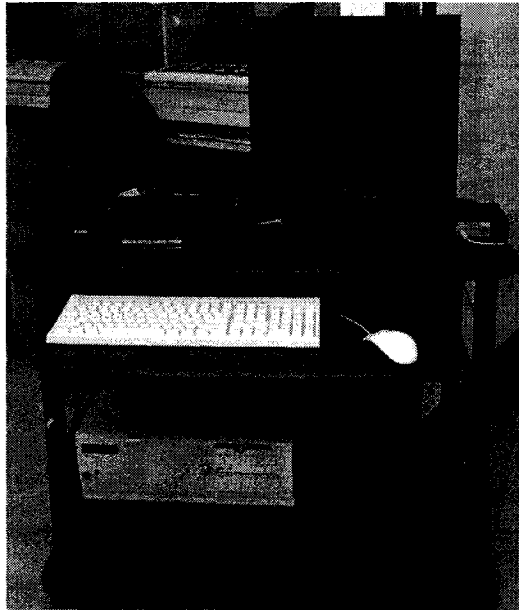


Figure 7-2: *The EMET controller is portable and can easily be linked to the FLEC and the linear accelerator through connectors.*

7.1.4 Integrated software for planning and delivery of EMET

Figure 7-3 shows the overall structure of the EMET planning and delivery software. Many routines were introduced to efficiently interface the different components of the EMET procedure. The software involves the management of more than 20000 lines of programming. Its structure was outlined to proceed with developing a graphical user interface.

7.1.5 Investigation of the clinical significance of EMET

We investigated the application of EMET treatment planning and delivery using the FLEC in the context of mixed beam treatment planning with conventional radiation therapy and IMRT. When applied as a sole treatment modality, the use of modulated electron beams exhibits undesirable dose heterogeneity within the target. Therefore, the combination of EMET with conventional photon beams, used in 3-dimensional conformal therapy (3D-CRT), is more of interest because it achieves better clinical outcome. Extensive comparisons between EMET and IMRT were provided to show the clinical advantages gained by the addition of EMET. The dosimetric evaluations showed that EMET preserves target conformity and dose homogeneity and improves sparing of

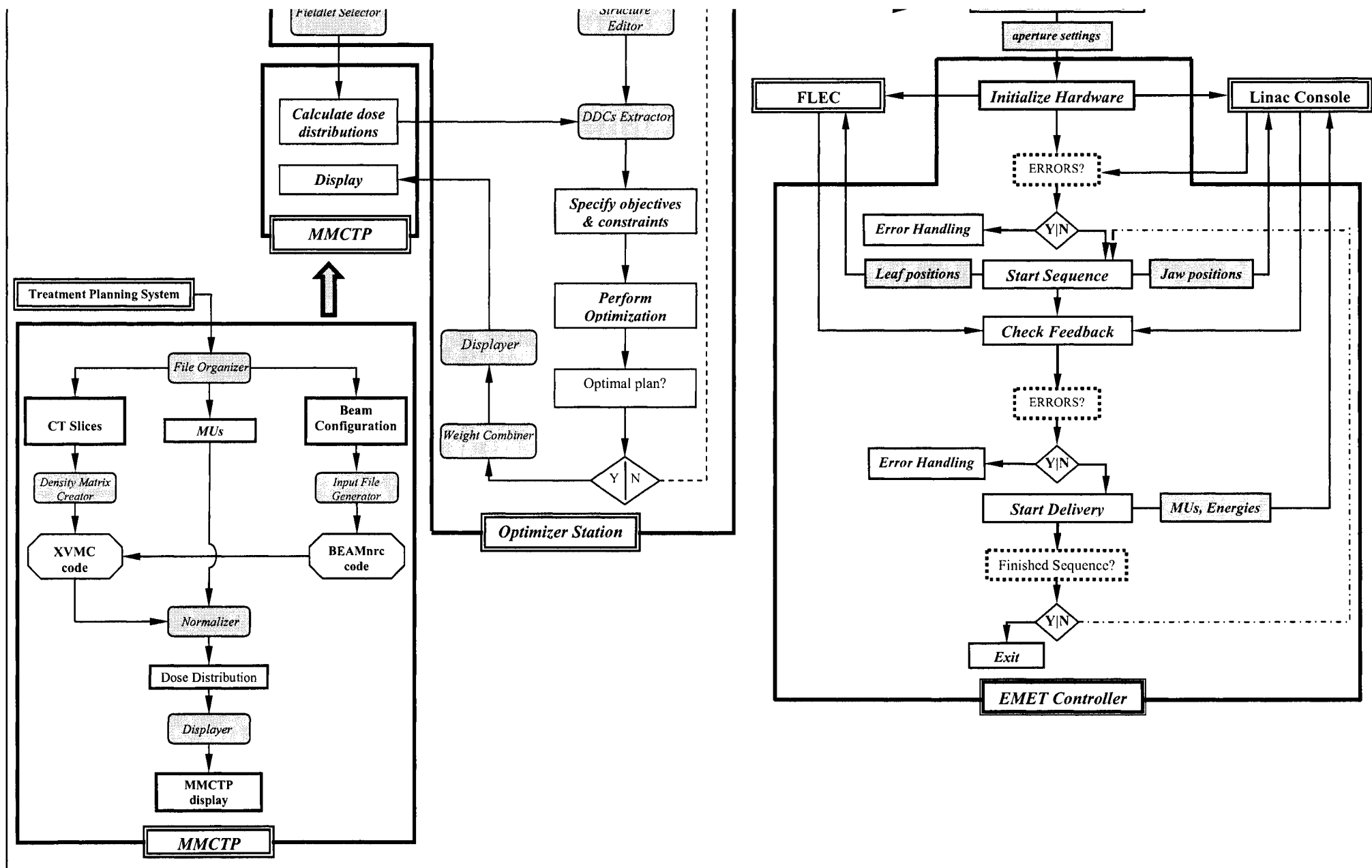


Figure 7-3: Flow chart of the software structure that was developed to perform Monte Carlo-based optimization and delivery for EMET.

the normal tissues. It also significantly reduces the estimated whole body dose. We showed that EMET could be a valuable added modality to the current treatment techniques especially when applied to superficially located tumors that are inherently difficult to plan using IMRT.

7.1.6 Validation of Monte Carlo calculations

The accuracy of the dose distributions obtained by our Monte Carlo system was verified. We started the validation by comparing the measured standard dosimetric data against the calculations of the simulated CL2300 CD linear accelerator for the electron energies 9, 12, 15, and 18 MeV. The confirmation of the accurate model was followed by a series of measurements to validate the FLEC configuration which involves the unconventional jaw collimation in the electron beam delivery. We compared the absorbed dose at a reference point by delivering different fieldlet distributions/energies to a standard phantom with the measured dose values obtained by an ionization chamber in the same geometry. Also, 1-D and 2-D dose distributions obtained from calculation and measurements were compared using the energy-independent tissue-equivalent radiochromic films. Complex intensity maps delivered with different energies/intensities were also compared to the calculation where they showed excellent agreement. Using radiochromic films for the validation of 2-D dose distributions that were obtained from energy modulated electron beams has never been reported before.

7.2 Future Work

Further improvements and development are still required in order to enhance the functionality of the FLEC performance and to expand its clinical applications. First, the use of EMET planning will have wider applications if it is integrated with Monte Carlo-based IMRT planning. The practice of radiation therapy will experience a significant shift if both the photon beamlets and the electron fieldlets are modulated with the same level of accuracy in the calculation and flexibility in the delivery. Second, we propose introducing dynamic movement of the leaves while the beam is under operation. We believe that the dynamic delivery increases the delivery efficiency compared to the present use of the step-and-shoot approach. The dynamic delivery also has the potential to feather the dose distribution by avoiding junctioning of the fieldlets. Third, we propose

to construct a new FLEC-specific applicator. Initially, the FLEC was developed to fit inside the clinical applicator provided by the manufacturer. This was necessary to show that the FLEC has the ability to complement the existing technology. However, we believe that another applicator will be more practical in order to avoid possible conflicts with the operation of the linear accelerator's electronics. The newly designed applicator can have more features that widen the area of application of the FLEC. For example, having a retractable applicator opens the possibility to use the FLEC for arc therapy and isocentric setups. Finally, technical modifications in the software structure and the management of the multiple routines are recommended. Moreover, the EMET planning will be facilitated with graphical user interface.

It is hoped that the results of this thesis and the future work based on it will improve the treatment planning process and ultimately provide better tumor control and avoid complications that affect the quality of life of cancer patients.

Appendix A

McGill Monte Carlo Treatment Planning (MMCTP)

McGill Monte Carlo treatment planning (MMCTP) system is an in-house developed software environment that integrates the research-aimed Monte Carlo codes with current and new treatment modalities and deliveries. Until the year 2000, Monte Carlo code packages remained mainly for research and development and were disconnected from the treatment planning clinical applications. At McGill University, we initiated a long term project dedicated to merge the theoretical knowledge of Monte Carlo with the applications of treatment planning procedure in the clinical environment. MMCTP system started with the development of simple programs that interface different Monte Carlo packages with the commercial treatment planning systems. It evolved to become a full research environment that uses multi modality and multi instance imaging in order to provide analysis tools for patient specific treatment planning.

This section discusses the clinical implementation of a Monte Carlo treatment planning system at McGill University. The steps involve determining the particle phase-space of the radiation source, defining the patient geometry including the inhomogeneity data, calculating the dose distributions, and developing the tools that display/analyze these dose distributions.

Modeling the beam

The EGSnrc/BEAMnrc [1] code system is used to simulate all linear accelerators that are available at our clinic. The code runs under the UNIX operating system and is designed to simulate the radiation beams for any radiation therapy source by defining its geometry through a series of individual component modules positioned perpendicularly

to the beam axis. The BEAM code produces data output in many forms for each simulation. The most useful output form, however, is the full phase space data that contains the energy, charge, position, direction, and the particles' history for all the particles in a certain scoring plane.

Al-Yahya [2] modeled the x-ray beams of Varian CL-2300 including modeling the 52-leaf Multi-Leaf Collimator (MLC). Interface routines that extract the beam parameters (jaws, MLC, isocenter) from the CadPlan system and present them to the BEAM code were introduced. Heath [3] developed an advanced component module that simulates the 120 leaves MLC in Varian CL-2100EX for both static and dynamic deliveries obtained from CORVUS IMRT treatment planning system. Dai [4] incorporated the simulation of the wedges for all x-ray beams. Electron beams were modeled for Varian CL-1800 by Doucet [5], Varian CL-2300 by Albaret [6], and Varian CL-2100 by Garry [7]. Albaret [6] developed a user code for transport of particles through irregularly shaped cutouts. All these models were extensively validated and their accuracies were verified to match the results of detailed measurements.

Modeling the patient

The phase space representations generated from the BEAM code are transported through the patient using the XVMC code [8]. The patient dose calculation is performed after converting the computed tomography (CT) images into mass densities to define the patient geometry. A C routine was written to combine the CT slices to create the density matrix required as an input for the XVMC code. Since the CT couch is not present at the time of the treatment, still incorporated in the CT data, it was necessary to remove the couch from the the CT images by setting CT numbers to air in the regions outside the body contour. The patient models consist of two-dimensional (2D) arrays of materials containing 128×128 voxels in the xy plane and n slices (depending on the patient) in the z direction. All slices have thicknesses that vary between 0.2 - 0.5 cm. The voxel dimensions vary between 0.2 - 0.4 cm depending on the resolution of the CT images that differs according to the current and time that are applied during the CT acquisition.

After reading the phase space file, the charged particles and the scattered radiation are traced through the patient geometry as defined by the patient-specific CT images, and finally produces a three dimensional dose distribution matrix.

Normalization

To generate a Monte Carlo calculated dose distribution for a conventional treatment plan, it is necessary to ensure that the same monitor units (MU) are applied to both conventional and Monte Carlo plans. The output data of a Monte Carlo simulation are reported as dose in each calculation voxel per particle incident from the source; however, measurements are reported in dose per MU. Calibration factors relating the Monte Carlo output to the dose per MU were established by performing Monte Carlo simulations under accelerator calibration conditions ($10 \times 10 \text{ cm}^2$, z_{max} , $SSD = 100 \text{ cm}$). It is important to note that the Monte Carlo calibration factors are energy dependent, unlike the clinical calibration value in terms of the dose to tissue which is fixed to 1 cGy/MU regardless of the energy used. For example: in x-ray beams, as the energy of the incident electron increases, the bremsstrahlung yield in the target, due to the dependence of the radiative stopping power on the energy, increases as well. Thus, the dose per incident particle reported by Monte Carlo is expected to have a higher value for an 18 MV beam in contrast to 6 MV beam. The linac, on the other hand, has been tuned to provide 1 cGy/MU at the point of maximum tissue dose for both energies. For this reason, a routine was introduced to add dose distributions resulting from applying different beam energies by assigning appropriate weights to each one. This ensures that the calculated dose distributions are consistent with the clinical specifications.

MMCTP environment

MMCTP system, built by Alexander [9], was designed to be compatible with the file structure implemented in the clinical environment. It has the flexibility to import from broad base data sources such as RTOG, DICOM, and CadPlan CART formats. Using a graphical user interface (GUI) that runs on a simple workstation, the commands to perform Monte Carlo calculations are sent through a standard secure-shell connection protocol to a computer cluster dedicated for lengthy computations. After the completion of the calculation, only the final dose distribution (in order of 3 Mbytes) is received at the local station where it is displayed on the GUI. The GUI was built using REAL Basic and it offers all the tools required for treatment planning procedures including external beam editing, image visualization options, contour editing, and dose analysis tools. Figure A-1 shows the MMCTP display with its various windows.

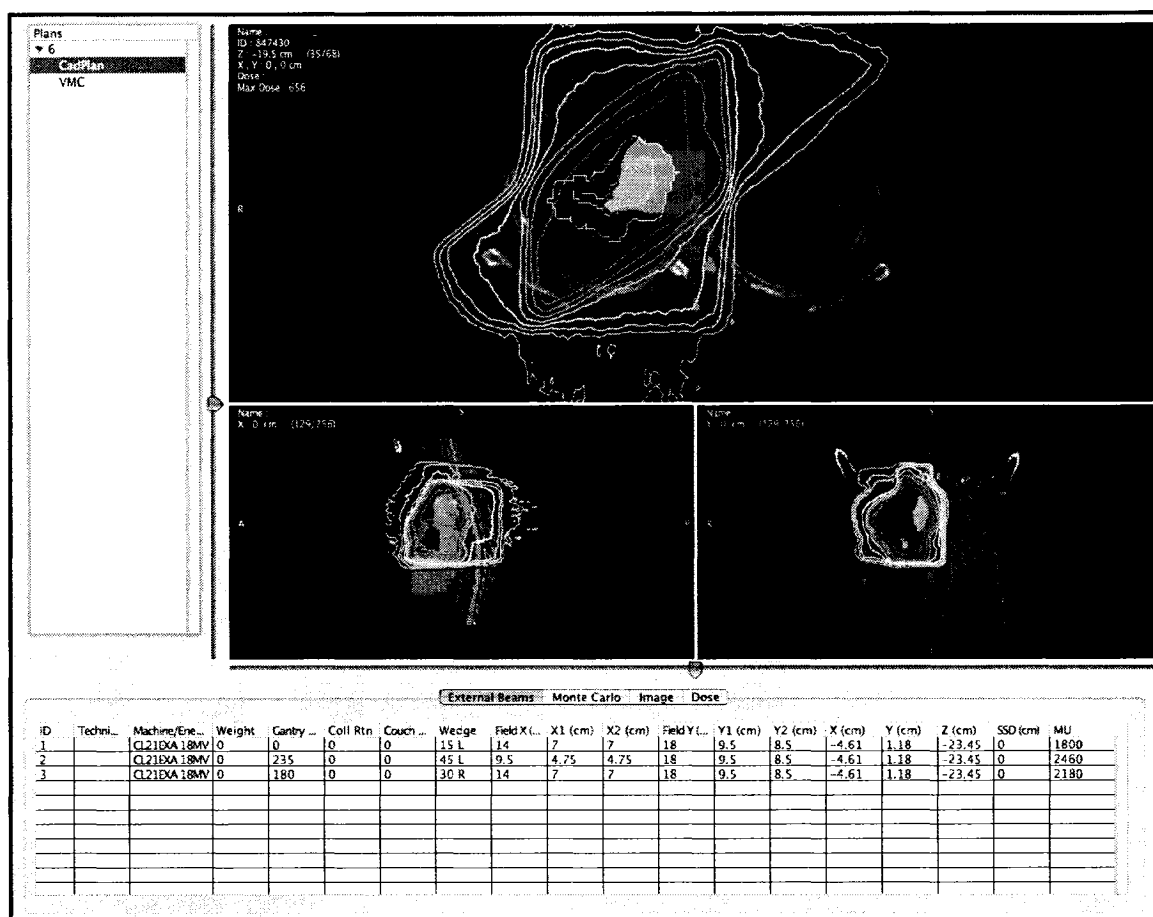


Figure A-1: The display of the main MMCTP window showing, in addition to the beam parameters list box, three canvas for axial, sagittal, and coronal views.

MMCTP converts the imported files into a new file structure that uncouples the private data from the parameters that are sent to the remote dose calculation engines. This design enables the use of an off-site cluster with a minimum amount of data transferred while maintaining the anonymity of the patient information. Alexander [9] tested MMCTP for its consistency of dealing with different Monte Carlo packages and treatment planning systems. All the consistency features were verified including coordinate transformation, beam and patient orientations, and dose calculations.

Conclusion

An in-house developed Monte Carlo treatment planning system was implemented, tested, and debugged. The development of this system involved programming different

routines in order to interface the different components to the existing treatment planning software. Figure A-2 shows a block diagram of the components of our system and summarizes the work that has been performed. The software is accessible from any computer regardless of its operating system. The MMCTP system enables us to proceed with detailed studies to evaluate the accuracy of the dose calculation algorithms implemented in current treatment planning systems.

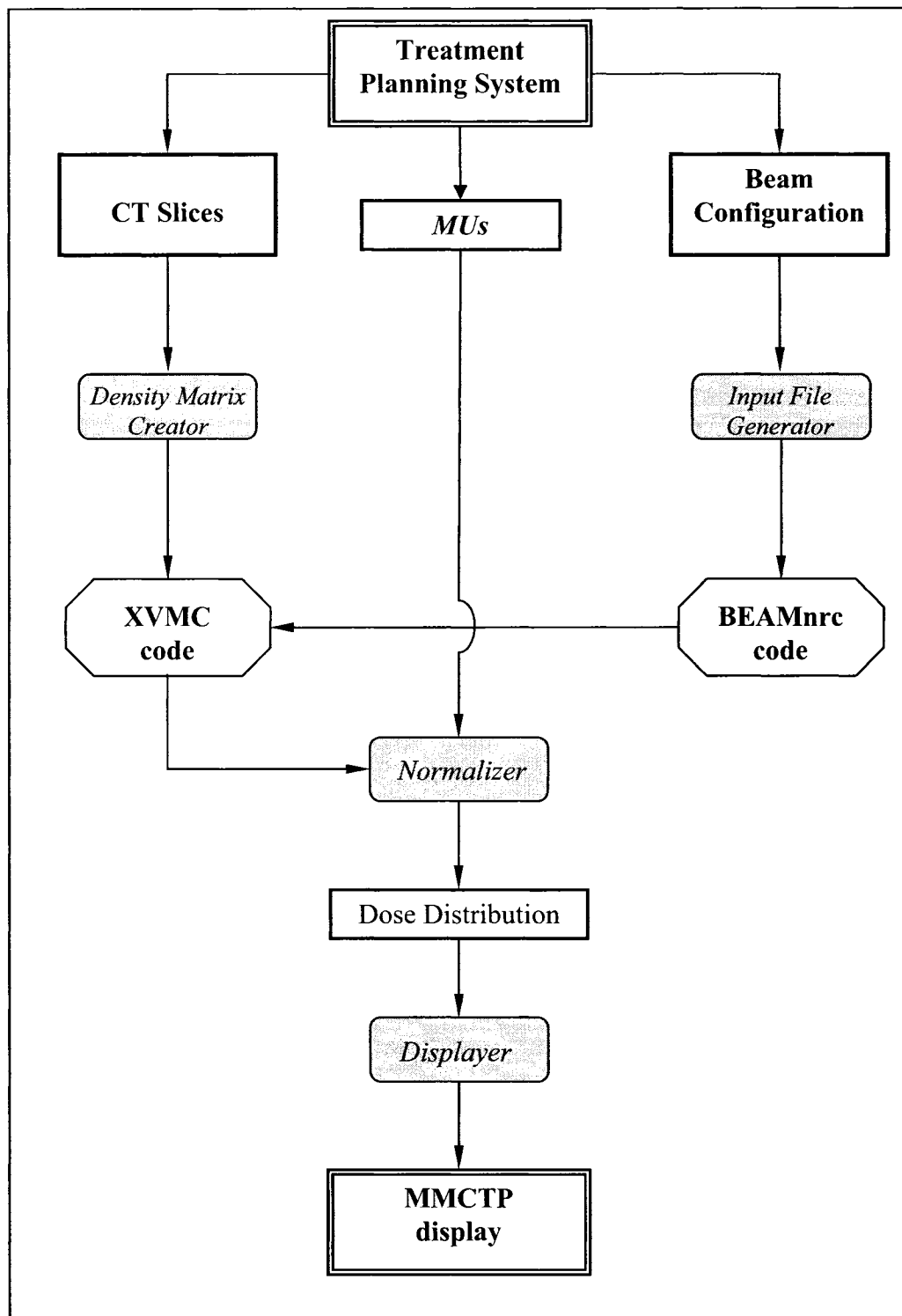


Figure A-2: Block diagram of the MMCTP structure. The shaded areas represent computer programs developed in-house.

References

- [1] D.W. Rogers, B.A. Faddegon, G.X. Ding, C.M. Ma, J. We, and T.R. Mackie, "BEAM: a Monte Carlo code to simulate radiotherapy treatment units," *Med. Phys.* **22**, 503-524 (1995).
- [2] Al-Yahya, Implementation and validation of Monte Carlo treatment planning for lung cancer patients. M.S. Thesis, Medical Physics Unit, McGill University, 2002.
- [3] E. Heath, Evaluation of the PEREGRINE Monte Carlo dose calculation code for 6 MV photon beams. M.S. Thesis, Medical Physics Unit, McGill University, 2003.
- [4] J. Dai, Validation of Monte Carlo techniques for 3D-CRT of lung cancer patients and comparative evaluation of treatment plans. M.S. Thesis, Medical Physics Unit, McGill University, 2004.
- [5] R. Doucet, M. Olivares, F. DeBlois, E.B. Podgorsak, I. Kawrakow, and J. Seuntjens, "Comparison of measured and Monte Carlo calculated dose distributions in inhomogeneous phantoms in clinical electron beams," *Phys. Med. Biol.* **48**, 2339-2354 (2003).
- [6] C. Albaret, Automatic system for Monte Carlo determination of cutout factors of arbitrarily shaped electron and experimental verification of Monte Carlo calculated dose distributions. M.S. Thesis, Medical Physics Unit, McGill University, 2004.
- [7] G. Garry, Study of novel techniques for verification imaging and patient dose reconstruction in external beam radiation therapy. Ph.D. Thesis, Medical Physics Unit, McGill University, 2006.
- [8] I. Kawrakow and M. Fippel, "Investigation of variance reduction techniques for Monte Carlo photon dose calculation using XVMC," *Phys. Med. Biol.* **45**, 2163-2183 (2000).
- [9] A. Alexander, MMCTP: A radiotherapy research environment for patient-treatment planning. M.S. Thesis, Medical Physics Unit, McGill University, 2006.

Appendix B

Waivers

Appendix B

The waivers from the publishers for the published manuscripts and the permission to use the reprinted figures are included below.

Signed waivers from co-authors of the unpublished manuscripts are also provided below.

Appendix B

The waivers

for to use

the reprints

Signed wa

are provided below.

Appendix B

for to use

the reprints

Signed wa

are provided below.



American Association of Physicists in Medicine

One Physics Ellipse
College Park, MD 20740-3846
(301) 209-3350
Fax (301) 209-0862
<http://www.aapm.org>

Office of the Executive Director

Angela R. Keyser
Phone: 301-209-3385 Fax: 301-209-0862
E-mail: akeyser@aapm.org

February 7, 2007

Khalid Al-Yahya
Medical Physics Unit
Montreal General Hospital, L5-113
1650 avenue Cedar
Montréal, Québec
H3G 1A4
Canada

Via Fax: 514-934-8229

Dear Mr. Al-Yahya:

The American Association of Physicists in Medicine hereby grants permission for Mr. Khalid Al-Yahya to use the material outlined below.

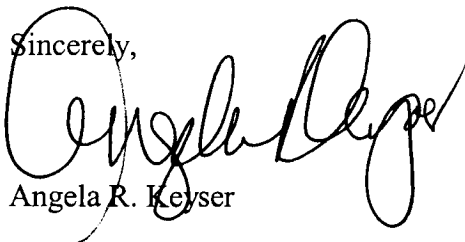
K.R. Hogstrom, R.A. Boyd, J.A. Antolak, M.M. Svatos, B.A. Faddegon, and J.G. Rosenman. "Dosimetry of a prototype retractable eMLC for fixed-beam electron therapy". *Medical Physics* 31, 2004; 443 - 462.

Figure 6

K. Al-Yahya, M. Schwartz, G. Shenouda, F. Verhaegen, C. Freeman, and J. Seuntjens. "Energy modulated electron therapy using a few leaf electron collimator in combination with IMRT and 3D-CRT: Monte Carlo-based planning and dosimetric evaluation". *Medical Physics* 32, 2005; 2976-2986.

K. Al-Yahya, F. Verhaegen, and J. Seuntjens. "Construction and dosimetry of a new automated collimator for delivery of Monte Carlo-based energy-intensity modulated electron therapy". Manuscript #06-696 submitted on November 20, 2006 (currently under revision).

Sincerely,



Angela R. Keyser



Print - Close Window

Date: Fri, 05 Jan 2007 12:17:24 -0500
From: "Khalid Alyahya" <alyahya@videotron.ca>
Subject: Fw: Al-YahyaMcGillUnivFB1-07.doc
To: "Khalid Al-Yahya" <ksyahya@yahoo.com>

----- Original Message -----

From: Bell, Folade (ELS)
To: kyahya@medphys.mcgill.ca
Sent: Friday, January 05, 2007 9:01 AM
Subject: Al-YahyaMcGillUnivFB1-07.doc

Date: January 5, 2007

Our ref: Al-YahyaMcGillUnivFB1-07

Mr. Khalid Al-Yahya
kyahya@medphys.mcgill.ca

Publication: Figure 3 from the *INTERNATIONAL JOURNAL OF RADIATION ONCOLOGY BIOLOGY PHYSICS*, V17(5): 1089-1094 © 1989 Elsevier Inc.

Figures 2 & 4 from the *INTERNATIONAL JOURNAL OF RADIATION ONCOLOGY BIOLOGY PHYSICS*, V51(4): 1142-1151 © 1989 Elsevier Inc.

As per your letter dated December 6, 2006, we hereby grant you permission to reprint the aforementioned material at no charge in your thesis for McGill University subject to the following conditions:

1. If any part of the material to be used (for example, figures) has appeared in our publication with credit or acknowledgement to another source, permission must also be sought from that source. If such permission is not obtained then that material may not be included in your publication/copies.
2. Suitable acknowledgment to the source must be made, either as a footnote or in a reference list at the end of your publication, as follows:

"Reprinted from Publication title, Vol number, Author(s), Title of article, Pages No., Copyright (Year), with permission from Elsevier."
3. Your thesis may be submitted to your institution in either print or electronic form.
4. Reproduction of this material is confined to the purpose for which permission is hereby given.
5. This permission is granted for non-exclusive world **English** rights only. For other languages please reapply separately for each one required. Permission excludes use in an electronic form. Should you have a specific electronic project in mind please reapply for permission.
6. This includes permission for the National Library of Canada to supply single copies, on demand, of the complete thesis. Should your thesis be published commercially, please reapply for permission.

Yours sincerely,
Foladé Bell
on behalf of Elsevier

For your convenience, please submit your future permissions requests online at:
<http://www.us.elsevierhealth.com/Licensing/permissions.jsp>



"Khalid Alyahya"
<kyahya@medphys.mcgill.ca>
a>

06/12/2006 19:54

To <permissions@iop.org>

cc

bcc

Subject: Permission Request

Dear Editor,

My name is Khalid Al-Yahya, a Ph.D. candidate at Medical Physics Unit, McGill University. I am in the process of depositing my thesis to the faculty of graduate studies and research in partial fulfillment of the requirements of the degree of Doctor of Philosophy. As part of the comprehensive literature review for the previous implementation of energy modulated electron therapy, I want to adapt some figures for representing results of previous works. I would like to have your permission to reprint the following figures in my thesis:

(1) Figure 1 from:

K.R. Hogstrom, M.D. Mills, and P.R. Almond, "Electron beam dose calculations," Phys. Med. Biol. 26, 445-459 (1981).

(2) Figure 1 and Figure 6 from:

C.M. Ma, T. Pawlicki, M.C. Lee, S.B. Jiang, J.S. Li, J. Deng, B. Yi, E. Mok, and A.L. Boyer, "Energy- and intensity-modulated electron beams for radiotherapy," Phys. Med. Biol. 45, 2293-2311 (2000).

The granted permission will be mentioned with acknowledgment of the source.

I would like to thank you in advance for your efforts.

Sincerely,

Khalid Alyahya
Medical Physics Unit
Montreal General Hospital, L5-113
1650 avenue Cedar
Montréal, Québec
H3G 1A4
Canada
Tel. (514) 934-8052
Fax. (514) 934-8229

PERMISSION TO REPRODUCE AS REQUESTED
IS GIVEN PROVIDED THAT:

- (a) the consent of the author(s) is obtained
- (b) the source of the material including author/editor, title, date and publisher is acknowledged.

IOP Publishing Limited
Dirac House
Temple Back
BRISTOL

8/12/06

BS1 6BE

Date

Rights & Permission



"Khalid Alyahya"
<kyahya@medphys.mcgill.ca>

06/12/2006 19:59

To <permissions@iop.org>

cc

bcc

Subject Request for permission (previously published manuscript)

Dear Editor,

My name is Khalid Al-Yahya, a Ph.D. candidate at Medical Physics Unit, McGill University. I am in the process of depositing my thesis to the faculty of graduate studies and research in partial fulfillment of the requirements of the degree of Doctor of Philosophy. My thesis is manuscript-based and I would like to ask for your permission to adapt/reprint one of previously published manuscripts. I would like to ask for your permission to reprint the following article

K. Al-Yahya, D. Hristov, F. Verhaegen, and J. Seuntjens, "Monte Carlo-based modulated electron beam treatment planning using a few leaf electron collimator - feasibility study," Phys. Med. Biol. 50, 847-857 (2005).

Your permissions will be acknowledged in the thesis and a copy of your permission letter will be included in a dedicated appendix.

Please accept my gratitude for your efforts,

Sincerely,

Khalid Alyahya
Medical Physics Unit
Montreal General Hospital, L5-113
1650 avenue Cedar
Montréal, Québec
H3G 1A4
Canada
Tel. (514) 934-8052
Fax. (514) 934-8229

PERMISSION TO REPRODUCE AS REQUESTED
IS GIVEN PROVIDED THAT:

- (a) ~~the consent of the author(s) is obtained~~
- (b) the source of the material including author/editor, title, date and publisher is acknowledged. ☒

IOP Publishing Limited
Dirac House
Temple Back
BRISTOL

8/12/06. *[Signature]*

BS1 6BE

Date

Rights & Permission

Ⓢ Please include the Internet address of the journal's homepage at:-
www.iop.org/journals/pmb

Thank you! *[Signature]*

Khalid Alyahya

From: "Ma, Charlie" <Charlie.Ma@fccc.edu>
To: "Khalid Alyahya" <kyahya@medphys.mcgill.ca>
Sent: February 13, 2007 5:35 PM
Subject: RE: Request of reprinting previously published material

Sure, you can use these figures in your thesis, if you properly reference the journal/year/pages/author, etc.

Good luck with your thesis write up!

 C-M Charlie Ma, Ph.D.
 Director, Radiation Physics
 Dept. of Radiation Oncology
 Fox Chase Cancer Center
 Room P-0049, 333 Cottman Av
 Philadelphia, PA 19111
 Tel: (215) 728-2996
 Fax: (215) 728-4789
 Email: charlie.ma@fccc.edu
<http://www.fccc.edu/research/pid/ma/index.html>

-----Original Message-----

From: Khalid Alyahya [mailto:kyahya@medphys.mcgill.ca]
Sent: Wednesday, February 07, 2007 3:10 PM
To: charlie.ma@fccc.edu
Subject: Request of reprinting previously published material

Dear Dr. Ma,

My name is Khalid Al-Yahya, a Ph.D. candidate at Medical Physics Unit, McGill University. I am in the process of depositing my thesis to the faculty of graduate studies and research in partial fulfillment of the requirements of the degree of Doctor of Philosophy. As part of the comprehensive literature review for the previous implementation of energy modulated electron therapy, I want to adapt some figures for representing results of previous works. I would like to have your permission to reprint the following figures in my thesis:

Figure 1 and Figure 6 from:

C.M. Ma, T. Pawlicki, M.C. Lee, S.B. Jiang, J.S. Li, J. Deng, B. Yi, E. Mok, and A.L. Boyer, "Energy- and intensity-modulated electron beams for radiotherapy," Phys. Med. Biol. 45, 2293-2311 (2000).

The granted permission will be mentioned with acknowledgment of the source.

I would like to thank you in advance for your cooperation.

Sincerely,

Khalid Alyahya
 Medical Physics Unit

23/02/2007

*Montreal General Hospital, L5-113
1650 avenue Cedar
Montréal, Québec
H3G 1A4
Canada
Tel. (514) 934-8052
Fax. (514) 934-8229*

Khalid Alyahya

From: "Kenneth R Hogstrom" <hogstrom@lsu.edu>
To: "Khalid Alyahya" <kyahya@medphys.mcgill.ca>
Sent: February 7, 2007 3:27 PM
Subject: Re: Request of Reprinting Previously Published Material

Approved.

Ken Hogstrom

"Khalid Alyahya"
<kyahya@medphys.mcgill.ca> To:
<hogstrom@lsu.edu>
cc:
Subject: Request of Reprinting Previously Published
Material
02/07/2007 02:06
PM

Dear Dr. Hogstrom:

My name is Khalid Al-Yahya, a Ph.D. candidate at Medical Physics Unit, McGill University. I am in the process of depositing my thesis to the faculty of graduate studies and research in partial fulfillment of the requirements of the degree of Doctor of Philosophy. As part of the comprehensive literature review for the previous implementation of energy modulated electron therapy, I want to adapt some figures for representing results of previous works. I would like to have your permission to reprint the following figures in my thesis:

Figure 1 from:
K.R. Hogstrom, M.D. Mills, and P.R. Almond, "Electron beam dose calculations," Phys. Med. Biol. 26, 445-459 (1981).

Figure 6 from:
K.R. Hogstrom, R.A. Boyd, J.A. Antolak, M.M. Svatos, B.A. Faddegon, and J.G. Rosenman, "Dosimetry of a prototype retractable eMLC for fixed-beam electron therapy," Med. Phys. 31, 443-462 (2004).

23/02/2007

The granted permission will be mentioned with acknowledgment of the source.

I would like to thank you in advance for your cooperation.

Sincerely,

Khalid Alyahya
Medical Physics Unit
Montreal General Hospital, L5-113
1650 avenue Cedar
Montréal, Québec
H3G 1A4
Canada
Tel. (514) 934-8052
Fax. (514) 934-8229

Appendix C

Reprints of the Published Papers

Monte Carlo based modulated electron beam treatment planning using a few-leaf electron collimator—feasibility study

Khalid Al-Yahya¹, Dimitre Hristov², Frank Verhaegen¹
and Jan Seuntjens¹

¹ Medical Physics Unit, McGill University, 1650 Cedar Avenue, Montreal H3G 1A9, Canada

² Siemens Medical Solutions, Inc., Oncology Care Systems, 4040 Nelson Avenue, Concord, CA 94520, USA

E-mail: kyahya@medphys.mcgill.ca

Received 6 July 2004, in final form 14 October 2004

Published 17 February 2005

Online at stacks.iop.org/PMB/50/847

Abstract

Energy modulated electron beam therapy with conventional clinical accelerators has lagged behind photon IMRT despite its potential to achieve highly conformal dose distributions in superficial targets. One of the reasons for this is the absence of an automated collimating device that allows for the flexible delivery of a series of variable field openings. Electron-specific multileaf collimators attached to the bottom of the applicator require the use of a large number of motors and suffer from being relatively bulky and impractical for head and neck sites. In this work, we investigate the treatment planning aspects of a proposed ‘few-leaf’ electron collimator (FLEC) that consists of four motor-driven trimmer bars at the end of the applicator. The device is designed to serve as an accessory to standard equipment and allows for the shaping of any irregular field by combination of rectangular fieldlets. Using a Monte Carlo model of the FLEC, dose distributions are optimized using a simulated annealing (SA) inverse planning algorithm based on a limited number of Monte Carlo pre-generated, realistic phantom-specific dose kernels and user-specified dose–volume constraints. Using a phantom setup with an artificial target enclosed by organs at risk (OAR) as well as using a realistic patient case, we demonstrate that highly conformal distributions can be generated. Estimates of delivery times are made and show that a full treatment fraction can be kept to 15 min or less.

(Some figures in this article are in colour only in the electronic version)

1. Introduction

Energy modulated electron therapy (EMET) has the ability to provide conformal dose distributions to superficial tumours for which it could compete with intensity modulated radiation therapy (IMRT). The high surface dose followed by a steep fall-off makes the electron beams well suited for treating shallow targets. However, EMET has not yet been clinically used to its full potential, in contrast to photon IMRT. The main reasons for this lag in clinical implementation are: (1) the lack of dosimetric accuracy of electron pencil beam algorithms in the presence of heterogeneities and beam modifiers and (2) the absence of a practical automated collimation device that allows the delivery of a series of different field openings (fieldlets) during one treatment. Although a high degree of accuracy of the dose calculation could be achieved if Monte Carlo techniques are used (Bielajew *et al* 1987, Kawrakow *et al* 1996, Ma *et al* 1997), the development of a beam shaping device that is able to preserve the electron beam characteristics and yet allow for flexible use of multiple fieldlets remains challenging.

In recent years, significant efforts have addressed the feasibility, implementation and clinical utility of EMET which employs a thin-leaf multileaf collimator attached onto a frame at the bottom of an existing electron applicator (Lee *et al* 2000, Ma *et al* 2000, Lee *et al* 2001, Ravindran *et al* 2002, Ma *et al* 2003, Hogstrom *et al* 2004). To automate such a collimator in a clinical setting, this approach requires the presence of a large number of motors at the bottom of the electron applicator and suffers from being relatively bulky and impractical to handle.

The use of inverse techniques for treatment planning of EMET is more complex than in photon beam IMRT since collimation has a profound effect on electron scattering and the dose gradients in a specific sub-field. In addition, accurate dose calculations in and near patient heterogeneities are essential for a successful application of EMET. Having detailed information about the effect of both the collimation devices and the complex patient geometry on the dose provided to the optimization algorithm would lead to a truly optimal treatment plan. Hence, the output and the dose distribution realized through the combination of multiple sub-fields require the electron transport to be faithfully modelled through the collimating system and inside the patient. Any optimization algorithm that does not make use of realistic dose deposition kernel data will inevitably produce segment weights that lead to suboptimal and/or undeliverable dose distributions.

In this work, we introduce an approach to deliver EMET plans using a simplified model for an automated collimation device. This feasibility study is based on Monte Carlo calculations where the fundamentals of electron transport and scattering through collimating devices and in the heterogeneous patient are all taken into account.

2. Materials and method

2.1. Design of few-leaf electron collimator

To facilitate the formation of irregular electron fields and to allow the flexible combination of different energies and intensities, a few-leaf electron collimator (FLEC) is proposed as an add-on accessory that could fit on a light-weight frame at the bottom of an electron applicator. In its most basic appearance (as shown in figure 1), this collimator consists of four blades (or trimmer bars) driven by motors so as to form arbitrary square or rectangular fields with an area between zero and nominally $9 \times 9 \text{ cm}^2$ (for the $15 \times 15 \text{ cm}^2$ electron applicator) and between zero and $14 \times 14 \text{ cm}^2$ (for the $20 \times 20 \text{ cm}^2$ electron applicator). Any irregular

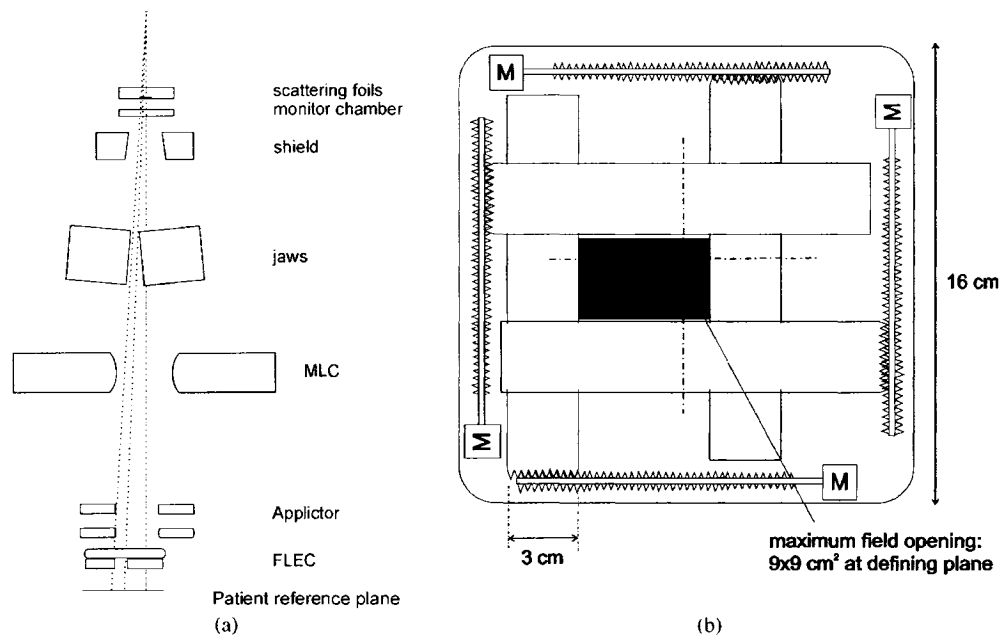


Figure 1. (a) Position of few-leaf electron collimator (FLEC) relative to other components in the accelerator (not to scale). (b) Schematic drawing of beam's eye view of FLEC.

irradiation field can be made up by a combination of rectangular and square fields which possibly could involve the use of collimator rotation in a more evolved stage. The function of the FLEC is an automated final re-collimation of electron fields, previously collimated by jaws and/or the photon MLC that will be used as backup collimation devices. Hence, the blades, made of copper, can be relatively thin. In our study, their thickness was 1.5 cm and their width was 3 cm. To first order, the delivery of complex dynamic electron fields will be performed in a step-and-shoot approach, whereby every sub-field is formed by simultaneous collimation of the electron beam by the jaws and the FLEC. We verified the ability of our clinical accelerators to dynamically control jaws when run in electron mode.

2.2. Monte Carlo calculations

In this study, the BEAM/EGSnrc (Rogers *et al* 1995) Monte Carlo code was used to simulate a CL2300 CD linear accelerator for the electron energies 6, 9, 12, 15, 18 and 22 MeV as well as for the photon energies of 6 and 18 MV. The transport parameters used in EGS accelerator simulations were $ECUT = AE = 700$ keV cutoff for electron transport, $PCUT = AP = 10$ keV for photon transport, and the electron step is 1% (i.e. $ESTEPE = 0.01$). After validation of the simulated beams against standard dosimetric data that include the validation of the model in the presence of the beam modifiers, the Monte Carlo model was used to generate a master phase space file above the jaws for all energies. The procedure for the selection and calculation of fieldlet arrangement is conducted as follows:

- (1) A user-specified number of fieldlets is geometrically selected and positioned to conform the shape of the projected target. The fieldlets are chosen such that they are matched at the edges of the projected 3D volume of the PTV. An algorithm for optimizing the best fieldlet configuration based on the 3D PTV contour is being developed. For the purpose of this feasibility study, the fieldlets were selected manually.

- (2) Using the master phase space file, we proceeded with the simulation of the fieldlet-specific jaw openings as well as with the lower part of the accelerator including the FLEC. For each fieldlet setting of FLEC, the secondary jaws are set so as to project an opening equal to the one projected by the FLEC plus a margin of 0.5 cm on all sides. The phase space file of a fully simulated fieldlet, for all energies, is scored at an SSD of 95 cm.
- (3) The final phase space file of the fieldlet is then transported through the patient geometry using the XVMC code (Fippel 1999, Kawrakow *et al* 2000). The patient is modelled by converting the CT data into a density matrix with a size of $128 \times 128 \times (\text{number of slices})$ with the dimensions of the voxel size varying from 0.25 to 0.35 cm.
- (4) Once the dose distribution of each fieldlet is generated, a Monte Carlo dose distribution given in absorbed dose to tissue per particle is converted to absorbed dose to tissue per monitor unit. This is obtained using energy-dependent calibration factors obtained from simulations that are performed under accelerator calibration conditions ($10 \times 10 \text{ cm}^2$, d_{max}). The Monte Carlo calculated dose distribution provided by each fieldlet—after it is ‘properly’ normalized—represents the dose deposition kernel whose weight is modulated by the optimization algorithm. The number of simulated particle histories was chosen to achieve a statistical uncertainty on the dose calculation of 1% or less per fieldlet.

2.3. Treatment plan optimization

Figure 2 shows a schematic diagram of the inverse treatment planning system. The optimization is performed using the simulated annealing (SA) algorithm proposed by Sait and Youssef (1999). The optimizer selects the fieldlets, their energies, and their associated intensities that correspond to the optimal plan while the rejected fieldlets receive the weight of zero.

The dose–volume objective function, $F^{\text{DV}}(\mathbf{w})$, is represented by

$$F^{\text{DV}}(\mathbf{w}) = F_{\text{TV}}^{\text{D}}(\mathbf{w}) + F_{\text{OAR}}^{\text{V}}(\mathbf{w})$$

where \mathbf{w} stands for the array of fieldlet weights, $F_{\text{TV}}^{\text{D}}(\mathbf{w})$ represents the (dose-based) target objective term and $F_{\text{OAR}}^{\text{V}}(\mathbf{w})$ represents the (volume-based) organs at risk (OAR) objective term. The objective functions are calculated as follows:

$$F_{\text{TV}}^{\text{D}}(\mathbf{w}) = \pi_{\text{TV}}^{\text{max}} \sum_{p \in \text{TV}} \Theta(D_{\text{TV},p}(\mathbf{w}) - D_{\text{TV}}^{\text{max}}) \left[\frac{D_{\text{TV},p}(\mathbf{w}) - D_{\text{TV}}^{\text{max}}}{D_{\text{TV}}^{\text{max}}} \right]^2 \\ + \pi_{\text{TV}}^{\text{min}} \sum_{p \in \text{TV}} \Theta(D_{\text{TV}}^{\text{min}} - D_{\text{TV},p}(\mathbf{w})) \left[\frac{D_{\text{TV}}^{\text{min}} - D_{\text{TV},p}(\mathbf{w})}{D_{\text{TV}}^{\text{min}}} \right]^2$$

and

$$F_{\text{OAR}}^{\text{V}}(\mathbf{w}) = \sum_l \pi_{\text{OAR}_l} \left[\frac{\sum_{p \in \text{OAR}_l} \Theta(D_{\text{OAR}_l,p}(\mathbf{w}) - D_{\text{OAR}_l}^{\text{max}}) dV - V_{\text{OAR}_l}^{\text{max}}}{V_{\text{OAR}_l}} \right]^2,$$

where $\pi_{\text{TV}}^{\text{max}}$ and $\pi_{\text{TV}}^{\text{min}}$ refer to the penalty parameters of the target maximum and minimum dose constraints, respectively, Θ defines the Heaviside or step function, and $D_{\text{TV},p}(\mathbf{w})$ is the dose deposited to point p of the target (denoted by TV) which contains a total of N_{TV} dose points. The dose to the target volume is constrained by the user-specified maximum and minimum dose $D_{\text{TV}}^{\text{max}}$ and $D_{\text{TV}}^{\text{min}}$ and relevant dose–volume relations for critical organs are specified by the dose–volume constraints of $(D_{\text{OAR}_l}^{\text{max}}, V_{\text{OAR}_l}^{\text{max}})$, where l labels all the organ constraints. Each

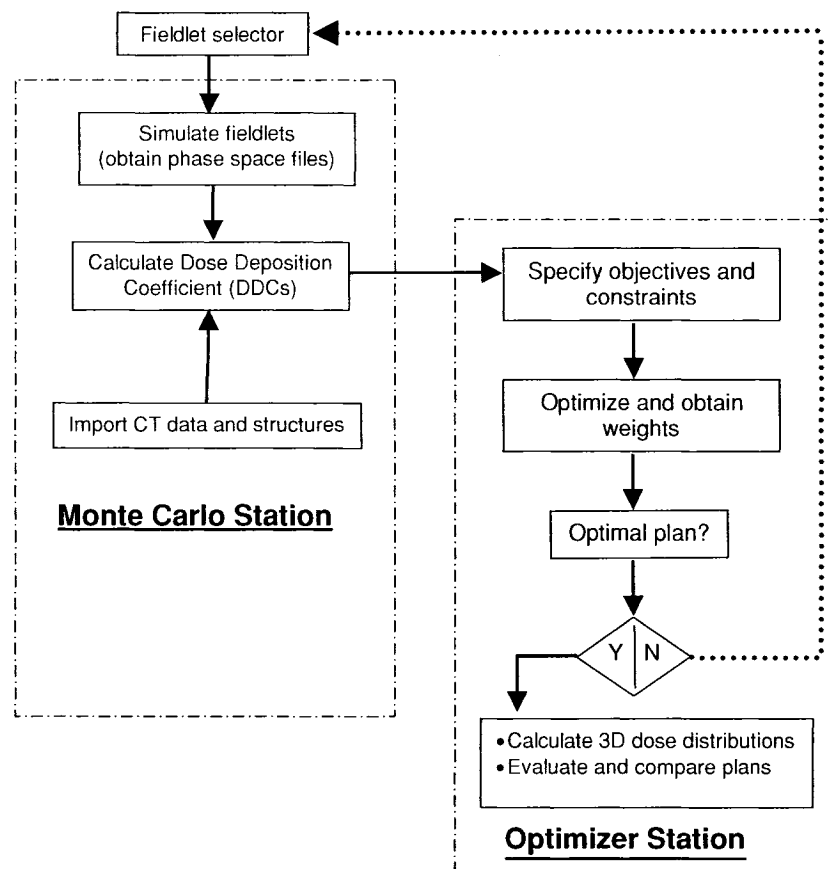


Figure 2. A schematic diagram of the current EMET procedure.

constraint in the OAR is assigned a penalty value π_{OAR} that weighs the individual penalty contribution to the overall objective function.

The optimization algorithm was developed in an in-house built inverse treatment planning system that is developed within a visual software environment (AVS 5.4, Advanced Visual Systems, MA), running under SUSE LINUX. Software has been developed to interface the optimizer with the Monte Carlo calculated kernels so that the dosimetric data as well as the contour data required for the optimization algorithm could be extracted. The software also extracts the dose deposition coefficients (DDCs) which define the relative dose contribution from each fieldlet to each voxel contained in a specific contour. Moreover, the optimal fluence data obtained by the optimization algorithm are interfaced again with the kernels and then fed back to the clinical planning system (CadPlan 6.2.7) to display the final dose distribution. Another optimization algorithm, based on the deterministic steep DVH minimization (Hristov *et al* 2002), has been developed within the same environment and objective function. It will be used for future studies for comparison with the simulated annealing algorithm to check the ability of both the algorithms to achieve the optimum optimization goals. That would include the study of the effect of the dependence of the generated fieldlet weights on the initial condition that might result in entrapment in a local minimum of the objective function if the deterministic approach is used.

Table 1. Target dose and organ dose–volume levels in EMET optimization for the phantom case.

Structure	Dose (Gy)	Volume (%)	Penalty value
Target	50	100	1
Target	60	0	1
Organ 1	40	2	0.3
Organ 1	30	10	0.3
Organ 2	40	2	0.3
Organ 2	30	10	0.3

Note that, since we work *a priori* with realistic and deliverable beam port dose distributions, there are no additional steps involved (analogous to an MLC leaf sequence calculator in IMRT) in determining the delivery of the distribution. The combined dose distribution is also truly optimized since the effects of both the presence of the heterogeneities as well as the bremsstrahlung produced by the collimation device are taken into account without the need to correct the final dose distribution for the leakage and transmission. As shown in figure 2, in the event that no convergence can be achieved in the optimization process with the existing fieldlets, new beams have to be added and the optimization process repeated. An example of such a case could be the need to reduce skin dose through the use of one or more conventionally shaped photon beams. As only a limited number of additional fieldlets would be required, the incremental time needed for this process is limited.

2.4. Treatment planning details

2.4.1. Simple water phantom. We have planned for EMET on a 3D homogeneous solid water phantom geometry as well as for a realistic head and neck case. For the homogeneous phantom case, contours and CT data were acquired from the CART files, the file format used by CadPlan treatment planning system. We used a phantom scanned through CT to emulate the planning procedure where our calculations will be performed. The target was drawn to be surrounded by critical structures shown in figure 3. The lateral extent of the target was 8 cm and the inferior–superior extent was 6 cm while the depth varies laterally. The isocentre was placed at the surface so that the phantom is at an SSD 100 cm. With each electron energy, five fieldlets were simulated: two of them were adjacent to cover the PTV laterally (along the x -axis) with a size of $4.5 \times 7 \text{ cm}^2$ each; two were chosen to cover the PTV widely (along the z -axis) with a size of $9 \times 3.5 \text{ cm}^2$, and one fieldlet that was of the size of $9 \times 7 \text{ cm}^2$ to properly cover the PTV. Table 1 summarizes the dose and dose–volume constraints prescribed for this case.

2.4.2. Head and neck case. For the head and neck case, we generated two plans: (1) the conventional tangential wedged photon beams with cutout-shaped electron boost and (2) EMET with four electron fields in addition to the wedged photon beams. In plan 1, the dose distribution was calculated after the simulation of the MLC-shaped wedged beams using our in-house Monte Carlo based treatment planning system. We acquired the beam modifiers as well as the monitor unit settings to perform the simulation for each beam and add the individual normalized dose distributions to be displayed in the clinical treatment planning system. In plan 2, the four electron fields were 9, 12, 15 and 18 MeV with six fieldlets each such that the PTV is fully covered. In addition, we considered each photon field as a fieldlet

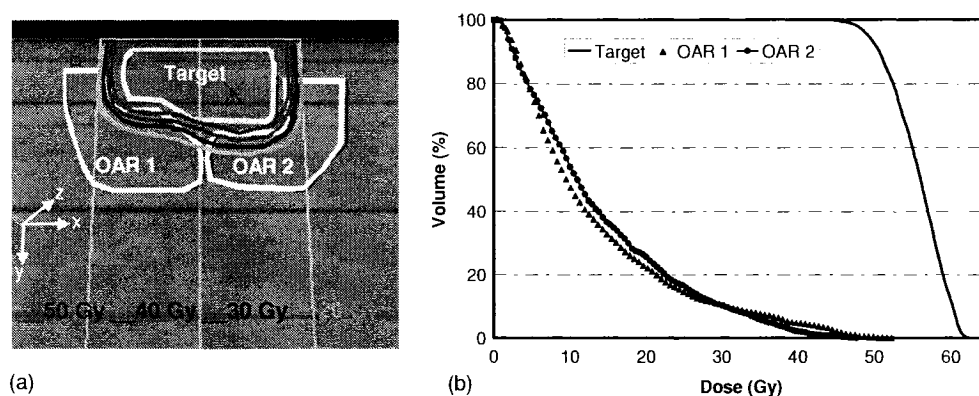


Figure 3. (a) Dose distribution of an optimized EMET plan and (b) DVHs for a hypothetical target and two organs at risk surrounding the PTV in a homogeneous solid water phantom scanned by CT (PTV is outlined in yellow).

and allowed the optimization algorithm to decide whether or not to use its contribution in the final plan.

3. Results and discussion

3.1. Homogeneous phantom

Using our automated EMET system, we calculated the dose distribution for an imaginary PTV outlined in a homogeneous solid water phantom that has been scanned by CT. Figure 3(a) shows the conformity of the isodose distribution obtained by EMET at the isocentre slice based on a 50 Gy prescription. The corresponding DVHs are shown in figure 3(b) for the PTV and the OARs. The DVH confirms the coverage of the PTV with the prescribed dose but it shows also the presence of hot spots due to the use of a limited number of fieldlets where the bulging effect that occurs at the edge of the fieldlets causes the appearance of dose heterogeneity wherever the fieldlets are junctioned. For this particular case, the effect could be reduced by the use of a photon field that covers the PTV to create more uniformity within the target. The hot spots could be eliminated by feathering the field edges using dynamic delivery of the fieldlets. Although it has not been implemented yet, it is a potential topic of future study.

3.2. Head and neck case

To demonstrate the ability of EMET to deal with more realistic scenarios, a plan was generated for a head and neck case and compared with the conventional treatment technique. Figure 4(a) shows the comparison between the Monte Carlo calculated isodose distribution for a conventional plan using two wedged and MLC-shaped photon beams boosted by a lateral 12 MeV electron beam with an optimized plan provided by EMET. It is shown that the EMET plan provides better conformity of the prescribed 50 Gy to the PTV as opposed to the conventional plan where the 50 Gy isodose line extends to cover more volume of the healthy tissues. It is also shown that the low-dose isodose line (20 Gy), obtained by EMET, covers a small volume compared to the conventional plan. If we consider any tissue outside the PTV as an OAR, then EMET would show superior behaviour in saving such an OAR. The

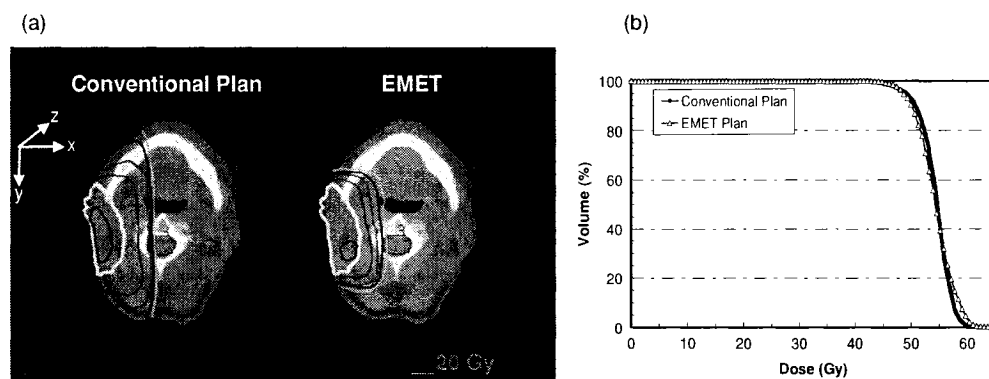


Figure 4. Comparison of (a) isodose distributions and (b) DVH for an outlined target using conventional two AP-PA wedged, MLC-shaped 6 MV beams mixed with one lateral 12 MeV electron beam and EMET technique using four fields of 9, 12, 15 and 18 MeV.

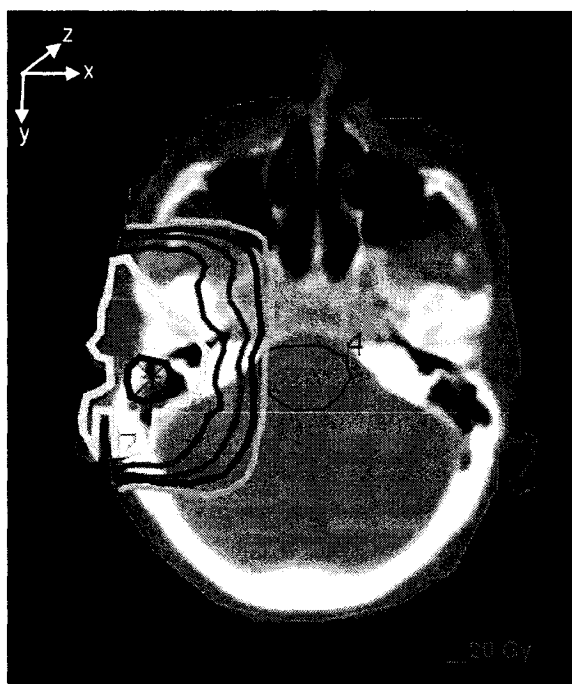


Figure 5. Dose distribution obtained by EMET shows that the algorithm takes the effect of the heterogeneity into account at the cost of the conformity.

DVHs, shown in figure 4(b), of both plans show that they both converge to the same maximum dose with more uniformity within the PTV if the conventional plan is used. Hot spots were observed to be spread along the PTV for the EMET plan due to the junctioning effect, while in the conventional plan the hotspots are localized in the soft tissue. Figure 5 shows the dose distribution obtained by EMET for a slice that contains part of the target located in bone tissues. It shows that the PTV is fully covered with the prescription dose of 50 Gy even though the slice shows a high level of heterogeneity. With the use of realistic Monte Carlo

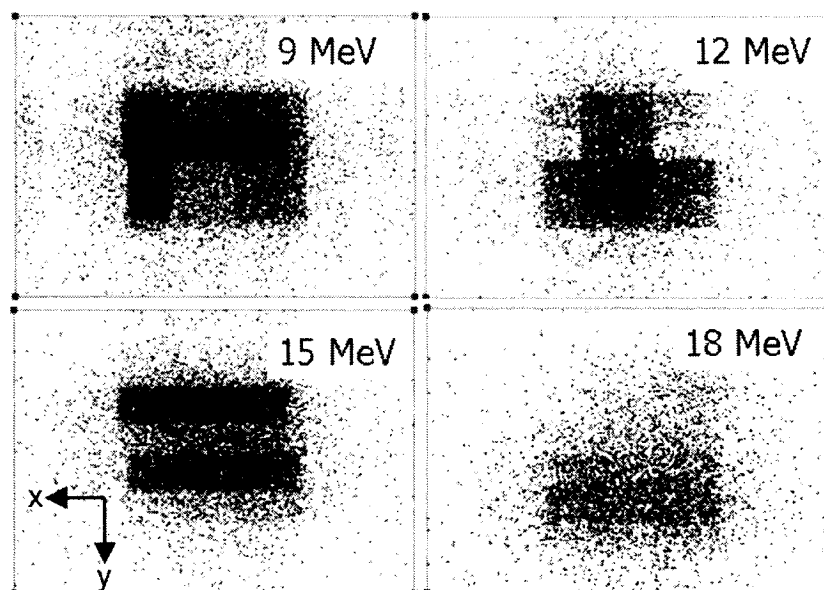


Figure 6. XY scatter plot for the weighted fluence obtained by the optimizer for each energy.

Table 2. The total number of the prescribed monitor units obtained by the optimizer over the whole treatment. The beam-on time required to deliver one fraction remains within a 5 min interval.

Fieldlet	9 MeV	12 MeV	15 MeV	18 MeV	6 MV	
1	2310	450	3000	0	ANT	0
2	7425	0	400	76	POS	1240
3	315	1408	1590	1372		
4	360	736	60	1892		
5	4750	36	0	0		
6	855	1536	120	252		
7	1980	0	270	1036		
8	495	0	0	0		

simulated fieldlets kernels *a priori*, where the patient heterogeneities have been accounted for in the optimization algorithm, the EMET plan is truly optimized with its initial requirements. However, due to the competing goals in the objective function between covering the PTV adequately and conforming the prescribed dose to it, the final outcome depends on which goal has higher priority. In this case, the coverage of the heterogeneous tissue came at the cost of the conformity.

The intensity maps for each energy field, obtained by weighing the Monte Carlo simulated fieldlets to their contribution provided by the optimizer, are shown in figure 6. The map shows the dominance of the 9 MeV electron field. Such dominance is due to the shallow depth of the tumour. There is also a significant fraction of the high energy electron fieldlets at the positions, which is attributed to the presence of bone tumour heterogeneity along the path of those specific fieldlets. Table 2 shows the final output provided by the optimizer converted to monitor unit settings. Note that these numbers represent the setting of the complete delivery and need to be fractionated based on the number of fractions prescribed by the physician.

The minimum output to be given by the optimizer was set to be one monitor unit, yet several fieldlets were given a zero weight including the anterior photon beam. The posterior photon beam, however, was given a relatively high weight which improved the homogeneity of the distribution as specified by the constraints.

The calculation time required to obtain phase files of 24 fieldlets used in this EMET plan was a total of 24 h with a 10 Pentium III CPUs cluster. Calculating all dose distributions based on the generated phase space files is estimated to be 30 min in the same cluster. The optimization process produces its results within 2 h. Most of the time consumed in the process is due to the production of the phase space files that could be significantly reduced by the use of the beam models or by building up a library of selected phase space files.

4. Conclusions

In this work, we studied the feasibility of a simplified collimation device to deliver conformal electron beam dose distributions. Our results show that EMET offers advantages over the conventional treatments and leads to a significant reduction of the dose delivered to the healthy tissues. In the case studied, the beam-on time for one fraction would be within 5 min if the accelerator was set to run 500 MU per minute. The transition time for the six fieldlets for each of the four energies used is estimated to be around 8 min based on the basic characteristics of standard motors and the pitch of typical driving screws. Given the fact that we used a limited number of fieldlets, the optimization algorithm could provide weights that conform to the target within reasonable delivery time. More work is needed in the selection of fieldlets and in investigating the use of beam models. A prototype of FLEC is under construction in our department. Comparisons between EMET and IMRT are being investigated and the feasibility of using a practical combined plan is underway.

Acknowledgments

This work has been partially supported by the Canadian Institute of Health Research (CIHR) operating grant MOP 57828. JS is a research scientist of the National Cancer Institute of Canada (NCIC) appointed with funds provided by the Canadian Cancer Society. The Saudi Arabian Cultural Bureau is also acknowledged for its financial contributions.

References

- Bielajew A F, Rogers D W O, Cygler J and Battista J J 1987 A comparison of electron pencil beam and Monte Carlo calculational methods *The Use of Computers in Radiation Therapy* ed I A D Bruinvis (Amsterdam: Elsevier)
- Fippel M 1999 Fast Monte Carlo dose calculation for photon beams based on VMC electron algorithm *Med. Phys.* **26** 1466–75
- Hogstrom K R, Boyd R A, Antolak J A, Svatos M M, Faddegon B A and Rosenman J G 2004 Dosimetry of a prototype retractable eMLC for fixed-beam electron therapy *Med. Phys.* **31** 443–62
- Hristov D, Stavrev P, Sham E and Fallone B G 2002 On the implementation of dose–volume objectives in gradient algorithms for inverse treatment planning *Med. Phys.* **29** 845–56
- Kawrakow I and Fippel M 2000 Investigation of variance reduction techniques for Monte Carlo photon dose calculation using XVMC *Phys. Med. Biol.* **45** 2163–83
- Kawrakow I, Fippel M and Friedrich K 1996 3D electron dose calculation using a voxel based Monte Carlo algorithm *Med. Phys.* **23** 445–57
- Lee M C, Jiang S B, Deng J, Li J S and Ma C-M 2001 Monte Carlo-based treatment planning for modulated electron beam radiation therapy *Phys. Med. Biol.* **46** 2177–99
- Lee M C, Jiang S B and Ma C-M 2000 Monte Carlo and experimental investigations of multileaf collimated electron beams for modulated electron radiotherapy *Med. Phys.* **27** 2708–18

- Ma C M, Ding M, Li J S, Lee M C, Pawlicki T and Deng J 2003 A comparative dosimetric study on tangential photon beams, intensity modulated radiation therapy (IMRT) and modulated electron radiotherapy (MERT) for breast cancer treatment *Phys. Med. Biol.* **48** 909–24
- Ma C M, Faddegon B A, Rogers D W O and Mackie T R 1997 Accurate characterization of Monte Carlo calculated electron beams for radiotherapy *Med. Phys.* **24** 401–6
- Ma C M, Pawlicki T, Lee M C, Jiang S B, Li J S, Deng J, Yi B, Mok E and Boyer A L 2000 Energy- and intensity-modulated electron beam radiotherapy for breast cancer *Phys. Med. Biol.* **45** 2947–67
- Ravindran B P, Singh R R, Brindha S and Sathyan S 2002 Manual multi-leaf collimator for electron beam shaping—a feasibility study *Phys. Med. Biol.* **47** 4389–96
- Rogers D W O, Faddegon B A, Ding G X, Ma C M, We J and Mackie T R 1995 BEAM: a Monte Carlo code to simulate radiotherapy treatment units *Med. Phys.* **22** 503–24
- Sait S M and Youssef H 1999 *Iterative Computer Algorithms with Applications in Engineering: Solving Combinatorial Optimization Problems* (Los Alamitos, CA: Angela Burgess)

Energy modulated electron therapy using a few leaf electron collimator in combination with IMRT and 3D-CRT: Monte Carlo-based planning and dosimetric evaluation

Khalid Al-Yahya^{a)}

Medical Physics Unit, McGill University, Montreal General Hospital, 1650 Cedar Avenue, Montreal, Quebec H3G 1A4, Canada

Matthew Schwartz and George Shenouda

Department of Radiation Oncology, McGill University Health Centre, Montreal General Hospital, 1650 Cedar Avenue, Montreal, Quebec H3G 1A4, Canada

Frank Verhaegen

Medical Physics Unit, McGill University, Montreal General Hospital, 1650 Cedar Avenue, Montreal, Quebec H3G 1A4, Canada

Carolyn Freeman

Department of Radiation Oncology, McGill University Health Centre, Montreal General Hospital, 1650 Cedar Avenue, Montreal, Quebec H3G 1A4, Canada

Jan Seuntjens^{b)}

Medical Physics Unit, McGill University, Montreal General Hospital, 1650 Cedar Avenue, Montreal, Quebec H3G 1A4, Canada

(Received 3 May 2005; revised 17 June 2005; accepted for publication 7 July 2005; published 30 August 2005)

Energy modulated electron therapy (EMET) based on Monte Carlo dose calculation is a promising technique that enhances the treatment planning and delivery of superficially located tumors. This study investigated the application of EMET using a novel few-leaf electron collimator (FLEC) in head and neck and breast sites in comparison with three-dimensional conventional radiation therapy (3D-CRT) and intensity modulated radiation therapy (IMRT) techniques. Treatment planning was performed for two parotid cases and one breast case. Four plans were compared for each case: 3D-CRT, IMRT, 3D-CRT in conjunction with EMET (EMET-CRT), and IMRT in conjunction with EMET (EMET-IMRT), all of which were performed and calculated with Monte Carlo techniques. For all patients, dose volume histograms (DVHs) were obtained for all organs of interest and the DVHs were used as a means of comparing the plans. Homogeneity and conformity of dose distributions were calculated, as well as a sparing index that compares the effect of the low isodose lines. In addition, the whole-body dose equivalent (WBDE) was estimated for each plan. Adding EMET delivered with the FLEC to 3D-CRT improves sparing of normal tissues. For the two head and neck cases, the mean dose to the contralateral parotid and brain stem was reduced relative to IMRT by 43% and 84%, and by 57% and 71%, respectively. Improved normal tissue sparing was quantified as an increase in sparing index of 47% and 30% for the head and neck and the breast cases, respectively. Adding EMET to either 3D-CRT or IMRT results in preservation of target conformity and dose homogeneity. When adding EMET to the treatment plan, the WBDE was reduced by between 6% and 19% for 3D-CRT and by between 21% and 33% for IMRT, while WBDE for EMET-CRT was reduced by up to 72% when compared with IMRT. FLEC offers a practical means of delivering modulated electron therapy. Although adding EMET delivered using the FLEC results in perturbation of target conformity when compared to IMRT, it significantly improves normal tissue sparing while offering enhanced target conformity to the 3D-CRT planning. The addition of EMET systematically leads to a reduction in WBDE especially when compared with IMRT. © 2005 American Association of Physicists in Medicine. [DOI: 10.1118/1.2011089]

Key words: Monte Carlo dosimetry, energy modulated electron therapy, intensity modulated radiation therapy, whole body dose

I. INTRODUCTION

Electron beams offer significant advantages over megavoltage photon beams in terms of delivery of high dose at shallow depths, rapid fall-off of the dose distribution beyond the

treatment volume, and low exit dose. Nevertheless, the use of modulated electron beams still lags behind that of photon intensity modulated radiation therapy (IMRT). Compared with IMRT, energy modulated electron therapy (EMET) has not been widely implemented due to problems inherent to

electron beams such as dosimetric accuracy and verification as well as a lack of systems for automatic delivery. Studies have shown the fundamental capability of modulated electron beams for the delivery of tailored dose distribution and different delivery approaches have been proposed.¹ An automated system of bolus modulation was proposed to design and produce patient specific bolus.²⁻⁵ But such system is expensive and planning and treatment with bolus-modulated electron beams remain time consuming and cumbersome.

Electron multileaf collimators (eMLCs)⁶⁻⁸ have been designed for use in their own support frame and have the potential to serve for modulated electron radiation therapy applications.⁸ Aside from being relatively bulky, due to the presence of a large number of motors in close proximity to the patient, automation of such a complex system has not been satisfactorily addressed.

We have recently proposed and studied the feasibility of a simplified "few-leaf electron collimator" (FLEC)⁹ for delivering EMET. The FLEC is designed as an added accessory tool able to automatically form a sequence of rectangular openings (fieldlets) to compose any irregular electron field. It consists of four copper bars driven by stepper motors that are electronically coupled to the motors controlling the photon jaws so that both of them simultaneously project the same opening at source to surface distance (SSD) of 100 cm. Being backed up by the jaws, the e-collimator blades have a thickness of only 1.1 cm and a width of 3 cm. These limited lateral dimensions ensure that the collimator fits within a regular clinical electron applicator.

The use of inverse planning techniques for EMET is more complex than for photon beam IMRT since collimation has a profound effect on electron scattering and the dose gradients in a specific fieldlet. In addition, accurate dose calculations in and near patient heterogeneities are essential to ensure that the optimizer has the dose information required for calculation of fieldlet weights that lead to an optimal treatment plan. Hence, the output and the dose distribution realized through the combination of multiple subfields requires faithful modeling of electron transport through the collimation system and inside the patient.

The total body dose resulting, mainly, from scatter and leakage in photon beams is considered to be a significant disadvantage to IMRT.¹⁰⁻¹² To deliver an equivalent target dose, IMRT techniques require a considerable increase in beam-on time compared to conventional techniques (between 2 and 5 times longer).^{13,14} The increased number of monitor units (MUs) leads to a greater whole-body dose to the patient due to the leakage and scattering of x-rays, hereby increasing the risk of radiation induced malignancies.¹⁵ In contrast, electron beams are not associated with the hazard of the increased total body dose due to the absence of the target and the flattening filter that produce and flatten photon beams and cause leaking and scattering away from the beam direction.

In this work, we investigated the clinical significance of a few-leaf collimator with an associated inverse Monte Carlo-based planning algorithm for electron beams. As the use of a limited number of electron fieldlets may result in undesirable

TABLE I. Objective function parameters used in treatment planning and optimization.

<i>Parotid cases</i>				
	Goal (Gy)	Vol below goal (%)	Min (Gy)	Max (Gy)
Target	60	2	57.5	68
	Limit (Gy)	Vol above limit(%)		Max (Gy)
Tissue	50	20		68
Eye(L)	40	2		45
Eye(R)	40	2		45
Lens(L)	8	1		8
Lens(R)	8	1		8
Spinal cord	40	4		45
Brain	50	33		53
Brain stem	50	33		53
Larynx	50	50		50
<i>Breast case</i>				
	Goal (Gy)	Vol below goal (%)	Min (Gy)	Max (Gy)
Target	50	3	48	55
	Limit (Gy)	Vol above limit(%)		Max (Gy)
Tissue	50	1		50
Heart	20	10		45
Lung	20	10		50

dose heterogeneity within the target when applied as a sole treatment modality, the combination of EMET with either traditional photon beams or IMRT beams is of greater interest because it achieves the conformity and target uniformity desired in an optimal plan with better sparing of normal tissues. EMET planning was thus performed either in conjunction with photon beams used in three-dimensional conformal therapy (EMET-CRT) or in conjunction with IMRT (EMET-IMRT). We studied three clinical cases: two parotid gland cases and a breast case. We estimated the whole body dose equivalent (WBDE) of the conventional 3D-CRT, IMRT, EMET-CRT, and EMET-IMRT plans using measured dose data at various distances from the isocenter. This work represents the results of a feasibility study and the full application of the technique awaits the implementation and validation of a QA program that verifies the accuracy of the delivery using similar techniques as those used in IMRT.

II. METHODS AND MATERIALS

A. Patient selection, volume definition, dose prescription

Two parotid cancer patients post-surgical resection previously treated with adjuvant radiation were selected. Each patient had been immobilized with a thermoplastic mask, and had had a planning computed tomography (CT) scan of the head and neck with 5 mm slices. The clinical target volume (CTV), planning target volume (PTV), and organs at risk (OARs) (brain, brain stem, spinal cord, eyes, lenses, larynx, and contralateral parotid) had been contoured for each patient. The CTV included the post-surgical bed and areas at risk for microscopic disease. The PTV included the CTV and

a 3 mm margin. The dose prescribed to the PTV was 60 Gy, at 2 Gy per fraction. For inverse planning, dose constraints to the OARs are seen in Table I.

One patient with left-sided breast cancer post-mastectomy previously treated with adjuvant radiation was selected. The patient had been immobilized with a breast board, and had had a planning CT scan of the thoracic cavity with 5 mm slices. The clinical target volume (CTV) and organs at risk (lungs, heart, contralateral breast, skin, and ribs) had been contoured. The skin was outlined for a depth of 2–3 mm. The CTV included the left chest wall as defined on the planning CT scan. The dose prescribed to the CTV was 50 Gy, at 2 Gy per fraction. For inverse planning, dose constraints to the OARs are seen in Table I. The IMRT plan dose constraints did not include the skin or ribs as we did not want to compromise the target coverage.

For all cases, the normal tissues excluding the OARs and target volumes were defined.

B. Treatment planning

1. Treatment planning system

To ensure consistency of the comparison between different plans, all plans computed in this work were Monte Carlo recalculated using the dose engine embedded in the McGill Monte Carlo Treatment Planning (MMCTP) system. This planning interface was developed with the capability of importing treatment plans from different planning systems from which it reads the CT data, beam arrangements and the MU prescription. After acquiring the plan information, the patient-specific beam arrangements are simulated using the Monte Carlo EGS/BEAMnrc package¹⁶ to obtain the phase space data (PSD) representing the beam energy and particle properties. For each energy, the MU calibration of the system is obtained based on a dose calculation in reference calibration conditions. The PSD of each beam is stored in a file from which each particle is transported through the patient density matrix [$256 \times 256 \times (\text{number of slices})$] derived from CT data (voxel size varying from 0.15 to 0.2 cm) using the fast Monte Carlo code XVMC.¹⁷ The beams are added based on their MU weights to obtain a final dose distribution displayed in MMCTP.

Simulation of the photon beams of all plans included importing the MLC file from the clinical treatment planning system (CadPlan®) and converting them to an input file readable by the DYNVMLC module¹⁸ in BEAM/EGSnrc. The DYNVMLC has the ability to fully model the details of the leaves used in the Millennium 120 leaf collimator including the difference on the thickness of the inner and the outer leaves, leaf holes, tips, air gaps. For dynamic delivery in IMRT plans, the leaf sequence files were extracted from the IMRT system station and converted to a format suitable for the BEAMnrc DYNVMLC component module in which the physical openings at the MLC plane are calculated and the MLC segments are sampled based on the MU settings. MMCTP is equipped to process the IMRT plan and provide a Monte Carlo-recalculated dose distribution for each approved plan. The wedges were simulated using the WEDGE

module developed by van der Zee and Welleweerd¹⁹ and modified to work within the BEAMnrc environment. While the validation of the simulations of DYNVMLC has been reported in another study,¹⁸ the simulations of the WEDGE module have been extensively studied over a wide set of experimental setups and the differences between measurements and calculations were less than 3%.

2. Energy modulated electron therapy planning

EMET was planned and the delivery was calculated as described in a previous study.⁹ Briefly, it involves the use of the automated FLEC in conjunction with Monte Carlo-calculation of patient-specific dose deposition coefficients (DDCs). Keeping the outer dimensions of the FLEC not larger than the currently existing standard electron applicators has the consequence that geometrical restrictions associated with the electron treatment of head and neck patients can be overcome. The weight of the FLEC is estimated to be around 3–4 kg in addition to the weight of a clinical electron treatment applicator. In the first order, the delivery of complex dynamic electron fields will be performed in a step-and-shoot approach, whereby every subfield is formed by simultaneous collimation of the electron beam by the jaws and FLEC. A complete fraction from a typical treatment plan consisting of a combination of 25 subfields of four energies can be delivered within a 15 min time frame.⁹ The DDCs are obtained by manual selection of suitable fieldlets that geometrically conform to the target followed by full Monte Carlo simulation of each fieldlet for all energies using the BEAMnrc code to obtain a phase space representation of the fieldlets. Particles from this phase space are then transported through the patient model using the XVMC code. The dose distribution of each simulated fieldlet is considered a kernel that is fed into an optimization algorithm. Each fieldlet's phase space file contains 2–6 million particles depending on its dimensions which results in a negligible latent uncertainty. In a previous study, the accuracy of the Monte Carlo engine for clinical electron beams has been commissioned and compared to measurements in heterogeneous phantoms and the overall accuracy was less than 3% near maximum dose.²⁰ The number of simulated histories was selected so as to achieve a statistical uncertainty within 2% or less per fieldlet in the voxels receiving 10% or more of maximum dose. Ma *et al.* illustrated that such small statistical uncertainties in modulated electron beams will not affect the final results represented in dose volume histogram (DVHs).²¹

The in-house developed optimization software operates under a graphical programming system (Application Visualization System, AVS Inc.) and uses the deterministic steep DVH minimization algorithm²² as an optimization technique. The software manages the extraction of the dosimetric information from the Monte Carlo calculated kernels which includes the contour data and the DDCs that characterize the relative dose contribution from each kernel to each point confined in an individual contour. Obtaining both contour

TABLE II. The total MUs to deliver the plans of the conventional 3D-CRT,^a EMET-CRT,^b IMRT,^c and EMET-IMRT.^b The addition of EMET reduces the photon beam contributions of the 3D-CRT and IMRT plans by transferring some weight to the electron beams. The electron MUs and the photon MUs are not additive since they contribute differently to the whole body dose.

<i>Case 1 (Parotid)</i>											
3D-CRT			EMET-CRT			IMRT			EMET-IMRT		
Energy	Angle	MU	Energy	Angle	MU	Energy	Angle	MU	Energy	Angle	MU
6 MV	345	142	6 MV	345	86	6 MV	240	259	6 MV	240	297
6 MV	200	141	6 MV	200	199	6 MV	280	199	6 MV	280	89
6 MV	270	97	6 MV	270	39	6 MV	310	226	6 MV	310	67
			6 MeV	270	48	6 MV	350	160	6 MV	350	131
			9 MeV	270	53	6 MV	30	216	6 MV	030	219
			12 MeV	270	251				6 MeV	270	50
									9 MeV	270	60
									12 MeV	270	279
<i>Case 2 (Parotid)</i>											
3D-CRT			EMET-CRT			IMRT			EMET-IMRT		
Energy	Angle	MU	Energy	Angle	MU	Energy	Angle	MU	Energy	Angle	MU
6 MV	10	165	6 MV	10	211	6 MV	330	209	6 MV	330	158
6 MV	190	155	6 MV	190	76	6 MV	100	209	6 MV	100	102
6 MV	90	134	6 MV	90	11	6 MV	130	207	6 MV	130	171
			9 MeV	90	159	6 MV	170	212	6 MV	170	111
			12 MeV	90	135	6 MV	30	198	6 MV	30	146
			15 MeV	90	320	6 MV	60	247	6 MV	60	206
									9 MeV	90	43
									12 MeV	90	74
									15 MeV	90	219
<i>Case 3 (Breast)</i>											
3D-CRT			EMET-CRT			IMRT			EMET-IMRT		
Energy	Angle	MU	Energy	Angle	MU	Energy	Angle	MU	Energy	Angle	MU
6 MV	302	205	6 MV	302	156	6 MV	302	207	6 MV	302	137
6 MV	127	205	6 MV	127	156	6 MV	312	184	6 MV	312	120
			6 MeV	46	370	6 MV	322	196	6 MV	322	101
			9 MeV	46	414	6 MV	127	185	6 MV	127	130
						6 MV	117	228	6 MV	117	144
						6 MV	107	243	6 MV	107	150
									6 MeV	46	570
									9 MeV	46	805

^aThe number of MUs is prescribed by the CadPlan treatment planning system.

^bThe number of MUs is prescribed by the EMET optimizer.

^cThe number of MUs is prescribed by the CORVUS treatment planning system.

Abbreviations: MU=Monitor Unit; 3D-CRT=three-dimensional conformal radiation therapy; EMET-CRT=energy modulated electron therapy in conjunction with three-dimensional conformal radiation therapy; IMRT=intensity modulated radiation therapy; EMET-IMRT=energy modulated electron therapy in conjunction with intensity modulated radiation therapy.

data and DDCs for the PTV and OARs is followed by assigning the prescription, the dose-volume constraints, and their related penalties. The EMET optimizer evaluates the role of each fieldlet in the overall dose distribution and assigns a relative weight to it. After an optimum plan is achieved, the EMET optimizer returns the energies of the contributing fieldlets along with their associated relative intensities in the form of number of MUs. Fieldlets that receive a weight of zero by the optimizer are considered rejected. In this work, the Monte Carlo simulated photon beams are

considered as fieldlets in both EMET-CRT and EMET-IMRT plans. The EMET optimizer determines the weight of the entire field in the same fashion it deals with an electron fieldlet. Thus, the optimizer reweighs the overall delivered IMRT treatment but does not change the leaf sequence of each of the individual IMRT fields.

3. Treatment techniques

For each patient, we have used four planning techniques that are summarized in Table II.

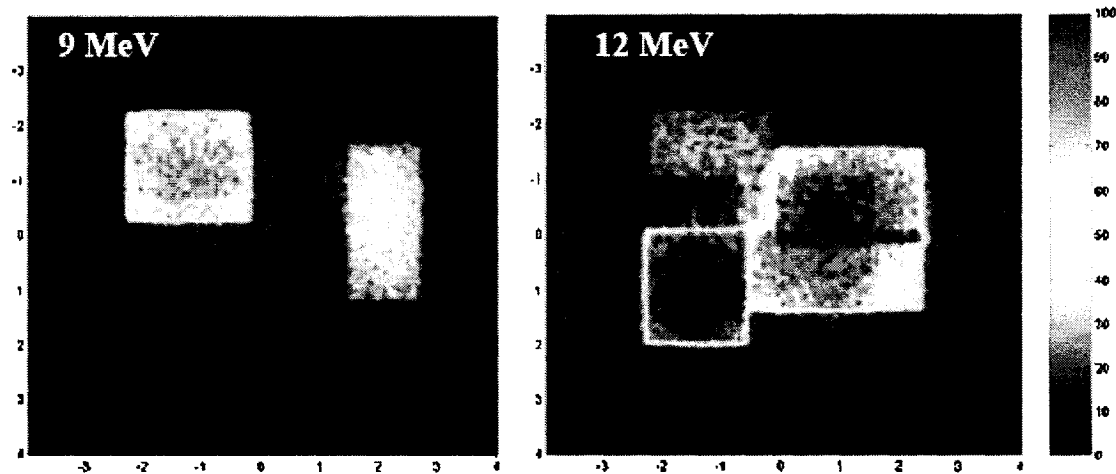


FIG. 1. The intensity map of two energy fields based on the relative weights assigned by the EMET optimizer. The intensity map is normalized to the fieldlet with the highest MUs.

Technique 1: 3D conformal radiotherapy (3D-CRT) technique

For each of the two parotid cases, three wedged 6 MV photon beams from a Varian Clinac 2100EX accelerator (Varian Medical Systems, Palo Alto, CA) were used. The perpendicular beams (the 270° beam for the first case and the 90° beam for the second case) were given a reduced weight to obtain a more homogeneous dose distribution. The fields were shaped by means of the beam's eye view (BEV) feature in ACQSIM (Philips, Andover, MA) and a 120 multileaf collimator (MLC) was used with a 6 mm consistent margin around the PTV to reduce the dose to the OARs. For the breast case, two tangential rectangular 6 MV photon fields were chosen based on the BEV feature to entirely cover the CTV. A wedge angle of 30° was selected to provide a uniform dose distribution within the CTV.

Technique 2: IMRT

The commercial inverse planning system (CORVUS 5.0, NOMOS Inc., Cranberry Township, PA) was used to generate the IMRT plans. The IMRT technique used five step-and-shoot 6 MV beam orientations for the first parotid case and six gantry angles for the second parotid case and the breast case. The optimization procedure was performed without considering the effect of tissue inhomogeneities. Although the CORVUS treatment planning system allows one to use heterogeneity corrections in the optimization procedure, Yang *et al.* showed that this leads to only a negligible difference when compared to the CORVUS plan obtained without the heterogeneity correction for coplanar plans.²³ The effect of this approximation is manifested as discrepancies between the predicted DVH by the optimization algorithm and the "actual" DVH obtained after calculating the dose distribution with Monte Carlo simulations which rigorously accounts for the effect of tissue inhomogeneities.

Once the IMRT plans are approved, leaf sequence files were produced for each beam orientation derived from the intensity maps required to achieve the fluence proposed by the optimization algorithm and the dose distribution is then recalculated by Monte Carlo methods.

Techniques 3 and 4: EMET-CRT and EMET-IMRT

For case 1, 10 fieldlets of 6, 9, and 12 MeV in addition to the newly weighted three beams of the conventional plan were selected for the EMET-CRT and the same electron fieldlets (with different intensities) were also selected in conjunction with the five IMRT fieldlets for the EMET-IMRT. Case 2 employed 12 fieldlets with energies of 9, 12, and 15 MeV. The intensity maps of the 9 and 12 MeV electron fields are shown in Fig. 1. The breast case used eight fieldlets of 6 and 9 MeV. Table II shows the MU settings for the four techniques where the settings of the EMET plans were provided by the EMET optimizer.

C. Plan evaluation parameters

For each case studied, the mean dose, minimum dose, and maximum dose to the target were calculated for each of the four plans. As per Nutting *et al.*,²⁴ the minimum dose is defined as the dose received by $\geq 99\%$ of the target volume and the maximum dose is defined as the dose received by $\leq 1\%$ of the target. DVHs were obtained for each of the four treatment plans for the target and OARs delineated. Only the mean dose and the maximum dose were reported for the OARs.

Conformity was compared by calculating the conformity index (COIN95) defined by Baltas *et al.*²⁵ for each plan. COIN95 is defined as the product of the fraction of the target covered by higher than 95% (PTV_{95}/PTV) of the prescribed dose and the ratio of the volume of the target receiving at least 95% of the prescribed dose to the total volume of tissue receiving at least 95% of the prescribed dose (PTV_{95}/V_{95}).

$$COIN95 = \frac{PTV_{95}}{PTV} \frac{PTV_{95}}{V_{95}}. \quad (1)$$

However, although COIN95 provides reasonable evaluation of the conformity surrounding the target for the high dose values, it does not consider the volume that lies in the low dose region. As shown in Fig. 2, having two plans

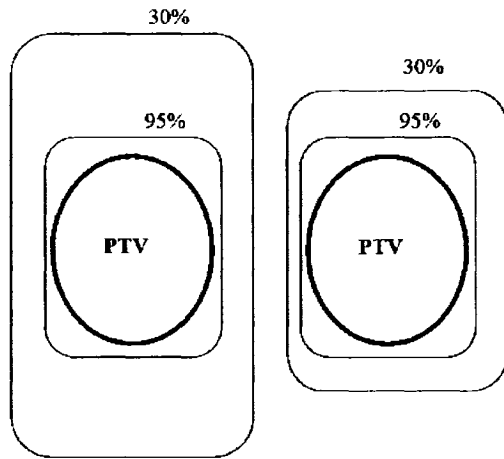


FIG. 2. Schematic diagram of two plans that have the same coverage of the 95% isodose line to the PTV volume but with different conformity of the low isodose lines. The conformity index (COIN95) will be equivalent for both plans despite their differences. The sparing index (SPIN50/10) could be used to differentiate between them.

delivering the same 95% coverage will not be differentiated by the COIN95 factor if one plan extends the 30% line to cover larger volume which is undesirable if it could be avoided. We therefore propose the use of a new term, the sparing index (SPIN50/10), to quantify the volume that receives between 50% and 10% of the prescribed dose. We have defined this as

$$SPIN50/10 = 1 - V_{10}^{50} \quad (2)$$

where V_{10}^{50} is the ratio of the volume of tissue that receives between 10% and 50% of the prescribed dose to the irradiated volume. The irradiated volume was defined as the volume of tissue that receives at least 0.5% of the prescribed dose. SPIN50/10 cannot stand alone without being evaluated in conjunction with COIN95 where both values, ideally, should approach 1.

We also used the homogeneity index HI90/110 to compare plans in terms of the ability to deliver homogeneous dose distribution to the target. HI90/110 is defined as the percentage of the target volume with a dose higher than 90% and lower than 110% of the prescribed dose. These parameters assist in evaluating plans that have comparable irradiated volumes since there is a central dependence of these parameters on the planning volume in relation to normal tissue.

D. Assessment of whole body dose-equivalent (WBDE)

The dose was measured using a cylindrical Farmer ionization chamber placed at a depth of 2 cm in a solid water phantom and positioned at 35, 55, 75 and 95 cm away from the edge of the field. To resemble the patient geometry, a semispherical solid water phantom that mimics a head was placed at the isocenter while the other parts of the body were mimicked using bolus bags to account for the effect of the internal scatter. Dose per MU was obtained for a 7×7 cm² field (a typical field collimated with jaws and FLEC used in

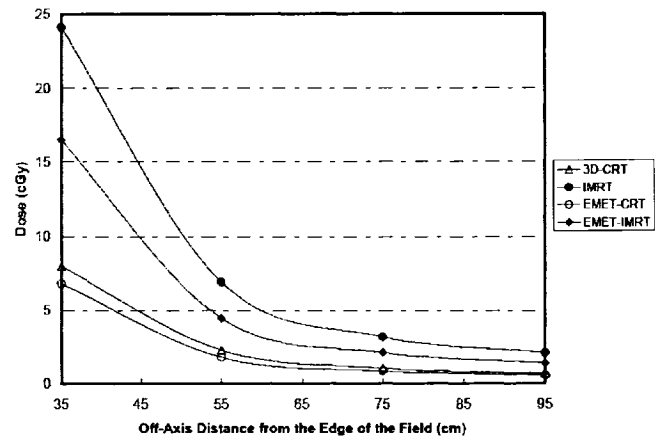


FIG. 3. Off axis dose at depth of 2 cm in a solid water phantom based on the number of MUs given by four techniques for the breast case.

EMET) at all energies (6, 9, 12, 15 MeV), as well as the dose per MU for 10×10 cm² of the 6 MV photon field which agreed with the results obtained by other authors.²⁶ Using the total number of MUs acquired from the CadPlan treatment planning system for the conventional plan, from the CORVUS treatment planning system for the IMRT plan, and from the EMET system for both the EMET-CRT and EMET-IMRT plan, WBDE was estimated by multiplying the total MUs of each field by the dose value per MU measured at 40 cm from the isocenter. This value was used as a reasonable approximation to determine WBDE resulting from the 60 Gy prescribed dose for head and neck cases and the 50 Gy prescribed dose for the breast case. Figure 3 illustrates the comparison of the behavior of the peripheral dose caused by the four techniques based on the total MUs prescribed for the breast case. It is important to note that this estimate of the total body dose assessment serves only as a first order approximation due to the vital dependence of the WBDE on the treatment technique of each plan. In this work, we have used WBDE only to relatively compare different planning techniques.

III. RESULTS

A. Parotid cancer cases

The isodose distributions of the four different plans with the DVHs of the outlined organs for the two cases are shown in Figs. 4(a) and 4(b). Table III shows the summary of the DVH analysis of the four treatment plans for each case where the minimum, maximum, and mean doses to the target are reported. COIN95, SPIN50/10, HI90/110, and the estimate for the WBDE are shown in Table IV.

The target was well covered by all four plans. However, the IMRT plan gave the highest conformity to the target, followed by the EMET-IMRT plan. The use of IMRT and EMET-CRT produced hot spots, but these were within the target volume and were considered acceptable. For case 2, the hot spots obtained with the EMET-CRT plan were within the air-filled cavities of the temporal bone in the mastoid air cells. Since the dose distribution was calculated by Monte

Carlo, the dose that is reported is the actual dose that is deposited in the air cavities. The hot spots with the IMRT plan were in the soft tissues due to the heterogeneities that were not taken into account in the optimization. As expected, the high isodose curves were very conformal with both the IMRT and EMET-CRT plans, but the low isodose curves for the IMRT plan contained a much larger volume of normal tissue compared with the EMET-CRT plan as seen in Fig. 4. This corresponds to the EMET-CRT plan having a much higher SPIN50/10 value than the IMRT plan (Table IV). If the SPIN50/10 is accepted as a measure of the ability of a given plan to spare the normal tissues in the low dose regions, then the EMET-CRT plan had a 47% higher sparing on average compared to the IMRT plan.

IMRT has been shown to reduce the dose to the contralateral parotid, brain, and spinal cord.^{24,27} In our series, IMRT decreased the mean dose to the contralateral parotid by 27% on average when compared to the 3D-CRT plan (Table III). The use of EMET-CRT further reduced the dose to the contralateral parotid dose by an additional 58%. The amount of normal brain tissue treated with a given technique is also an important issue when comparing different treatment techniques. The mean dose to the brain was 27% lower on average with the EMET-CRT plan as compared to the IMRT plan. The maximum dose to the spinal cord was 22% lower on average with the EMET-CRT plan when compared to the IMRT plan.

The estimate of WBDE (in mSv) is shown in Table IV. The WBDE was lowest for the EMET-CRT plans and the highest for the IMRT plans for all cases. The use of EMET-CRT resulted in a 69% decrease in the whole body dose on average compared to the IMRT plan.

B. Left breast cancer post-mastectomy case

Table III summarizes the quantitative comparison between different plans for the target volume and OARs. The minimum, maximum, and mean doses to the target, ipsilateral lung, heart, skin overlying the treated breast, and ribs are given for each of the treatment plans. COIN95, SPIN50/10, HI90/110, and the WBDE are given for each plan in Table IV. Figure 4(c) compares the isodose distributions for each of the treatment plans. The mean doses to the target were similar with each of the plans. However, when using the conformity index, the EMET-IMRT plan had the highest conformity followed by the IMRT plan, EMET-CRT plan, and the 3D-CRT plan the lowest. EMET-CRT gave the most homogeneous dose distribution to the target as shown by the HI90/110 seen in Table IV. The SPIN50/10 showed that the 3D-CRT plan had highest value due to the poor conformity, shown in COIN95, that increased the volume of normal tissues irradiated with high isodose lines while lessening the volume covered by low isodose lines. The sparing of the 3D-CRT plan is followed by the EMET-CRT plan, EMET-IMRT plan, and the IMRT plan.

An important concern with left-sided breast cancer patients treated with radiotherapy is the dose to the heart. Table III gives the doses to the heart according to the different

techniques. The 3D-CRT technique gave the lowest mean heart dose followed by the EMET-CRT plan, EMET-IMRT plan, and the IMRT plan. The use of EMET-CRT in this case gave a similar conformity as IMRT, but with a decrease in the dose to the heart. The EMET-CRT plan gave a 47% lower mean heart dose and a 41% lower maximum heart dose as compared to the IMRT plan.

The ipsilateral lung often receives significant dose with conventional radiotherapy using tangential fields. Table III shows the doses to the ipsilateral lung by the different techniques. The EMET-IMRT technique gave the lowest mean dose to the lung, which resulted in a 10% decrease in the mean lung dose compared to the IMRT plan. The dose to the contralateral lung was negligible since it was not in the path of any irradiation field. In addition, the skin and rib doses were analyzed, and the IMRT plan gave the lowest mean doses to each. The higher mean dose to the skin seen with the EMET-CRT plan is likely due to the location of the CTV 3–4 mm below the surface so that the skin is in the buildup region. However, the maximum skin dose was the highest with IMRT and the lowest with EMET-CRT. The increased dose to the skin seen with IMRT is likely due to the fact that the skin is in the buildup region for photons, and IMRT uses multiple tangential beams to deliver a homogenous dose to the target. This effect has been seen with patients treated with IMRT for head and neck cancers.²⁸ The EMET-CRT plan had an 8% lower maximum skin dose when compared to the IMRT plan.

WBDE is shown in Table IV. It was lowest for the EMET-CRT plan followed by the 3D-CRT plan, EMET-IMRT plan, and the IMRT plan. The EMET-CRT plan was 72% lower than the IMRT plan with respect to the estimated whole body radiation dose.

IV. DISCUSSION

In this study, we introduce a novel EMET technique using a FLEC as a modality for use in conjunction with 3D-CRT and/or IMRT in the context of mixed beam treatment planning and delivery. The automated FLEC circumvents the challenge of remotely shaping the electron fields required for the clinical application of EMET. This technique was applied to two parotid cases and a breast case for which comparisons with Monte Carlo-recalculated conventional 3D-CRT and IMRT plans were performed. Although the FLEC involves the use of limited beam ports and large fieldlets compared to the fine MLC beamlets used in IMRT, the results show a significant overall improvement in several parameters used to analyze treatment plans.

A. 3D-CRT vs EMET-CRT

Conformity is significantly enhanced when EMET was added to the 3D-CRT plan. The conformity effect was more pronounced with the breast case where the high isodose lines extend to the lung covering some portion of it with the prescribed dose while with EMET-CRT plan, as shown in Fig. 4, the 45 Gy isodose line conforms to the breast tissues, sparing the lung from irradiation by high doses. The volume of lung

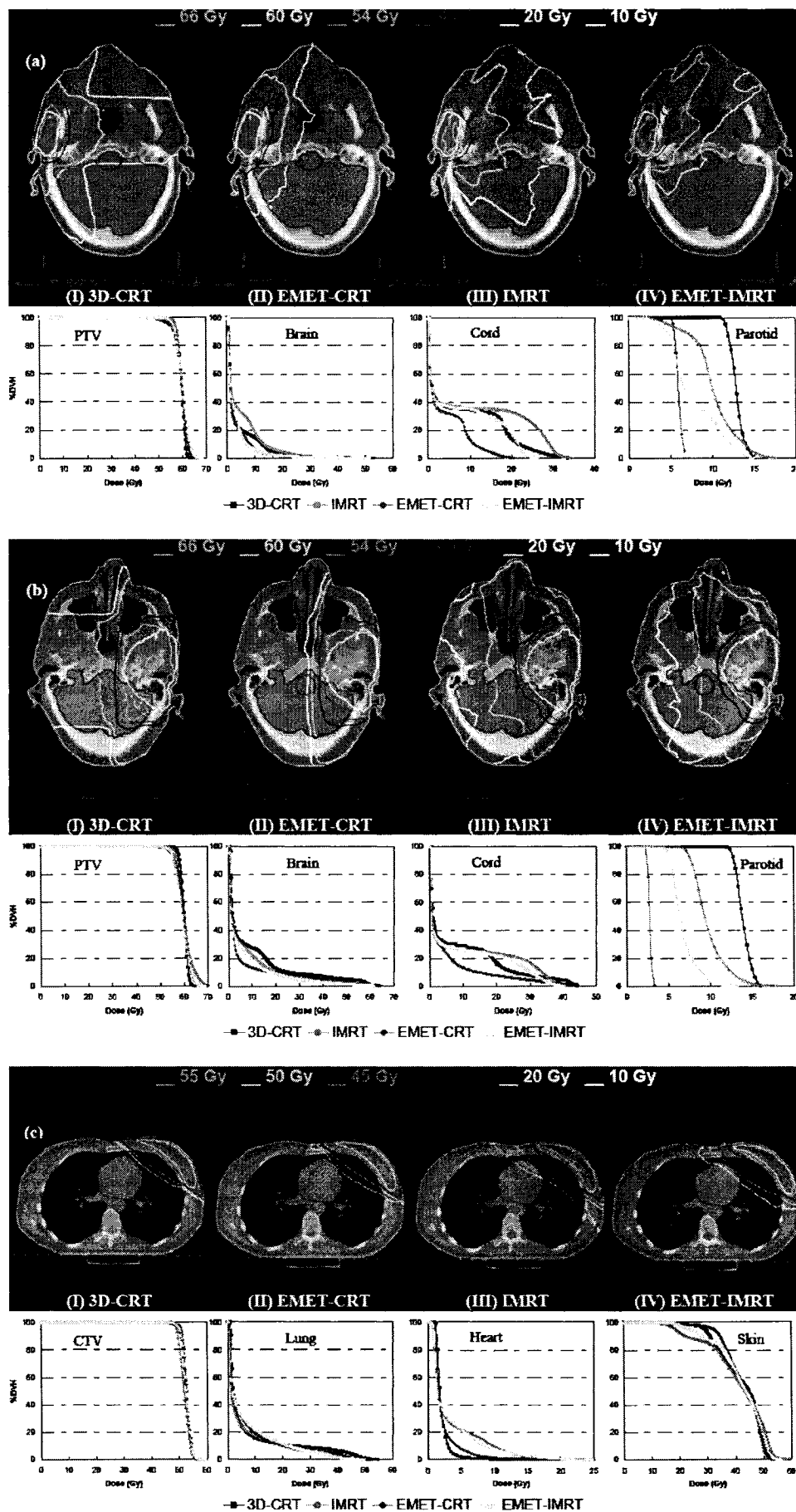


FIG. 4. A comparison of the Monte Carlo calculated dose distributions and DVHs for all outlined organs produced by four plans: (I) 3D-CRT, (II) EMET-CRT, (III) IMRT, and (IV) EMET-IMRT; (a) and (b) are for the two parotid cases and (c) is for the breast case.

TABLE III. Comparison of dose for PTV and OARs using four planning techniques. The overall statistical uncertainties of all plans were less than 2%.

Plan	PTV			Brain		Brain stem		Cord		Contralateral parotid	
	Mean	Min	Max	Mean	Max	Mean	Max	Mean	Max	Mean	Max
<i>Case 1 (Parotid)</i>											
3D-CRT	59.1	49.6	62.2	3.60	24.5	16.0	19.9	7.5	31.6	12.7	14.7
IMRT	59.7	55.9	64.7	4.82	29.2	17.2	25.1	9.9	32.2	9.9	16.3
EMET-CRT	59.5	50.7	63.6	2.79	23.9	7.4	11.3	3.8	18.2	5.7	6.7
EMET-IMRT	59.9	54.7	65.4	2.9	23.5	9.1	14.5	7.2	24.2	7.5	14.3
<i>Case 2 (Parotid)</i>											
3D-CRT	59.9	56.9	63.1	9.01	59.3	18.4	29.3	8.1	43.2	13.7	15.7
IMRT	60.3	55.1	68.9	6.64	52.2	17.8	38.4	8.6	39.9	9.5	15.1
EMET-CRT	59.6	52.2	65.9	5.94	55.4	5.3	18.7	4.6	40.7	2.5	3.1
EMET-IMRT	59.3	53.2	66.1	6.15	51.8	14.0	34.5	7.8	37.3	6.5	11.1
Plan	Breast			Lung		Heart		Skin		Ribs	
	Mean	Min	Max	Mean	Max	Mean	Max	Mean	Max	Mean	Max
<i>Case 1 (Breast)</i>											
3D-CRT	52.4	47.3	55.5	14.3	48.7	2.1	6.2	41.7	51.9	12.2	52.2
IMRT	51.7	48.1	56.3	11.2	42.8	4.3	17.2	40.7	55.6	9.5	49.4
EMET-CRT	52.5	48.5	55.4	12.4	45.1	2.3	10.1	42.6	51.4	11.8	49.9
EMET-IMRT	52.4	48.7	56.2	10.1	41.3	3.8	17.3	41.7	53.7	10.3	49.5

Abbreviations: min=minimum dose; max=maximum dose; mean=mean dose; 3D-CRT=three-dimensional conformal radiation therapy; EMET-CRT=energy modulated electron therapy in conjunction with three-dimensional conformal radiation therapy; IMRT=intensity modulated radiation therapy; EMET-IMRT=energy modulated electron therapy in conjunction with intensity modulated radiation therapy.

that receives the prescribed dose as seen from the DVH was reduced by 50% using EMET. Sparing was also significantly improved with the use of EMET-CRT in both head and neck cases, leading to considerable reduction of the mean dose to all OARs including the contralateral parotid. Sparing could also be achieved by replacing the lateral photon field with a lateral conventional cutout-shaped electron field. However, this would lead to extremely unfavorable heterogeneities in the dose distribution appearing as an extended tail in the DVH of the PTV. Target dose uniformity was affected by the addition of EMET to the 3D-CRT in the head and neck cases, but the reduction to the HI90/110 caused by EMET remained modest. Homogeneity could possibly be enhanced by assigning more penalty to it in the optimization procedure but this will cause competing goals in the objective function that might sacrifice conformity and/or reduce sparing of the other organs. In the breast case, however, the homogeneity of the dose distribution was improved with the use of EMET. The addition of a relatively large number of electron MUs did not increase the WBDE; EMET-CRT showed systematic reduction of the WBDE by reducing the photon MUs which are the dominant source of radiation outside the beam and replacing them with electron MUs which make a minimal contribution to the whole body dose.

B. IMRT vs IMRT-EMET

Optimizing the EMET fieldlets with the IMRT whole fields that are added to form the IMRT-EMET plan does not represent the best possible optimization as only the weight of

the entire IMRT field is varied and not the weight of the individual beamlets since the current technology has not yet been clinically implemented for Monte Carlo based optimization of photon beams. Using EMET-IMRT for the head and neck cases showed reduced conformity relative to IMRT alone. This is not the case for the breast case where conformity was enhanced with the EMET-IMRT plan. This is attributed to the relative large size of the fieldlets compared to the projection of the small PTV. In the parotid cases, due to the small size of the PTV, the effect of the edges of the fieldlets appeared to be significant while this effect diminished in the breast case where a large target is irradiated. Overall, homogeneity is preserved with the addition of EMET. Sparing, however, systematically improves with EMET due to the lower exit dose of electrons compared to photons. Improvement of sparing was seen as the SPIN50/10 as well as the mean dose and the maximum dose to the OARs, all of which were consistently reduced when EMET fields were optimized with IMRT. EMET-IMRT has the advantage of lowering the WBDE because of the reduction of the photon beam-on time.

C. IMRT vs EMET-CRT

Although the conformity achieved by IMRT cannot be challenged with the EMET-CRT due to the use of rather large fieldlets, the sparing attained by EMET-CRT is superior even with such limited fieldlets. The significant reduction of dose to the contralateral parotid suggests that EMET-CRT has the potential to improve the quality of life, while the reduction of

TABLE IV. Comparison of treatment planning evaluation parameters of the four planning techniques.

	Plan	COIN95 ^a	SPIN50/10 ^b	HI90/110 ^c	WBDE ^d (mSv)
<i>Case 1</i>					
(Parotid)	3D-CRT	0.56	0.49	0.957	9.4
	IMRT	0.68	0.52	0.997	26.3
	EMET-CRT	0.59	0.77	0.956	8.9
	EMET-IMRT	0.62	0.59	0.985	20.8
<i>Case 2</i>					
(Parotid)	3D-CRT	0.54	0.69	0.987	11.3
	IMRT	0.69	0.61	0.935	31.8
	EMET-CRT	0.62	0.88	0.957	9.4
	EMET-IMRT	0.64	0.60	0.973	23.4
<i>Case 3</i>					
(Breast)	3D-CRT	0.30	0.93	0.949	8.5
	IMRT	0.54	0.67	0.956	25.7
	EMET-CRT	0.43	0.88	0.980	7.2
	EMET-IMRT	0.57	0.71	0.960	17.4

^aCOIN95=Conformity index.^bSPIN50/10=Sparing index.^cHI90/110=Homogeneity index.^dWBDE=Whole body dose equivalent

Abbreviations: 3D-CRT=three-dimensional conformal radiation therapy; EMET-CRT=energy modulated electron therapy in conjunction with three-dimensional conformal radiation therapy; IMRT=intensity modulated radiation therapy; EMET-IMRT=energy modulated electron therapy in conjunction with intensity modulated radiation therapy.

dose to the spinal cord is important since it allows the patient to receive further radiation treatment if needed. Target dose homogeneity was modestly improved with the breast case where the hot spots caused by the tangential effect of the IMRT fields could be avoided. The maximum dose to the skin in the breast case was reduced by 8% with EMET-CRT compared to IMRT. In the second parotid case, the hot spots in the IMRT plan were in the soft tissues while they were in the air cavities in the EMET-CRT plan. This effect cannot be differentiated when comparisons are made through DVHs only but it might have clinical implications. This study also underlies the concern of the inclusion of the air cavities in the PTV especially when true Monte Carlo optimization is implemented.²⁹ For the WBDE, EMET-CRT shows major reduction of the estimate of WBDE (in the order of 70%).

V. CONCLUSION

In summary, we investigated the use of energy modulated electron beam treatment planning and delivery using a few-leaf electron collimator in a context of mixed beam treatment planning with conventional radiation therapy and IMRT. We used Monte Carlo techniques to calculate treatment plans for conventional 3D-CRT planning and IMRT alone or combined with EMET. We have shown that EMET delivered with the FLEC could be a valuable addition to current treatment techniques especially when applied to superficially located tumors that are inherently difficult to plan using IMRT. Since the FLEC can be readily automated and remotely controlled, the complexity of EMET delivery will not exceed what is deemed acceptable in IMRT. The characteristics of

quality assurance procedures are expected to be similar to those for IMRT treatments. For two head and neck cases and for one breast case we showed that target conformity and homogeneity are preserved while drastically improving normal tissue sparing. As a result of reducing the number of photon MUs for delivery, the addition of EMET systematically leads to a reduction in whole body dose, especially when compared to IMRT. The application of EMET to other treatment sites is currently being investigated.

ACKNOWLEDGMENTS

This work has been supported in part by the Canadian Institutes of Health Research through Grant No. MOP 57828 and by National Cancer Institute of Canada, Terry Fox Foundation, Grant No. 016298. K.A. acknowledges support from the Saudi Cultural Bureau. J.S. is a Research Scientist of the National Cancer Institute of Canada appointed with funds provided by the Canadian Cancer Society.

^aElectronic mail: kyahya@medphys.mcgill.ca^bAuthor to whom correspondence should be addressed; electronic mail: jseuntjens@medphys.mcgill.ca¹K. R. Hogstrom, J. A. Antolak, R. J. Kudchadker, C. M. Ma, and D. D. Leavitt, "Modulated electron therapy," in: *Intensity-Modulated Radiation Therapy: The State of the Art: Proceedings of the 2003 Summer School*, edited by J. R. Palta and T. R. Mackie (Medical Physics, Madison, 2003), pp. 749–786.²D. A. Low, G. Starkschall, S. W. Bujnowski, L. L. Wang, and K. R. Hogstrom, "Electron bolus design for radiotherapy treatment planning: bolus design algorithms," *Med. Phys.* **19**, 115–124 (1992).³D. A. Low, G. Starkschall, N. E. Sherman, S. W. Bujnowski, J. R. Ewton, and K. R. Hogstrom, "Computer-aided design and fabrication of an electron bolus for treatment of the paraspinal muscles," *Int. J. Radiat. Oncol., Biol., Phys.* **33**, 1127–1138 (1995).⁴G. H. Perkins, M. D. McNeese, J. A. Antolak, T. A. Buchholz, E. A. Strom, and K. R. Hogstrom, "A custom three-dimensional electron bolus technique for optimization of postmastectomy irradiation," *Int. J. Radiat. Oncol., Biol., Phys.* **51**, 1142–1151 (2001).⁵R. J. Kudchadker, K. R. Hogstrom, A. S. Garden, M. D. McNeese, R. A. Boyd, and J. A. Antolak, "Electron conformal radiotherapy using bolus and intensity modulation," *Int. J. Radiat. Oncol., Biol., Phys.* **53**, 1023–1037 (2002).⁶M. C. Lee, S. B. Jiang, and C. M. Ma, "Monte Carlo and experimental investigations of multileaf collimated electron beams for modulated electron radiation therapy," *Med. Phys.* **27**, 2708–2718 (2000).⁷C. M. Ma, T. Pawlicki, M. C. Lee, S. B. Jiang, J. S. Li, J. Deng, B. Yi, E. Mok, and A. L. Boyer, "Energy- and intensity-modulated electron beams for radiotherapy," *Phys. Med. Biol.* **45**, 2293–2311 (2000).⁸K. R. Hogstrom, R. A. Boyd, J. A. Antolak, M. M. Svatos, B. A. Faddegon, and J. G. Rosenman, "Dosimetry of a prototype retractable eMLC for fixed-beam electron therapy," *Med. Phys.* **31**, 443–462 (2004).⁹K. Al-Yahya, D. Hristov, F. Verhaegen, and J. Seuntjens, "Monte Carlo-based modulated electron beam treatment planning using a few leaf electron collimator—feasibility study," *Phys. Med. Biol.* **50**, 847–857 (2005).¹⁰E. Glatstein, "Intensity-modulated radiation therapy: the inverse, the converse, and the perverse," *Semin. Radiat. Oncol.* **12**, 272–281 (2002).¹¹A. C. Paulino and M. Skwarchuk, "Intensity-modulated radiation therapy in the treatment of children," *Med. Dosim.* **27**, 115–120 (2002).¹²D. Verellen and F. Vanhavere, "Risk assessment of radiation-induced malignancies based on whole-body equivalent dose estimates for IMRT treatment in the head and neck region," *Radiat. Oncol.* **53**, 199–203 (1999).¹³Intensity Modulated Radiation Therapy Collaborative Working Group, "Intensity-modulated radiotherapy: current status and issues of interest," *Int. J. Radiat. Oncol. Biol. Phys.* **51**, 880–914 (2001).¹⁴D. Followill, P. Geis, and A. Boyer, "Estimates of whole-body dose

- equivalent produced by beam intensity modulated conformal therapy," *Int. J. Radiat. Oncol., Biol., Phys.* **38**, 667–672 (1997).
- ¹⁵E. J. Hall and C. S. Wu, "Radiation-induced second cancers: the impact of 3D-CRT and IMRT," *Int. J. Radiat. Oncol., Biol., Phys.* **56**, 83–88 (2003).
 - ¹⁶D. W. Rogers, B. A. Faddegon, G. X. Ding, C. M. Ma, J. We, and T. R. Mackie, "BEAM: a Monte Carlo code to simulate radiotherapy treatment units," *Med. Phys.* **22**, 503–524 (1995).
 - ¹⁷I. Kawrakow and M. Fippel, "Investigation of variance reduction techniques for Monte Carlo photon dose calculation using XVMC," *Phys. Med. Biol.* **45**, 2163–2183 (2000).
 - ¹⁸E. Heath and J. Seuntjens, "Development and validation of a BEAMnc component module for accurate Monte Carlo modelling of the Varian dynamic Millennium multileaf collimator," *Phys. Med. Biol.* **48**, 4045–4063 (2003).
 - ¹⁹W. van der Zee and J. Welleweerd, "A Monte Carlo study on internal wedges using BEAM," *Med. Phys.* **29**, 876–885 (2002).
 - ²⁰R. Doucet, M. Olivares, F. DeBlois, E. B. Podgorsak, I. Kawrakow, and J. Seuntjens, "Comparison of measured and Monte Carlo calculated dose distributions in inhomogeneous phantoms in clinical electron beams," *Phys. Med. Biol.* **48**, 2339–2354 (2003).
 - ²¹C. M. Ma, J. S. Li, S. B. Jiang, T. Pawlicki, W. Xiong, L. H. Qin, and J. Yang, "Effect of statistical uncertainties on Monte Carlo treatment planning," *Phys. Med. Biol.* **50**, 891–907 (2005).
 - ²²D. Hristov, P. Stavrev, E. Sham, and B. G. Fallone, "On the implementation of dose-volume objectives in gradient algorithms for inverse treatment planning," *Med. Phys.* **29**, 848–856 (2002).
 - ²³J. Yang, J. Li, L. Chen, R. Price, S. McNeeley, L. Qin, L. Wang, W. Xiong, and C. M. Ma, "Dosimetric verification of IMRT treatment planning using Monte Carlo simulations for prostate cancer," *Phys. Med. Biol.* **50**, 869–878 (2005).
 - ²⁴C. M. Nutting, C. G. Rowbottom, V. P. Cosgrove, J. M. Henk, D. P. Dearnaley, M. H. Robinson, J. Conway, and S. Webb, "Optimisation of radiotherapy for carcinoma of the parotid gland: a comparison of conventional, three-dimensional conformal, and intensity-modulated techniques," *Radiother. Oncol.* **60**, 163–172 (2001).
 - ²⁵D. Baltas, C. Kolotas, K. Geramani, R. F. Mould, G. Ioannidis, M. Kekchidi, and N. Zamboglou, "A conformal index (COIN) to evaluate implant quality and dose specification in brachytherapy," *Int. J. Radiat. Oncol., Biol., Phys.* **40**, 515–524 (1998).
 - ²⁶M. Stovall, C. R. Blackwell, J. Cundiff, D. H. Novack, J. R. Palta, L. K. Wagner, E. W. Webster, and R. J. Shalek, "Fetal dose from radiotherapy with photon beams: report of AAPM Radiation Therapy Committee Task Group No. 36," *Med. Phys.* **22**, 63–82 (1995).
 - ²⁷C. M. Bragg, J. Conway, and M. H. Robinson, "The role of intensity-modulated radiotherapy in the treatment of parotid tumors," *Int. J. Radiat. Oncol., Biol., Phys.* **52**, 729–738 (2002).
 - ²⁸N. Lee, C. Chuang, J. M. Quivey, T. L. Phillips, P. Akazawa, L. J. Verhey, and P. Xia, "Skin toxicity due to intensity-modulated radiotherapy for head-and-neck carcinoma," *Int. J. Radiat. Oncol., Biol., Phys.* **53**, 630–637 (2002).
 - ²⁹C. Boudreau, E. Heath, J. Seuntjens, O. Ballivy, and W. Parker, "IMRT head and neck treatment planning with a commercially available Monte Carlo based planning system," *Phys. Med. Biol.* **50**, 879–890 (2005).

Bibliography

- AAPM, "A protocol for the determination of absorbed dose from high-energy photon and electron beams," *Med. Phys.* **10**, 741-771 (1983).
- AAPM, "Total skin electron therapy: technique and dosimetry," Report no 23, American Association of Medical Physicists (December 1987).
- C. Akazawa, "Treatment of the scalp using photon and electron beams," *Med. Dosim.* **14**, 129-131 (1989).
- C. Albaret, Automatic system for Monte Carlo determination of cutout factors of arbitrarily shaped electron and experimental verification of Monte Carlo calculated dose distributions. M.S. Thesis, Medical Physics Unit, McGill University, 2004.
- A. Alexander, MMCTP: A radiotherapy research environment for patient-treatment planning. M.S. Thesis, Medical Physics Unit, McGill University, 2006.
- P.R. Almond, "The physical measurements of electron beams from 6 to 18 MeV: absorbed dose and energy calibration," *Phys. Med. Biol.* **12**, 13-24 (1967).
- P.R. Almond, P.J. Biggs, B.M. Coursey, W.F. Hanson, M.S. Huq, R. Nath, and D.W. Rogers, "AAPM's TG-51 protocol for clinical reference dosimetry of high-energy photon and electron beams," *Med. Phys.* **26**, 1847-1870 (1999).
- K. Al-Yahya, Implementation and validation of Monte Carlo treatment planning for lung cancer patients. M.S. Thesis, Medical Physics Unit, McGill University, 2002.
- K. Al-Yahya, D. Hristov, F. Verhaegen, and J. Seuntjens, "Monte Carlo-based modulated electron beam treatment planning using a few leaf electron collimator - feasibility study," *Phys. Med. Biol.* **50**, 847-857 (2005).
- K. Al-Yahya, M. Schwartz, G. Shenouda, F. Verhaegen, C. Freeman, and J. Seuntjens, "Energy modulated electron therapy using a few leaf electron collimator in combination with IMRT and 3D-CRT: Monte Carlo-based planning and dosimetric evaluation," *Med. Phys.* **32**, 2976-2986 (2005).
- P. Andreo and A.E. Nahum, "Stopping-power ratio for a photon spectrum as a weighted sum of the values for monoenergetic photon beams," *Phys. Med. Biol.* **30**, 1055-1065 (1985).
- P. Andreo and A. Brahme, "Stopping power data for high-energy photon beams," *Phys. Med. Biol.* **31**, 839-858 (1986).
- P. Andreo, A. Nahum, and A. Brahme, "Chamber-dependent wall correction factors in dosimetry," *Phys. Med. Biol.* **31**, 1189-1199 (1986).

- P. Andreo, "Monte Carlo techniques in medical radiation physics," *Phys. Med. Biol.* **36**, 861-920 (1991).
- J.A. Antolak, M.R. Bieda, and K.R. Hogstrom, "Using Monte Carlo methods to commission electron beams: a feasibility study," *Med. Phys.* **29**, 771-786 (2002).
- H. Attix, *Introduction to radiological physics and radiation dosimetry* (Whily & Son, New York, NY, 1986).
- D. Baltas, C. Kolotas, K. Geramani, R.F. Mould, G. Ioannidis, M. Kekchidi, and N. Zamboglou, "A conformal index (COIN) to evaluate implant quality and dose specification in brachytherapy," *Int. J. Radiat. Oncol. Biol. Phys.* **40**, 515-524 (1998).
- A.S. Beddar and S. Krishnan, "Intraoperative radiotherapy using a mobile electron LINAC: a retroperitoneal sarcoma case," *J. Appl. Clin. Med. Phys.* **6**, 95-107 (2005).
- M.J. Berger, "Monte Carlo calculation of the penetration and diffusion of fast charged particles," *Methods Comput. Phys.* **1**, 135-215 (1963).
- H. Bethe and W. Heitler, "On the stopping of fast particles and on the creation of positive electrons," *Proc. Roy. Soc.* **146**, 0083-0112 (1934).
- H.J. Bhabha, "The scattering of positrons by electrons with exchange on Dirac's theory of the positron," *Proc. Roy. Soc.* **154**, 0195-0206 (1936).
- A.F. Bielajew, D.W. Rogers, J. Cygler, and J.J. Battista, "A comparison of electron pencil beam and Monte Carlo calculation methods," in: *The Use of Computers in Radiation Therapy*, edited by A.D. Bruinvis (Elsevier, Amestrdam, 1987).
- A.F. Bielajew and D.W.O. Rogers, "PRESTA - the parameter reduced electron-step transport algorithm for electron Monte-Carlo transport," *Nucl. Inst. Methods B* **18**, 165-181 (1987).
- P.J. Biggs, A.L. Boyer, and K.P. Doppke, "Electron dosimetry of irregular fields on the Clinac 18," *Int. J. Radiat. Oncol. Biol. Phys.* **5**, 433-440 (1979).
- P. Bjork, T. Knoos, and P. Nilsson, "Measurements of output factors with different detector types and Monte Carlo calculations of stopping-power ratios for degraded electron beams," *Phys. Med. Biol.* **49**, 4493-4506 (2004).
- M. Blomquist and M. Karlsson, "Test procedures for verification of an electron pencil beam algorithm implemented for treatment planning," *Radiother. Oncol.* **39**, 271-286 (1996).
- M. Blomquist, M.G. Karlsson, B. Zackrisson, and M. Karlsson, "Multileaf collimation of electrons--clinical effects on electron energy modulation and mixed beam therapy depending on treatment head design," *Phys. Med. Biol.* **47**, 1013-1024 (2002).
- J.E. Bond, R. Nath, and R.J. Schulz, "Monte Carlo calculation of the wall correction factors for

- ionization chambers and Aeq for ^{60}Co gamma rays," *Med. Phys.* **5**, 422-425 (1978).
- M.L. Boone, P.R. Almond, and A.E. Wright, "High-energy electron dose perturbations in regions of tissue heterogeneity," *Ann. N. Y. Acad. Sci.* **161**, 214-232 (1969).
- T. Bortfeld, J. Burkelbach, R. Boesecke, and W. Schlegel, "Methods of image reconstruction from projections applied to conformation radiotherapy," *Phys. Med. Biol.* **35**, 1423-1434 (1990).
- C. Boudreau, E. Heath, J. Seuntjens, O. Ballivy, and W. Parker, "IMRT head and neck treatment planning with a commercially available Monte Carlo based planning system.," *Phys. Med. Biol.* **50**, 879-890 (2005).
- A.L. Boyer, P. Geis, W. Grant, and M. Carol, "Modulated beam conformal therapy for head and neck tumors," *Int. J. Radiat. Oncol. Biol. Phys.* **39**, 227-236 (1997).
- C.M. Bragg, J. Conway, and M.H. Robinson, "The role of intensity-modulated radiotherapy in the treatment of parotid tumors," *Int. J. Radiat. Oncol. Biol. Phys.* **52**, 729-738 (2002).
- A. Brahme, I. Lax, and P. Andreo, "Electron beam dose planning using discrete Gaussian beams. Mathematical background," *Acta Radiol. Oncol.* **20**, 147-158 (1981).
- A. Brahme, "Geometric parameters of clinical electron beams," *Acta Radiol. Suppl.* **364**, 11-19 (1983).
- A. Brahme, "Design principles and clinical possibilities with a new generation of radiation therapy equipment. A review," *Acta Oncol.* **26**, 403-412 (1987).
- A. Brahme, "Optimal setting of multileaf collimators in stationary beam radiation therapy," *Strahlenther. Onkol.* **164**, 343-350 (1988).
- J.F. Briesmeister, "MCNP-a general Monte Carlo n-particle transport code, Version 4C Technical Report No LA-13709-M Los Alamos National Laboratory," (2000).
- J. Coleman, C. Park, J.E. Villarreal-Barajas, P. Petti, and B. Faddegon, "A comparison of Monte Carlo and Fermi-Eyges-Hogstrom estimates of heart and lung dose from breast electron boost treatment," *Int. J. Radiat. Oncol. Biol. Phys.* **61**, 621-628 (2005).
- D.J. Convery and S. Webb, "Generation of discrete beam-intensity modulation by dynamic multileaf collimation under minimum leaf separation constraints," *Phys. Med. Biol.* **43**, 2521-2538 (1998).
- J.E. Cygler, J.J. Battista, J.W. Scrimger, E. Mah, and J. Antolak, "Electron dose distributions in experimental phantoms: a comparison with 2D pencil beam calculations," *Phys. Med. Biol.* **32**, 1073-1086 (1987).
- J.E. Cygler, G.M. Daskalov, G.H. Chan, and G.X. Ding, "Evaluation of the first commercial Monte Carlo dose calculation engine for electron beam treatment planning," *Med. Phys.*

- 31, 142-153 (2004).
- J.E. Cygler, C. Lochrin, G.M. Daskalov, M. Howard, R. Zohr, B. Esche, L. Eapen, L. Grimard, and J.M. Caudrelier, "Clinical use of a commercial Monte Carlo treatment planning system for electron beams," *Phys. Med. Biol.* **50**, 1029-1034 (2005).
- J. Dai, Validation of Monte Carlo techniques for 3D-CRT of lung cancer patients and comparative evaluation of treatment plans. M.S. Thesis, Medical Physics Unit, McGill University, 2004.
- S.K. Das, M. Bell, L.B. Marks, and J.G. Rosenman, "A preliminary study of the role of modulated electron beams in intensity modulated radiotherapy, using automated beam orientation and modality selection," *Int. J. Radiat. Oncol. Biol. Phys.* **59**, 602-617 (2004).
- J.F. Dempsey, D.A. Low, S. Mutic, J. Markman, A.S. Kirov, G.H. Nussbaum, and J.F. Williamson, "Validation of a precision radiochromic film dosimetry system for quantitative two-dimensional imaging of acute exposure dose distributions," *Med. Phys.* **27**, 2462-2475 (2000).
- J. Deng, M.C. Lee, and C.M. Ma, "A Monte Carlo investigation of fluence profiles collimated by an electron specific MLC during beam delivery for modulated electron radiation therapy," *Med. Phys.* **29**, 2472-2483 (2002).
- S. Devic, J. Seuntjens, G. Hegyi, E.B. Podgorsak, C.G. Soares, A.S. Kirov, I. Ali, J.F. Williamson, and A. Elizondo, "Dosimetric properties of improved GafChromic films for seven different digitizers," *Med. Phys.* **31**, 2392-2401 (2004).
- S. Devic, J. Seuntjens, E. Sham, E.B. Podgorsak, C.R. Schmidlein, A.S. Kirov, and C.G. Soares, "Precise radiochromic film dosimetry using a flat-bed document scanner," *Med. Phys.* **32**, 2245-2253 (2005).
- G.X. Ding, J.E. Cygler, G.G. Zhang, and M.K. Yu, "Evaluation of a commercial three-dimensional electron beam treatment planning system," *Med. Phys.* **26**, 2571-2580 (1999).
- G.X. Ding, J.E. Cygler, C.W. Yu, N.I. Kalach, and G. Daskalov, "A comparison of electron beam dose calculation accuracy between treatment planning systems using either a pencil beam or a Monte Carlo algorithm," *Int. J. Radiat. Oncol. Biol. Phys.* **63**, 622-633 (2005).
- G.X. Ding, D.M. Duggan, C.W. Coffey, P. Shokrani, and J.E. Cygler, "First macro Monte Carlo based commercial dose calculation module for electron beam treatment planning--new issues for clinical consideration," *Phys. Med. Biol.* **51**, 2781-2799 (2006).
- R. Doucet, M. Olivares, F. DeBlois, E.B. Podgorsak, I. Kawrakow, and J. Seuntjens, "Comparison of measured and Monte Carlo calculated dose distributions in

- inhomogeneous phantoms in clinical electron beams," *Phys. Med. Biol.* **48**, 2339-2354 (2003).
- F.C.P. du Plessis, A. Leal, S. Stathakis, W. Xiong, and C.M. Ma, "Characterization of megavoltage electron beams delivered through a photon multi-leaf collimator (pMLC)," *Phys. Med. Biol.* **51**, 2113-2129 (2006).
- J. Dutreix and A. Dutreix, "Film dosimetry of high-energy electrons," *Ann. N. Y. Acad. Sci.* **161**, 33-43 (1969).
- M.A. Ebert and P.W. Hoban, "Possibilities for tailoring dose distributions through the manipulation of electron beam characteristics," *Phys. Med. Biol.* **42**, 2065-2081 (1997).
- K.E. Ekstrand and R.L. Dixon, "The problem of obliquely incident beams in electron-beam treatment planning," *Med. Phys.* **9**, 276-278 (1982).
- L. Eyges, "Multiple Scattering with Energy Loss," *Phys. Rev.* **74**, 1534-1535 (1948).
- B.A. Faddegon, C.K. Ross, and D.W. Rogers, "Forward-directed bremsstrahlung of 10- to 30-MeV electrons incident on thick targets of Al and Pb," *Med. Phys.* **17**, 773-785 (1990).
- B.A. Faddegon, C.K. Ross, and D.W. Rogers, "Angular distribution of bremsstrahlung from 15-MeV electrons incident on thick targets of Be, Al, and Pb," *Med. Phys.* **18**, 727-739 (1991).
- M. Fippel, I. Kawrakow, and K. Friedrich, "Electron beam dose calculations with the VMC algorithm and the verification data of the NCI working group," *Phys. Med. Biol.* **42**, 501-520 (1997).
- M. Fippel, "Fast Monte Carlo dose calculation for photon beams based on VMC electron algorithm," *Phys. Med. Biol.* **26**, 1466-1475 (1999).
- S. Flampouri, P.M. Evans, F. Verhaegen, A.E. Nahum, E. Spezi, and M. Partridge, "Optimization of accelerator target and detector for portal imaging using Monte Carlo simulation and experiment," *Phys. Med. Biol.* **47**, 3331-3349 (2002).
- D. Followill, P. Geis, and A. Boyer, "Estimates of whole-body dose equivalent produced by beam intensity modulated conformal therapy," *Int. J. Radiat. Oncol. Biol. Phys.* **38**, 667-672 (1997).
- G. Garry, Study of novel techniques for verification imaging and patient dose reconstruction in external beam radiation therapy. Ph.D. Thesis, Medical Physics Unit, McGill University, 2006.
- A.T. Gauer, A.D. Albers, A.F. Cremers, A.R. Harmansa, A.R. Pellegrini, and A.R. Schmidt, "Design of a computer-controlled multileaf collimator for advanced electron radiotherapy," *Phys. Med. Biol.* **51**, 5987-6003 (2006).

- GEANT, Application Software Group Computing and Networks Division-Detector Description and Simulation Tool, in: CERN Program Library Long Writeup W5013 (CERN, Geneva, 1995).
- GEANT4 <http://geant4.web.cern.ch/geant4/> (2003).
- E. Glatstein, "Intensity-modulated radiation therapy: the inverse, the converse, and the perverse," *Semin. Radiat. Oncol.* **12**, 272-281 (2002).
- A.D. Green, Modeling of dual foil scattering systems for clinical electron beams. M.S. Thesis, University of Texas Health Science Center, 1991.
- E. Grusell, A. Montelius, A. Brahme, G. Rikner, and K. Russell, "A general solution to charged particle beam flattening using an optimized dual-scattering-foil technique, with application to proton therapy beams," *Phys. Med. Biol.* **39**, 2201-2216 (1994).
- J.A. Halbeib, "Structure and operation of the ITS code system," in: *Transport of Electrons and Photons*, edited by T.M. Jenkins, W.R. Nelson, A. Rindi (Plenum, New York, 1988), pp. 249-262.
- E.J. Hall and C.S. Wu, "Radiation-induced second cancers: the impact of 3D-CRT and IMRT," *Int. J. Radiat. Oncol. Biol. Phys.* **56**, 83-88 (2003).
- D. Harder, "Energiespektren schneller Elektronen in verschiedenen Tiefen," in: *Symp. on High-Energy Electrons*, edited by A. Zuppinger, G. Poretti (Springer, Berlin, 1965), pp. 260.
- E. Heath, Evaluation of the PEREGRINE Monte Carlo dose calculation code for 6 MV photon beams. M.S. Thesis, Medical Physics Unit, McGill University, 2003.
- E. Heath, J. Seuntjens, and D. Sheikh-Bagheri, "Dosimetric evaluation of the clinical implementation of the first commercial IMRT Monte Carlo treatment planning system at 6 MV," *Med. Phys.* **31**, 2771-2779 (2004).
- J.S. Hendricks, K.J. Adam, T.E. Booth, J.F. Briesmeister, L.L. Carter, L.J. Cox, J.A. Favorite, R.A. Forster, G.W. McKinney, and R.E. Prael, "Present and future capabilities of MCNP," *Appl. Radiat. Isot.* **53**, 857-861 (2000).
- G. Hettinger and C. Pettersson, "Determination of Frick G-value for 30 MeV electrons with the use of a calorimetric technique," in: *Symp. on High-Energy Electrons (Montreaux, Switzerland)*, edited by A. Zuppinger, G. Poretti (Springer, Berlin, 1965), pp. 57-61.
- K.R. Hogstrom, M.D. Mills, and P.R. Almond, "Electron beam dose calculations," *Phys. Med. Biol.* **26**, 445-459 (1981).
- K.R. Hogstrom and R.S. Fields, "Use of CT in electron beam treatment planning: current and future development," in: *Computed Tomography in Radiation Therapy*, edited by C.C. Ling (Raven, New York, 1983), pp. 241-252.

- K.R. Hogstrom, M.D. Mills, J.A. Meyer, J.R. Palta, D.E. Mellenberg, R.T. Meoz, and R.S. Fields, "Dosimetric evaluation of a pencil-beam algorithm for electrons employing a two-dimensional heterogeneity correction," *Int. J. Radiat. Oncol. Biol. Phys.* **10**, 561-569 (1984).
- K.R. Hogstrom and D.D. Leavitt, "Dosimetry of electron arc therapy," in: *Radiation Oncology Physics 1986: Proc. 1986 Summer School of the AAPM*, edited by H. Elson, C. Born (AIP, New York, 1987), pp. 265-295.
- K.R. Hogstrom, R.G. Kurup, A.S. Shiu, and G. Starkschall, "A two-dimensional pencil-beam algorithm for calculation of arc electron dose distributions," *Phys. Med. Biol.* **34**, 315-341 (1989).
- K.R. Hogstrom, "Clinical Electron Beam Dosimetry: Basic Dosimetry Data," in: *AAPM 1990 Summer School*, edited by A.J. Purdy (American Institute of Physics, New York, 1992), pp. 390-490.
- K.R. Hogstrom and R.E. Steadham, "Electron beam dose computation," in: *Teletherapy: Present and Future. 1996 Proc. Summer School of the AAPM*, edited by J.R. Palta, T.R. Mackie (Advanced Medical Publishing, Madison, WI, 1996), pp. 137-174.
- K.R. Hogstrom, R.E. Steadham, P.F. Wong, and A.S. Shiu, "Monitor unit calculations for electron beams," in: *Monitor Unit Calculations for External Photon and Electron Beams*, edited by J.P. Gibbons (Advanced Medical Publishing, Madison, WI, 2000), pp. 113-125.
- K.R. Hogstrom, J.A. Antolak, R.J. Kudchadker, C.M. Ma, and D.D. Leavitt, "Modulated Electron Therapy," in: *Intensity-Modulated Radiation Therapy, The State of the Art: Proceedings of the 2003 Summer School*, edited by J.R. Palta, T.R. Mackie (Medical Physics Publishing, Madison, 2003), pp. 749-786.
- K.R. Hogstrom, R.A. Boyd, J.A. Antolak, M.M. Svatos, B.A. Faddegon, and J.G. Rosenman, "Dosimetry of a prototype retractable eMLC for fixed-beam electron therapy," *Med. Phys.* **31**, 443-462 (2004).
- K.R. Hogstrom and P.R. Almond, "Review of electron beam therapy physics," *Phys. Med. Biol.* **51**, R455-489 (2006).
- D. Hristov, P. Stavrev, E. Sham, and B.G. Fallone, "On the implementation of dose-volume objectives in gradient algorithms for inverse treatment planning," *Med. Phys.* **29**, 848-856 (2002).
- H. Huizenga and P.R. Storchi, "Numerical calculation of energy deposition by broad high-energy electron beams," *Phys. Med. Biol.* **34**, 1371-1396 (1989).
- S. Hyodynmaa, A. Gustafsson, and A. Brahme, "Optimization of conformal electron beam

- therapy using energy- and fluence-modulated beams," *Med. Phys.* **23**, 659-666 (1996).
- "Intensity-modulated radiotherapy: current status and issues of interest," *Int. J. Radiat. Oncol. Biol. Phys.* **51**, 880-914 (2001).
- International Atomic Energy Agency Technical Report No. 277: Absorbed dose determination in photon and electron beams: an international code of practice (IAEA, Vienna, 1987).
- International Commission of Radiation Units and Measurements Report No. 24: Determination of absorbed dose in a patient irradiated by x or gamma rays in radiotherapy procedures (ICRU, Washington, D.C., 1976).
- International Commission of Radiation Units and Measurements Report No. 33: Radiation quantities and units (ICRU, Washington, D.C., 1980).
- International Commission of Radiation Units and Measurements Report No. 35: Radiation dosimetry: electron beams with energies between 1 and 50 MeV (ICRU, Washington, D.C., 1984).
- International Commission of Radiation Units and Measurements Report No. 50: Prescription, recording, and reporting photon beam therapy (ICRU, Washington, D.C., 1993).
- J.J. Janssen, D.E. Riedeman, M. Morawska-Kaczynska, P.R. Storchi, and H. Huizenga, "Numerical calculation of energy deposition by high-energy electron beams: III. Three-dimensional heterogeneous media," *Phys. Med. Biol.* **39**, 1351-1366 (1994).
- R. Jeraj, P.J. Keall, and P.M. Ostwald, "Comparisons between MCNP, EGS4 and experiment for clinical electron beams," *Phys. Med. Biol.* **44**, 705-717 (1999).
- D. Jette, "Electron beam dose calculations," in: *Radiation Therapy Physics*, edited by A.R. Smith (Springer, Berlin, 1995), pp. 95-121.
- S.B. Jiang, T. Pawlicki, and C.-M. Ma, An aperture-based inverse planning algorithm for modulated electron radiation therapy, in: Engineering in Medicine and Biology Society, 2000. Proceedings of the 22nd Annual International Conference of the IEEE, Vol. 1 (2000) 116-118 vol.111.
- S.B. Jiang, T. Pawlicki, E. Gracia, T. Guerrero, M.C. Lee, J.S. Li, J. Deng, D.R. Goffinet, A.L. Boyer, and C.M. Ma, "Modulated electron radiation therapy: A new treatment modality," *Int. J. Radiat. Oncol. Biol. Phys.* **48**, 218 (2000).
- A. Kapur, C.M. Ma, E.C. Mok, D.O. Findley, and A.L. Boyer, "Monte Carlo calculations of electron beam output factors for a medical linear accelerator," *Phys. Med. Biol.* **43**, 3479-3494 (1998).
- M. Karlsson, H. Nystrom, and H. Svensson, "Electron beam characteristics of the 50-MeV racetrack microtron," *Med. Phys.* **19**, 307-315 (1992).

- M. Karlsson and B. Zackrisson, "Matching of electron and photon beams with a multi-leaf collimator," *Radiother. Oncol.* **29**, 317-326 (1993).
- M. Karlsson and B. Zackrisson, "Exploration of new treatment modalities offered by high energy (up to 50 MeV) electrons and photons," *Radiother. Oncol.* **43**, 303-309 (1997).
- M.G. Karlsson, M. Karlsson, and B. Zackrisson, "Intensity modulation with electrons: calculations, measurements and clinical applications," *Phys. Med. Biol.* **43**, 1159-1169 (1998).
- M.G. Karlsson, M. Karlsson, and C.M. Ma, "Treatment head design for multileaf collimated high-energy electrons," *Med. Phys.* **26**, 2161-2167 (1999).
- C.J. Karzmark and N.C. Pering, "Electron linear accelerators for radiation therapy: history, principles and contemporary developments," *Phys. Med. Biol.* **18**, 321-354 (1973).
- C.J. Karzmark, "Advances in linear accelerator design for radiotherapy," *Med. Phys.* **11**, 105-128 (1984).
- C.J. Karzmark, C. Nunan, and E. Tanabe, *Medical Electron Accelerator* (McGraw Hill, New York, 1993).
- I. Kawrakow, M. Fippel, and K. Friedrich, "3D electron dose calculation using a Voxel based Monte Carlo algorithm (VMC)," *Med. Phys.* **23**, 445-457 (1996).
- I. Kawrakow and M. Fippel, "Investigation of variance reduction techniques for Monte Carlo photon dose calculation using XVMC," *Phys. Med. Biol.* **45**, 2163-2183 (2000).
- I. Kawrakow, "Accurate condensed history Monte Carlo simulation of electron transport. I. EGSnrc, the new EGS4 version," *Med. Phys.* **27**, 485-498 (2000).
- I. Kawrakow, D.W. Rogers, and B.R. Walters, "Large efficiency improvements in BEAMnrc using directional bremsstrahlung splitting," *Med. Phys.* **31**, 2883-2898 (2004).
- P.J. Keall and P.W. Hoban, "Super-Monte Carlo: a 3-D electron beam dose calculation algorithm," *Med. Phys.* **23**, 2023-2034 (1996).
- F.M. Khan, W. Sewchand, and S.H. Levitt, "Effect of air space and depth dose in electron beam therapy," *Radiology* **126**, 249-251 (1978).
- F.M. Khan, K.P. Doppke, K.R. Hogstrom, G.J. Kutcher, R. Nath, S.C. Prasad, J.A. Purdy, M. Rozenfeld, and B.L. Werner, "Clinical electron-beam dosimetry: report of AAPM Radiation Therapy Committee Task Group No. 25," *Med. Phys.* **18**, 73-109 (1991).
- F.M. Khan, *The Physics of Radiation Therapy* (Lippincott, Williams & Wilkins, Philadelphia, PA, 2003).
- E.E. Klein, D.A. Low, and J.A. Purdy, "Changes in electron beam dosimetry with a new scattering foil-applicator system on a CL2100C," *Int. J. Radiat. Oncol. Biol. Phys.* **32**,

- 483-490 (1995).
- E.E. Klein, Z. Li, and D.A. Low, "Feasibility study of multileaf collimated electrons with a scattering foil based accelerator," *Radiother. Oncol.* **41**, 189-196 (1996).
- E.E. Klein, "Modulated electron beams using multi-segmented multileaf collimation," *Radiother. Oncol.* **48**, 307-311 (1998).
- H.M. Kooy and H. Rashid, "A three-dimensional electron pencil-beam algorithm," *Phys. Med. Biol.* **34**, 229-243 (1989).
- R.J. Kudchadker, K.R. Hogstrom, A.S. Garden, M.D. McNeese, R.A. Boyd, and J.A. Antolak, "Electron conformal radiotherapy using bolus and intensity modulation," *Int. J. Radiat. Oncol. Biol. Phys.* **53**, 1023-1037 (2002).
- R.J. Kudchadker, J.A. Antolak, W.H. Morrison, P.F. Wong, and K.R. Hogstrom, "Utilization of custom electron bolus in head and neck radiotherapy," *J. Appl. Clin. Med. Phys.* **4**, 321-333 (2003).
- J.S. Laughlin, "Calorimetric determination of absorbed dose with electrons," in: *Symp. on High-Energy Electrons (Montreaux, Switzerland)*, edited by A. Zuppinger, G. Poretti (Springer, Berlin, 1965), pp. 65-71.
- I. Lax, A. Brahme, and P. Andreo, "Electron beam dose planning using Gaussian beams. Improved radial dose profiles," *Acta Radiol. Suppl.* **364**, 49-59 (1983).
- I. Lax and A. Brahme, "Electron beam dose planning using Gaussian beams. Energy and spatial scaling with inhomogeneities," *Acta Radiol. Oncol.* **24**, 75-85 (1985).
- I. Lax, "Inhomogeneity corrections in electron-beam dose planning. Limitations with the semi-infinite slab approximation," *Phys. Med. Biol.* **31**, 879-892 (1986).
- D.D. Leavitt, J.R. Stewart, J.H. Moeller, W.L. Lee, and G.A. Takach, Jr., "Electron arc therapy: design, implementation and evaluation of a dynamic multi-vane collimator system," *Int. J. Radiat. Oncol. Biol. Phys.* **17**, 1089-1094 (1989).
- D.D. Leavitt, J.R. Stewart, J.H. Moeller, and L. Earley, "Optimization of electron arc therapy doses by multi-vane collimator control," *Int. J. Radiat. Oncol. Biol. Phys.* **16**, 489-496 (1989).
- D.D. Leavitt, J.R. Stewart, and L. Earley, "Improved dose homogeneity in electron arc therapy achieved by a multiple-energy technique," *Int. J. Radiat. Oncol. Biol. Phys.* **19**, 159-165 (1990).
- D.D. Leavitt, L. Earley, and J.R. Stewart, "Design and production of customized field shaping devices for electron arc therapy," *Med. Dosim.* **15**, 25-31 (1990).
- M.C. Lee, S.B. Jiang, and C.M. Ma, "Monte Carlo and experimental investigations of multileaf

- collimated electron beams for modulated electron radiation therapy," *Med. Phys.* **27**, 2708-2718 (2000).
- M.C. Lee, S.B. Jiang, J. Deng, J.S. Li, and C.M. Ma, "Monte Carlo-based treatment planning for modulated electron beam radiation therapy," *Phys. Med. Biol.* **46**, 2177-2199 (2001).
- M.C. Lee, J. Deng, J. Li, S.B. Jiang, and C.M. Ma, "Monte Carlo based treatment planning for modulated electron beam radiation therapy," *Phys. Med. Biol.* **46**, 2177-2199 (2001).
- N. Lee, C. Chuang, J.M. Quivey, T.L. Phillips, P. Akazawa, L.J. Verhey, and P. Xia, "Skin toxicity due to intensity-modulated radiotherapy for head-and-neck carcinoma," *Int. J. Radiat. Oncol. Biol. Phys.* **53**, 630-637 (2002).
- J.S. Li, T. Pawlicki, J. Deng, S.B. Jiang, E. Mok, and C.M. Ma, "Validation of a Monte Carlo dose calculation tool for radiotherapy treatment planning," *Phys. Med. Biol.* **45**, 2969-2985 (2000).
- J.G. Li, S.S. Williams, D.R. Goffinet, A.L. Boyer, and L. Xing, "Breast-conserving radiation therapy using combined electron and intensity-modulated radiotherapy technique," *Radiother. Oncol.* **56**, 65-71 (2000).
- E.P. Lief, A. Larsson, and J.L. Humm, "Electron dose profile shaping by modulation of a scanning elementary beam," *Med. Phys.* **23**, 33-44 (1996).
- E.P. Lief, Y.C. Lo, and J.L. Humm, "Electron wedges for radiation therapy," *Int. J. Radiat. Oncol. Biol. Phys.* **40**, 233-243 (1998).
- S.C. Lillicrap, P. Wilson, and J.W. Boag, "Dose distributions in high energy electron beams: production of broad beam distributions from narrow beam data," *Phys. Med. Biol.* **20**, 30-38 (1975).
- C.C. Ling, C. Burman, C.S. Chui, G.J. Kutcher, S.A. Leibel, T. LoSasso, R. Mohan, T. Bortfeld, L. Reinstein, S. Spirou, X.H. Wang, Q. Wu, M. Zelefsky, and Z. Fuks, "Conformal radiation treatment of prostate cancer using inversely-planned intensity-modulated photon beams produced with dynamic multileaf collimation," *Int. J. Radiat. Oncol. Biol. Phys.* **35**, 721-730 (1996).
- D.A. Low, G. Starkschall, S.W. Bujnowski, L.L. Wang, and K.R. Hogstrom, "Electron bolus design for radiotherapy treatment planning: bolus design algorithms," *Med. Phys.* **19**, 115-124 (1992).
- D.A. Low, G. Starkschall, N.E. Sherman, S.W. Bujnowski, J.R. Ewton, and K.R. Hogstrom, "Computer-aided design and fabrication of an electron bolus for treatment of the paraspinal muscles," *Int. J. Radiat. Oncol. Biol. Phys.* **33**, 1127-1138 (1995).
- C.M. Ma, B. Faddegon, D.W. Rogers, and T.R. Mackie, "Accurate characterization of Monte

- Carlo calculated electron beams for radiotherapy," *Med. Phys.* **24**, 401-406 (1997).
- C.M. Ma, E. Mok, A. Kapur, T. Pawlicki, D. Findley, S. Brain, K. Forster, and A.L. Boyer, "Clinical implementation of a Monte Carlo treatment planning system," *Med. Phys.* **26**, 2133-2143 (1999).
- C.M. Ma, T. Pawlicki, M.C. Lee, S.B. Jiang, J.S. Li, J. Deng, B. Yi, E. Mok, and A.L. Boyer, "Energy- and intensity-modulated electron beams for radiotherapy," *Phys. Med. Biol.* **45**, 2293-2311 (2000).
- C.M. Ma, J.S. Li, T. Pawlicki, S.B. Jiang, J. Deng, M.C. Lee, T. Koumrian, M. Luxton, and S. Brain, "A Monte Carlo dose calculation tool for radiotherapy treatment planning," *Phys. Med. Biol.* **47**, 1671-1689 (2002).
- C.M. Ma, M. Ding, J.S. Li, M.C. Lee, T. Pawlicki, and J. Deng, "A comparative dosimetric study on tangential photon beams, intensity-modulated radiation therapy (IMRT) and modulated electron radiotherapy (MERT) for breast cancer treatment," *Phys. Med. Biol.* **48**, 909-924 (2003).
- C.M. Ma, J.S. Li, S.B. Jiang, T. Pawlicki, W. Xiong, L.H. Qin, and J. Yang, "Effect of statistical uncertainties on Monte Carlo treatment planning," *Phys. Med. Biol.* **50**, 891-907 (2005).
- A. Mack, G. Mack, D. Wertz, S.G. Scheib, H.D. Bottcher, and V. Seifert, "High precision film dosimetry with GAFCHROMIC films for quality assurance especially when using small fields," *Med. Phys.* **30**, 2399-2409 (2003).
- T.R. Mackie and J.J. Battista, A macroscopic Monte Carlo method for electron beam dose calculations: a proposal, in: *Proc. 8th Conf. of Use of Computers in Radiation Therapy* (IEEE, Toronto, 1984) 123-127.
- T.R. Mackie, J.W. Scrimger, and J.J. Battista, "A convolution method of calculating dose for 15-MV x rays," *Med. Phys.* **12**, 188-196 (1985).
- T.R. Mackie, T.W. Holmes, P.J. Reckwerdt, and J. Yang, "Tomotherapy: optimized planning and delivery of radiation therapy," *Int J Imag Syst Tech* **6**, 43-55 (1995).
- M.H. Maor, R.S. Fields, K.R. Hogstrom, and J. van Eys, "Improving the therapeutic ratio of craniospinal irradiation in medulloblastoma," *Int. J. Radiat. Oncol. Biol. Phys.* **11**, 687-697 (1985).
- R.C. McCall, R.D. McIntyre, and W.G. Turnbull, "Improvement of linear accelerator depth-dose curves," *Med. Phys.* **5**, 518-524 (1978).
- B.M. McCurdy and S. Pistorius, "Photon scatter in portal images: physical characteristics of pencil beam kernels generated using the EGS Monte Carlo code," *Med. Phys.* **27**, 312-320 (2000).

- L.K. McNeely, G.M. Jacobson, D.D. Leavitt, and J.R. Stewart, "Electron arc therapy: chest wall irradiation of breast cancer patients," *Int. J. Radiat. Oncol. Biol. Phys.* **14**, 1287-1294 (1988).
- D.L. McShan, B.A. Fraass, and R.K. Ten Haken, "Dosimetric verification of a 3-D electron pencil beam dose calculation algorithm," *Med. Phys.* **21**, 13-23 (1994).
- M.L. Meurk, D.A. Goer, G. Spalek, and T. Cook, "The Mobetron: a new concept for IORT," in: *Intraoperative Radiation Therapy in the Treatment of Cancer: 6th Int. IORT Symposium and 31st San Francisco Cancer Symposium (September 1996) (Frontiers of Radiation Therapy and Oncology vol 31)*, edited by J.L. Meyer, W. Hinkelbein (Karger, Basle, 1997), pp. 65-70.
- M. Miften, M. Wiesmeyer, A. Kapur, and C.M. Ma, "Comparison of RTP dose distributions in heterogeneous phantoms with the BEAM Monte Carlo simulation system," *J. Appl. Clin. Med. Phys.* **2**, 21-31 (2001).
- M.D. Mills, K.R. Hogstrom, and P.R. Almond, "Prediction of electron beam output factors," *Med. Phys.* **9**, 60-68 (1982).
- M.D. Mills, K.R. Hogstrom, and R.S. Fields, "Determination of electron beam output factors for a 20-MeV linear accelerator," *Med. Phys.* **12**, 473-476 (1985).
- M.D. Mills, L.C. Fajardo, D.L. Wilson, J.L. Daves, and W.J. Spanos, "Commissioning of a mobile electron accelerator for intraoperative radiotherapy," *J. Appl. Clin. Med. Phys.* **2**, 121-130 (2001).
- R. Mohan, C. Chui, and L. Lidofsky, "Differential pencil beam dose computation model for photons," *Med. Phys.* **13**, 64-73 (1986).
- C. Moller, "Zur Theories des Durchgangs schneller Elektronen durch Materie," *Ann. Phys.* **14**, (1932).
- X. Mu, L. Olofsson, M. Karlsson, R. Sjogren, and B. Zackrisson, "Can photon IMRT be improved by combination with mixed electron and photon techniques?," *Acta Oncol.* **43**, 727-735 (2004).
- R. Muller-Runkel and S.H. Cho, "Evaluation of a commercial three-dimensional electron pencil beam algorithm," *Med. Phys.* **24**, 91-101 (1997).
- A.E. Nahum, "Water/air mass stopping power ratios for megavoltage photon and electron beams," *Phys. Med. Biol.* **23**, 24-38 (1978).
- A.E. Nahum and M. Kristensen, "Calculated response and wall correction factors for ionization chambers exposed to ^{60}Co gamma rays," *Med. Phys.* **9**, 925-929 (1982).
- A. Nahum, "Overview of photon and electron Monte Carlo," in: *Monte Carlo Transport of*

- Photons and Electrons*, edited by T.M. Jenkins, W.R. Nelson, A. Rindi (Plenum, New York, 1988).
- National Cancer Institute 2006 <http://www.cancer.gov> .
- W.R. Nelson, H. Hirayama, and D.W. Rogers, "The EGS4 code system, Stanford Linear Accelerator Center Report SLAC-265," (1985).
- H. Neuenschwander, T.R. Mackie, and P.J. Reckwerdt, "MMC--a high-performance Monte Carlo code for electron beam treatment planning," *Phys. Med. Biol.* **40**, 543-574 (1995).
- A. Niroomand-Rad, C.R. Blackwell, B.M. Coursey, K.P. Gall, J.M. Galvin, W.L. McLaughlin, A.S. Meigooni, R. Nath, J.E. Rodgers, and C.G. Soares, "Radiochromic film dosimetry: recommendations of AAPM Radiation Therapy Committee Task Group 55. American Association of Physicists in Medicine," *Med. Phys.* **25**, 2093-2115 (1998).
- C.M. Nutting, C.G. Rowbottom, V.P. Cosgrove, J.M. Henk, D.P. Dearnaley, M.H. Robinson, J. Conway, and S. Webb, "Optimisation of radiotherapy for carcinoma of the parotid gland: a comparison of conventional, three-dimensional conformal, and intensity-modulated techniques," *Radiother. Oncol.* **60**, 163-172 (2001).
- M. Olivares-Pla, E.B. Podgorsak, and C. Pla, "Electron arc dose distributions as a function of beam energy," *Med. Phys.* **24**, 127-132 (1997).
- L. Olofsson, M.G. Karlsson, and M. Karlsson, "Photon and electron collimator effects on electron output and abutting segments in energy modulated electron therapy," *Med. Phys.* **32**, 3178-3184 (2005).
- P.M. Ostwald and T. Kron, "Variation in calculated effective source-surface distances with depth," *Phys. Med. Biol.* **41**, 2067-2078 (1996).
- L. Paelinck, B.D. Smedt, N. Reynaert, M. Coghe, W.D. Gersem, C.D. Wagter, B. Vanderstraeten, H. Thierens, and W.D. Neve, "Comparison of dose-volume histograms of IMRT treatment plans for ethmoid sinus cancer computed by advanced treatment planning systems including Monte Carlo," *Radiother. Oncol.* (2006).
- S. Pai, L.E. Reinstein, G. Gluckman, Z. Xu, and T. Weiss, "The use of improved radiochromic film for in vivo quality assurance of high dose rate brachytherapy," *Med. Phys.* **25**, 1217-1221 (1998).
- J.R. Palta and T.R. Mackie, *Intensity modulated radiation therapy - the state of the art* (Medical Physics Publishing, Madison, WI, 2004).
- J.P. Patau, C.E. Vernes, M. Terrissol, and M. Malbert, "Calcul des caracteristiques qualitatives (TEL, F.Q., equivalent de dose) d'un faisceau de photons de freinage a usage medical, par simulation de sa creation et de son transport," in: *Proc. the 6th Symposium on*

- Microdosimetry*, edited by J. Booz, H.G. Ebert (Harwood Academic, London, 1978), pp. 579-588.
- A.C. Paulino and M. Skwarchuk, "Intensity-modulated radiation therapy in the treatment of children," *Med. Dosim.* **27**, 115-120 (2002).
- G.H. Perkins, M.D. McNeese, J.A. Antolak, T.A. Buchholz, E.A. Strom, and K.R. Hogstrom, "A custom three-dimensional electron bolus technique for optimization of postmastectomy irradiation," *Int. J. Radiat. Oncol. Biol. Phys.* **51**, 1142-1151 (2001).
- D.J. Perry and J.G. Holt, "A model for calculating the effects of small inhomogeneities on electron beam dose distributions," *Med. Phys.* **7**, 207-215 (1980).
- A.P. Pinkerton, "Comparison of calorimetric and other methods for the determination of absorbed dose," *Ann. N. Y. Acad. Sci.* **161**, 63-76 (1969).
- E.B. Podgorsak, P. Metcalfe, and J. Van Dyk, "Medical Accelerators," in: *The Modern Technology of Radiation Oncology*, edited by J. Van Dyk (Medical Physics Publishing, Madison, 1999), pp. 351-435.
- R.A. Popple, R. Weinber, J.A. Antolak, S.J. Ye, P.N. Pareek, J. Duan, S. Shen, and I.A. Brezovich, "Comprehensive evaluation of a commercial macro Monte Carlo electron dose calculation implementation using a standard verification data set," *Med. Phys.* **33**, 1540-1551 (2006).
- R.A. Price, G.E. Hanks, S.W. McNeeley, E.M. Horwitz, and W.H. Pinover, "Advantages of using noncoplanar vs. axial beam arrangements when treating prostate cancer with intensity-modulated radiation therapy and the step-and-shoot delivery method," *Int. J. Radiat. Oncol. Biol. Phys.* **53**, 236-243 (2002).
- B.P. Ravindran, I.R. Singh, S. Brindha, and S. Sathyan, "Manual multi-leaf collimator for electron beam shaping--a feasibility study," *Phys. Med. Biol.* **47**, 4389-4396 (2002).
- D.M. Roback, F.M. Khan, J.P. Gibbons, and A. Sethi, "Effective SSD for electron beams as a function of energy and beam collimation," *Med. Phys.* **22**, 2093-2095 (1995).
- D.W. Rogers, B.A. Faddegon, G.X. Ding, C.M. Ma, J. We, and T.R. Mackie, "BEAM: a Monte Carlo code to simulate radiotherapy treatment units," *Med. Phys.* **22**, 503-524 (1995).
- D.W. Rogers, C.M. Ma, B.R. Walters, G.X. Ding, D. Sheikh-Bagheri, and G.G. Zhang, "BEAMnrc Users Manual, National Research Council of Canada, Ottawa, Report PIRS-0509(A)G," (2002).
- D.W. Rogers, "Fifty years of Monte Carlo simulations for medical physics," *Phys. Med. Biol.* **51**, R287-301 (2006).
- F. Rohlich and B.C. Carlson, "Positron-electron difference in energy loss and multiple

- scattering," Phys. Rev. **93**, 38 (1953).
- RSICC <http://www-rsicc.ornl.gov/SOFTWARE.html> (2003).
- S.M. Sait and H. Youssef, *Iterative Computer Algorithms with Applications in Engineering: Solving Combinatorial Optimization Problems* (Angela Burgess, Los Alamitos, CA, 1999).
- N. Sakthi, P. Keall, I. Mihaylov, Q. Wu, Y. Wu, J.F. Williamson, R. Schmidt-Ullrich, and J.V. Siebers, "Monte Carlo-based dosimetry of head-and-neck patients treated with SIB-IMRT," Int. J. Radiat. Oncol. Biol. Phys. **64**, 968-977 (2006).
- A. Samuelsson, S. Hyodynmaa, and K.A. Johansson, "Dose accuracy check of the 3D electron beam algorithm in a treatment planning system," Phys. Med. Biol. **43**, 1529-1544 (1998).
- S.M. Seltzer, "Electron-photon Monte Carlo calculations: the ETRAN code," Appl. Radiat. Isot. **42**, 917 (1991).
- J. Sempau, "An algorithm for Monte Carlo simulation of coupled electron-photon transport," Nucl. Inst. Methods B **132**, 377 (1997).
- J. Seuntjens, A. Van der Plaetsen, H. Thierens, and M. Piessens, "Comparison of measured and calculated dose distributions in lung after electron beam treatment of the chest wall," Med. Phys. **21**, 1959-1968 (1994).
- J.P. Seuntjens and P.N. Mobit, *Recent developments in accurate radiation dosimetry* (Medical Physics Publishing, Madison, 2002).
- J. Seuntjens, J. Dai, E. Heath, K. Al-Yahya, and W. Parker, Retrospective Monte Carlo study of conformal lung cancer treatment plans (abstract), in: *Current Topics In Monte Carlo Treatment Planning, Advanced Workshop* (McGill University, 2004).
- R.J. Shalek and C.E. Smith, "Chemical dosimetry for the measurement of high-energy photons and electrons," Ann. N. Y. Acad. Sci. **161**, 44-62 (1969).
- E. Sham, *Simulated annealing algorithm for inverse treatment planning*. M.S. Thesis, Medical Physics Unit, McGill University, 2002.
- D. Sheikh-Bagheri, I. Kawrakow, B.R. Walters, and D.W. Rogers, "Monte Carlo simulations: efficiency improvements techniques and statistical considerations," in: *Integrating new technologies into the clinic: Monte Carlo and Image-Guided Radiation Therapy-Proceedings of 2006 AAPM Summer School*, edited by (Medical Physics Publishing, Madison, WI, 2006), pp. 71-91.
- A.S. Shiu, V.A. Otte, and K.R. Hogstrom, "Measurement of dose distributions using film in therapeutic electron beams," Med. Phys. **16**, 911-915 (1989).
- A.S. Shiu and K.R. Hogstrom, "Pencil-beam redefinition algorithm for electron dose

- distributions," *Med. Phys.* **18**, 7-18 (1991).
- C.G. Soares, D.G. Halpern, and C.K. Wang, "Calibration and characterization of beta-particle sources for intravascular brachytherapy," *Med. Phys.* **25**, 339-346 (1998).
- E. Spezi and D.G. Lewis, "Full forward Monte Carlo calculation of portal dose from MLC collimated treatment beams," *Phys. Med. Biol.* **47**, 377-390 (2002).
- G. Starkschall, A.S. Shiu, S.W. Bujnowski, L.L. Wang, D.A. Low, and K.R. Hogstrom, "Effect of dimensionality of heterogeneity corrections on the implementation of a three-dimensional electron pencil-beam algorithm," *Phys. Med. Biol.* **36**, 207-227 (1991).
- J.R. Stewart, D.D. Leavitt, and J. Prows, "Electron arc therapy of the chest wall for breast cancer: rationale, dosimetry, and clinical aspects," *Front. Radiat. Ther. Oncol.* **25**, 134-150 (1991).
- M. Stovall, C.R. Blackwell, J. Cundiff, D.H. Novack, J.R. Palta, L.K. Wagner, E.W. Webster, and R.J. Shalek, "Fetal dose from radiotherapy with photon beams: report of AAPM Radiation Therapy Committee Task Group No. 36," *Med. Phys.* **22**, 63-82 (1995).
- K. Sultanem, H.K. Shu, P. Xia, C. Akazawa, J.M. Quivey, L.J. Verhey, and K.K. Fu, "Three-dimensional intensity-modulated radiotherapy in the treatment of nasopharyngeal carcinoma: the University of California-San Francisco experience," *Int. J. Radiat. Oncol. Biol. Phys.* **48**, 711-722 (2000).
- R.K. Ten Haken, B.A. Fraass, and R.J. Jost, "Practical methods of electron depth-dose measurement compared to use of the NACP design chamber in water," *Med. Phys.* **14**, 1060-1066 (1987).
- D.I. Thwaites, A.R. DuSautoy, T. Jordan, M.R. McEwen, A. Nisbet, A. Nahum, and W.G. Pitchford, "The IPEMB code of practice for electron dosimetry for radiotherapy beams of initial energy from 2 to 50 MeV based on an air kerma calibration. Institution of Physics and Engineering in Medicine and Biology," *Phys. Med. Biol.* **41**, 2557-2603 (1996).
- J.G. Trump, K.A. Wright, W.W. Evans, J.H. Anson, H.F. Hare, J.L. Fromer, G. Jacque, and K.W. Horne, "High energy electrons for the treatment of extensive superficial malignant lesions," *Am. J. Roentgenol. Radium. Ther. Nucl. Med.* **69**, 623-629 (1953).
- M. Tubiana, *Introduction to Radiobiology* (Taylor & Francis, New York, 1990).
- S.S. Tung, A.S. Shiu, G. Starkschall, W.H. Morrison, and K.R. Hogstrom, "Dosimetric evaluation of total scalp irradiation using a lateral electron-photon technique," *Int. J. Radiat. Oncol. Biol. Phys.* **27**, 153-160 (1993).
- J.V. Turian, B.D. Smith, D.A. Bernard, K.L. Griem, and J.C. Chu, "Monte Carlo calculations of output factors for clinically shaped electron fields," *J. Appl. Clin. Med. Phys.* **5**, 42-63

- (2004).
- S.C. van der Marck and A. Hogenbirk, "ORANGE, a new, fast dose engine for radiotherapy treatment planning," *Radiat. Prot. Dosimetry*. **115**, 517-521 (2005).
- W. van der Zee and J. Welleweerd, "A Monte Carlo study on internal wedges using BEAM," *Med. Phys.* **29**, 876-885 (2002).
- W. van der Zee, A. Hogenbirk, and S.C. van der Marck, "ORANGE: a Monte Carlo dose engine for radiotherapy," *Phys. Med. Biol.* **50**, 625-641 (2005).
- D. Verellen, N. Linthout, D. van den Berge, A. Bel, and G. Storme, "Initial experience with intensity-modulated conformal radiation therapy for treatment of the head and neck region," *Int. J. Radiat. Oncol. Biol. Phys.* **39**, 99-114 (1997).
- D. Verellen and F. Vanhavere, "Risk assessment of radiation-induced malignancies based on whole-body equivalent dose estimates for IMRT treatment in the head and neck region," *Radiother. Oncol.* **53**, 199-203 (1999).
- F. Verhaegen, R. Symonds-Tayler, H.H. Liu, and A.E. Nahum, "Backscatter towards the monitor ion chamber in high-energy photon and electron beams: charge integration versus Monte Carlo simulation," *Phys. Med. Biol.* **45**, 3159-3170 (2000).
- F. Verhaegen, C. Mubata, J. Pettingell, A.M. Bidmead, I. Rosenberg, D. Mockridge, and A.E. Nahum, "Monte Carlo calculation of output factors for circular, rectangular, and square fields of electron accelerators (6-20 MeV)," *Med. Phys.* **28**, 938-949 (2001).
- F. Verhaegen and J. Seuntjens, "Monte Carlo modelling of external radiotherapy photon beams," *Phys. Med. Biol.* **48**, R107-164 (2003).
- S. Webb, "Optimization by simulated annealing of three-dimensional, conformal treatment planning for radiation fields defined by a multileaf collimator: II. Inclusion of two-dimensional modulation of the x-ray intensity," *Phys. Med. Biol.* **37**, 1689-1704 (1992).
- S. Webb, *Intensity modulated radiation therapy* (Institute of Physics Publishing, Bristol, UK, 2000).
- B.L. Werner, F.M. Khan, and F.C. Deibel, "A model for calculating electron beam scattering in treatment planning," *Med. Phys.* **9**, 180-187 (1982).
- J. Yang, J. Li, L. Chen, R. Price, S. McNeeley, L. Qin, L. Wang, W. Xiong, and C.M. Ma, "Dosimetric verification of IMRT treatment planning using Monte Carlo simulations for prostate cancer," *Phys. Med. Biol.* **50**, 869-878 (2005).
- C.X. Yu, M.J. Symons, M.N. Du, A.A. Martinez, and J.W. Wong, "A method for implementing dynamic photon beam intensity modulation using independent jaws and a multileaf collimator," *Phys. Med. Biol.* **40**, 769-787 (1995).

- B. Zackrisson and M. Karlsson, "Matching of electron beams for conformal therapy of target volumes at moderate depths," *Radiother. Oncol.* **39**, 261-270 (1996).
- G.G. Zhang, D.W. Rogers, J.E. Cygler, and T.R. Mackie, "Monte Carlo investigation of electron beam output factors versus size of square cutout," *Med. Phys.* **26**, 743-750 (1999).